TELEVISION BANDWIDTH COMPRESSION BY INTERPOLATION

A Thesis submitted by Peter Charles John Hill for the Degree of Doctor of Philosophy in the Faculty of Engineering of the University of London.

The Electrical Engineering Department,
Imperial College,
London, S.W.7.

March, 1960

ABSTRACT

The present day conventional TV signal is highly redundant from an Information-Theoretical standpoint; redundancies result from the statistical structure of the video signal itself and also from certain psycho-physical limitations in human vision. Removal of these redundancies may lead to bandwidth reduction in the signal which may then be transmitted over a channel of reduced capacity. Economic considerations apart, success of any such band-saving system depends ultimately upon favourable subjective assessment.

A bandwidth compression scheme is proposed in which the unnecessarily high field repetition rate, set to obviate picture flicker on display and not justified by the time resolution of the human eye, is reduced for narrow band transmission by a factor of four. Periodically selected full rate fields are stretched in time and successively transmitted over the relay as in conventional television. The line receiver functions so as to provide the received fields in real time and also the interlaced fields and missing frames by a process of interpolation. The interpolation is such that the contours represented by large brightness gradients are geometrically preserved together with their motion, with the restriction that edges are assumed to be linear over three adjacent lines and moving uniformly over three consecutive frames; near-horizontal contours and fast vertical motions fall outside the system's

contour preserving capabilities. A '<u>picture transformer</u>',an optico-mechanical machine with electronic control, has been constructed in order to test and demonstrate the principle of '<u>contour interpolation</u>' with stationary pictures. The device simulates the receiver routine for 2:1 field interpolation at speeds around one ten-thousandth that of television and provides results in photographic form for subjective appraisal.

The Thesis concludes by extending the principles to fully electronic interpolation schemes and includes basic system designs for two, four, and eight-to-one TV compression using presently available conventional equipment.

ACKNOWLEDGEMENTS

The author wishes to acknowledge the constant advice and encouragement he has received, during the course of his work, from his supervisor Professor D. Gabor, Dr.-Ing., F.Inst.P.,M.I.E.E.,F.R.S.

In addition the author wishes to thank Professor A. Tustin, M.Sc., M.I.E.E., Head of the Electrical Engineering Department, Imperial College, for affording the facilities of the Electronics Laboratory and the Electrical Workshops; also Dr. M.E. Haine, Research Manager of the Siemens Edison Swan Research Laboratory for supplying the photoconductive cells; Mr. W. Green for constructing much of the basic mechanical hardware; and Mr. L. Boroff for his assistance in constructing "pointolite" lamp assemblies.

The Chief Engineer of the British Broadcasting Corporation is to be thanked for granting the author a Research Scholarship, thus enabling him to carry out his work at Imperial College during the period 1956-59. The author is also appreciative of the interest taken in the project by Mr. W. Proctor Wilson, C.B.E., Head of Research Department and Mr. W.K. Newson, Engineering Recruitment Officer, both of the British Broadcasting Corporation.

/

CONTENTS

1. INTRODUCTION.

Television is the art of instantaneous transmission of a time varying scene at one point through a communication channel to an observer at another point. The present day system, involving periodic scanning which converts the simultaneous spatial brightness information into a sequential temporal signal, has been chosen as a compromise between the economic and practicable limitations of the resulting engineering system and the psycho-physical limitations of the human eye.

The channel bandwidth (just over 3 Mc/sec for the British 405 line, 50 field/sec, 2 : 1 interlaced system) is set for uniform-rate transmission of maximum detail pictures of fixed horizontal and vertical resolution and field repetition rate. As a result of inter-element, inter-line and inter-field correlations, the information rate of transmitted TV pictures is non-uniform; Information Theory shows that channel efficiency may be increased by averaging out the information rate and matching the channel (including the observer) to it. One result of this is a potential bandwidth reduction which offers many attractive advantages: increased efficiency in the utilisation of waveband space in the RF spectrum allotted to television, with a potential increase in picture definition, or provision of space for a colour signal; possibility of intercontinental television using a short wave carrier or submarine link; direct recording of video signals on magnetic tape using conventional methods, are a few. As the realisation of compression schemes is costly, their chief application will be in TV relaying where the economics is not so important as in broadcasting, compatibility is irrelevant and achievement of results is important.

The following sections describe the application of Information Theory to television and give a short survey of work on bandwidth compression together with a bibliography.

1.1 INFORMATION - THEORETICAL BACKGROUND TO TELEVISION BANDWIDTH COMPRESSION

1.11 Information Source and Channel Capacity.

The most important results in the theory can be compressed into two classical formulas due to SHANNON (1) which are conceptually simple but difficult to interpret and apply in practice. The first relates to the information source:

$$H = -\sum_{1}^{N} P_i \log_2 P_i \quad \text{bits/symbol} \qquad (1.1)$$

gives the information per symbol in an N symbol alphabet, if P_i is the probability of the i^{th} symbol. These symbols may be amplitude values of picture elements, groups of elements forming known shapes, complete lines, etc. To transmit N' symbols per second with ideal coding requires a channel of capacity N'H bits/sec. Channel capacity is given by

$$C_{MAX} = W\log_2 (1 + P/N) \text{ bits/sec.} \qquad (1.2)$$

with W the waveband, P/N the mean signal to noise power ratio assuming Gaussian signals and noise. The result is approximately valid for restricted signal powers, and represents an efficiency which can only be approached in practice; it also shows how the three parameters may be interchanged still maintaining constant channel capacity.

In the light of these formulas then, reduction of bandwidth is achieved by exchanging it for savings in average power, which are obtained by uniformly distributing the signal power over the frequency spectrum; this is done by equalising the symbol probabilities to maximise H in equation 1.1 and transmitting the resulting 'Gaussian' sequence uniformly in time.

The overall potential compression factor for the picture source-observer channel may be computed : Assuming 32 intensity levels (the number required to reproduce a subjectively satisfactory picture has been investigated by GOODALL[(2)]) and 400^2 elements, the orthodox channel can transmit $32^{160,000}$ possible pictures with its capacity of about 30×10^6 bits/sec for a 3Mc/sec bandwidth and p-p signal/RMS noise ratio of 30 dB*; real pictures are not Gaussian however, and also the result of studies in visual perception [(3)] indicates that the human intake rate is perhaps 50 bits/sec at most; this yields a potential compression of a few millions to one!

Information Theory can show what may be achieved but gives no indication of its realisation.

---

* Unless stated otherwise, the British system will be assumed in the remainder of the text, using the American nomenclature of field and frame rather than the British frame and picture.

1.12 Possibilities in Television Bandwidth Compression.

There are two distinct types of redundancy in conventional video signals; the first is statistical redundancy and results from the various picture correlations, the second is human or non-statistical redundancy, resulting from limitations in human vision; they can be combatted, theoretically at least, by statistical and nonstatistical coding respectively. Under these headings, the various known redundancies will be listed, together with an indication of their reduction possibilities.

STATISTICAL REDUNDANCY :

1. Inter-element correlations. Measurement of second-order or transition probabilities for real pictures indicates a possible saving. If the brightness intensity of one picture point is 'i', the information given by the next is from SHANNON's formula

$$H = -\sum_{k} P_i(k) \log_2 P_i(k) \qquad (1.3)$$

which is a maximum for all $P_i(k)$ equal. Statistical coding (of the Shannon-Fano type)[4] or variable velocity scanning will equalise the transition probabilities and reduce the redundancy. Higher order transition probabilities should yield an increased saving. (The first order distribution is not expected to provide any worthwhile gain.)

2. Inter-line correlations. Since high vertical coherence is characteristic of pictures, adjacent lines are highly correlated unless

they contain 'surprises'; an alphabet of line symbols would be very large and the resultant saving from statistical coding small. The high correlation however does suggest an economy by transmitting only a fraction of the full number of lines/field and predicting or interpolating the remainder at the receiver.

3. Inter-frame correlations. Except for complete scene changes, there is a strong temporal coherence between adjacent frames. Power and/or bandwidth reduction may be theoretically achieved by transmitting frame-difference signals only, until a 'surprise' frame occurs[(5)]; alternatively, the transmitter sends a reduced number of frames and the receiver interpolates the missing ones. Coding complete pictures is obviously absurd but redundancy could be reduced theoretically by coding typical scenic areas (dress material, grass, sky, etc.) and indexing these from a suitable store at the receiver.

4. Spectrum redundancies. As a result of the scanning mechanism involved in orthodox TV, the video signal frequency spectrum consists of harmonics of the line scanning frequency, and with each of these is grouped a number of discrete sidebands spaced by the field frequency[(6)]. The spectrum structure is dependent on the horizontal correlation (Wiener's Theorem - the autocorrelation function is the Fourier - transform of the smoothed power spectrum), the power distribution in the line harmonic sidebands is dependent on the vertical correlation, and the modulation of the field harmonics depends on frame coherence or motion detail.

The 'gaps' in this spectrum may be used to accommodate additional information[7] (this is precisely what is done in the N.T.S.C. Colour System).

6. Quantisation. The present TV channel has a video bandwidth of 3Mc/s at a S/N ratio of 30 to 35 dB <u>at the output</u> (the actual transmission channel must be rather better - around 50-60 dB). With 30 dB signal: noise, $\log_2(1 + P/N) = 10$ which is sufficient to transmit just over 1000 levels whereas 32 are enough [2]. This represents a redundancy of about one half, assuming completely uncorrelated picture elements.

<u>NON-STATISTICAL REDUNDANCY</u> :

1. Field frequency redundancy. The present field rate of 50 cycles/sec is designed to remove flicker at conventional display brightness intensities and is not justified by the time resolution of the eye. Exploitation of this leads to reduced field transmission rates with the receiver making up the full number by suitable interpolation or repetition. (cf. frame repetition in conventional cinematography).

2. The eye concentrates and tends to hook on to object edges (brightness transients) and is relatively poor in its ability to determine the absolute brightness of large areas[8]; this suggests separate channels for 'edge' and 'large area' information.

3. The eye is unable to notice the exact amplitude and shape of short brightness transients and the number of perceptible contrast levels appears to be an inverse function of frequency[8].

This indicates a saving by grading the number of quantising levels according to frequency band with a band divided video signal, and is equivalent to taper-quantizing the 'rate-of-change-' signal.

4. Visual acuity falls off with decreasing field brightness,[9] a redundancy which may be reduced by transmitting fewer samples i.e. a reduced waveband, in the low brightness regions.

5. Visual resolving power peaks into a very narrow cone-angle and in particular falls off at the edges of the picture <u>if</u> subjective interest is concentrated at the centre-region of the display.[10]. In such a case, bandwidth economy may be achieved at the picture edges. In general, this may be extended to a compression scheme in which only the 'interest areas' of the picture are sent with full resolution.

6. Human redundancy, which cannot be exploited using present-day techniques, results from the compressed visual transmission in the observer's eye-brain channel.

The above list of non-statistical redundancies is by no means exhaustive; it must be emphasised that compression schemes reducing redundancies (statistical and human) are not necessarily independent, and any large saving must result from the combination of two or more <u>independent</u> schemes; the ultimate criterion of success depends on favourable subjective assessment.

1.2 SURVEY OF TELEVISION BANDWIDTH COMPRESSION RESEARCH.

Rather than give a chronological account of previous work in this field, this short survey will attempt to list the various attacks on the problem as under the headings given in Section 1.12 above.

The first order probability distribution for pictures has been measured by KRETZMER[11]; the results showed that first order statistics are not 'stationary' and that no saving could be expected from efficient coding with a 32 level picture. The second order probability distribution has been measured by SCHREIBER[12] using analogue equipment at TV rates and also by STODDARD[13] using digital equipment to determine the joint probability distribution of the 32-level quantized intensity of adjacent signal samples. Stoddard's derived conditional entropy of 1.24 bits for a medium detail picture indicates a 4 : 1 redundancy in specifying the second element of each pair with the same uncertainty as the first. SCHREIBER[14] has also measured third order statistics but with disappointing results; the potential channel capacity savings indicated by the work of Kretzmer and Schreiber is reviewed theoretically by CAPON[15] who also describes the measurement of autocorrelation functions of still pictures using optical equipment.

The removal of first order correlations has been investigated by HARRISON[16] in experiments with linear prediction in television; he explores the possibilities in using suitably weighted samples derived from 'previous sample', 'slope', 'previous-line', 'planar and circular' points, to predict the next signal sample using a computer. The reduced power in the error signal ('actual' minus 'predicted' values) indicates the possible saving; he showed that the gain provided by slope and planar prediction is only incrementally greater than that afforded by previous value prediction.

Several velocity modulation schemes have been proposed in which inter-element correlations are effectively reduced. In 1934 a variable velocity scanning system was described by BEDFORD and PUCKLE[17]; the system transmits a display scanner waveform which brightness-modulates the trace of a fixed intensity writing CRT spot, and assumes therefore, on an information theory basis, a directly proportional 'picture detail' - brightness law. In schemes proposed by SCHRÖTER[18], CHERRY and GOURIET[19], the measure of picture detail is taken as the square of the rate of change of brightness intensity[20] and the scanning speed is varied inversely with this quantity. The potential gain of 4 or 5 by this method cannot be fully exploited because surprisingly high detail lines would be incompletely scanned, and also because the scanner feedback mechanism becomes unstable if the maximum scanning speed is more than about 3 times the mean. NOVIK[21] has analysed mathematically velocity modulation as a function of rise time of TV signal changes. CHERRY, PRASADA and HOLLOWAY[22] have proposed an 'Open Loop' television compression system in which picture detail is quantised into a few discrete levels and the signal is sampled at a quantised rate dependent on that detail; the amplitude modulated pulses are shuffled into time-uniformity and the final spacing defines the compressed bandwidth - this work is still in its initial stages. GOURIET[23] describes an alternative scheme in which significant brightness changes and their positions are transmitted in separate or multiplexed channels as equi-spaced amplitude modulated pulses; assuming the channels to carry independent information and the number of significant changes per line to be 6% of the number of line elements[20], Gouriet computes a theoretical channel capacity saving of around 7 : 1 and also describes the instrumentation of a practicable system which approaches that compression figure. Bandwidth saving based on the direct transmission of co-ordinates of picture elements which indicate a brightness change by at least one minimum perceptible increment is described theoretically by TSUKKERMAN[24]. A non-uniform scanning system suitable for 2-level facsimile-type transmission, and usable when constancy of frame rate is irrelevant, is described by HAYNES and HOGER[25]; in their system, a precisely controlled spot resting time removes the edge-transient from the channel, the bandwidth being determined by the average 'edge-rate'.

The 'Dot Arresting' system of SCHLESINGER[26] substantiated the theory that the eye tends to concentrate and hook onto brightness transients (although it is unable to notice the exact amplitude and shape of such changes), a fact which has suggested to several workers the possibility of limited amplitude specification of high frequency detail. KRETZMER[27] describes 'hyperquantising' in two frequency bands, with about half the number of amplitude levels in the high frequency band, and also 'taper-quantising' on the per-element difference signal based on the assumption that the eye is more sensitive to errors in small amplitude changes than large ones. Another hyperquantizing system, developed by ANDO[28], transmits the high-frequency components as a two level pulse train indicating contour positions, polarities and widths; the pulse width information is used to form simple triangular shaped transients in the reformed picture the results of which are claimed to be promising. In the experimental system of SCHREIBER, KNAPP, and KAY[29], the high frequency transients are synthesised from a digital code signal giving the location and quantized amplitude of the edges and added to the low frequency signal which is separately transmitted in analogue form. An alternative system involving coarse quantisation in the high frequency regions has been simulated by JULESZ[30] on the IBM 704 computer; only 'surprise' samples are transmitted and the receiver linearly interpolates intervening samples with a maximum consecutive interpolation of 16 Nyquist intervals; suitable coding would provide a 2 : 1 compression in such a scheme. Computer simulation has also been used by GRAHAM and KELLY[31] for a 'predictive quantizing' system in which observer coding is achieved by employing fine quantum steps for small prediction errors and coarse steps when the predictor is surprised; YOUNGBLOOD[32], ABOUDI and FANO[33] are investigating rate of change quantizing which, even without statistical encoding, provides a potential redundancy reduction. Youngblood has also suggested combining slope quantisation with interpolation schemes and this work is being extended by CUNNINGHAM[34] who programmes a computer to average the intensity levels of 3 by 3 and 5 by 5 sample blocks and obtain a full high frequency picture by algebraic interpolation between these data blocks.

A 2 : 1 bandwidth reduction scheme, dependent upon the periodic structure of the video signal frequency spectrum, has recently been described by BELL and HOWSON[35]; the band 1·5 - 3.0 Mc/s amplitude modulates a sub-carrier of frequency equal to an odd multiple of the half-line frequency and the lower side band is 'frequency interleaved' with the first band of 0 - 1.5 Mc/s. Results show that subcarrier dot crawling which is tolerable with still pictures becomes very noticeable with picture movement. The effect of movement of, and in, TV pictures on the frequency spectrum has been theoretically investigated by the Engineering Division of the Australian Post Office[36] and this Division has also investigated the relation between auto-correlation, power spectra and entropy bounds in video signals[37] [38] [39].

The general problem of TV bandwidth reduction and coding has been discussed by SEYLER[40], GRAHAM[41], DELBORD[42] and POWERS and STARAS[43].

1.3 BIBLIOGRAPHY - TELEVISION BANDWIDTH COMPRESSION

1. SHANNON, C.E., WEAVER, W., The Mathematical Theory of Communication University of Illinois Press, Urbana, 1949.

2. GOODALL, W.W., Television By Pulse Code Modulation, B.S.T.J., (Bell System Technical Journal) 30, pp 33-49, 1951.

3. SZILKAI, G.C., Some Studies in the Speed of Visual Perception, I.R.E. Trans. Information Theory, I.T.-2, P.125, September, 1956

4. OLIVER, B.M., Efficient Coding, B.S.T.J., 31, 4, 1952.

5. KELL, R.D., and B.T.H. Ltd., British Patent No. 341811.

6. MERTZ, P., GRAY, W.A., Theory of Scanning and its Relation to the Transmitted Signal in Telephotography and Television, B.S.T.J. 13, p.464, 1934.

7. BELL, D.A., Information Theory and its Engineering Applications, Pitman, London, pp 92-96, 1953.

8. EVANS, R.M., Sharpness and Contrast in Projected Pictures, Journal of the S.M.P.T.E. (Society of Motion Picture and Television Engineers), Convention Record, Los Angeles, October 1956.

9. JESTY, L.C., PHELP, N.R., Evaluation of Picture Quality with Special Reference to Television Systems, Marconi Review, 14, 102, 1951.

10. JESTY, L.C., Television as a Communication Problem, Proc. I.E.E., 99, IIIA, No. 20, p. 761, 1952.

11. KRETZMER, E.R., Statistics of Television Signals, B.S.T.J., 31, July, 1952.

12. SCHREIBER, W.F., Probability Distributions of Television Signals, Ph. D. Thesis, Harvard, 1953.

13. STODDARD, J.C., Measurement of Second-Order Probability Distributions of Pictures by Digital Means, M.I.T. Research Lab. of Electronics, Tech. Report, 302, 1955.

14. SCHREIBER, W.F. The Measurement of Third Order Probability Distribution of Television Signals, I.R.E. Trans. Information Theory, Vol. 1-T2, 3, pp 94 - 105, September 1956.

15. CAPON, J., Bounds to the Entropy of Television Signals, M.I.T. Research Lab. of Electronics, Tech. Report 296, May 1955.

16. HARRISON, C.W., Experiments with Linear Prediction in Television, B.S.T.J., 31, p. 764, July, 1952.

17. BEDFORD, L.H., PUCKLE, O.S., A Velocity Modulation Television System, Journal I.E.E., 75, p.63, 1934.

18. SCHRÖTER, F., 'Speicherempfang und Differenzbild Fernshen', Archiv. der Elektrischen Ubertragung, 7, p. 63, 1953.

19. CHERRY, E.C., GOURIET, G.G., Some Possibilities for the Compression of TV Signals by Re-coding, Symposium on Communication Theory, London, 1952, Butterworth Scientific Press, 1953.

20. GOURIET, G.G., A Method of Measuring Television Picture Detail and its Applications. Electronic Eng., 24, p. 306, 1952.

21. NOVIK, D.A., A Method of Compressing the Bandwidth of a Television Channel, Zh., teckh., Fiz., 26, No. 4, pp900-10, 1956 (In Russian).

22. CHERRY, E.C., PRASADA, B., (Imperial College) and HOLLOWAY, D.G., (B.T.R. Ltd.,) Proposed New 'Open Loop' System of Television Compression, Provisional Patent, October 1957. No. 32376/58.

23. GOURIET, G.G. Bandwidth Compression of a Television Signal, Proc. I.E.E., Part B., 104, No. 15, p. 265, May, 1957.

24. TSUKKERMAN, I.I, Transmission of Coordinates of Television Picture Elements, Radiotecknika, 13, 4, pp 77-9, 1958 (In Russian).

25. HAYNES, N.E., Hoger, D.T., Stop-Go Scanning Saves Spectrum Space, Electronics, 31, 39, pp 84-88, September 1958.

26. SCHLESINGER, K., Dot Arresting Improves TV Picture Quality, Electronics, 24, No. 9, p. 96, September 1951.

27. KRETZMER, E.R., Reduced Alphabet Representation of Television Signals, I.R.E., Convention Record, Part 4, pp 140-7, March, 1956.

28. ANDO, H., Quantizing System of Higher Components of TV Signals, J. Inst. Elect. Comm. Eng. Japan, 42, 5, May 1959.

29. SCHREIBER, W.F., KNAPP, C.F., KAY, N.D., Synthetic Highs - An Experimental TV Bandwidth Reduction System, Journal of the S.M.P.T.E., 68, pp 525-537, August, 1959.

30. JULESZ, B., A Method of Coding Television Signals Based on Edge Detection. B.S.T.J., 38, 4, July, 1959.

31. GRAHAM, R.E., KELLY, J.L., A Computer Simulation Chain for Research on Picture Coding, I.R.E. Convention Record, Part 4, pp 41-6, August 1958.

32. YOUNGBLOOD, W.A., Picture Processing. Quarterly Progress Report 54, M.I.T. Research Lab. of Electronics, p. 138, July, 1958.

33. ABOUDI, R.W., FANO, R.M., The Effect of Slope Quantisation in Picture Transmission. Quarterly Progress Report, 41, M.I.T., Research Lab. of Electronics, April, 1953.

34. CUNNINGHAM, J.E., Picture Processing. Quarterly Prog. Rep. 54, M.I.T. Research Lab. of Electronics, p. 138, July 1959.

35. BELL, D.A., HOWSON, E.A., Two to One Television Bandwidth Reduction Scheme, Unpublished, Brit. I.R.E., Television Convention, Cambridge, July 1959.

36. COMM. OF AUSTRALIA (P.G. Dept.) ENG DIV. RES. REP. No. 4465, The Effect of Movement of and in Television Pictures on the Frequency Spectrum of the Video Signal.

37. KORPEL, A., Measurements in the Power Spectrum of TV Signals, Comm, of Australia (P.G. Dept.) Eng. Div. Research Lab. Rep. 4632.

38. COMM. OF AUSTRALIA (P.G. Dept.) ENG. DIV. RES. LAB. REP. No. 4503. Relationships between Auto-Correlation Functions and Entropy

Bounds in TV Picture Signals.

39. COMM. OF AUSTRALIA (P.G. Dept.) ENG. DIV. RES. LAB. REP. No. 4405, The Frame Difference Signal of Television Picture Signals.

40. SEYLER, A.J. Bandwidth Reduction in Television Relaying I-II, Proc. Inst. R.E. Australia, 16, 7, 8, pp 218-25, 261-276, July, August 1955.

41. GRAHAM, R.E., Communication Theory Applied to Television Coding, Acta Electronica, 2, No. 1-2, 1958.

42. DELBORD, Y.L., Bandwidth Reduction Systems and Their Application to TV. Acta Electronica, 2, No. 1-2, 1958.

43. POWERS, K.H., STARAS, H., Some Relations between TV Picture Redundancy and Bandwidth Requirements, Trans. A.I.E.E., 76, pp 492-6, 1957.

44. DEUTSCH, S., The Possibilities of Reduced Television Bandwidth, I.R.E. Transactions on Broadcast and Television Receivers, 1956.

2. THE PRINCIPLE OF CONTOUR INTERPOLATION (1) (2)

2.1 INTRODUCTION

The most wasteful redundancy in conventional television systems is the unnecessarily high field repetition rate justified only by flicker suppression. One of the two interlaced fields in each frame provides little additional information and the frame frequency (30/s in the U.S. and 25/s in Europe) is not justified by the time resolution of the eye. It is known that 16 frame/sec cinematography with a shutter frequency of 48/sec is subjectively satisfactory, and also that in systems with 'optical equalisation' in which one picture fades continuously into the next, the frame rate may be reduced to 6/sec. or less. This indicates a possible saving of 8 to 1 in television : 2 from the saving of every second interlaced field and 4 from the saving of 3 frames in 4.

'Contour interpolation' takes in two data simultaneously (as compared with one in conventional television and thousands in visual perception) and recognises one type of pattern - a short length of an outline assumed to be straight; it provides a system for displaying motion over the best optical equalisation systems.

2.2 LINEAR AND CONTOUR INTERPOLATION.

2.21 Linear Interpolation.

Linear Interpolation represents optical equalisation and is illustrated in Fig. 2.1(a). Lines 1 and 2 can be considered as next-but-one lines in one frame (adjacent lines in one interlaced field) or as corresponding lines in next-but-one frames. If the line signals are $S_1(t)$ and $S_2(t)$, the interpolated line signal is given by

$$S_{12}(x) = \frac{1}{2} S_1 (x) + \frac{1}{2} S_2(x) \qquad .....(2.1)$$

and this preserves sharp edges only if they are vertical and stationary, whereas slanting contours and moving edges are blurred; normal detail is accurately interpolated if there is a linear variation in intensity between corresponding elements of lines 1 and 2. It is probable that linear interpolation could be used for halving the frame frequency in orthodox television.

2.22 <u>Contour Interpolation</u>.

Contour Interpolation is more intelligent in preserving sharp outlines and is illustrated in Fig. 2.1(b). If a step function commences at t_1 in line 1 and t_2 in line 2, the interpolated signal is given by

$$S_{12}(t - \tfrac{1}{2}\overline{t_1 + t_2}) = \tfrac{1}{2}S_1(t - t_1) + \tfrac{1}{2}S_2(t - t_2) \qquad .....(2.2)$$

and is a step function commencing at $\frac{1}{2}(t_1 + t_2)$ with the mean amplitude of steps S_1 and S_2. This is the correct guess for a <u>uniformly</u> moving edge and a good approximation for other outlines which are not too capricious.

One method of mechanisation is shown in Fig. 2.2; the top sketch shows the contour (narrow zone of steep intensity gradient) cut by the two lines 1 and 2 at x_1 and x_2, and assuming it is important enough (the gradient exceeds a certain absolute value) the procedure is as follows: Two scanning spots, vertically aligned, proceed at equal

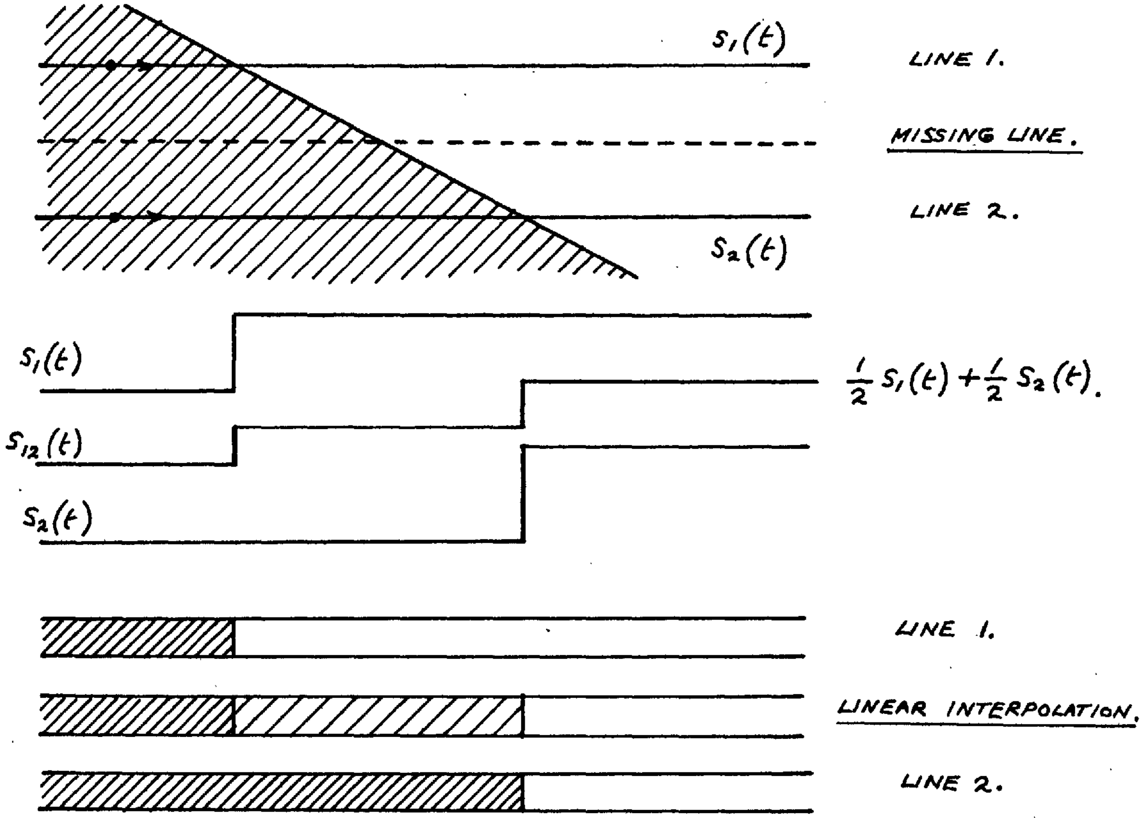

(a) LINEAR INTERPOLATION

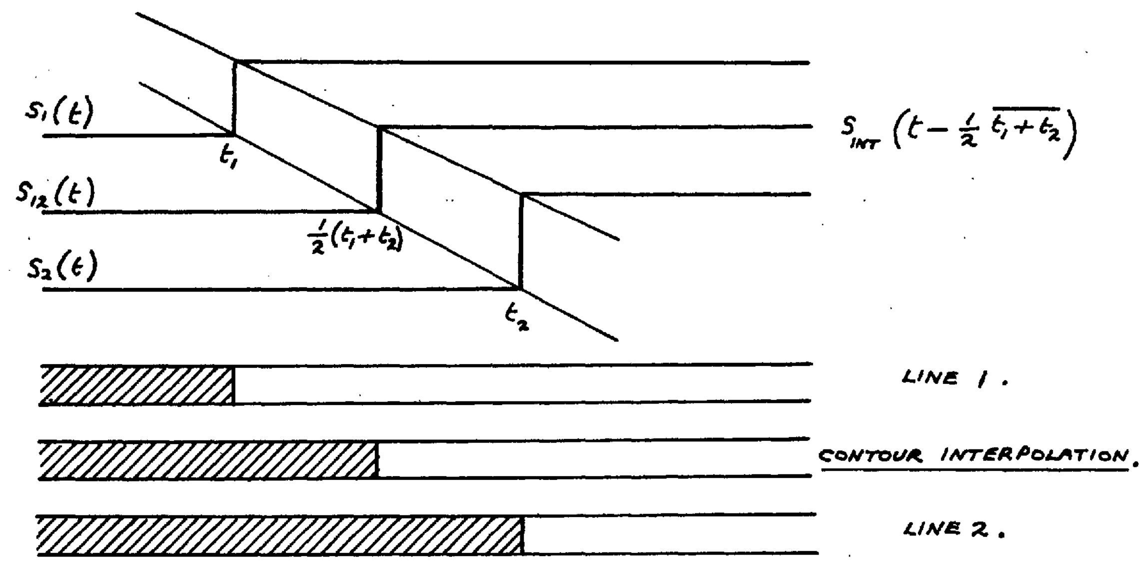

(b) CONTOUR INTERPOLATION

FIG. 2·1 LINEAR AND CONTOUR INTERPOLATION.

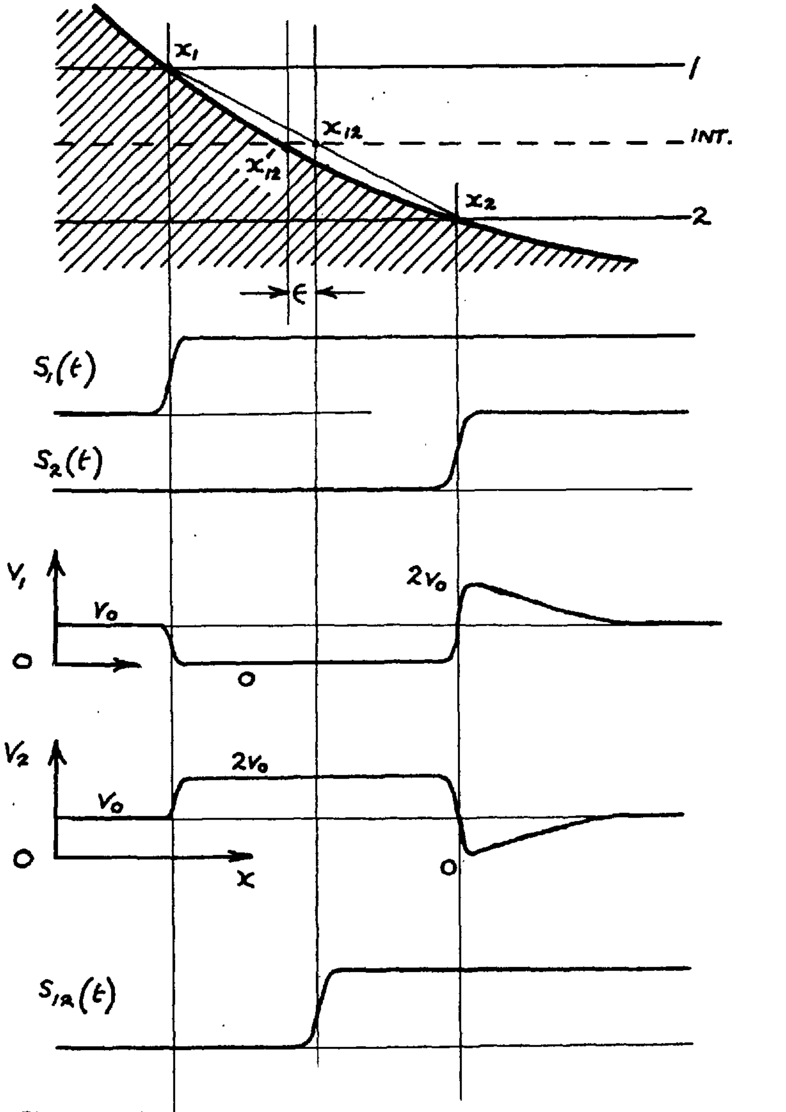

FIG. 2·2

CONTOUR INTERPOLATION WITH OVERSHOOT.

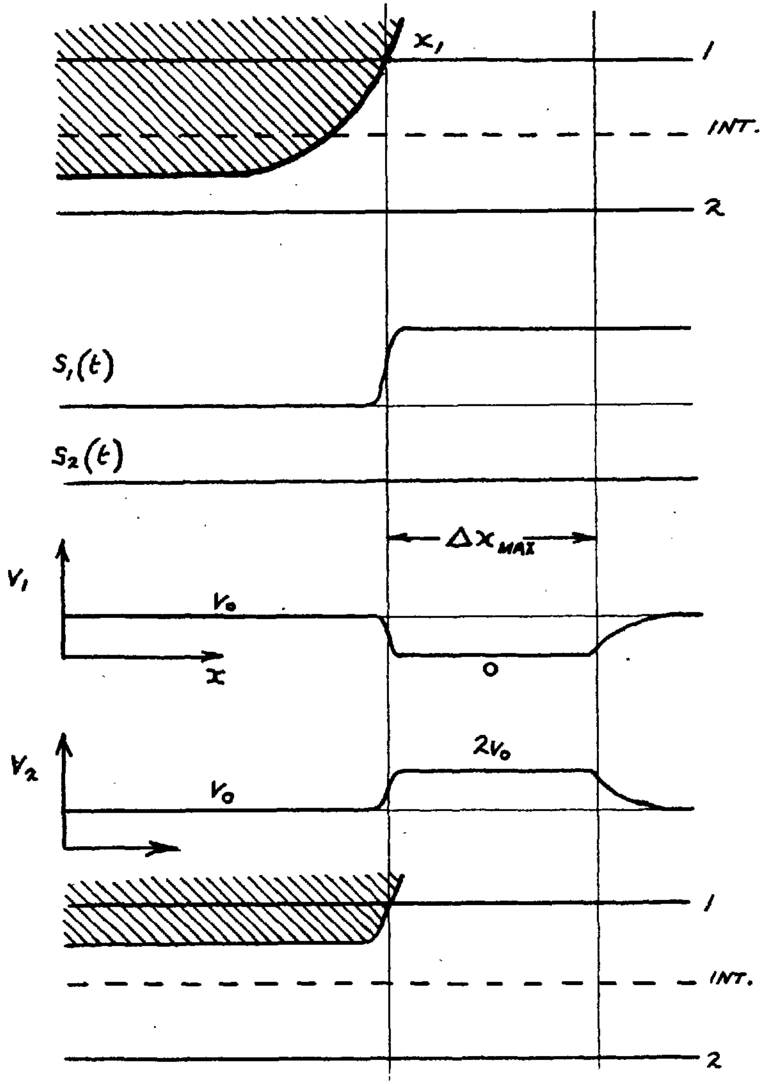

FIG. 2·3 'MISSING CONTOUR' ROUTINE.

velocity v_o along lines 1 and 2. When the first one reaches the contour (in the sketch, the upper one at x_1) it stops dead, and the second proceeds instantaneously at double speed $2v_o$ until it finds the other end of the contour. The second spot then stops dead, the first jumps up to double speed and subsequently the first spot is decelerated and the second accelerated until they are again vertically aligned and proceeding with equal uniform speed v_o; in this process the mean spot velocity $\frac{1}{2}(v_1 + v_2)$ is constant and equal to v_o, the speed of the interpolating spot. The intensity of the interpolated line is derived by the following signal distribution rule:

$$s_{12} = \frac{v_1 s_1 + v_2 s_2}{v_1 + v_2} \qquad \text{.....(2.3)}$$

which includes the rule for linear interpolation when $v_1 = v_2 = v_o$; in contour interpolation each spot contributes to the interpolated intensity in proportion to its velocity and the velocity plots in the sketch represent the signal weightings. In the contour-search region, the whole signal is transferred to the moving spot i.e. with $v_1 = 0$, $v_2 = 2v_o$, we have $s_{12} = s_2$, and this is the correct result if this region is either structureless, or contains vertical detail, or is a stationary background of any type in the case of frame interpolation. The advantage of the velocity overshoot-routine after the second spot finds the contour is that it puts the correct amplitude in the contour itself, a refinement which may be unimportant because of the inability of the eye to notice the exact amplitude of short brightness transients.

A modified routine is available in case the second spot misses the contour and this is illustrated in Fig. 23. The control of the contour-search mechanism is such that if, after a distance Δx_{max} after the arrested first spot position, the second has failed to find the contour, the two velocities return to the normal value v_o <u>without overshoot</u> and this has the effect of terminating the contour below the first line.

For interpolation between adjacent field lines, the distance Δx_{max} may be set at 6 - 8 spot widths restricting the interpolation to contours inclined more steeply than 1 in 3 or 1 in 4 to the horizontal. If the searching distance is too great there is too great a risk in finding a spurious contour in the interval.

For frame interpolation, the maximum searching distance Δx_{max} corresponds to the maximum distance a contour has moved between two transmitted frames and therefore sets an upper bound to the horizontal velocity of motion for which the above routine is effective. Transmission of one frame in four provides a time interval of 0.16 sec and, assuming an object moving across the complete picture width (say 400 elements) in two seconds, to be the fastest motion we need consider, this gives an object shift of 32 points in the interframe period. Experimentation must show whether with $\Delta x_{max} \doteqdot 30$ picture points there is too great a chance of hooking onto the wrong contour.

2.3 FUNCTIONAL ELEMENTS OF CONTOUR INTERPOLATION SYSTEMS

There are five basic functional elements in a contour interpolation system and they may be listed as follows :

1. INPUT STORE: Sequential line data must be stored and available simultaneously, i.e. two lines in one field or corresponding lines in two frames/fields.
2. TWO SENSING ORGANS: These may be moving spots with an organ which decides when the contour interpolation mechanism shall be put into and out of action.
3. VELOCITY MODULATING ORGAN: Performs the contour searching routine when put into action by the above organ.
4. SIGNAL DISTRIBUTOR: An organ which weights the data from the two sensing organs according to the scanning velocities and adds them.
5. OUTPUT STORE: To store the interpolated signals when they are not instantaneously transmitted.

A line or field contour interpolation system is shown in schematic form in Fig. 2.4; in this diagram the two sensing organs have been expanded into two scanners, contour detector- gates and a control circuit and it should be noted that each sensing organ scanner provides separate control and main writing channels; this allows the control action to be advanced on the main interpolating channel and compensates for switching delays in the velocity modulator feedback circuit and signal distributor, it also obviates possible instability in variable velocity scanning systems which work to a resolution of a fraction of a picture point.

A complete compression system involves a <u>transmitter</u> which stores

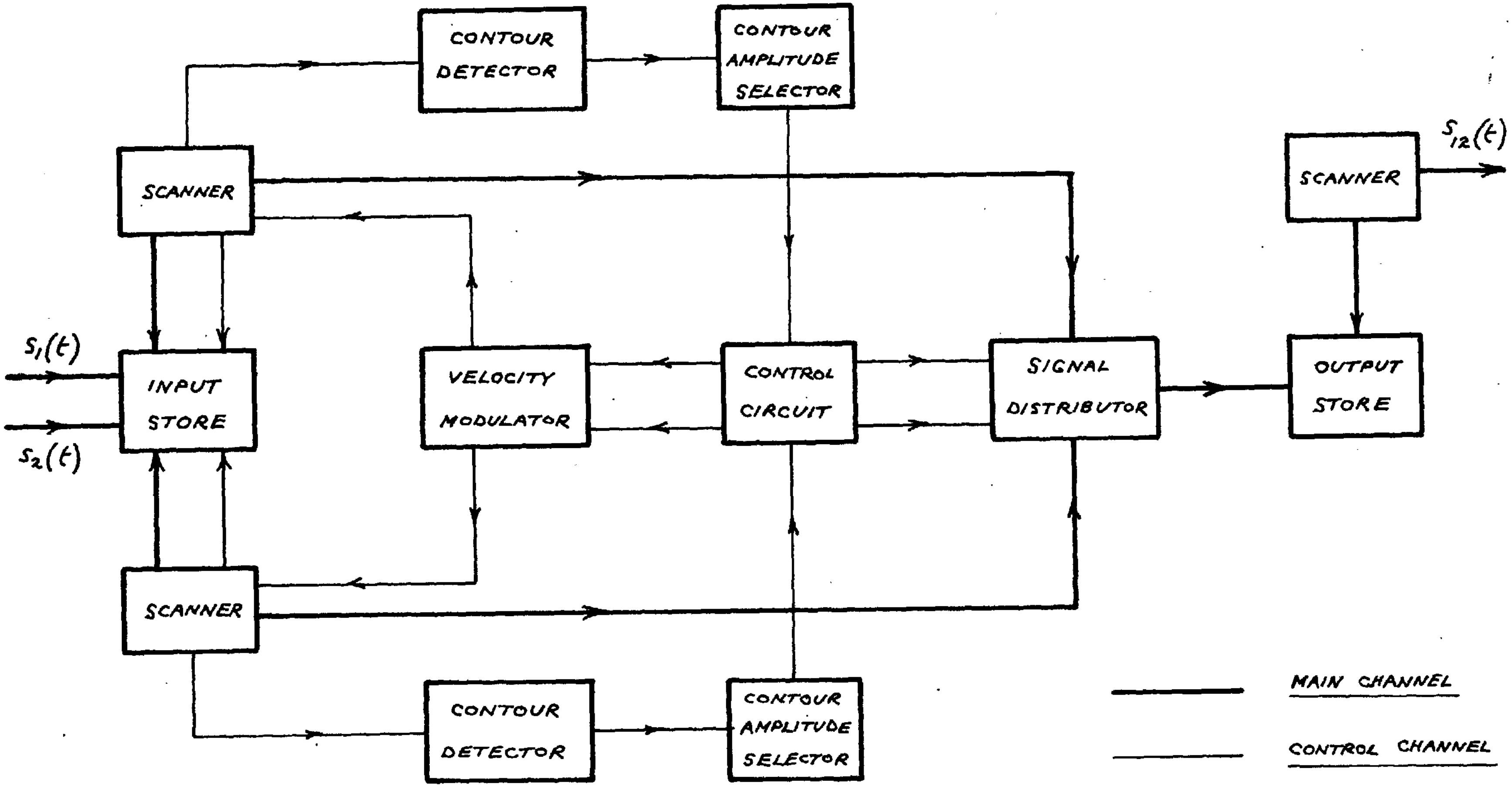

FIG 2·4. BLOCK DIAGRAM OF A LINE 'CONTOUR INTERPOLATION' SYSTEM.

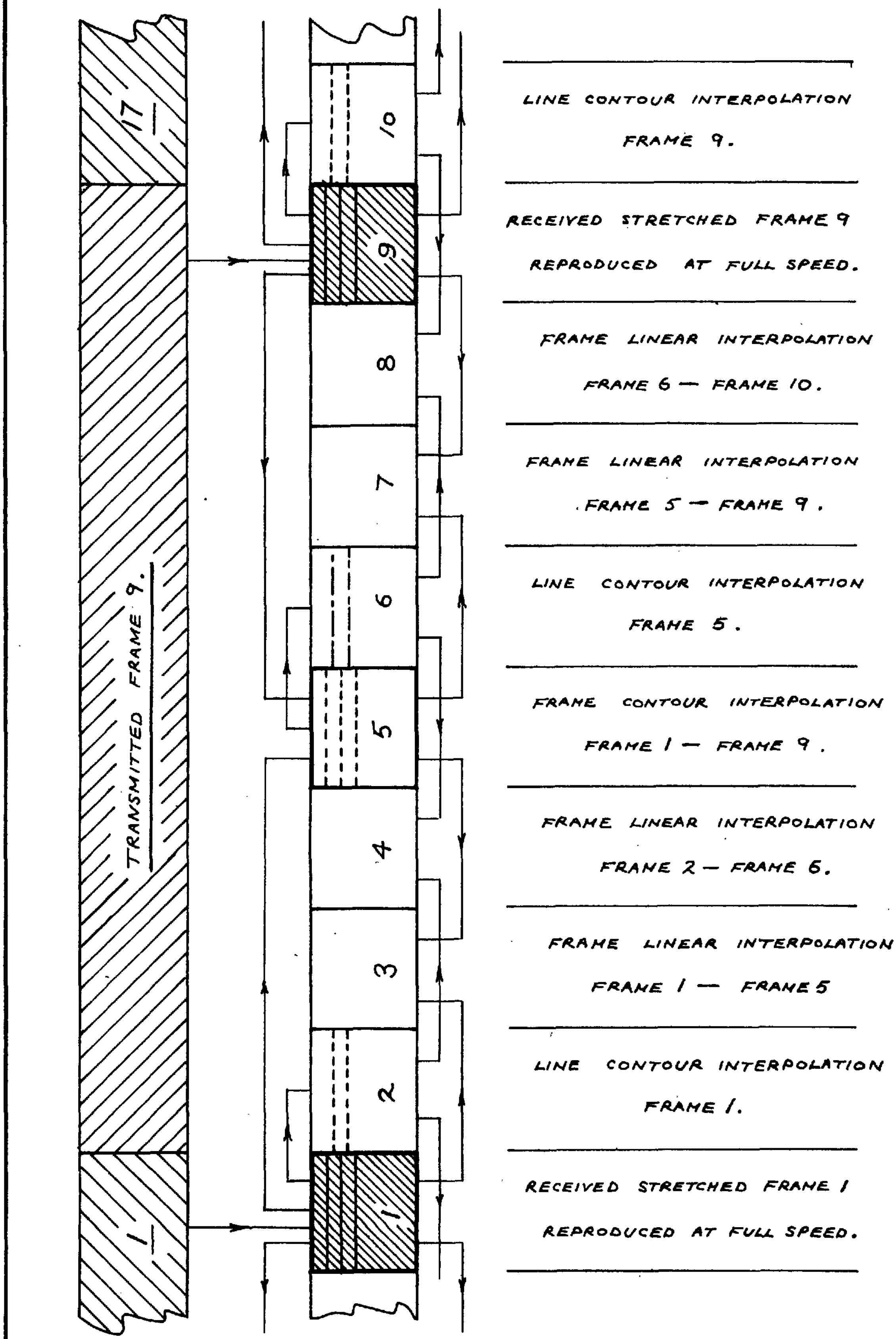

FIG. 2:5 A TELEVISION TRANSMISSION SYSTEM WITH 8:1 COMPRESSION.

selected fields, frames or both, and 'stretches' these uniformly in time, and a receiver with field and/or frame contour interpolation which compresses the received signals into real time and produces the missing signals by interpolation. An 8:1 compression scheme is shown diagrammatically in Fig. 2.5 To progress from the broad functional scheme to electronic realisation is not an easy matter and this is discussed in Chapter 6. It was decided to test the principles involved in contour interpolation initially in a slow speed device working at a rate of about 1/10,000 that of television and this work is described in Chapters 3, 4 and 5.

2.4 SPECIAL FEATURES AND LIMITATIONS OF INTERPOLATION SYSTEMS

It is useful at this stage to consider the theoretical advantages of this form of bandwidth compression and also particular expected limitations in the ultimately derived television pictures.

2.41 Special Advantages of Bandwidth Saving by Interpolation.

Compared with other forms of bandwidth compression, contour interpolation possesses the following outstanding advantages:

(1) Contour Interpolation offers a fixed high compression ratio; a figure of 8:1 is not too sanguine compared with about 3:1 in rate equalisation systems.

(2) In the interpolation system, complexity in the terminal equipment lies mainly in the line receiver; the transmitter for signal stretching is comparatively trivial.

(3) The stretched signals for channel transmission are slow

speed conventional picture signals which may be subsequently _independently_ further compressed in bandwidth by a tandem rate equaliser or statistical coder.

(4) Interpolation systems are compatible with Standards Conversion and these functions may be combined in transmission.

(5) For fixed bandwidth channels, signals may be time-multiplexed if transmitted unstretched.

(6) Direct monitoring of the transmitted compressed signal is possible using a simple long-persistence display.

2.42 _Limitations in Contour Interpolation_.

We shall list in this section, certain obvious picture-motion types of programme in which contour interpolation fails. As in conventional transmissions, suitable programme editing removes objectionable failure-effects and ultimate picture quality must be assessed subjectively.

(1) In field and frame interpolation only those contours which exceed the pre-set threshold engage the mechanism. Low _intensity_ slope edges are equalised with linear interpolation; this is no great disadvantage if we assume that subjective interest lies mainly in the large intensity gradients.

(2) A contour 'detector' which works with the picture rate-of-change signal is also sensitive to _geometrical_ contour slope and the output is weighted, increasing with this slope to the horizontal. For a given rate-of-change threshold, near horizontal contours will be undetected completely. This may be advantageous with very low slope edges

where the searching mechanism would turn off prior to finding the second edge point and the second point would present another 'initial' contour.

(3) In field interpolation, the system is able to recognise changes in geometrical edge slope once in every two ultimate scanning lines and in frame interpolation, accelerations are detected at half the conventional rate for 2:1 compression.

(4) 'Surprise' information, such as sharp corners and fast motion with associated suddenly revealed contours, will beat the system, if the spurious contours are detected and taken to be coherent. In frame interpolation it might be necessary to adopt further criteria to ensure that detected edge points are coherent. A simple criterion might be contour brightness phase identity which would certainly deal effectively with close patterning in field interpolation where the pattern structure coalesces with the normal contour routine.

(5) The vertical resolution to horizontal structures (e.g. grids) is immediately halved in field interpolation and the spurious patterning which is present with such structures(normally avoided in programme material) would be more objectionable than in conventional systems. In particular, a horizontal bar pattern of vertical wavelength equal to two conventional line widths is totally missed in 2:1 interpolation, the resultant frame showing a uniform area of intensity lying on or between the two bar intensities and dependent upon the relative positions of scanning lines and bars.

(6) Vertical motions which take the present system to the limit will not bear compression by horizontal interpolation. This

would include fast ball games taken vertically and possibly mouth movements in certain types of speech.

2.5 REFERENCES

1. GABOR, D., 'Television Compression by Contour Interpolation', Written communication, received September, 1956.

2. GABOR, D., 'Television Compression by Contour Interpolation' N.2 del Supplemento al Vol.13, Serie X, del Nuovo Cimento - pp. 467-473.

3. THE PICTURE TRANSFORMER

The picture transformer is a device which has been built for testing and demonstrating at slow speed the principle of 2:1 field contour interpolation in television. It is an instrument which consists essentially of a facsimile transmitter and receiver in which the transmission of alternate lines is purely optical with mechanical synchronisation; the optical transmission is modulated by electronically controlled mechanical devices which operate according to the previously described routine.

As an instrument, it is of interest in itself, as it could be incorporated with conventional picture transmitter/receiver equipment enabling the users to transmit at full bandwidth for half the radio time; this economic saving is particularly valuable for multiple picture transmission. As early as 1934, the London - Melbourne Air Race finish was transmitted back to London on facsimile equipment as a sequence of 35mm. cinematograph frames[(1)], and today 'Telecine' frames are successively transmitted through the transatlantic cable link and recorded on conventional film.[(2)]

In the picture transformer, the original record, a paper print or drawing, is placed on a rotating picture drum and scanned with 0.15mm. spots with a double line spacing of 0.30mm. The generated 60 x 70mm. picture is recorded on conventional '120' size film carried by a second drum, and a full recording consists in an interpolation (200 lines) followed or preceded by the transcription of the original 200 lines which are interlaced with the others; for this purpose a 'half-line shift' is provided. The maximum transformation rate aimed at in the design is 1 picture element per millisecond i.e. a maximum 'horizontal bandwidth' of around 500 c.p.s. A variable speed (10:1) motor drive provides 7 forward scanning rates from 500 to 50 c.p.s. plus a fast reverse drive. The apparatus is completely light tight and may be operated under normal lighting conditions.

The complete picture transformer (minus the control circuitry) is shown in Plate 1 with the cover plates removed to show the interior construction and components. We now briefly describe the general mechanical hardware of the apparatus and its facilities and then proceed to describe in full detail the functional components. The design and operation of the electronic control circuits are given in the following chapter.

3.1 BASIC HARDWARE OF THE PICTURE TRANSFORMER

A scale drawing (Fig. 3.1) of the picture transformer is attached to the end of this thesis; the motor drive and light source assemblies are not shown but appear later in this chapter.

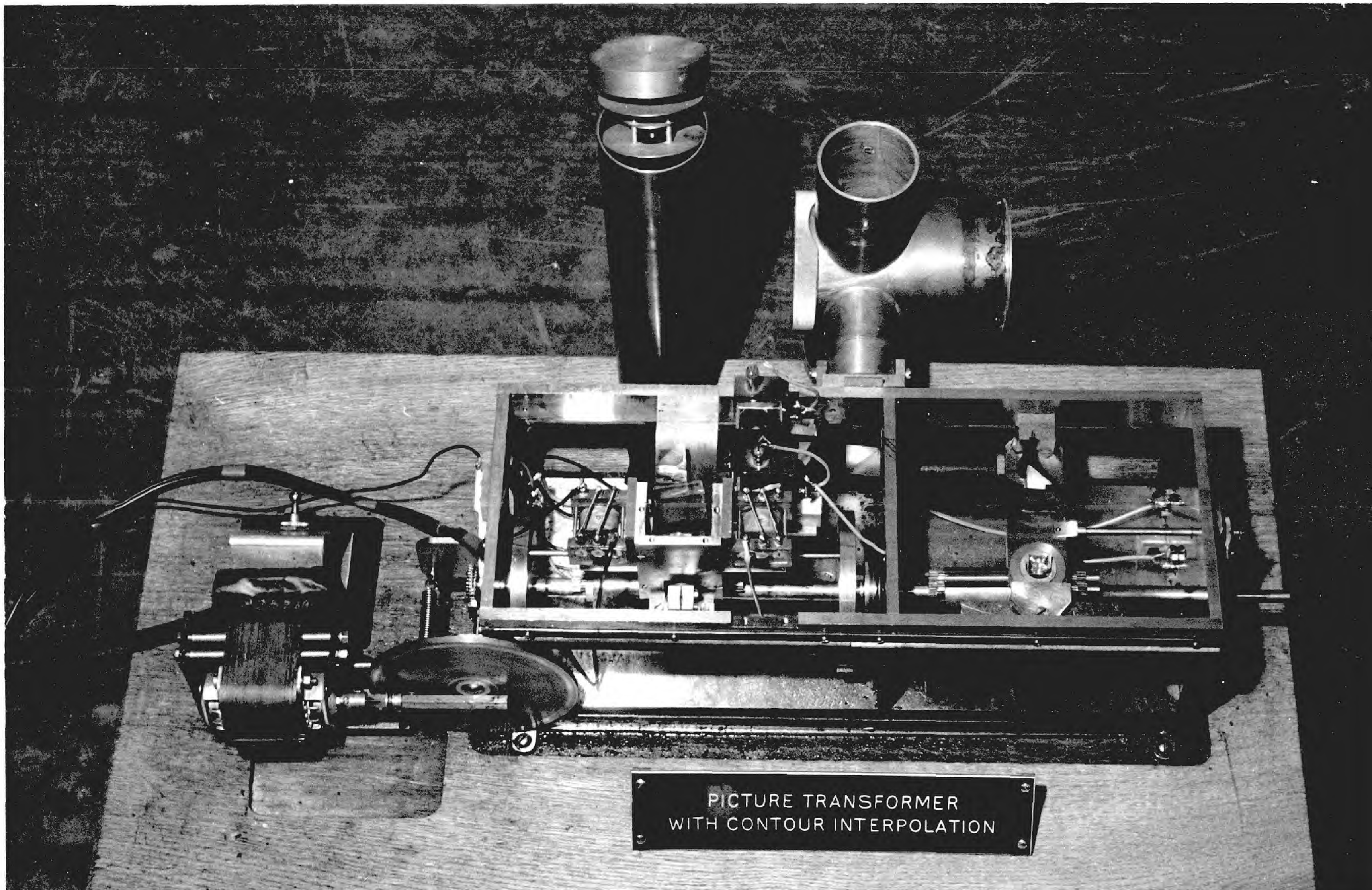

— PLATE 1 —

3.11 General Construction

The picture transformer has a fabricated steel base frame, ground on top and milled at the sides. The end plates are pinned and screwed to the base and a centre-plate divides the apparatus into separate 'writing' and 'reading' sections; two steel side bar members join the sides of the three plates at the top of the apparatus. Through these plates runs a tubular silver steel shaft carrying two drums, each with 1" diameter and 2½" length, which is motor driven at the 'reading' end. The drums are pinned through free axial slots in the tube wall into a brass rod with a 0.3 mm. pitch screw section (80 threads/inch) at the 'writing' end, thus enabling them to revolve with the tubular shaft and precess along it with double line spacing. Fig. 3.2 shows the picture and film drums together with the slotted spool retaining mechanisms. The tubular shaft also carries two brass wheel-flange assemblies (Fig. 3.3) which provide mechanical drive to the velocity modulator.

The optical circuit is supported by two ground steel cross-bars and a rectangular steel platform fixed to the underside of the side bars of the transformer; the optic axis is set at 3_3" above the top of the apparatus base. The 'half-line shift' facility is provided by making the writing cross bar a swinging arm (Fig. 3.4). The optical-drive lamp assembly fits into a brass lamp tube which is inset into the steel side bar.

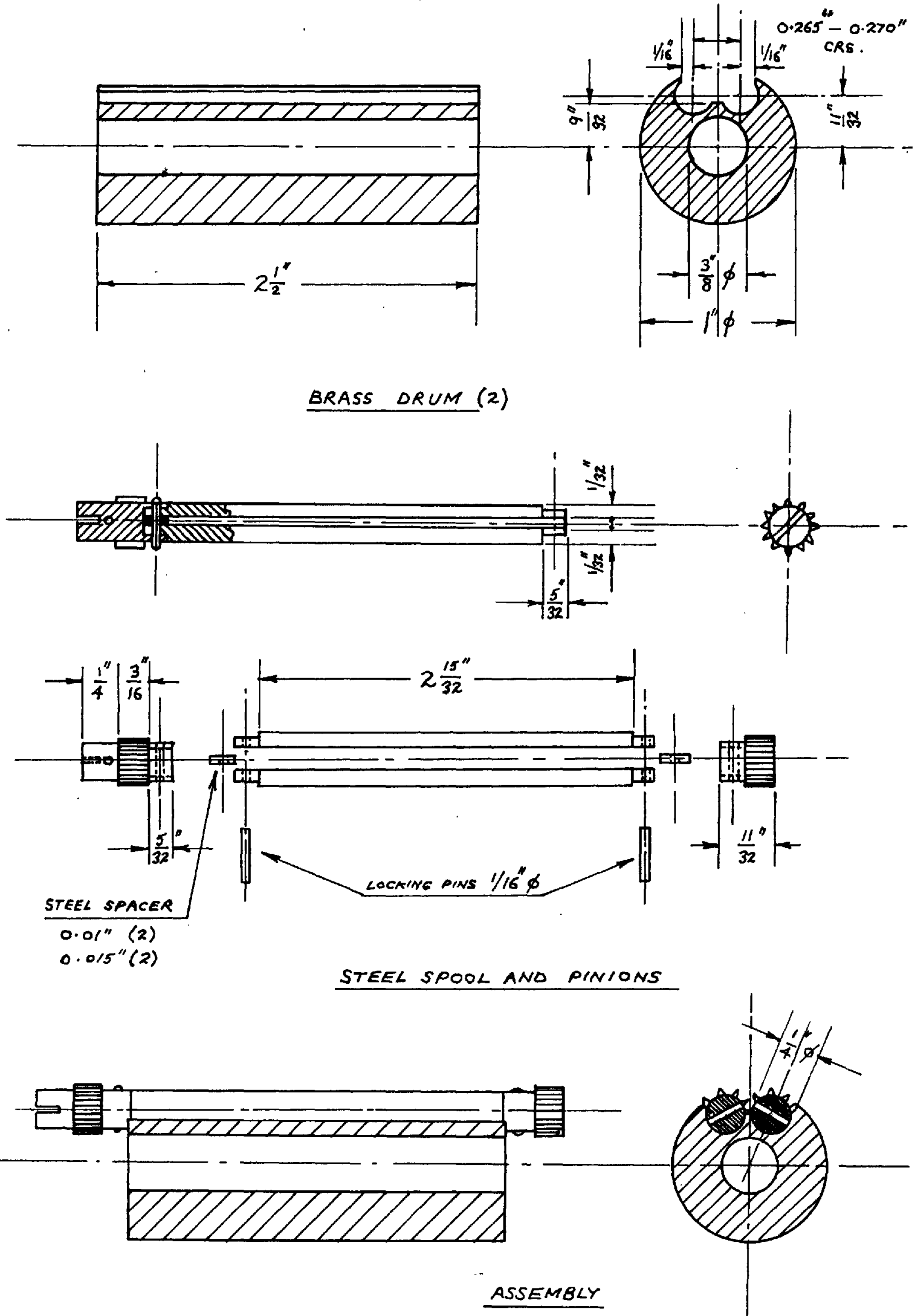

SCALE: FULL SIZE

FIG. 3·2 PICTURE–FILM DRUMS AND RETAINING MECHANISMS.

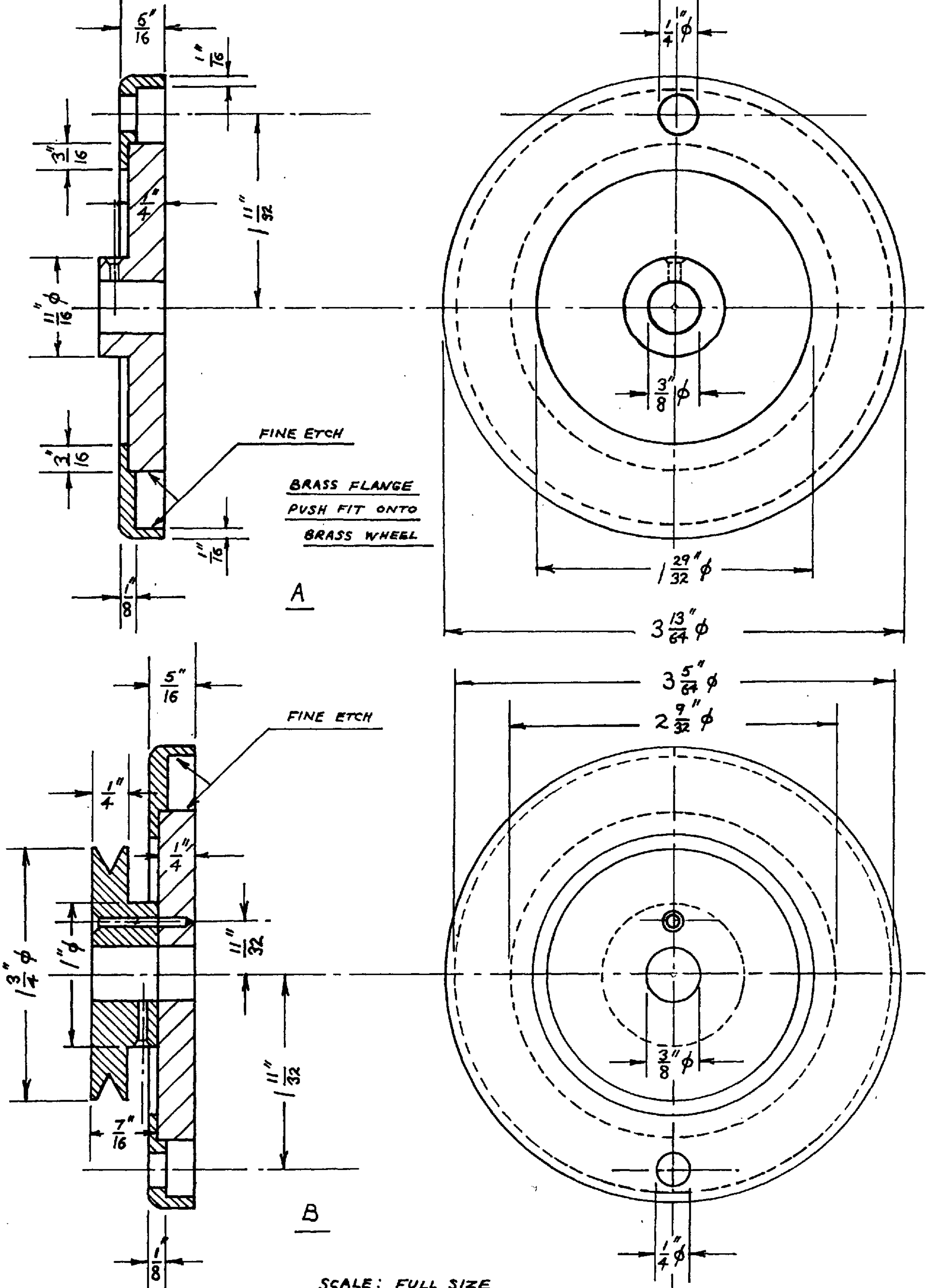

FIG. 3·3 WHEEL FLANGE ASSEMBLY FOR PICTURE TRANSFORMER

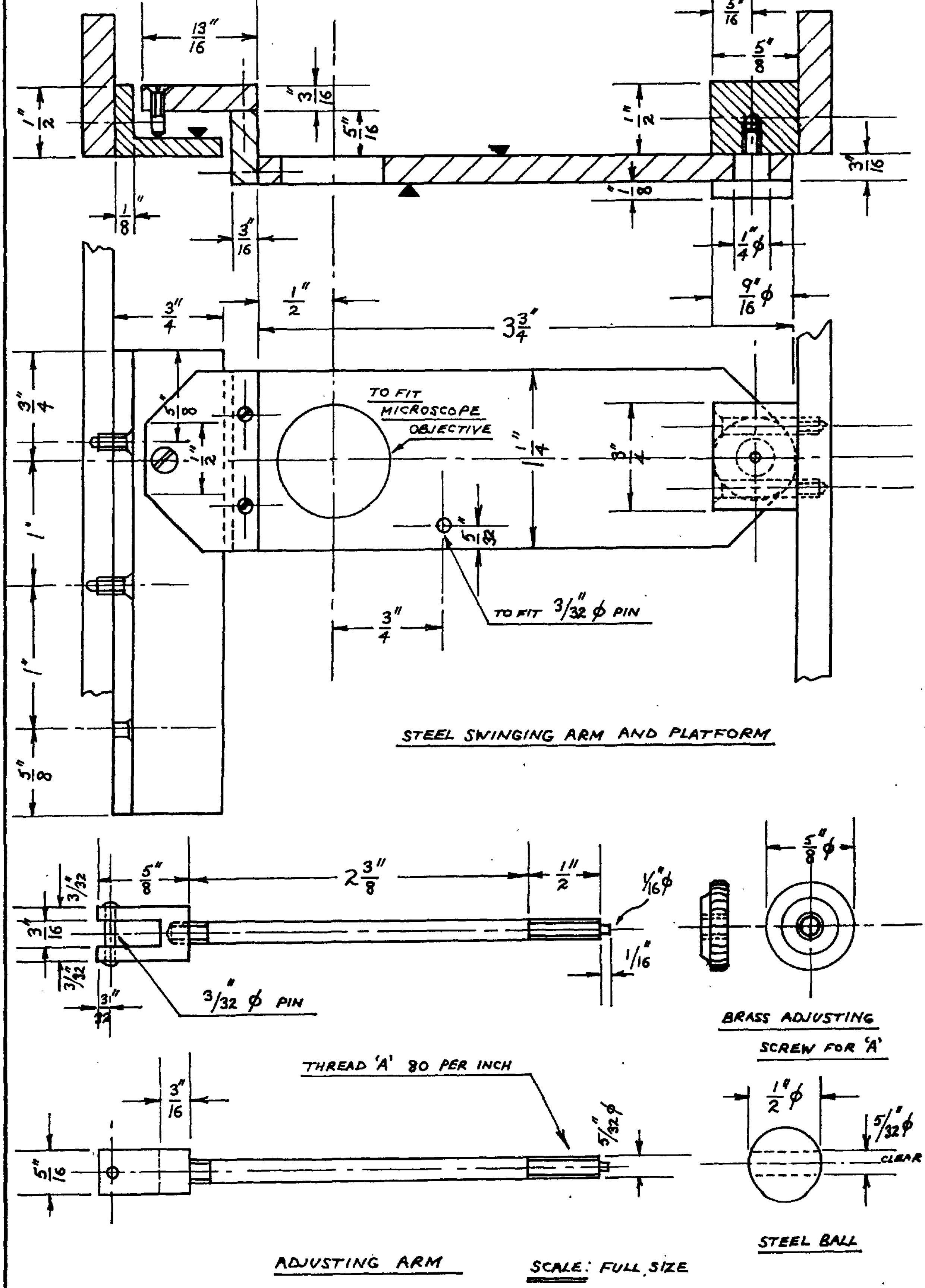

FIG. 3·4 SWINGING ARM FOR PICTURE TRANSFORMER

The velocity modulator with its actuator assembly is mounted onto the reading steel cross bar above the microscope objective and the signal distributor is placed on the ground surface of the apparatus base. Electrical connections to the modulators are made via a Plessey multiway connector inserted into the reading-box end-plate. The photocell screened output leads are taken through to the writing box and terminate on two Belling Lee co-axial sockets screwed to the writing-box end-plate.

Both the reading and the writing sections are made light-tight with independent top and side cover plates cut from 16 Gauge mild steel. The side-plates run in steel guides with black velvet sliding surfaces to ensure complete screening. The cover plate nearest to the picture drums contains a small red filter window for picture scanning observation and also carries a Johnson 'Film Loading bag' at the writing section for loading and unloading film under normal lighting conditions.

The apparatus is rigidly screwed to a 1" Japanese Oak base plate and is electrically mains earthed.

3.12 The Motor Drive Assembly (Fig. 3.5)

The motor drive is supplied from a 40watt Garrard shaded pole induction motor, and provides a speed step down ratio variable in 7 discrete steps between and including the limits 240:1 and 20:1. This

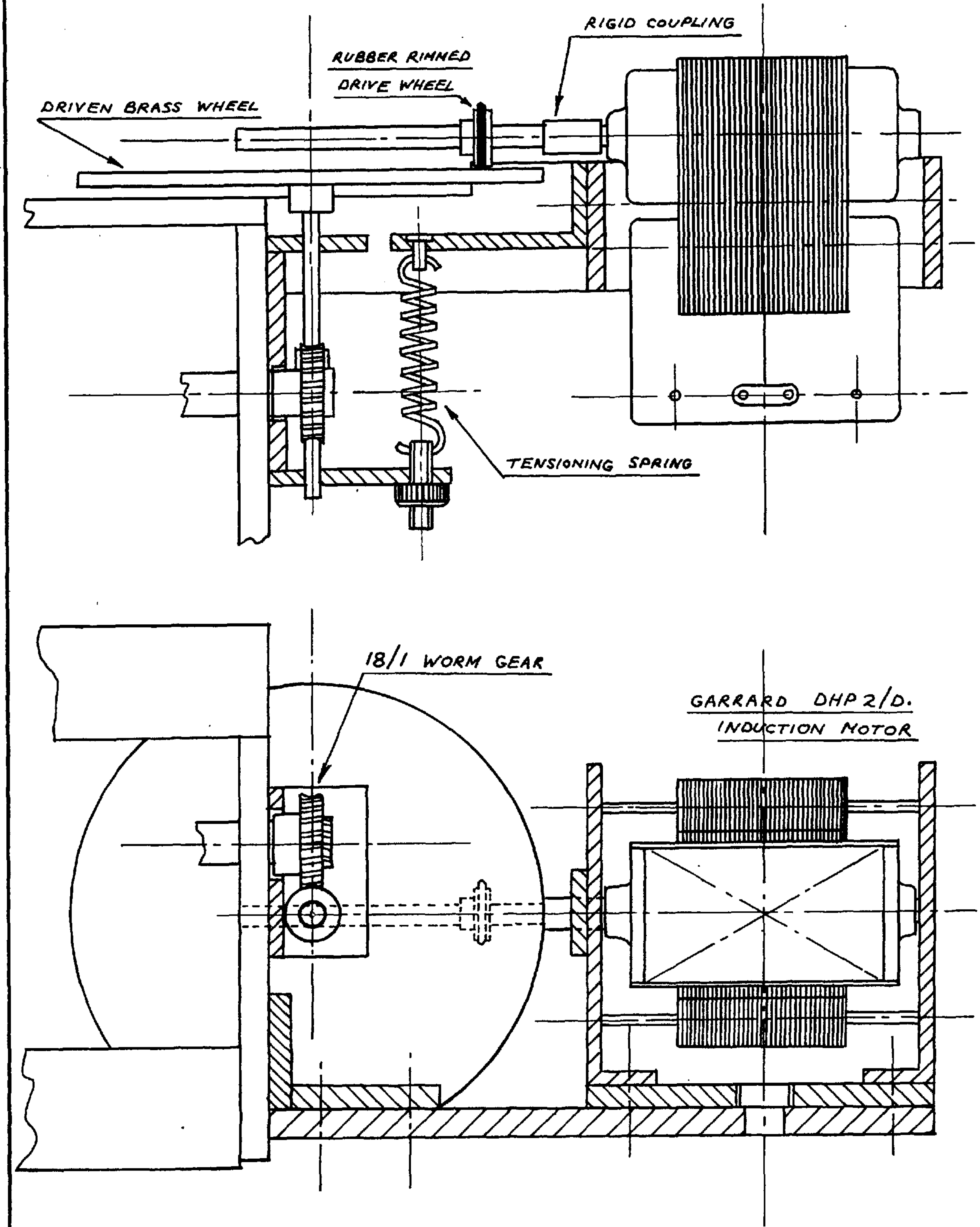

FIG. 3·5 MOTOR DRIVE FOR PICTURE TRANSFORMER

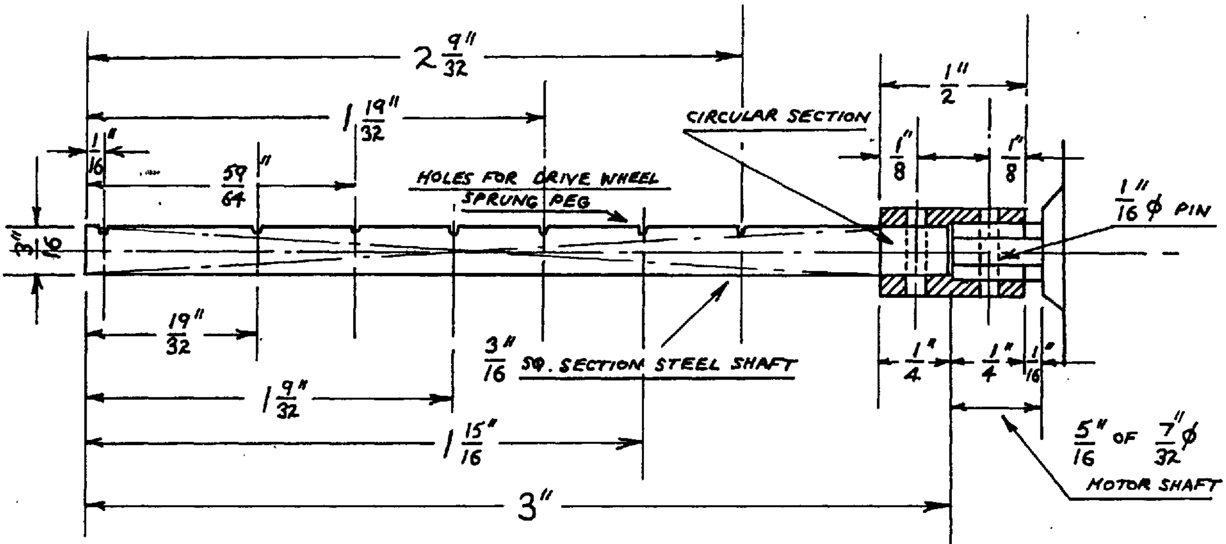

SCALE: 1½ X FULL SIZE

MOTOR EXTENSION SHAFT AND BRASS COUPLING.

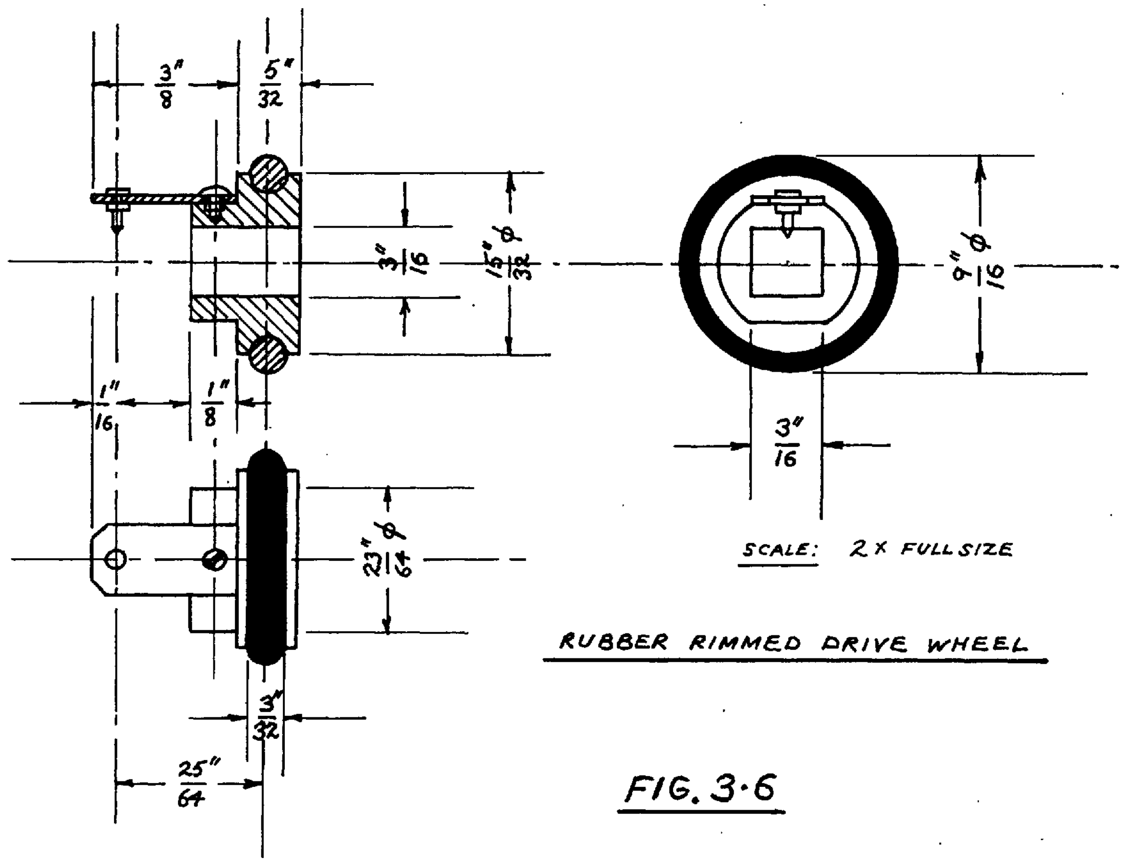

SCALE: 2X FULLSIZE

RUBBER RIMMED DRIVE WHEEL

FIG. 3·6

COMPONENTS FOR MOTOR DRIVE OF PICTURE TRANSFORMER.

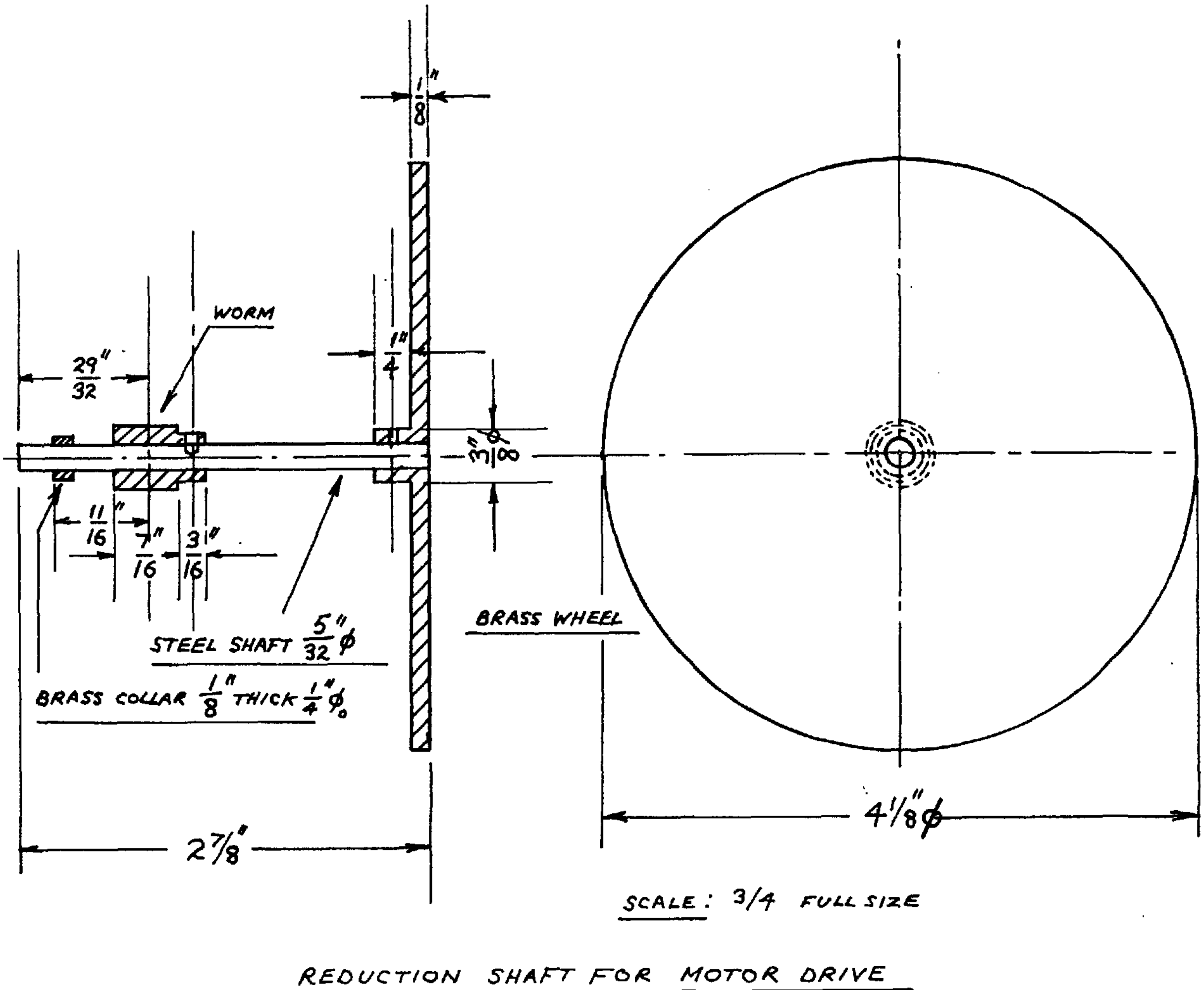

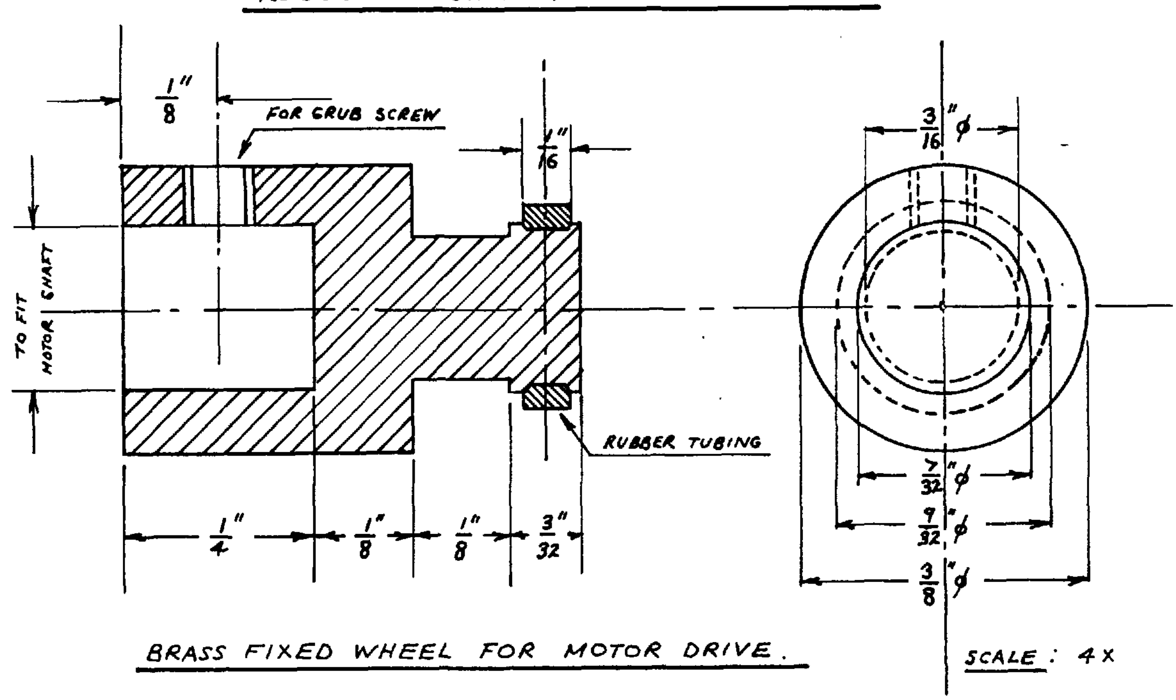

FIG. 3·7 MOTOR DRIVE COMPONENTS FOR PICTURE TRANSFORMER

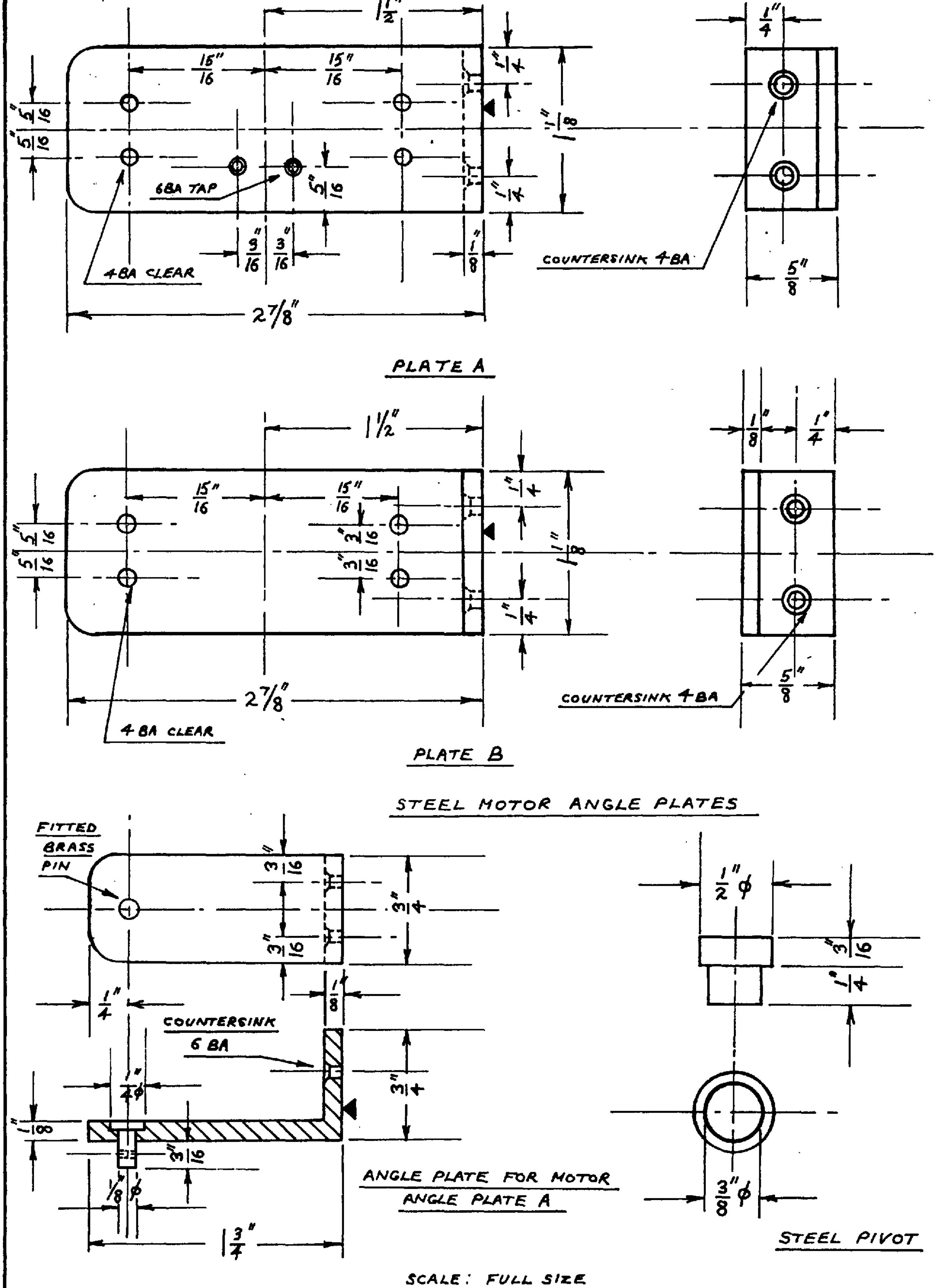

FIG 3·8 COMPONENTS FOR MOTOR DRIVE OF PICTURE TRANSFORMER

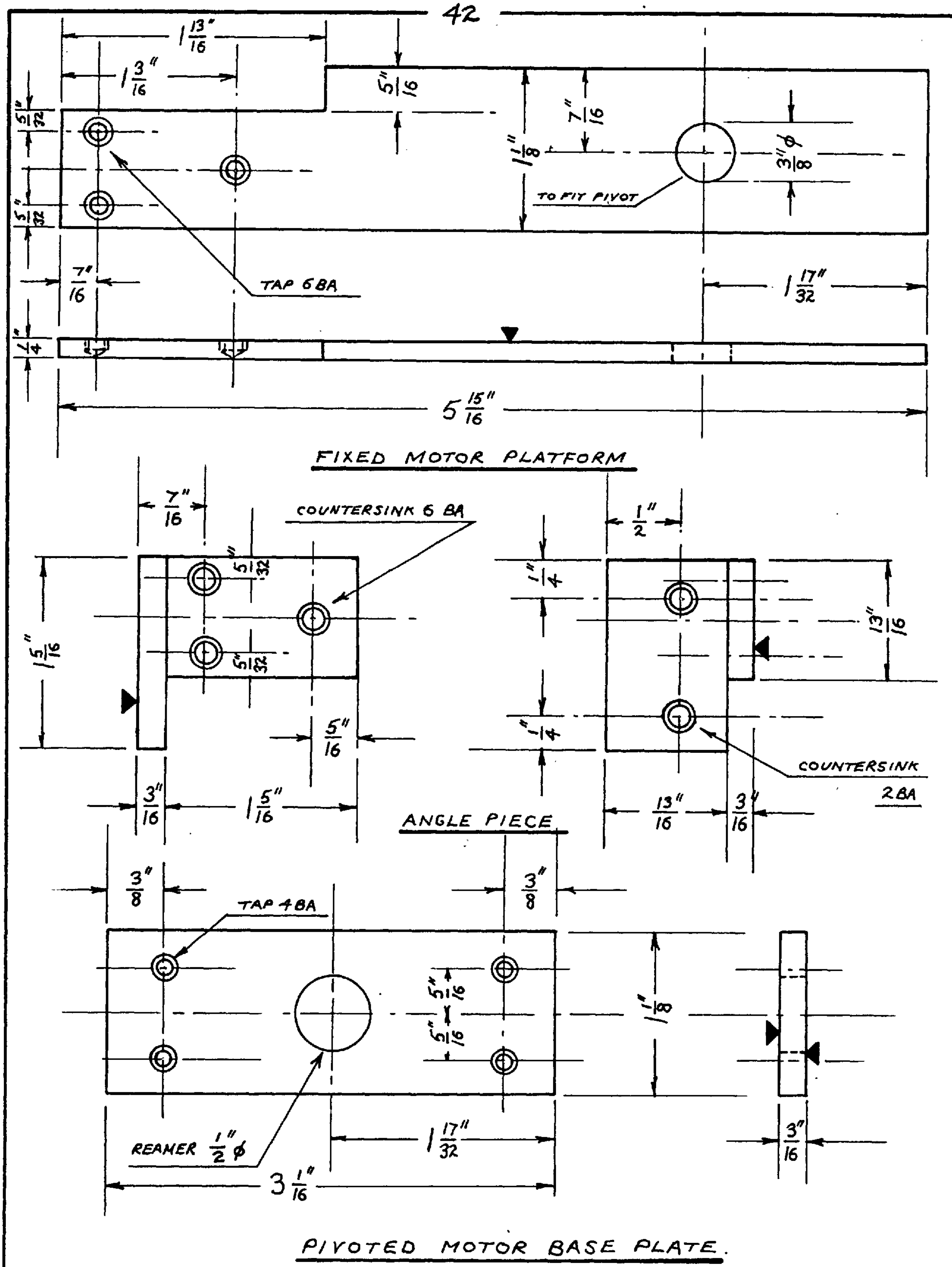

SCALE: FULL SIZE

FIG. 3·9

COMPONENTS FOR MOTOR DRIVE OF PICTURE TRANSFORMER

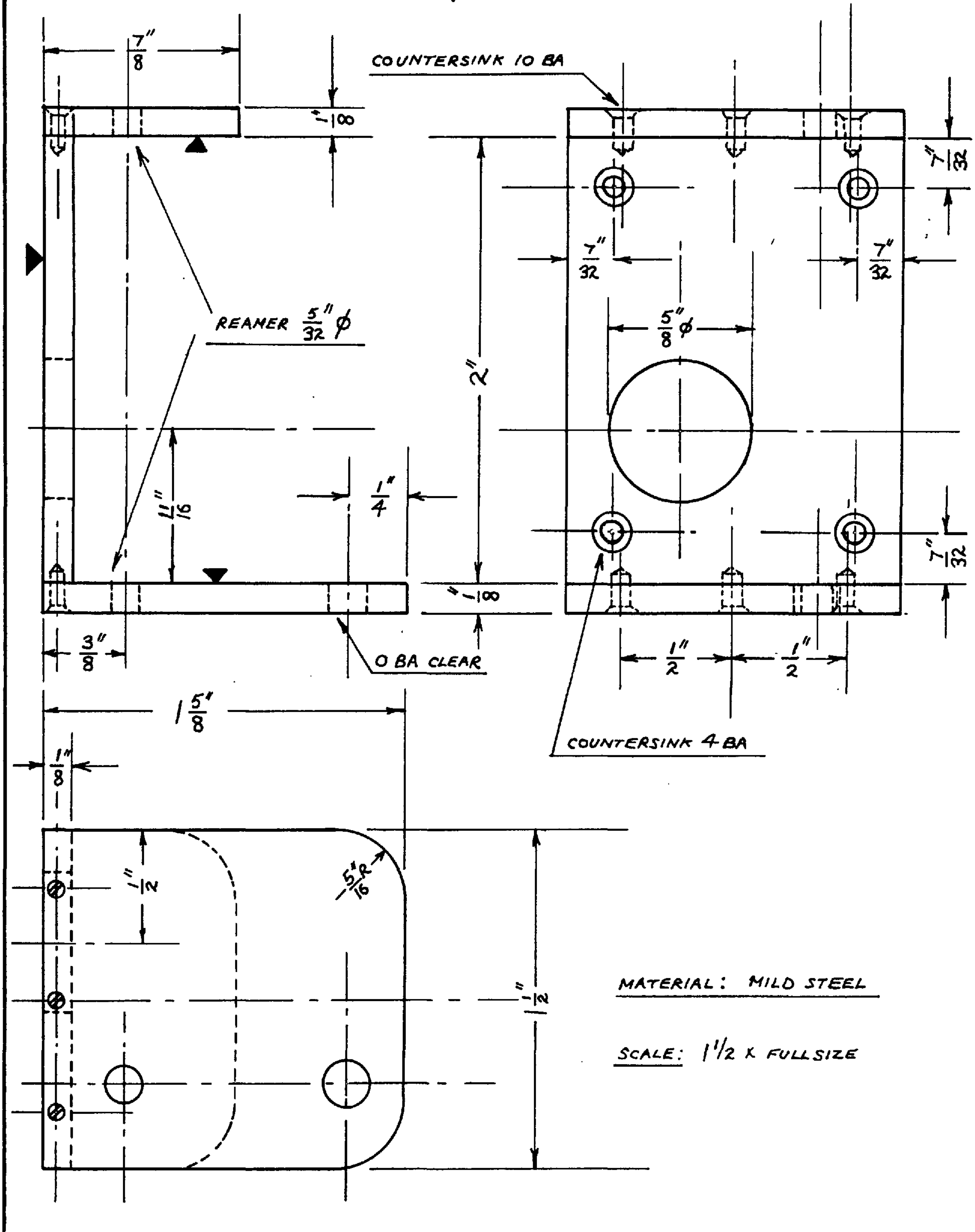

MOUNT FOR WHEEL-WORM REDUCTION SHAFT

FIG. 3·10

COMPONENTS FOR MOTOR DRIVE OF PICTURE TRANSFORMER is achieved in two stages; the first stage is a variable position wheel drive onto a brass plate; and the second stage is an 18:1 reduction worm gear, the driven wheel of which is fixed to the picture transformer tubular shaft. The complete assembly is supported on a steel platform anchored to the end plate of the apparatus.

Table 3.1 Scanning Velocities for 0.15mm Picture Element.

SPEED RANGE	PERIOD FOR 200 LINES	SCANNING VELOCITY	PICTURE ELEMENT	HORIZONTAL BANDWIDTH
EXTRA SLOW	1000 secs.	16mm/sec	10.0msec	50 C.P.S.
1	496	32	5.0	100
2	396	40	4.0	125
3	320	50	3.25	155
4	244	64	2.5	200
5	152	105	1.5	333
6	76	210	0.75	666

Six of the seven forward speeds and a 'reverse gear' are provided by a square section steel motor extension shaft carrying a rubber rimmed drive wheel (Fig. 3.6), and the 'extra slow' speed is provided by a fixed rubber rimmed brass wheel (Fig. 3.7) which fits the motor shaft directly. Both wheels are spring loaded onto the brass reduction plate with an adjustable steel tensioning spring attached at one end to the pivoted motor housing (Figs. 3.8, 3.9), and at the other to the fixed worm-reduction plate bearing mount. (Fig. 3.10)

Table 3.1 gives the measured drive speeds in terms of scanning velocities and equivalent horizontal bandwidths; the reversing time for 200 lines is just over 2 minutes.

3.2 OPTICS OF PICTURE TRANSFORMER.

The function of the optics is to provide two separate optical channels; two main beams which simultaneously scan alternate lines on the picture drum via a velocity modulator recombining through a signal distributor to write interpolated lines at the receiving drum, and two advanced control beams scanning the same lines one or two picture points ahead of the previous beams and transmitting the pick-up signals to two photocells for controlling the modulator and distributor routine previously described.

3.21 Overall Description of Optical System.

The basic optical system of the picture transformer is shown in Fig. 3.11. A point source (Pointolite lamp) illuminates an aperture plate via a collimating lens; the total magnification in the optical tract is 30 and with writing/reading spots 0.15mm diameter, the apertures are made 4.5mm diameter with centre spacings of 1-2 diameters. The optimum spacing is a matter for experiment as this depends upon the total closed loop reaction time of the modulators.

Physical separation of the main and control beams may be augmented by wavelength separation, using red light (above 5000 A.U.) for control, as photocells have good sensitivity in this region, and blue light for writing as films respond well in the blue-green region. Suitable Wratten filters are No.25 (RED) and No.38A (BLUE); the disadvantage of filtering is that it increases the attenuation in the optical tract and with perfect collimation it is not necessary; with imperfect collimation contral-main beam cross-talk leads to instability and then filtering, frequency selective or otherwise, is the solution.

After passing the aperture plate, the approximately collimated light beams fall on a beam splitter cube, with near equal reflection and transmission coefficients. The reflected beams pass through the moving mask of the signal distributor (explained later) and onto two biprisms; the first horizontally diverges each beam by two spot diameters (9mm) at the second which re-aligns each beam pair. The two control beams pass through the 'sensing' prism or double beam splitter which is inoperative in the forward direction and the two main beams pass under it.

The four beams are then reflected at a 90° prism, turning them at

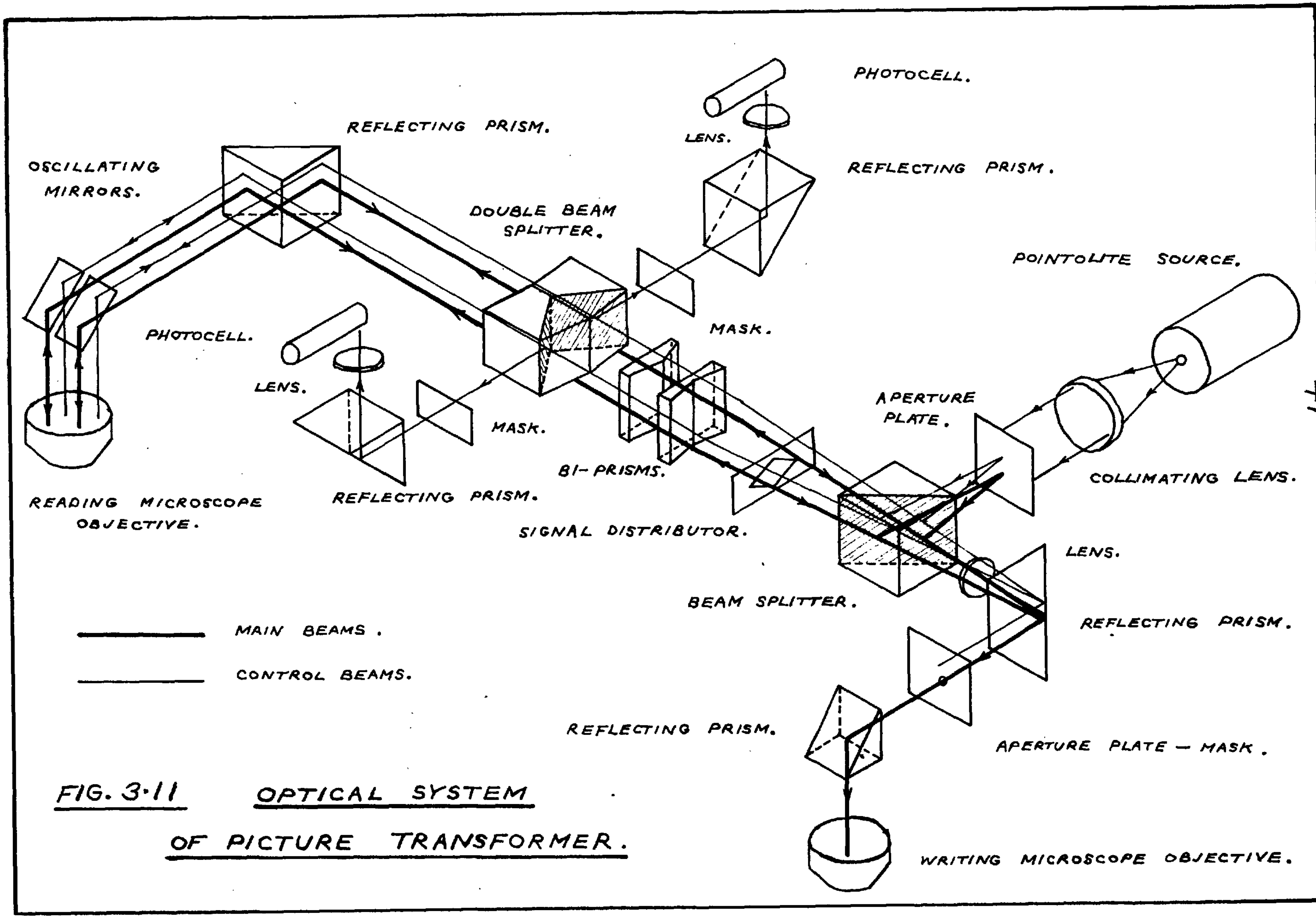

FIG. 3·11 OPTICAL SYSTEM OF PICTURE TRANSFORMER.

right angles and inverting their order, towards two small oscillating mirrors which are normally at 45° to the horizontal. These mirrors effect the velocity modulation and present the four beams to a 30X microscope objective with a focal length of ¼", and numerical aperture 0.5. The velocity modulation is described in detail later on.

After reflection at the picture drum, all beams return on the same paths on which they came; it is essential to prevent interline crosstalk by ensuring that each beam is not reflected back by the wrong mirror and this is achieved by placing black partitions between the beam pairs; the movement of the oscillating mirrors (assuming small amplitudes) is eliminated in the return path.

The return rays are turned through 90° by the reflecting prism and the control pair are semi-reflected outwards by the sensing double beam splitter towards 90° prisms; these turn the beams upwards and small short focus lenses focus each beam onto the photosensitive area of a photocell. With filtered beams, any main beam interaction is eliminated by placing a red filtering mask in the optical tract prior to the lens-photocell system.

The main beams pass back underneath the sensing prism and are recombined by the two bi-prisms and pass through the oscillating mask once again. This mask may be placed just before or just after (as in the figure) the bi-prisms, and in the final design it worked out more convenient to perform the signal weighting prior to recombination. The signal distributor mask must not operate on the control beam and is allowed to weight the lower beams only by limiting the mask height to just over one beam diameter. Normally, one half of each semicircular beam is transmitted by the mask aperture.

The weighted combination writing beam next passes back to the beam splitter cube where it is semi-transmitted through into the writing box to two reflecting prisms and a 40X microscope objective (4mm, 0.7.N.A.) for writing the spot on the film drum. The writing objective has a shorter focal length than the reading one since the apparent aperture is closer to it than to the latter; this equalises picture and film drum scanning spot diameters to approximately 0.15mm. The control beam is eliminated by a mask placed to stop it after transmission through the beam splitter; there is no advantage in blue filtering both beams at this point as they are still physically separated, and any control-to-main beam interaction is negligible as the control beam undergoes an additional double beam-splitter transmission compared with the main beam.

The above describes the ideal optical system with perfectly collimated beams. Initial scan tests with the picture transformer showed that exact collimation was impossible and the best writing results (largest signal amplitudes) were obtained by (a) allowing the collimating lens (a 2" microscope objective with numerical aperture 0.15) to focus the pointolite source at a point near the reading reflecting prism and (b) by relying upon geometrical spacing alone for the main and control channel separation. These measures successfully combatted the prohibitively large attenuations in the main and control tracts to give sensible signals at the photocells and film drum. The auxiliary effects are:

(i) The beams cross prior to the oscillating mirrors. The vertical inversion puts the main spot in advance of the control; this was corrected by placing a <u>roof prism</u> between the mirrors and reflecting prism. The horizontal inversion simply interchanges lines 1 and 2 at the picture drum.

(ii) Interchannel crosstalk at the photocells is large with the sensing prism by-passed on the forward transmission by the main beam. Filtering prior to the cells is impracticable with such low control signals involved and it was found that simple filter attenuation at the first aperture plate could eliminate modulator instability and still write a good half-tone signal.

(iii) Unwanted glass-to-air surface reflections or 'ghosts' are more troublesome with uncollimated beams since the usual precaution of tilting the surfaces a few degrees away from normality may be cancelled in the worst case. The beam splitter cube possesses a large ghost/signal ratio since the stray reflection is the high level direct semi-transmission of the aperture plate image, and the signal is the low level picture return beam. This ghost was eliminated by increasing the separation of the wanted from the unwanted signal with an auxiliary lens placed just beyond the beam splitter inside the writing section.

A bad 'ghost' from the reading reflecting prism was eliminated by increasing the distance of this prism from the double-beam splitter to reduce the main beam reflection from 90° and to increase the effective tilt.

(iv) The above described auxiliary lens is also required to re-focus the writing beam at a point between the two reflecting prisms; at this point an aperture plate eliminates the strays and passes only the wanted beam; movement of this aperture corrects for unequal signal weightings - these result from unequal mirror reflection coefficients, inequality in each half of the sensing prism and incorrect mask setting of the signal distributor.

It is possible to calculate approximately the attentuations in the optical tracts. Beam splitters at best possess an efficiency of 1/3 (Maxwells theory gives 25% transmission, 25% reflection, and 50% absorption); a large numerical aperture objective will capture only about $\frac{1}{4}$ of the reflected light with the half which transmitted the initial beam; the signal distributor reduces the total intensity by $\frac{1}{2}$ and the biprism splits the control beam into half. Ignoring reflection inefficiencies at mirrors and reflecting prisms, and assuming perfect collimation, the attenuation in the control tract from aperture plate to photocell is certainly not less than 3.2.2.3.4.3. $\doteqdot$ 450X and the attenuation in the writing tract between the aperture plate and writing aperture, is probably greater than 3.2.4.3. $\doteqdot$ 450/6 X. With an aperture separation of 2 spot diameters, the minimum attenuation is 9X at the aperture plate for each beam; hence the total source system-to-photocell control tract attenuation is at least 4000X and the main tract attenuation about the same, if we assume that filtering at the aperture plate and stopping at the writing end accounts for a factor of 6. Pointolite sources are available with Candle Powers up to 150 C.P.; photocells have sensitivities ranging from about 100uA/Lumen for the gas-filled cell, to about 3A/Lumen for the photoconductive cell; and conveniently fast films such as Kodak 'Verichrome Pan' Film (29° Scheiner) are available with 'middle characteristic' (density of 1.2 approx.) exposures of less than 0.1 Metre-candle-secs, for writing speeds between 15 and 100 mm/sec with a 0.15 mm spot. The above quoted attenuations are not prohibitively large therefore; the choice of light source and film speed are discussed below.

3.22 Component Design.

(a) Point Source and Collimator. The light flux from a lens-point source combination is directly proportional to source brightness and the square of the lens numerical aperture. A short focus micro-scope objective (2", 0.15 N.A.) was selected for the collimator and a 30 C.P. Pointolite Lamp, 100% overrun (about 120 C.P.), for the point source, the small glass bulb enabling the shortfocus lens to be used. (a 150 C.P. Pointolite was rejected because the incremental brightness gain of 150/120 is offset by the much smaller numerical aperture lens necessitated by the very large bulb.) The 30 C.P. bulb operates normally on 200 Volt D.C. with an arc current of 0.45A between a tungsten bead (anode) and Ioniser, and the arc is initiated with an Ioniser current of 4.5A for 3 seconds. A 400 volt D.C. supply with a potentiometer control ranging from 200v upwards was used for overrunning the lamp (ionising at 200v and arcing with 200-400 volts dependent upon required writing flux). The bulb was operated horizontally. The brass lamp housing and lens tube are shown in sectional form by Fig. 3.12. A small focus adjustment is given by sliding the lamp housing back tube, which is welded into the main one, over the tubular lens mount. The design ensures that the pointolite tungsten bead lies on the optic axis of the picture transformer. A light chimney (Fig.3.13) has been included to provide adequate draught around the overrun bulb.

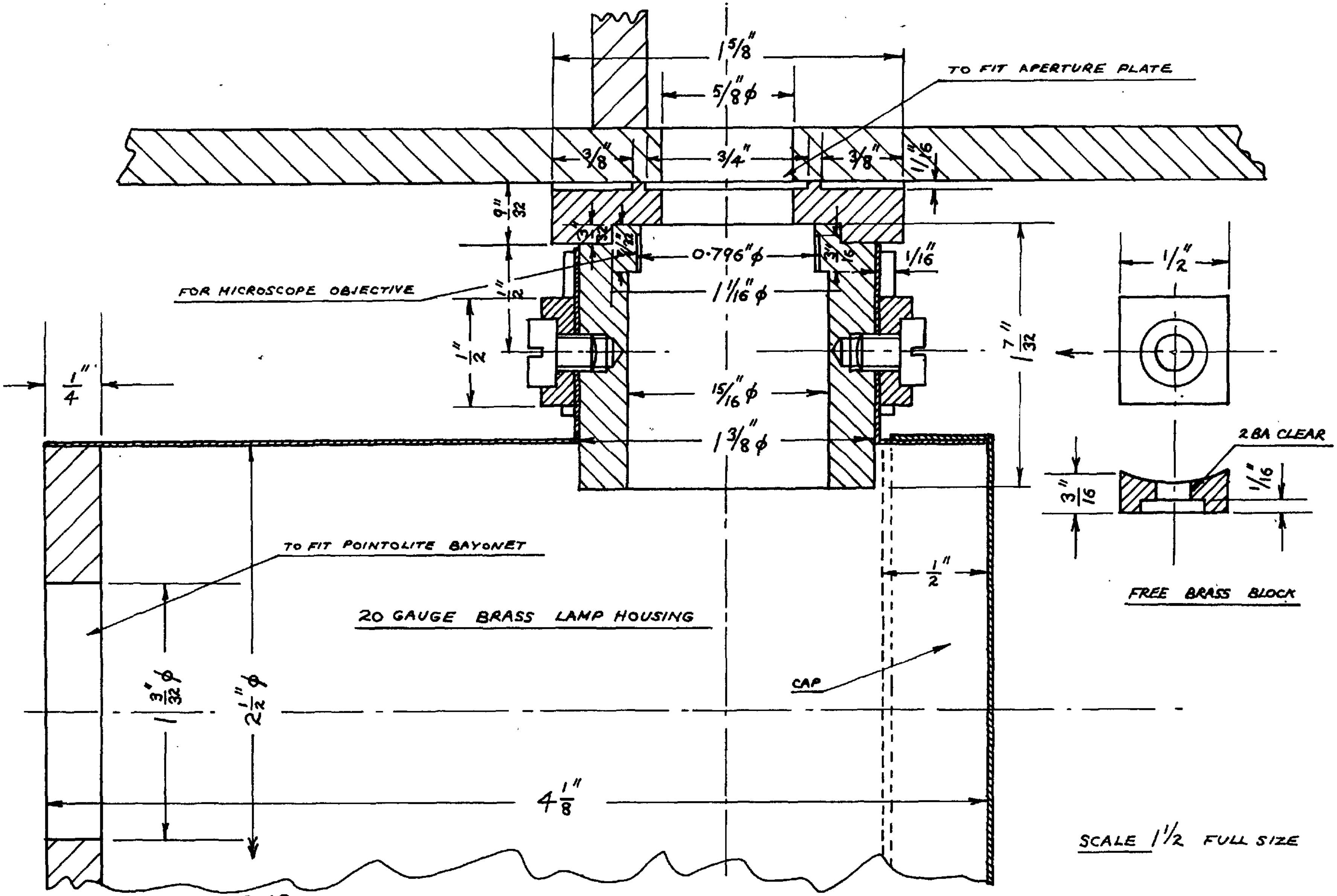

FIG. 3·12 LAMP HOUSING AND LENS TUBE

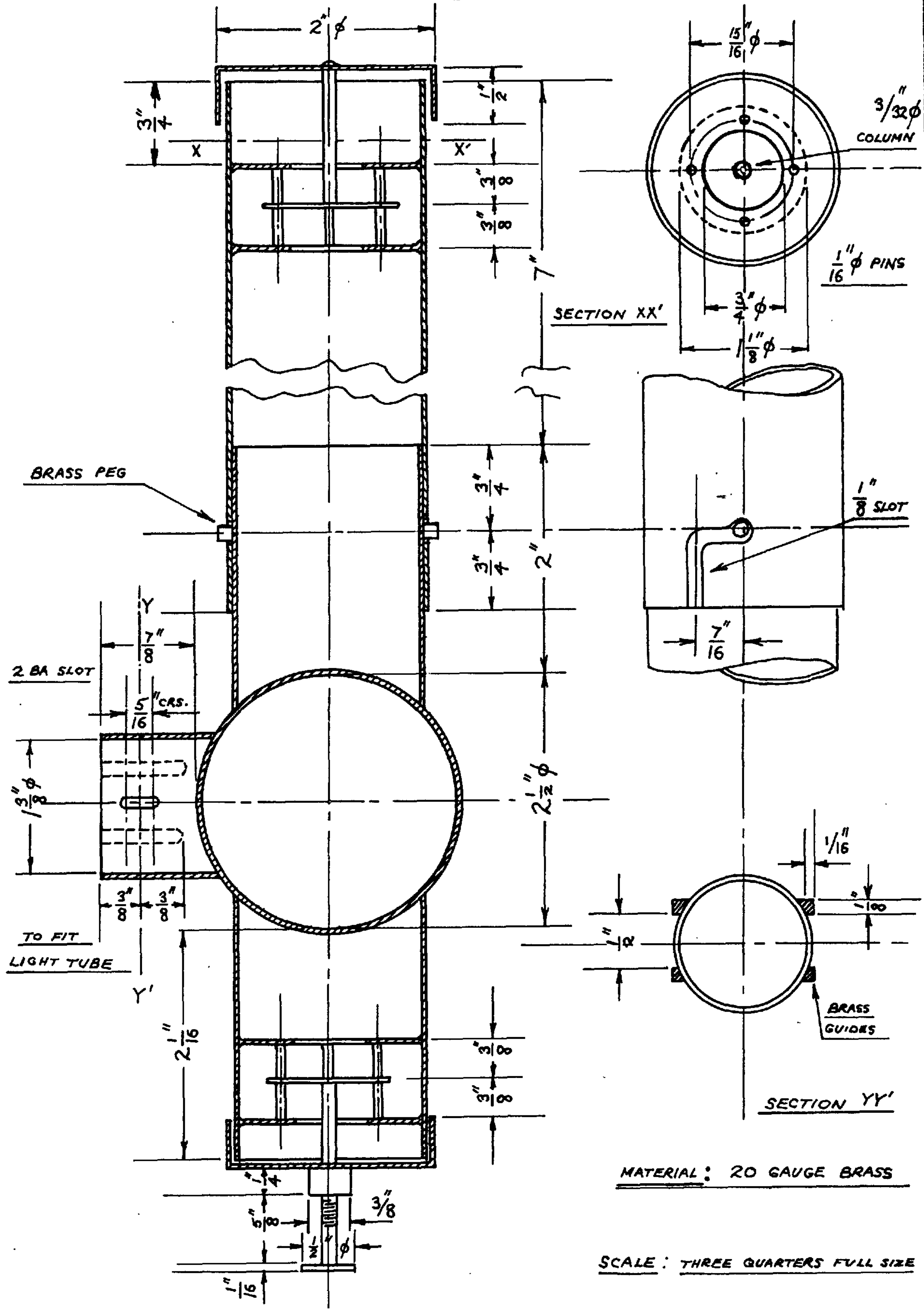

FIG. 3·13 LIGHT CHIMNEY FOR PICTURE TRANSFORMER.

The lamp life with the above operation was limited to a few hours; as a result of this, and because the manufacturers (A.E.I. Lamp and Lighting Co. Ltd.) ceased production of 30 C.P. bulbs, some modified lamps were constructed; 150 C.P. Foitolite assemblies, with new filaments wound by hand from 0.008" diameter tungsten wire, were inserted into small pyrex bulbs, with a nitrogen gas pressure of 6" mercury. (The manufacturers quote 3" with the <u>large</u> bulb). The advantages are (i) the lamp is run <u>normally</u> on 230 volt A.C. and (ii) the assembly is inherently more sturdy in operation with double tungsten bead arcing, and with the filament used only for ionising. Small porous tungsten chips were included inside the bulb for abrasively cleaning the glass interior surface; despite conventional de-gassing of the assemblies in the bulb evacuation process, light attenuating deposits form on the glass inner surface. In operation, the twin beads are placed in line along the optic axis such that the foremost one only contributes to the driving flux.

The flux output from the above system is evaluated as follows: assuming a <u>point</u> source of intensity I candle-power to be at a distance ℓ from a perfect lens of entrance radius r, the collected flux ϕ is given by $\phi = \frac{4\pi I r^2}{\ell^2}$ -------------------- (3.1)

With I = 150, r = 0.5 cm (for the 2" objective) and ℓ = 4cm, Equation (3.1) gives ϕ = 30 lumens. A more exact formula is derived in

Appendix 7.3 for a finite size spherical source. Equation (17) gives

$$E = \frac{I}{8L^2} \cdot \frac{3D-2(Rs+R)}{D-2(Rs+R)} \text{ lumens/cm}^2 \text{ ------------ } (3.2)$$

with I the source candle-power, D the source to lens distance, L the source to entrance pupil distance, Rs and R apparent lens and source radii respectively. With 0.15 N.A. lens, and D = 4 cms. R = 1.5 mm (hot bead of 150 C.P. assembly), we have L = 1cm, and Rs = 0.45 cms. Substituting in (3.2) gives E = 63 lumen cm^{-2} or $\phi = E\pi R_s^2 = 40$ lumens. The efficiency of the above system, assuming unity transmission through the lens, is given by $\phi/4\pi I \doteq 2\%$.

The aperture plate is a 1/32" brass plate with 2 circular holes 4.5 mm diameter spaced vertically by 4.5 - 9 mm, depending upon the requirement.

(b) Beam Splitters. (Ref. to Fig. 3.14) The beam splitter cube consits of two $48^\circ - 84^\circ - 48^\circ$ reflecting Crown glass prisms (Prism A) with the largest faces 'C' cemented together with Canada Balsam with a semireflecting film interface. The double beam splitting sensing prism (Prism B) is a four component crown glass combination cemented with Canada Balsam; Interfaces k_1, k_2 and j_1, j_2 contain the semi-reflecting film and the interface between k_2 and j_2 is blackened to prevent interchannel interference in the forward path. All transmission air-glass surfaces possess a 3° tilt to reduce 'ghosting'.

The semi-reflecting films of both beam splitters are gold and have been evaporated onto the prism faces using conventional laboratory evaporation technique[(3) (4)]. The evaporating currents and durations to produce the desired films were determined experimentally by evaporating gold onto glass slide specimens 15 mm square, and visually comparing the results with two calibrated filters of transmissions 50% and 75%. A film with 75% transmission prior to contacting with a further glass surface gives a final result of near equality in transmission and reflection. This was checked visually in a very elementary way: the cemented slides (and final prisms) were placed vertically on black velvet with a white paper strip placed underneath one edge and obliquely to the glass; the transmitted and reflected rays were monitored together by observing them back through the glass. Prior to evaporation the prisms were cleaned with detergent, caustic soda, dilute Nitric Acid and a Tessler coil discharge. An even film was ensured by centering the pertinent prism face above the evaporator boat and maintaining a small 'capture' solid angle. In particular, both halves of the sensing prism were spluttered simultaneously.

Both beam splitters are mounted upon optically flat paxolin bases; the sensing prism base is tunnelled to allow the main beam to underpass it.

<u>(c) The Bi-prisms.</u> (Ref. to Fig. 3.14) Each bi-prism is made up of two $28^\circ \pm 10'$ Crown glass prism components (Prism D). The

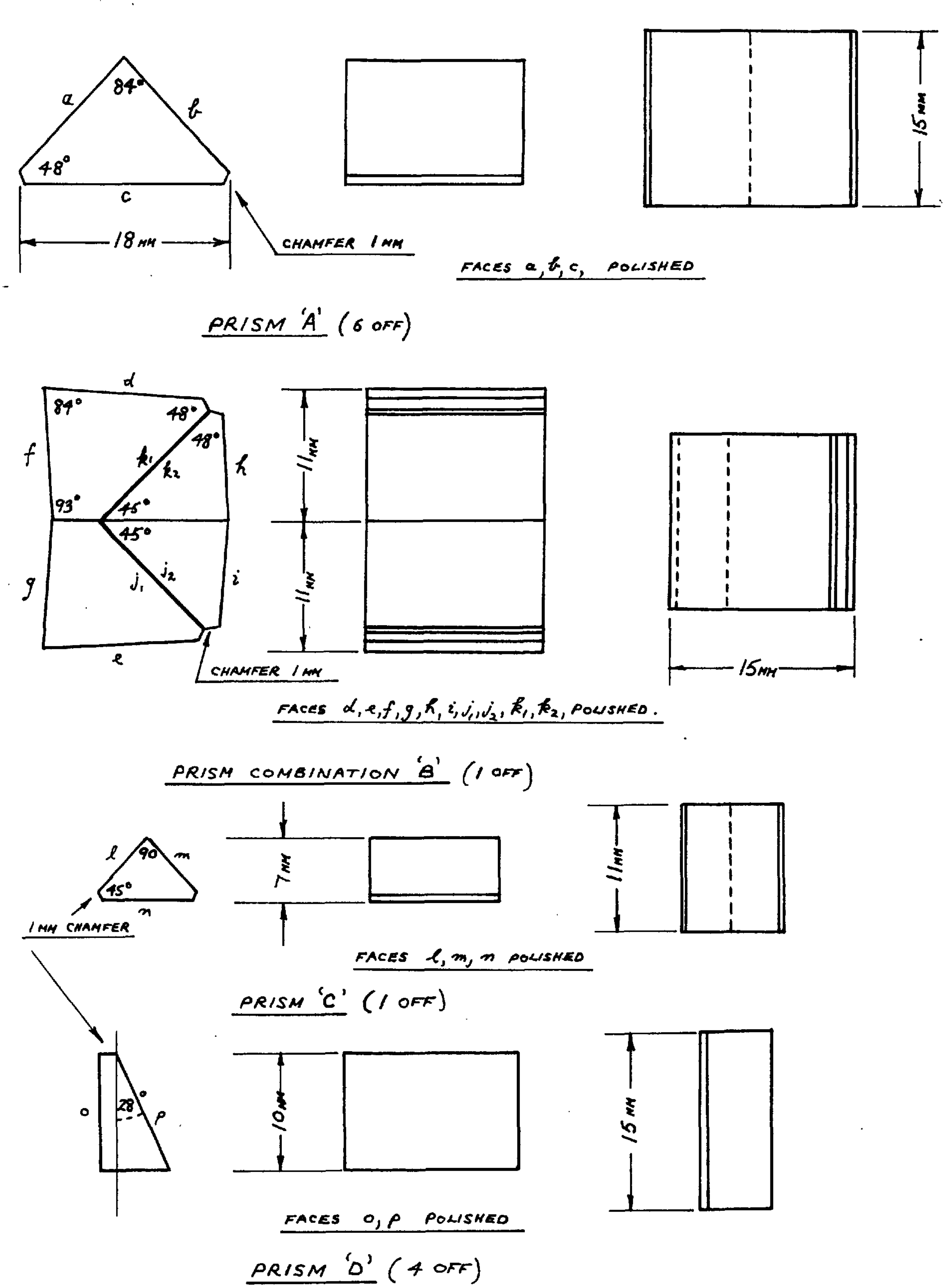

FIG.3·14 CROWN GLASS PRISMS FOR PICTURE TRANSFORMER deflection given by a small angle prism x° is approximately $x(\mu-1) \doteqdot x/2$ for μ(glass) = 1.5. The first biprism splits the 4.5 mm diameter beams into two pairs of semicircular beams of half width, diverging by 28°. The required total separation of 9 mm is reached at a distance (4.5 - 1.125)/ Sin 14° mm beyond the biprism i.e. 15 mm. At this point is placed the second biprism which re-collimates the beams by deflecting them back by 14° before the control pair enter, and the main pair underpass, the sensing prism. (Fig. 3.15). Both prisms have been mounted on flat paxolin bases.

(d) The 5 Reflecting Prisms (Ref. to Fig. 3.14) Four of these are 48° - 84° - 48° Crown glass prisms (Prism A) tilted 3° to reduce 'ghosting'. The prism prior to the writing objective (Prism C) handles the single interpolated spot and is made 45° - 90° - 45°. The two prisms for deflecting the control beams vertically towards the photocells have been mounted on identically dimensioned brass prisms with ground bases; the 45° brass faces are channelled 1 mm deep to provide adequate glass-air surfaces. Small shortfocus ($\frac{3}{4}$") lenses for photocell focus are held just above the prism top faces by paxolin side plates affixed to the brass bases. The two horizontally deflecting prisms are mounted on flat paxolin bases and the small writing prism is placed on top of the microscope objective lens mount.

(e) Oscillating Mirrors. Each mirror has been cut from a 1 mm

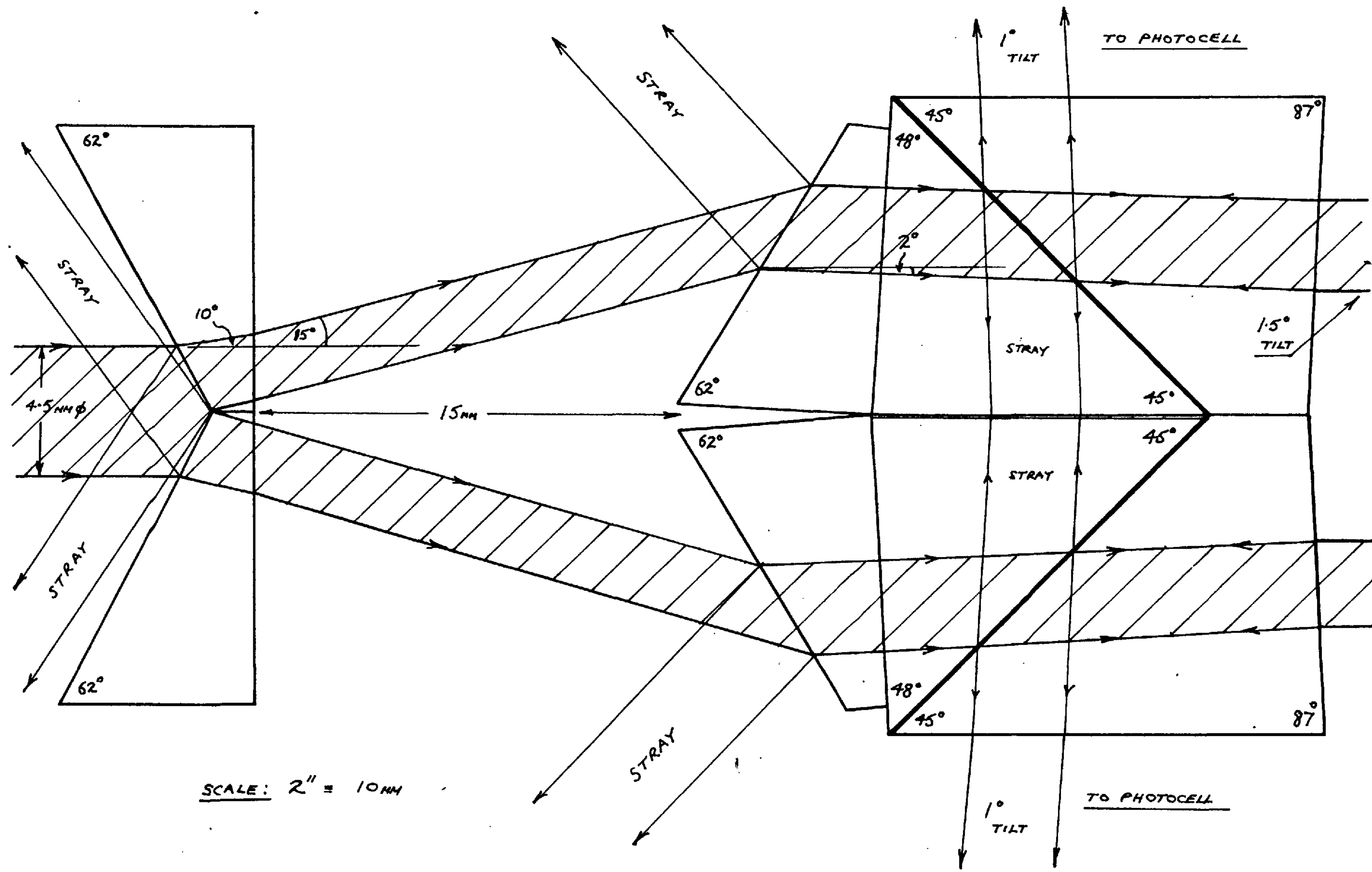

FIG. 3·15 BI-PRISM AND SENSING PRISM RAY DIAGRAM FOR THE CONTROL BEAMS.

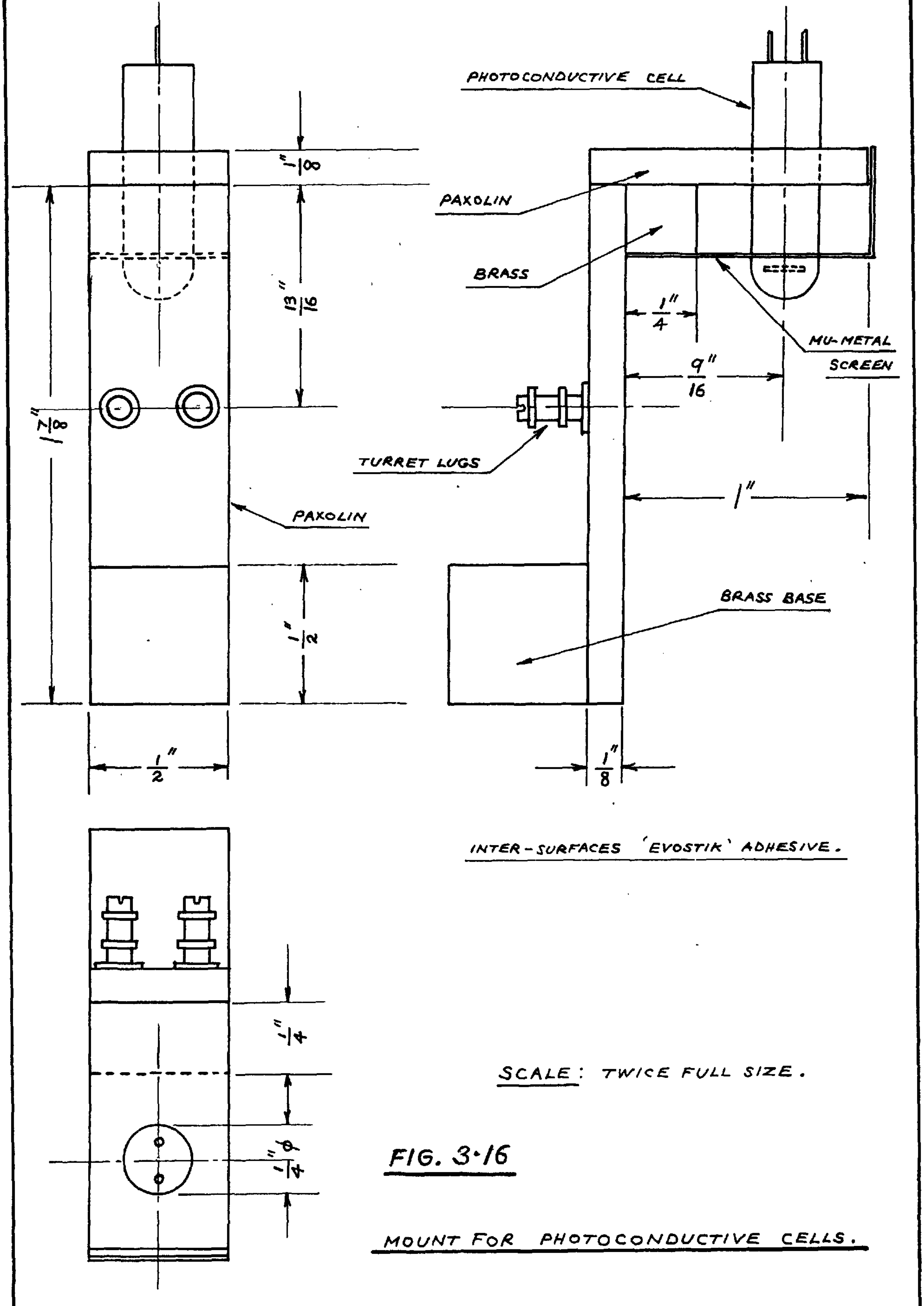

FIG. 3·16

MOUNT FOR PHOTOCONDUCTIVE CELLS.

thick glass microscope slide and is rectangular, $\frac{1}{4}$" across and 9/16" long. The reflecting surfaces were prepared by evaporating aluminium directly onto the glass under vacuum; these surfaces have been left untreated.

(f) The Photocells. With 40 Lumen driving flux and a control tract attenuation of at least 4000 times gives a peak signal of 0.01 lumen at the cells. Including reflection losses the peak-to-peak signal at each cell is unlikely to exceed 0.001 L. The following photocells were considered:

(i) Gas-filled photovoltaic cell 55 CG: Sensitivity of about 100 uA/L at 0.005L with a 1 M load resistance; large area cathode. High impedance, low level output. Bandwidth limited to around 1 kc/sec.

(ii) Phototransistor OCP71: Sensitivity about 0.3A/L; low impedance output; 1 mm square sensitive area; thermally sensitive.

(iii) Photoconductive Cadmium Sulphide Cell: Sensitivity about 1A/L; 1.5 mm square sensitive area; bandwidth limited to about 1 Kc/sec.

The photoconductive cell was selected on grounds of high level output, thermal stability, and compatible element size. Each cell is mounted on a cubical brass base assembly (Fig. 3.16) and is optically aligned by sliding on the picture transformer ground steel 'prism platform'.

(g) Moving Arm for Interlace. The mechanical design of the arm is given in Fig. 3.4. If the reflecting prism is positioned at radius Rp from the bar fulcrum, the adjusting arm at radius R_A, and the objective at radius Ro, then n revolutions of the adjusting screw of pitch P moves the objective a distance $nPRo/R_A$ relative to the drum. In addition, the optical beam is deflected by angle $2nP/R_A$ and for a spot focussed at the writing drum from infinity, the deflection relative to the drum is $-2nPf/R_A$, with f the focal length of the writing objective. Resultant deflection is given by $\delta = nPR_o/R_A - 2nPf/R_A$

For perfect interlace, $\delta = P/2$, (since P has been made equal to the scanning line pitch) and this gives $n = \dfrac{R_A}{2Ro-4f} \doteqdot \dfrac{R_A}{2R_o}$ - - - -(3.3)

since for the X40 objective, $2f < Ro$. With R_A = 5.5 cm, and Ro = 7.5 cm, Equation (3.3) gives n = 0.37 turn, i.e. 135°. Theoretically therefore, a 135° turn of the adjusting screw on the swinging 'writing' arm should move the writing spot exactly between lines for perfect interlace.

3.23 Testing the Optical Circuit.

Prior to incorporating the above described optical system with the picture transformer, the optical attenuation of each component was experimentally determined by the method of substitution. The procedure was as follows: Light from a 30 candle power pointolite was collimated by a 2", 0.15 N.A. microscope objective and led past a motor driven vane interrupter which square-wave modulated the beam at 50 c.p.s. The modulated beam was passed through a red or blue filtered 4.5 mm diameter aperture, depending upon the measurement to be performed, and finally passed to the optical circuit with prisms arranged such that the output beam terminated at a gas-filled photocell (Mullard 55 CG); the cell output measurement was performed by amplifying the ac-voltage signal with a high gain (40dB) single audio pre-amplifier (EF86) and coupling the amplifier output to the A_1 amplifier of a Cossor oscilloscope 1035.

The fundamental optical circuit was a single reflecting prism (48° - 84° - 48°) turning the beam through a right-angle. The reflection efficiency of this prism was determined by augmenting the circuit with two identical prisms and observing the relative decrease in photocell signal; a linear photocell response was assumed with the small intensities involved. The remaining components were determined by augmenting, for transmission measurements, and replacing, for reflection measurements, the single reflecting prism with the pertinent components. Care was taken to ensure that the ultimate signal beam always fell upon the same area of the cell photocathode. With chromatically selective beam splitters and a photocell response peaking in the red to infra-red region, the measurements performed only yield approximate attenuations for components operating in the final optical system in which the beam splitters handle filtered transmitted/reflected outputs from each other.

Table 3.2 below summarises the results obtained, and enables the attenuations in the control and main writing tracts to be computed:

COMPONENT	CIRCUIT 1	CIRCUIT 2	REFLECTING RED (25)	TRANSMITTING RED (25)	REFLECTING BLUE (38A)	TRANSMITTING BLUE (38A)
Reflecting Prism	1 reflecting Prism	3 reflecting Prism	0.92	-	0.92	-
Beam Splitt. Cube	1 Refl. Prism	Beam Splitt, /plus Refl. prism(trans)	0.45	0.23	0.40	0.18
Sensing Prism(both halves	1 Refl. Prism	Beam Splitt /plus Refl. prism(trans)	0.43	0.18	0.48	0.18
Bi-Prism	1 Refl. Prism	Bi-Prism plus Refl. Prism	- -	0.45	-	0.45
Oscillating Mirrors	1 Refl. Prism	Single Mirror	0.90	-	0.90	-
X30 Objective and White card	3 Refl. Prisms	3 Refl. Prisms sensing Prism Objective/card	0.12	-	0.12	-
Blue Filter Wratten 38A	1 Refl. Prism	Refl. Prism plus Filter	-	0.40	-	0.90
Red Filter Wratten 25	1 Refl. Prism	Refl. Prism plus Filter	-	0.92	-	0.50

ATTENUATION IN THE CONTROL TRACT

	Transmission
Aperture Plate, 4.5 mm Ø aperture	0.11
Beam Splitter Cube Reflecting	0.45
Bi-Prisms (0.9 x 0.45)	0.41
Signal Distributor Mask	1.00
Sensing Prism Transmitting Red	0.23
Reflecting Prism	0.92
Oscillating Mirrors	0.90
Picture and Objective (peak white)	0.12
Oscillating Mirrors	0.90
Reflecting Prism	0.92
Sensing Prism Reflecting Red	0.43
Reflecting Prism	0.92
Supplementary Lens (theoretical)	0.9
Transmission through photocell glass (theoretical)	0.9
TOTAL TRANSMISSION	1.2×10^{-4}

ATTENUATION IN MAIN WRITING TRACT

	Transmission
Aperture Plate, 4.5 mm ∅ aperture	0.11
Beam Splitting Cube Reflecting	0.45
Bi-Prisms (0.9 x 0.45)	0.41
Signal Distributor Mask	0.50
Sensing Prism (omitted)	1.00
Reflecting Prism	0.92
Oscillating Mirrors	0.90
Picture and Objective(peak white)	0.12
Oscillating Mirrors	0.90
Reflecting Prism	0.92
Sensing Prism (omitted)	1.00
Signal Distributor (transmits fully ½ initially passed)	1.00
Bi.Prisms (recombine and attenuate 0.9 x 0.9)	1.62
Beam Splitter Cube Transmitting Red	0.23
Auxiliary Lens (theoretical)	0.90
Masking Plate (1 mm ∅).	0.05
Reflecting Prism	0.92
Reflecting prism	0.92
Objective	0.9

TOTAL TRANSMISSION 1.1×10^{-5}

Hence with 40 lumens initial flux, each photocell receives a peak signal flux of 0.005 lumens; also the writing flux at the film drum is 4.4×10^{-4} lumens, approximately one tenth of the control flux, for a peak white picture. This writing flux is concentrated in a 0.15 mm spot or, allowing for spreading on the film and assuming that the spot just fills half the line spacing (80 per inch), is concentrated in a 1/80" ∅ spot (factor of ½ for spreading); this gives an illumination of approximately 5000 lumen metre^{-2}. Running the picture transformer at 50 c.p.s. horizontal bandwidth (spot period 10 millisecs) gives a peak exposure on the film of 50 lumen metre^{-2} seconds i.e. 50 Metre-Candle-Seconds, which is certainly past the middle point of the density-exposure characteristic of medium fast panchromatic film (Kodak Ltd., quote an exposure of 0.2 Metre-candle- seconds for a density of 1.2 with Verichrome Pan Film, 29° Scheiner).

Alignment of the optical circuit is described in Sec. 5.21 of Chapter 6.

3.3 THE VELOCITY MODULATOR

The function of this organ is to carry out the velocity modulation routine previously described, each time the pilot spots encounter a sufficiently pronounced amplitude gradient, with a minimum of response time. The mean velocity of the spots is the peripheral speed of the picture drum, and only the velocity difference must be applied to the mirrors <u>synchronised</u> to the drum speed.

Possibilities for this modulation include :

(1) Driving the mirrors mechanically and controlling the drive with electromechanical transducers; this has the advantage of direct synchronisation to the picture drum scanning speed, and is the method which has been adopted.

(2) Attaching the mirrors to two moving coil meter-type systems and driving the coils with ramp functions of current of slopes depending upon picture scanning velocity.

(3) Direct mirror deflection with an electromechanical transducer; piezoelectric bimorph elements and magnetic deflectors are possibilities; a magnetic system would be difficult to control linearly.

If a mirror behind a lens with a focal length f tilts by an angle x, the reflected ray rotates by 2x and the focussed spot by a distance 2fx assuming the spot to be in the focal plane of the lens. Hence half the required modulation is achieved if the axis of rotation of the mirrors is at 2f from the drum and it connects with a lever 2f long with the drum surface. i.e. the spot instantaneously starts to follow the rotating picture and spot motion is arrested relative to it.

It is impossible to present the mirror axis $\frac{1}{2}$" from the drum with a $\frac{1}{4}$" reading objective from dimensional considerations and also because the picture/drum must not be damaged. However, a lever of length r engaging with a drum of radius R gives the same result, providing they satisfy the relation:

$$r = 2fR/Ro$$

where Ro is the radius of the picture drum. For the contour chasing routine, the same tilt must be applied to the second mirror but with opposite sign; in a similar way, this may be performed by connecting the second mirror with a flange rotating with the picture drum. Unfortunately when applied to the picture transformer design, the second flange radius works out embarrassingly large. Both engaging drum and flange may be made conveniently small if the mirrors work through an angular reduction mechanism.

The realisation of the velocity modulator is based upon the above considerations. The modulator functions optically, is driven mechanically and the control is electronic and performed by magnetic actuators.

3.31 General Design and Operation

The final device is illustrated in Plate 2 and Fig. 3.17 shows a sketch approximately to scale and full size. The two mirrors are carried on independent shafts and are fixed on a balance arm which may be horizontally deflected, such that when one engages with the inner rotating surface, the other engages with the outer flange on the opposite

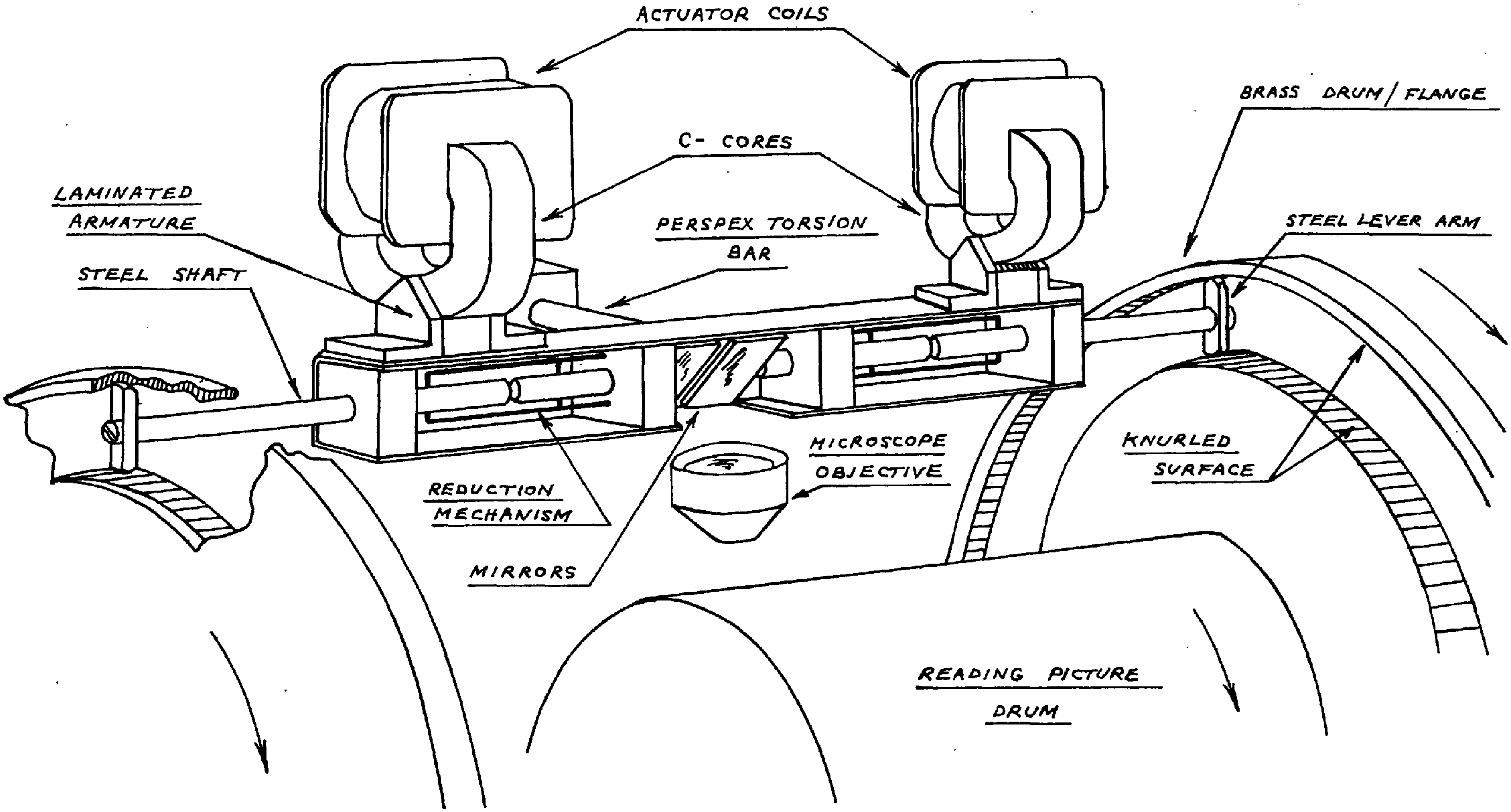

FIG. 3·17 THE VELOCITY MODULATOR.

side. The balance arm is about 160 mm long and the motion required for engaging it is between 0.1 to 0.2 mm; the response time aimed at is 1 millisecond.

The lever arms are about 5 mm long and they engage with the drum, radius 29 mm, or with the flange, radius 39 mm, respectively. The tilt angles become exactly equal and opposite if we make the inner arm radius 4.3 mm and the outer one 5.7 mm long since,

$$\frac{R}{r} \cdot \frac{2f}{Ro} = \frac{39.12}{5.7.13} = \frac{29.12}{4.3.13} = 6.2$$

where f = 6 mm and Ro is taken to be 13 mm ($\frac{1}{2}$" radius plus picture paper thickness). The angular motion is too large by a factor of 6.2 and a reduction mechanism is incorporated. This is effected by dividing each mirror shaft and coupling the two components by two horizontally end-fixed spring steel wires pinned to them; each wire is cantilever deflected by the driven steel shaft and the reduced deflection some distance down the wire is transmitted to the second shaft carrying the mirror. A long straight wire deflected in the cantilever mode exhibits a cubic deflection profile, providing a deflection distance proportional to the cube of the distance from the fixed end. Rigid coupling pins are therefore inserted into the inner and outer sections of the divided silver steel shaft at a distance ratio of $1:6.2^{1/3}$ or about 1:1.8 from the clamped ends. For small angular deflections where $\sin\theta / \theta \rightarrow 1$ this gives angular reductions

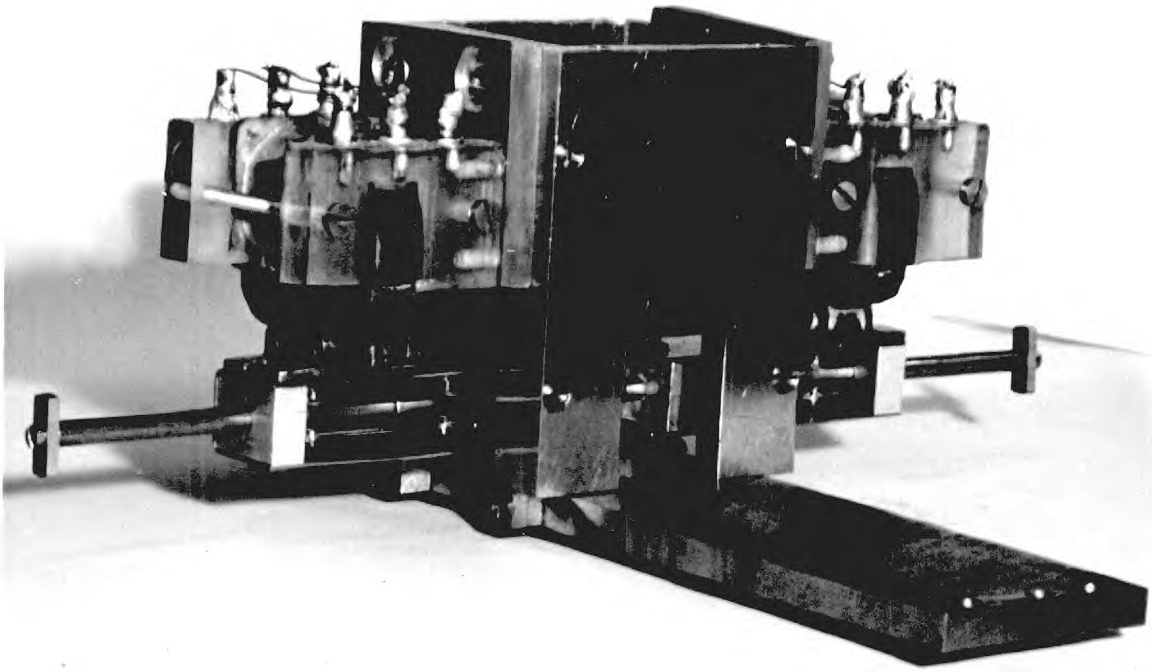

PLATE 2: THE VELOCITY MODULATOR

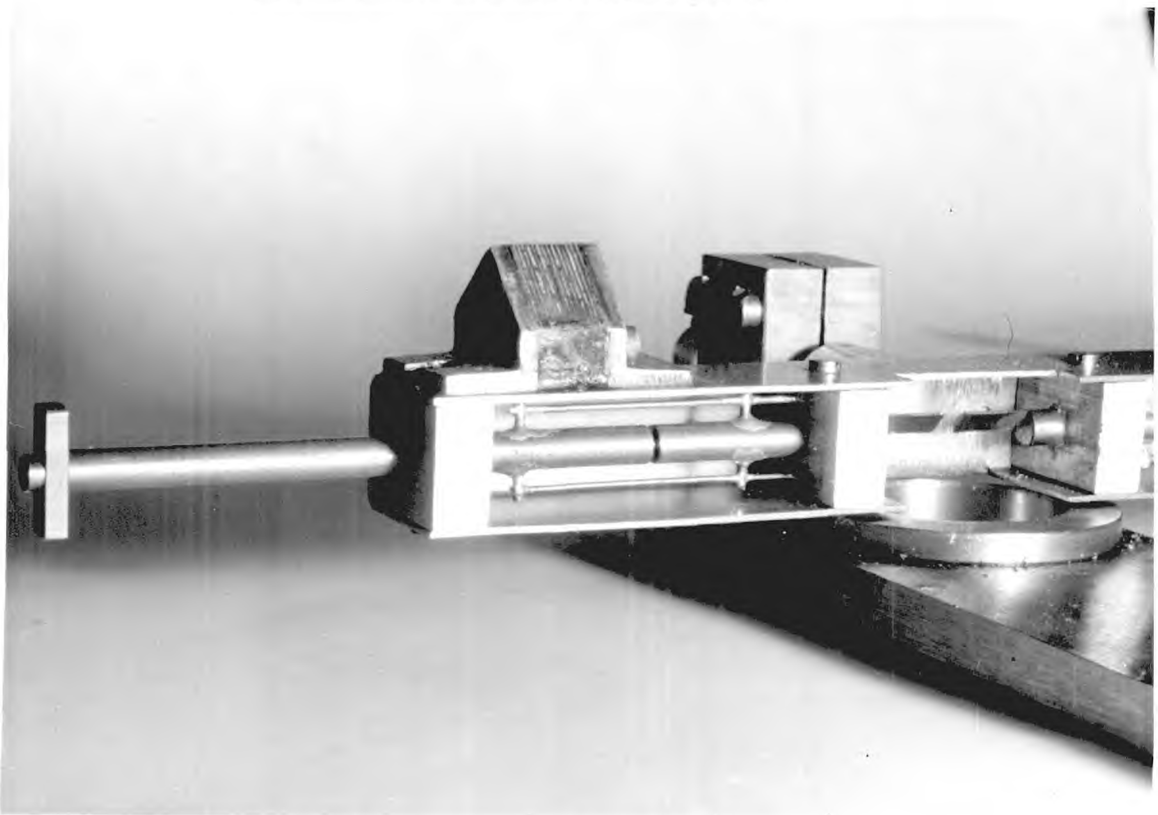

PLATE 3: THE REDUCTION MECHANISM

of 6.2 : 1 as required. The actual design is rather more complicated since the spring steel wire exhibits a torsional deflection mode in addition to the above; this is elaborated in a later section. The reduction gear also provides the restoring force from the cantilever and torsional stiffness of the coupling wires; the restoration must be performed within the minimum picture element period and should be aperiodic. Damping is provided by the frictional aluminium bearings carrying the shaft sections.

The advantage of the reduction mechanism is that it provides a convenient method for stopping the mirrors beyond the maximum excursion required (apart from any electronically controlled limit). The maximum searching distance Δx_{MAX} over which we need scan is about 6 to 8 picture points; this means 0.45 mm (3 points) for each mirror. With a focal length of 6 mm this corresponds to angular deflections of $\pm$ 0.45/12 = 0.0375, about 2°. The lever arm maximum deflection is then 12.4° and this is easily realised by making the lever arm profile circular over 12.4° only; this gives 1.0 and 1.3 mm widths at the inner and outer lever arm peripheries.

The restoring torque for the balance arm is provided by a Perspex torsion shaft. Perspex material is chosen because of its excellent damping qualities. The natural undamped frequency of vibration of a torsional shaft of radius r, length L and modulus of rigidity G carrying an inertia I is given by :

$$w_n^2 = \frac{\pi r^4 G}{2LI} \qquad \text{--------- } 3.4$$

With a shear modulus for perspex about 3 x 10^{10} dyne cm^{-2} and an estimated moment of inertia of 500 gm cm^2 for the balance arm, a torsional shaft ¼" diameter (radius 0.3 cm), L= 1 cm gives a natural frequency w_n of about 900 radian sec^{-1}, or roughly 150 cycle sec^{-1}. With damping, the restoring time is of the order of 3 milliseconds and corresponds to 3 picture points at the maximum scanning speed.

The balance arm is switched by magnetic actuators placed above it; in operation, one of the two laminated 'Stalloy' armatures attached to the balance arm is vertically attracted by its core-coil system when the coil is energised with a large current pulse. The active side of the balance arm therefore engages the lever arm in the flange and produces double velocity scanning; the non-active side performs the spot arresting mechanism. The magnetic actuators are to be described more fully later on (Section 3.32). It is possible to estimate roughly the forces which the actuators must exert on the balance arm by assuming that the arm is to be tilted a maximum amplitude of 0.1 mm at the armature position in 1 millisecond. The tilt angle is 0.1/40 = 1/400 rds. for armatures situated halfway along the arm; this gives an angular acceleration of $\frac{2}{400} \cdot 10^6$ or 5 x 10^3 rd sec^{-2} assuming constant acceleration in motion. With an inertial moment of 500 gm cm^2, the initial torque required to produce this acceleration is 2.5×10^6 dyne-cm, and this gives a force of 500 gms wt. with the armatures placed 4 cm from the balance arm axis; this actuator force, increases inversely as the square of the magnetic gap distance (working below saturation) and compensates for the retarding restoring torque supplied by the Perspex torsion bar. With the large forces involved it is obviously expedient to work the magnetic circuit with as large an initial magneto-motive force as is practicable with the available winding space and allowable thermal dissipation. The armatures contribute to the inertia of the balance arm and their position on the balance arm should be optimised in order to minimise the response time.

The previously described 'overshoot' routine may be realised with this modulator if the damping of the balance arm is not aperiodic such that on releasing the attracted armature, the torsional stiffness of the Perspex bar reverses the arm tilt and the lever arms engage the opposite rotating surfaces. The disadvantage of this method of overshoot is that the tilt reversal is a double amplitude swing and if the control spot advance is set to compensate for the switch-on delay, it will be late for the switch off; moreover, the 'missing contour' routine must be performed without overshoot and so it is necessary to control the overshoot electronically, if it is required, and simply reverse the torque instantaneously by energising the second actuator.

The drum/flange design has been given in Fig.3.3 and they are constructed from brass; the engaging surfaces have been etched with a fine Merlin wheel; the etch resolution is within that of the picture points and the circular profiles of the steel lever arms are similarly knurled to match. Damage to the knurled surfaces is negligible with forces of the order of 200 gm.wt. acting at the contact points.

The balance arm (Fig.3.18) has been designed from maximum rigidity and minimum inertia considerations; the frame consists of four aluminium blocks housed in a 0.020" thick steel U-channel open at the mirror faces. It was found that welding the blocks to the channel in order to minimise the inertia produced distortion of the balance arm, and consequently they have been inserted with three small steel screws apiece. The lever arm shafts and the coupled mirror shafts are $\frac{1}{8}$" diameter silver steel. The oscillating mirrors, $\frac{1}{4}$" by 9/16" and 1 mm thick have been fixed onto the flats of the inner shafts by 'Araldite' casting resin used as a cement. The mirrors, set at 45° to the horizontal, slightly overlap the steel channel and to accommodate their motion, a rectangular recess has been cut into the top and bottom horizontal steel faces of the channel.

The lever arms are made from 1/16" steel and have been cut from a 10 mm diameter knurled disc; the centre hole is offset 0.3 mm to

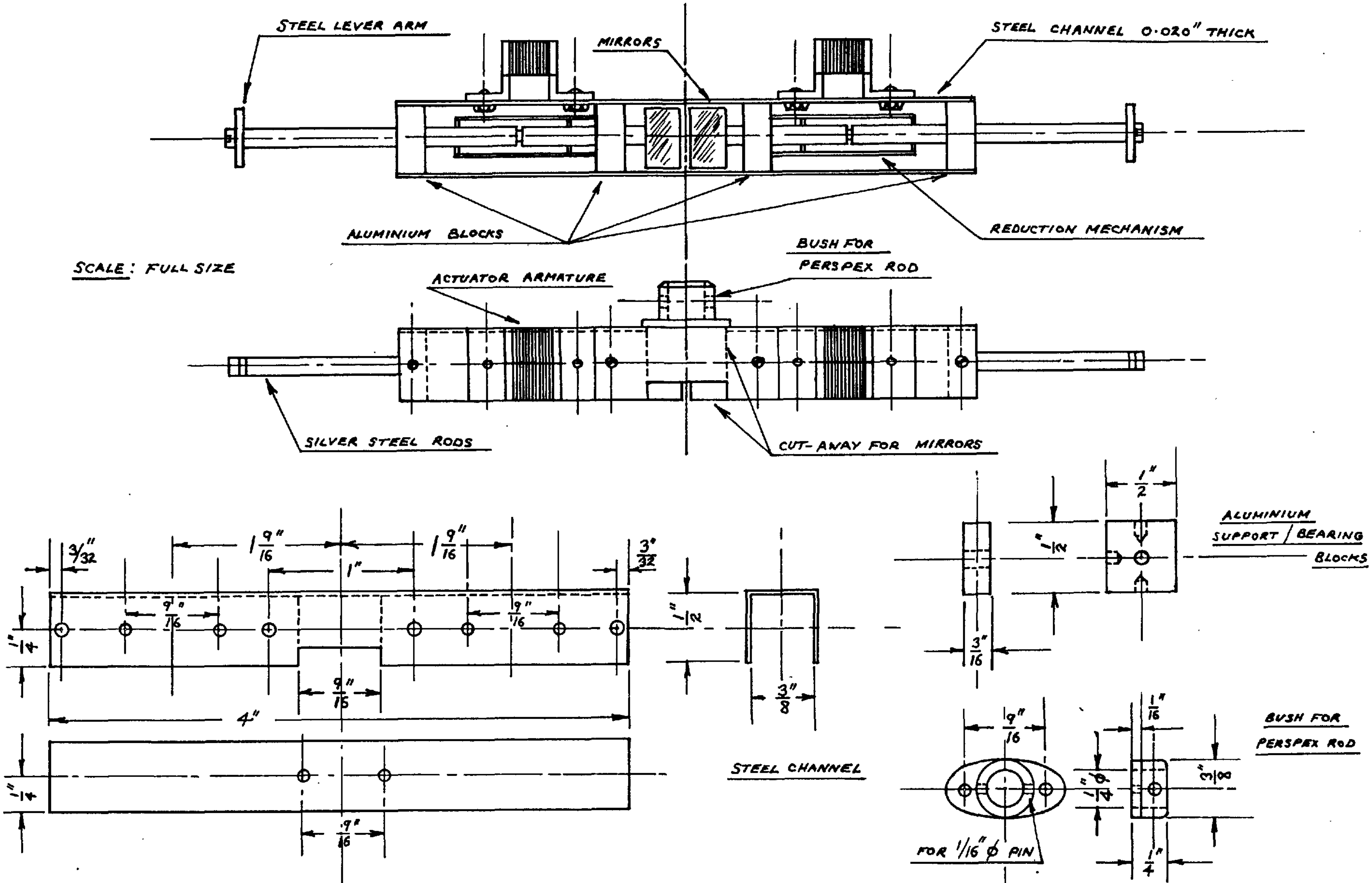

FIG. 3·18 THE VELOCITY MODULATOR

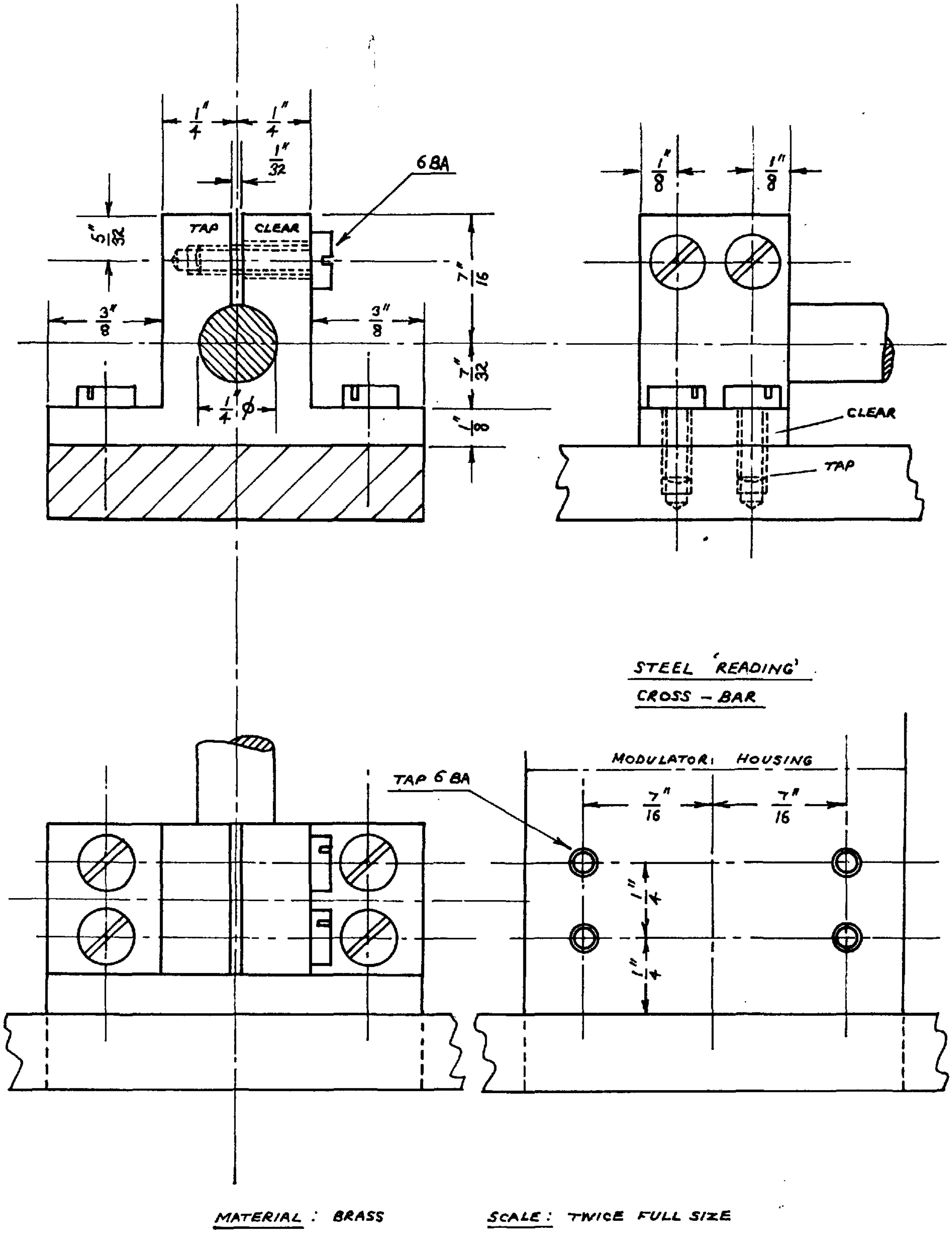

FIG. 3·19 END MOUNT FOR PERSPEX TORSION BAR OF VELOCITY MODULATOR

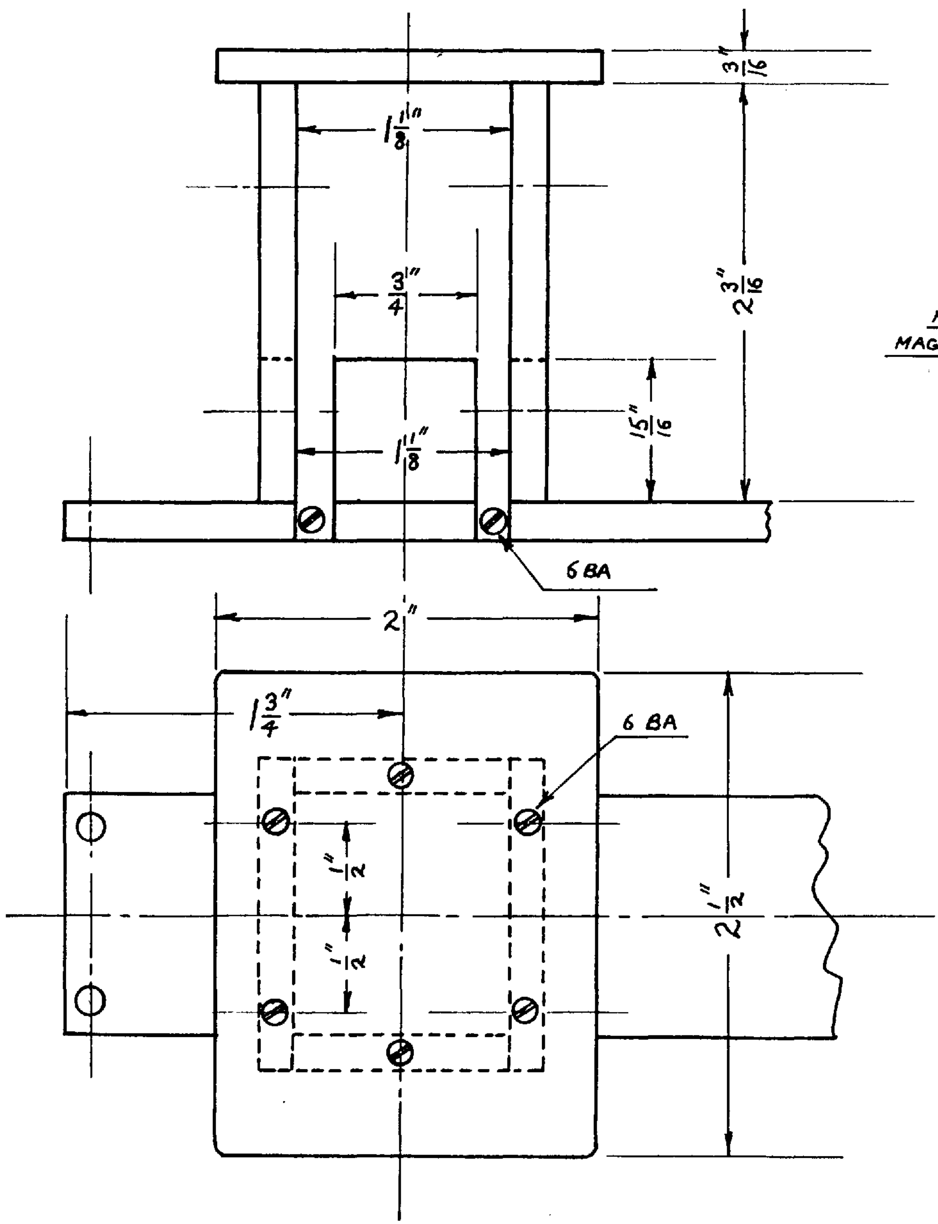

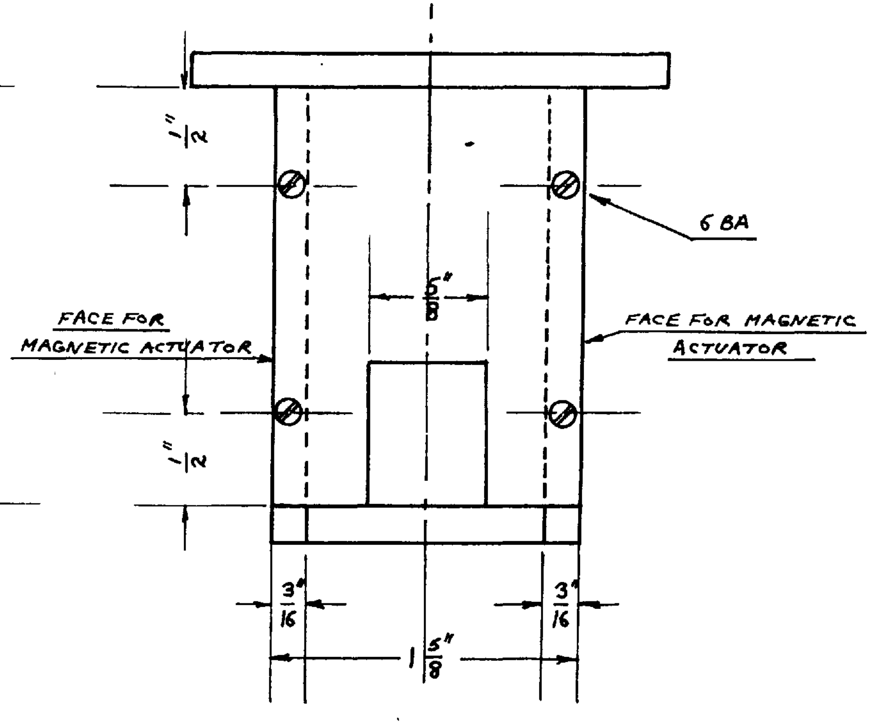

MATERIAL: STEEL   SCALE: FULL SIZE

FIG. 3·20

MOUNTING BRIDGE FOR MAGNETIC ACTUATORS OF VELOCITY MODULATOR provide the necessary asymmetrical lever radii of 4.7 and 5.3 mm. These arms have been screwed into the silver steel shafts with large head-diameter screws.

A brass bush, screwed into the back of the balance arm holds the torsion bar by providing a tight push fit ¼" dia. and a 1/16" dia. steel retaining pin. It is essential to reduce any slackness at this point to a minimum, as it is liable to give backlash in the cantilever deflection of the torsion bar, thereby upsetting the balance at the two lever arms. Bearing slackness in the silver steel coupled shafts is also detrimental to the position balancing of the deflected balance arm and to minimise this, the two shaft sections form an additional bearing at the common ends by running 7/32" of the inner end of the lever arm shaft into the mirror shaft. The other end of the torsion bar, and hence the entire balance arm with it, is gripped by a sprung brass end-mount shown in Fig. 3.19. This end-mount has a ground base and is screwed to the steel 'reading' cross-bar of the picture transformer at the end opposite to the lamp assembly (Fig.3.1) with four 6BA screws. This mount provides the facility for setting up the balance arm in the quiescent position; vertical adjustment is obtained by introducing 0.001" spacer plates between the cross-bar and the mount base, and angular adjustment is performed by enlarging the split in the top of the mount with a wedge and gently tapping round the balance arm. Due to eccentricity in the drum-flange assembly, these settings were found to be extremely critical.

The magnetic actuator system is carried by a ground steel bridge screwed to the 'reading' cross-bar of the picture transformer (Fig.3.20) and the vertical centre-line of this mounting bridge passes through the oscillating mirror axis. The base of the mount is tunnelled through the four sides to allow the balance arm, the perspex torsion bar, and the four light beams to pass through.

We now describe in detail, the magnetic actuator system, the balance arm switching performance, and the design of the angular reduction mechanism in turn.

3.32 Design and Construction of the Magnetic Actuators.

(1) DESIGN

The power requirement of each actuator is derived from the following criteria:

(i) Assuming linear motion of the balance arm subsequent to actuator energisation, the initial torque T_i required from a single actuator, placed at distance r from the torsion bar, to yield a response τ seconds for an actuator deflection of $\hat{y}$ is given by,

$$T_i = \frac{2I\hat{y}}{\tau^2 r} \qquad \text{---------- (3.5)}$$

where I is the total inertial moment of the balance arm including the armatures. With I = 700 gm cm^2 (experimentally determined - Sec. 3.33), $\hat{y}$ = 0.1 mm at r = 40 mm, and τ = 0.001 secs, equation 3.5 gives $T_i = 3.5 \times 10^3$ gm-cm, i.e. with r = 40 mm, the INITIAL force <u>F ≑ 10 Newton</u>.

(ii) At peak angular deflection, the torsion bar provides a restoring torque $\hat{T}_R$ given by:

$$\hat{T}_R = \frac{4\pi^2 I f_n^2 y}{r} \quad \text{---------} \quad (3.6)$$

where f_n is the natural frequency of the balance arm; With f_n = 200 c.p.s., equation 3.6 gives $\hat{T}_R$ = 2.5 Newton-metre, i.e. a FINAL restoring FORCE at the actuator <u>$\hat{F}_R$ = 60 Newton</u>

(iii) The lever arm shafts of the mirror angular reduction gear require a total maximum downward pressure $\hat{P}$ at the maximum deflection $\hat{\theta}$ given by :

$$\hat{P} = \frac{k_o \hat{\theta}}{p\mu} \quad \text{-----------} \quad (3.7)$$

where p is the lever-arm radius, μ the coefficient of dynamic friction between lever profile and etched drum/flange, and k_o the dynamic stiffness of the lever arm shaft at deflection $\hat{\theta}$.

Equation 3.7 gives $\hat{P}$ = 13 Newton, for $\hat{\theta} = 12^o$, ko = 5.6×10^{-5} Nm. deg^{-1} (see Sec. 3.34); p = 5×10^{-3} metre, and a pessimistic minimum μ = 0.01. With actuators placed at 4 cm from the mid-point of the 8 cm radius balance arm, this gives a total required actuator force $\hat{F}_M$ of approximately 50 Newton for FRICTIONAL drive of the reduction gear. $\hat{F}_M = 50$ Newton

The required maximum actuator force F_{MAX} for peak deflection of the balance arm is given by $F_{MAX} = \hat{F}_R + \hat{F}_M \doteqdot 100$ Newton, and this must be provided when the magnetic gap is closed; the 'fitting' magnetic gap is assumed to be 0.05 mm (roughly 0.002") and the initial gap is 0.05 $+\Delta g$ mm where Δg is the peak gap displacement. The actuators incorporate a $\frac{1}{4}$" square cross section, grain orientated silicon steel C- core yoke with a 90°V- cut and a 90° armature prism made up of 0.014" thick Stalloy laminations (Figs. 3.21,3.22,3.23). With this arrangement, $\Delta g = 0.1/\sqrt{2}$ for an armature vertical deflection $\hat{y} = 0.1$ mm; the initial gap $g_i = 0.12$ mm therefore. We design on the initial force requirement (i) above, i.e. Fi = 10 Newton.

The vertical force of attraction Fv of the armature into the V-cut C- core is given by:

$$Fv = \frac{tdBgi^2}{\eta_o} \qquad \text{- - - - - - - - - -} \quad (3.8)$$

where t is the vertical core-armature height, d the core-armature breadth, and Bg_i the magnetic flux density in the air gap; η_o is the permeability of free space. With $t = d = \frac{1}{4}$", Fv = Fi = 10 Newton, $\eta_o = 4\pi \times 10^{-7}$, Equation 3.8 gives $B_{gi} = 0.62$ Wb. metre^{-2}. The saturation flux density of silicon steel is 1.6 Wb metre $^{-2}$ and this is reached before the gap closes to 0.05 mm; hence the maximum force with this system is given by substituting $Bg_i = 1.6$ Wb/m^2 in Equation

3.8 above and $\hat{F}_v$ = 40 Newton. This is taken to be sufficient because ideally the reduction mechanism drive of $\hat{F}_M$ = 50 Newton is supplied by engaging the lever arms, rather than slipping them on the large inertial drum/flange system.

The AMPERE TURNS required is given by $\frac{Bg_i . 2g_i}{\mu_o}$ where g_i is the initial normal gap distance in metres. With g_i = 0.12 mm this gives AT = 120 Ampere-turns, assuming the yoke (C-core) to have negligible magnetic reluctance.

The linear static self - INDUCTANCE L of the actuator is given by

$$L = \frac{\sqrt{2}Bg.t.d.N}{I} \quad \text{----------} \quad (3.9)$$

with Bg the gap flux density with a magnetomotive force NI Ampere-turns, and t.d the magnetic cross section of the core. Choosing I = 100 mA and N = 1200 turns to satisfy AT = 120, Equation 3.9 gives an initial inductance Li = 0.41 Henries with Bg = Bg_i = 0.62 Wb metre^{-2} The maximum periodic working of the coils gives a RMS current of $100/\sqrt{2}$ = 70 mA. Choosing a maximum diameter copper wire of 38 Gauge (with a rating of 42 mA for 1500A/sq.inch) the current density is 2500 A which is not excessive with randomly pulsed working.

The TIME-CONSTANT T of the magnetic circuit at the moment of switching is given by Li/Rc where Rc is the coil resistance. With 38 Gauge enamelled copper wire Rc is under 100Ω for 1200 turns on a

$\frac{3}{4}$" C-core. For an electrical time constant of 0.001 second, the voltage source impedance must be 4 kΩ, in addition, the time-varying inductance introduced by the decreasing magnetic gap contributes a resistive term.

The estimated mean ACTUATOR POWER to be developed for balance arm deflection is given by $k\hat{y}^2/ 2\tau r^2$ where k is the torsional stiffness of the torsion bar and other symbols are as above; this gives 1.25 Watts and so may be supplied by a small audio power stage.

The positioning of the armatures on the balance arm (r = 1 9/16") has been dictated by space considerations; we now justify the final design position by observing that the following criteria are to be satisfied:

(a) The initial angular acceleration of the balance arm is to be maximised.

(b) At peak deflection, the actuators must provide sufficient torque to deflect the Perspex torsion bar and hold the lever arms in the knurled drum/flange surfaces.

The first criterion (see the accompanying sketch Fig.3.24) is satisfied as follows : Assume one actuator is pulsed from an initial gap of g_i to a final gap g_o and let $\hat{y} = g_i - g_o$. Then if δ is the deflection of the lever arm shafts at their extremities distance R from the torsion bar, we have

$$\delta = R\hat{y}/r \qquad \text{-------------} \quad (3.10)$$

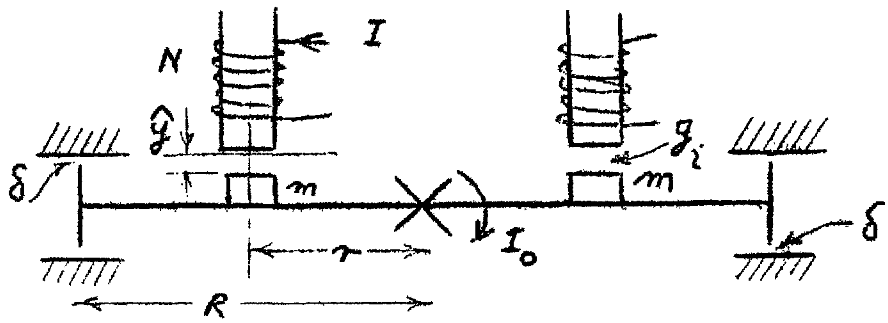

FIG. 3.24

Also, the initial angular acceleration $/\ddot{\theta}/\ t = o$ is given by

$$/\ddot{\theta}/_{t=o} = \frac{Fi\ .r}{I_o + 2mr^2} \qquad (3.11)$$

where Fi is the initial actuator vertical attraction, I_o the moment of inertia of the balance arm only, and m the mass of the armature. From Equation (3.8), we have,

$$F_i = \frac{\eta_o I^2 N^2 t.d}{(\hat{y} + g_o)^2} \qquad (3.12)$$

with symbols as above; inserting (3.12) and (3.10) into (3.11) we have:

$$/\ddot{\theta}/_{t=o} = \frac{\eta_o I^2 N^2 td}{\left(g_o + \frac{\delta r}{R}\right)^2 \left(\frac{I_o}{r} + 2mr\right)} \qquad (3.13)$$

and this is maximised by putting $\frac{d}{dr}\left\{/\ddot{\theta}/t = o\right\} = 0$ from (3.13);

or, minimising the denominator of (3.13), we have :

$$\left(\frac{6\delta m}{R}\right) r^3 + (2g_o m)r^2 + \left(\frac{\delta I_o}{R}\right) r - I_o g_o = 0 \qquad (3.14)$$

Inserting into Equation 3.14 the values δ = 0.2 mm, m = 7 gm (experimentally determined), R = 78 mm, g_o = 0.1 mm, I_o = 500 gm cm^2, and solving by Newtons Approximation Method, r = 25 mm i.e. 1".

The second criterion is satisfied by making r as large as possible since the final torque T_f provided by the actuators is directly proportional to this quantity:

$$T_f = \left(\frac{\eta_o I^2 N^2 t.d}{go^2} \right) r \qquad \text{------------ (3.15)}$$

Equation 3.14 and 3.15 justify the choice for r of 40 mm.

(2) CONSTRUCTION

The cores used in the actuators are 'Telmag' $\frac{3}{4}$ HWR grain - orientated silicon steel C- cores; the V- cuts were performed by the makers, Telcon Ltd. Each core carries a coil former, constructed from card and strengthened with Shellac, carrying a 1500 turn winding of 38 Gauge enamelled copper wire; the windings have been split into three sections to enable either actuator to perform as a 'moving-iron' pick-up device when the other is current driven for frequency testing of the balance arm.

Each core half has been set into an Araldite side-plate (Fig.3.23) and the casting alignment was set from the normally cut face of each core using the same fixing jig for all four components. The assembly is shown in Fig. 3.22, the two Araldite plates are held with two long

8 BA bolts inserted in the plane contained by the joined normal core faces, and both are screwed onto a brass back-plate.

The armatures, constructed from 0.014" thick Stalloy transformer laminations, are shown in Fig.3.21 and Plate 3. The triangular laminations were cut roughly to size and both sides painted with a solution of levigated aluminium oxide in amyl acetate; after allowing them to dry, each armature was assembled by sticking 16 laminations between two steel angle pieces with a Paxolin spacer base. Each armature was machined down to fit one of the assembled actuator cores. To remove conducting burrs from the lamination ends, the top faces of the armatures were deplated after prior cleaning in 70% H_2SO_4 with lead as cathode under the following conditions: 600 mA was passed for 10 minutes followed by 300 mA for the same period, and the derived insulation was subsequently checked. The roof of each armature was finally painted with a dilute Shellac solution for protection.

Measurements performed on the actuators provided the following results: Total resistance of 1500 turn coils = 62Ω, with an equi-turn 3 section coil of section resistances, 17Ω, 20Ω, 25Ω. Inductance measurements using a Marconi Universal Bridge gave:

Actuator A, with the matched armature strapped in position:

At frequency 1 Kc/sec, L = 740 mH, Q = 21.6

10 Kc/sec, L = 700 mH, Q = 7.5

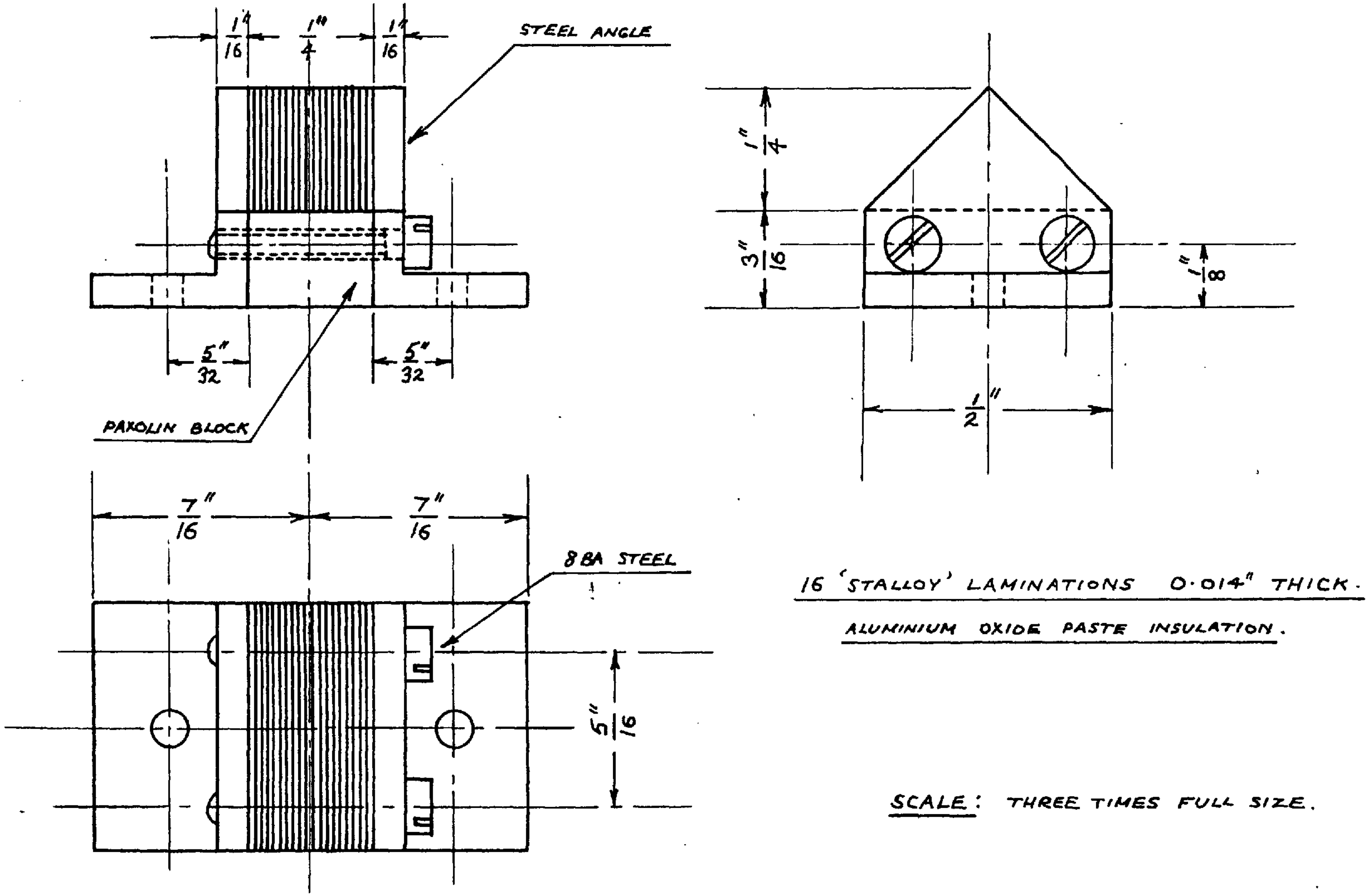

FIG. 3·21 LAMINATED 'STALLOY' ARMATURES FOR VELOCITY MODULATOR

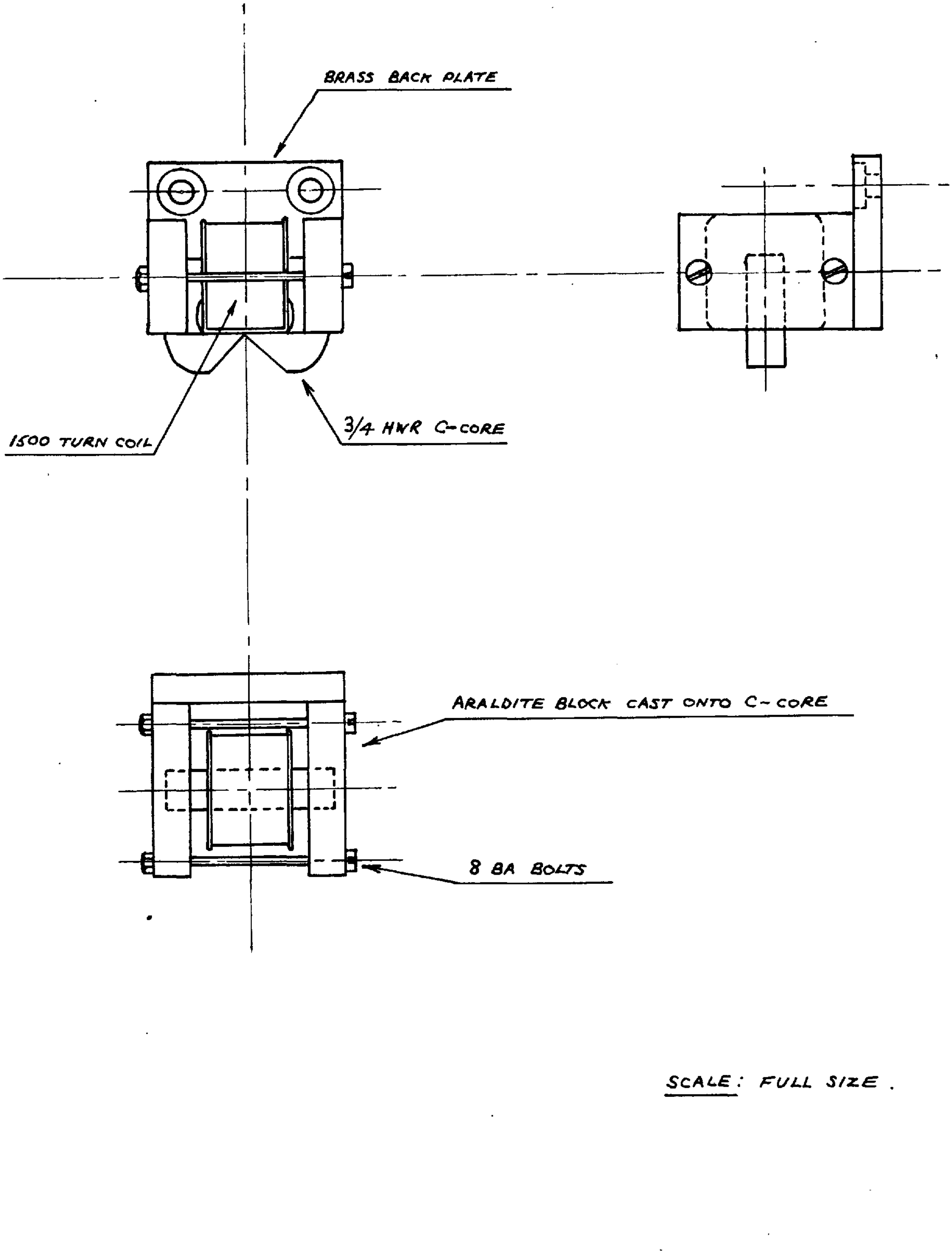

FIG. 3·22 CORE-COIL ASSEMBLY FOR VELOCITY MODULATOR

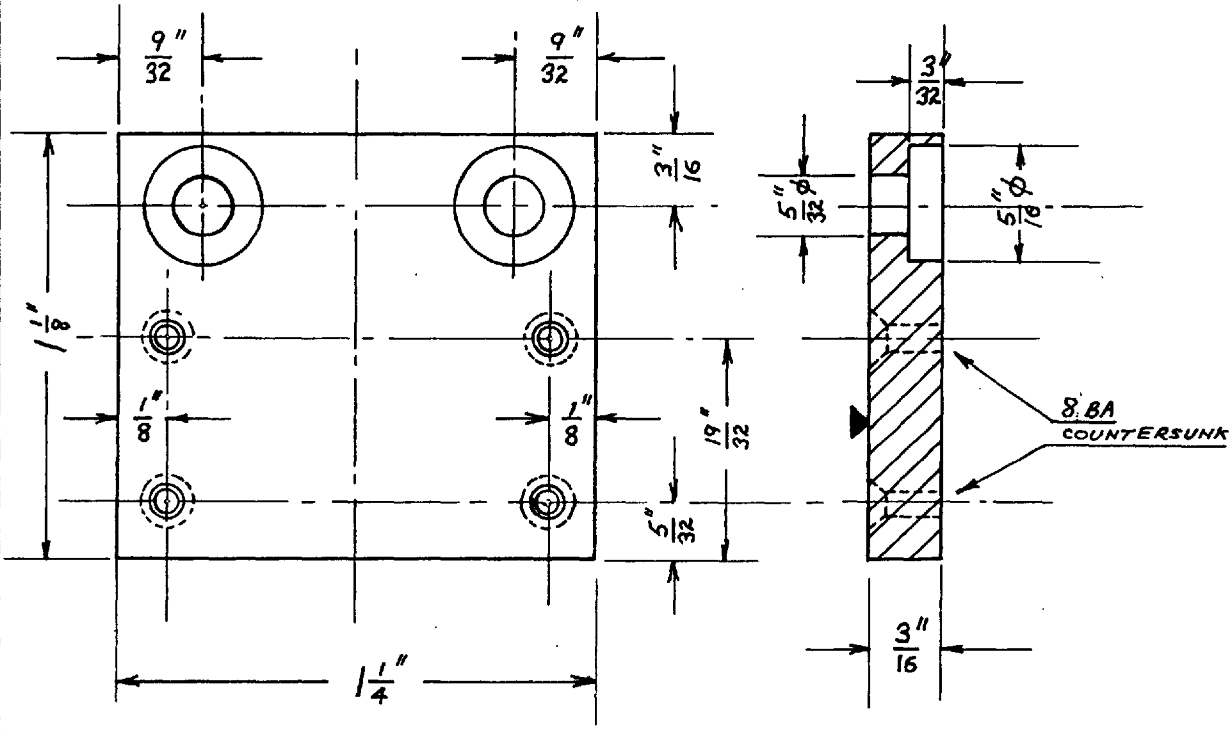

BRASS BACK PLATE FOR CORE-COIL ASSEMBLY.

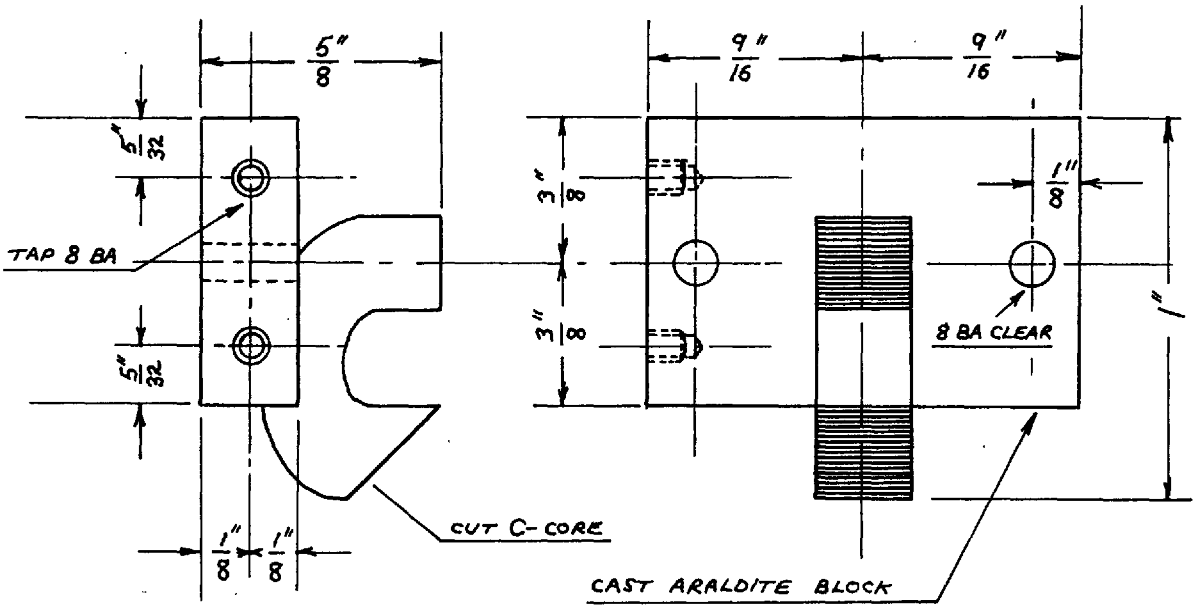

ACTUATOR C-CORE AND ARALDITE PLATE.

SCALE: TWICE FULL SIZE.

FIG. 3·23 VELOCITY MODULATOR ACTUATOR COMPONENTS.

Armature removed,

At frequency 1 Kc/sec, L = 260 mH, Q = 16.2

10 Kc/sec, L = 240 mH, Q = 11.0

Actuator B with armature strapped in position:

At frequency 1 Kc/sec, L = 550 mH, Q = 18.7

10 Kc/sec, L = 500 mH, Q = 6.8

Armature removed,

Frequency 1 Kc/sec, L = 220 mH, Q = 15.4

10 Kc/sec, L = 180 mH, Q = 10.8

The above incremental inductance and coil Q values indicate the core-armature 'iron losses'; at 1 Kc/sec, working on the basis of coil copper losses only, the value of Q should be $0.74 \times 2\pi \cdot 10^3/62 = 75$ for actuator A, compared with the experimental value of about 22.

The armature-actuator pairs have been carefully positioned and aligned; the procedure for this was as follows:

(i) Spacers, 0.008" thick, were fitted between both lever-arm drum/flange surfaces and the balance arm was set with the torsion bar fixed in the end-mount. The spacers were removed to check the equilibrium and clearance with drum motion, and re-inserted again.

(ii) The actuator core-coil assemblies were lightly screwed into the sides of the steel mounting bridge.

(iii) Spacers, 0.004" thick were fitted onto the two sloping magnetic surfaces of the armatures which were then approximately positioned on the top surface of the balance arm steel channel.

(iv) The coils were energised with 25 mA direct current to ensure good fitting surfaces between armatures, spacers, and cores; with the core-coil assemblies firmly affixed to the mounting bridge, the armatures were set onto the balance arm with 'Araldite D' Casting Resin, at room temperature. All spacers were removed once the armatures had firmly set on the balance arm.

With the balance arm mechanically adjusted with the torsion bar set, and the magnetic actuators exactly fitting the armatures, the velocity modulator is ready for operation.

3.33 Frequency and Transient Testing of the Balance Arm Dynamics.

The purpose of this testing was to verify that the design provided the response required for satisfactory switching, and in particular to investigate the damping and spurious oscillation modes in the torsional operation of the balance arm.

Prior to testing, the moment of inertia of the balance arm (without armatures) was experimentally determined by comparing its period of angular oscillation, when suspended horizontally by a 40 cm long, 38 Gauge spring steel wire attached to the torsion bar mounting bush, with that of a known inertia similarly suspended. The known inertia was a rectangular brass bar of inertial moment 66.2 gm cm^2 which gave a natural frequency of 65 c.p.s.; the balance arm natural frequency was 25 c.p.s. and assuming the natural frequency to be inversely proportional to the square root of inertia, this gave a balance arm inertia of 450 gm cm^2. The mass of each armature was found to be 6.5gm. and with these placed at 4 cm from the pertinent vibration axis, the total inertial moment of balance arm is 660 gm cm^2.

The shear modulus of Perspex was also determined by measuring the static torsional stiffness of a 20 cm long, 3/16" dia. circular rod; shear modulus G is obtained from the formula $G = 2\,lk/\pi r^4$ and with $r = 3/16"$, $l = 20$ cm, $k = 0.4$ Nm/rd, $G = 4 \times 10^9\ N/m^2$

For a balance arm undamped natural frequency of 200 c.p.s., and an inertial moment 660 gm cm^2, the required torsion bar stiffness is 100 $Nm.rd^{-1}$ (this has been met by the actuator design) and with 5/16" available length for mounting bush to end-mount displacement, this gives a Perspex bar diameter $d = 2\left(\frac{2lk}{\pi G}\right)^{\frac{1}{4}} = 0.66$ cm. i.e. 0.26" dia.

The first frequency test was performed with a Perspex rod 0.25" dia. and active length 5/16".

In the frequency testing, the method was to sinusoidally current drive one actuator from an audio power valve, and use the other as a moving iron pick up. Available output transformers failed to provide a sufficient current step-up and consequently the output valve (6BW6) was allowed to drive the actuator coil directly, with the quiescent anode current providing a steady polarising field. One of the 500 turn coils on the other actuator was fed with 48 mA direct current to provide a steady magnetic flux which could be modulated with armature motion and the modulation picked up as a voltage on the remaining 1000 turns.

With a valve drive current of $I_d = Io + Ia \sin wt$, the torque T supplied by the first actuator is proportional to I_d^2 i.e.

$$T \propto Io^2 + 2IoIa \sin wt + Ia^2 \sin^2 wt$$ and providing that $Ia \ll Io$, the sinusoidal driving torque T (W) is given by

$$T\ (W) = 2IoI_a \sin wt \qquad \text{------------(3.16)}$$

where Io is the polarising steady anode current, and Ia the peak 'signal' current of frequency $\underline{w}$ rd sec^{-1}. The complex stiffness k (jw) is defined by $T(jw) = k(jw)\ \theta\ (jw)$ and for small vibrations, θ (jw) is proportional to the magnetic gap width $g_s(jw)$ and $k(jw) \propto I_a(jw)/g_s(jw)$. If the polarising field in the moving iron actuator is derived from a current Io in No turns, then the instantaneous flux ϕ (t) flowing through the pick up coil is given by :

$$\phi\ (t) = \frac{AIoNo\eta o}{g_o + g_s\ (t)} \qquad \text{-------(3.17)}$$

when $g_o + g(t)$ is the instantaneous total magnetic gap at time t and

A is the core cross-sectional area. The open circuit Voltage E_n developed across an n turn pick-up coil is given by :

$$E_n = n\dot{\phi}(t) = - AIoNon\eta o\ (g_o + g_s(t))^{-2} \cdot \dot{g}_s\ (t) \quad - - (3.18)$$

and if $/g_s\ (t)\ / \ll g_o$, Equation 3.18 gives,

$$En = - \frac{jAIoNon\eta ow.}{g_o^2}\ g_s\ (jw) \quad - - - - - - - - - - - - (3.19)$$

This latter equation shows that the relative amplitude response with frequency may be determined by plotting the normalised open circuit voltage from the pick-up coil, weighted by the factor 1/w. for constant current drive against frequency w i.e. plotting the reciprocal of the amplitude of the complex stiffness $/k(jw)/^{-1}$ versus frequency.

The experimental procedure was as follows: The 6BW6 power valve was voltage driven on its control grid from a B.S.R. low frequency oscillator, and the signal current in the driven actuator was maintained constant over the frequency range by varying the grid signal and monitoring the voltage developed across a small resistor (100Ω) placed in series with the coil; the signal current amplitude was kept well below the standing anode current of the valve and the quiescent gap on the pick-up actuator was made large so that Eq. 3.19 above was valid. The output voltage from the pick-up coil was measured on a Cossor Oscilloscope.

The results are tabulated below; the first frequency response

(Table 3.3) exhibits a torsional resonant frequency $f_{R_1} = 76$ c.p.s. and a cantilever mode resonant frequency $f_{R_2} = 175$ c.p.s; this response, plotted in Fig. 3.25 in normalised form, showed that the torsion bar was presenting too low a torsional stiffness by twisting within the bush fitting on the balance arm. The bush was subsequently strengthened and made a tight fit for the Perspex rod. The result of this is tabulated in Table 3.4 and plotted in Fig. 3.26 as a frequency response; the torsional resonant frequency has been increased to $f_{R_1} = 123$ c.p.s. and the cantilever mode resonant frequency f_{R_3} to 230 c.p.s. The ancillary mode, $f_{R_2} = 133$ c.p.s. has been introduced and results from flexing of the back of the balance arm steel channel from the torsion bar bush. Multiple ancillary modes were introduced when an attempt was made to remove the cantilever mode by replacing the Perspex rod with a steel bar of rectangular cross-section; the scheme was finally abandoned because of the spurious flexing and also because steel does not possess the same excellent damping qualities as Perspex. The frequency characteristic shown in Fig. 3.26 is for the final device as used in the picture transformer.

The above described set-up for frequency testing was also used to display the transient response of the balance arm; the sinusoidal input was replaced by 10 m.sec pulses at 20 c.p.s. P.R.F., and the pick-up coil voltage waveform displayed on an oscilloscope for

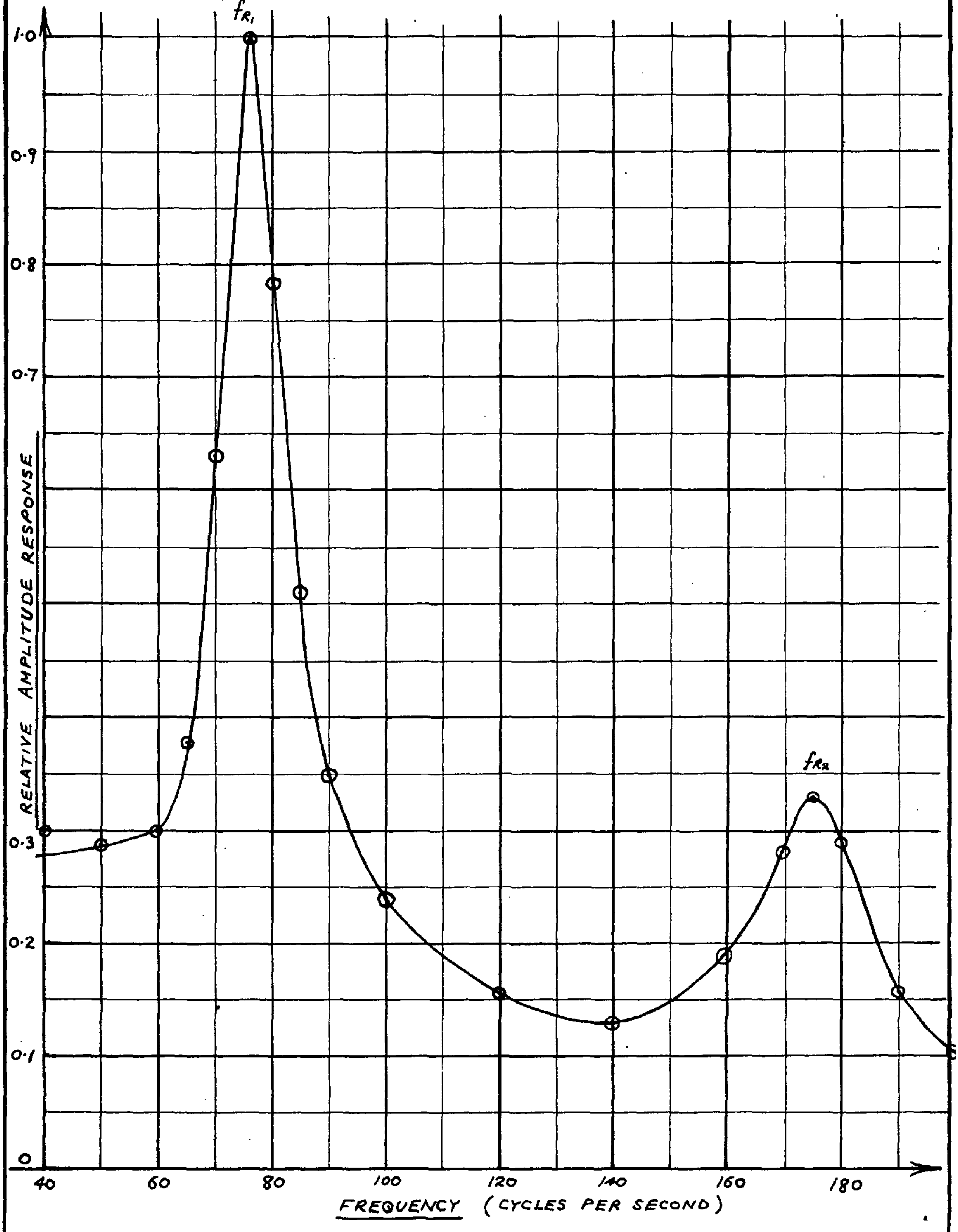

FIG. 3·25 FREQUENCY RESPONSE OF TRIAL BALANCE ARM OF THE VELOCITY MODULATOR

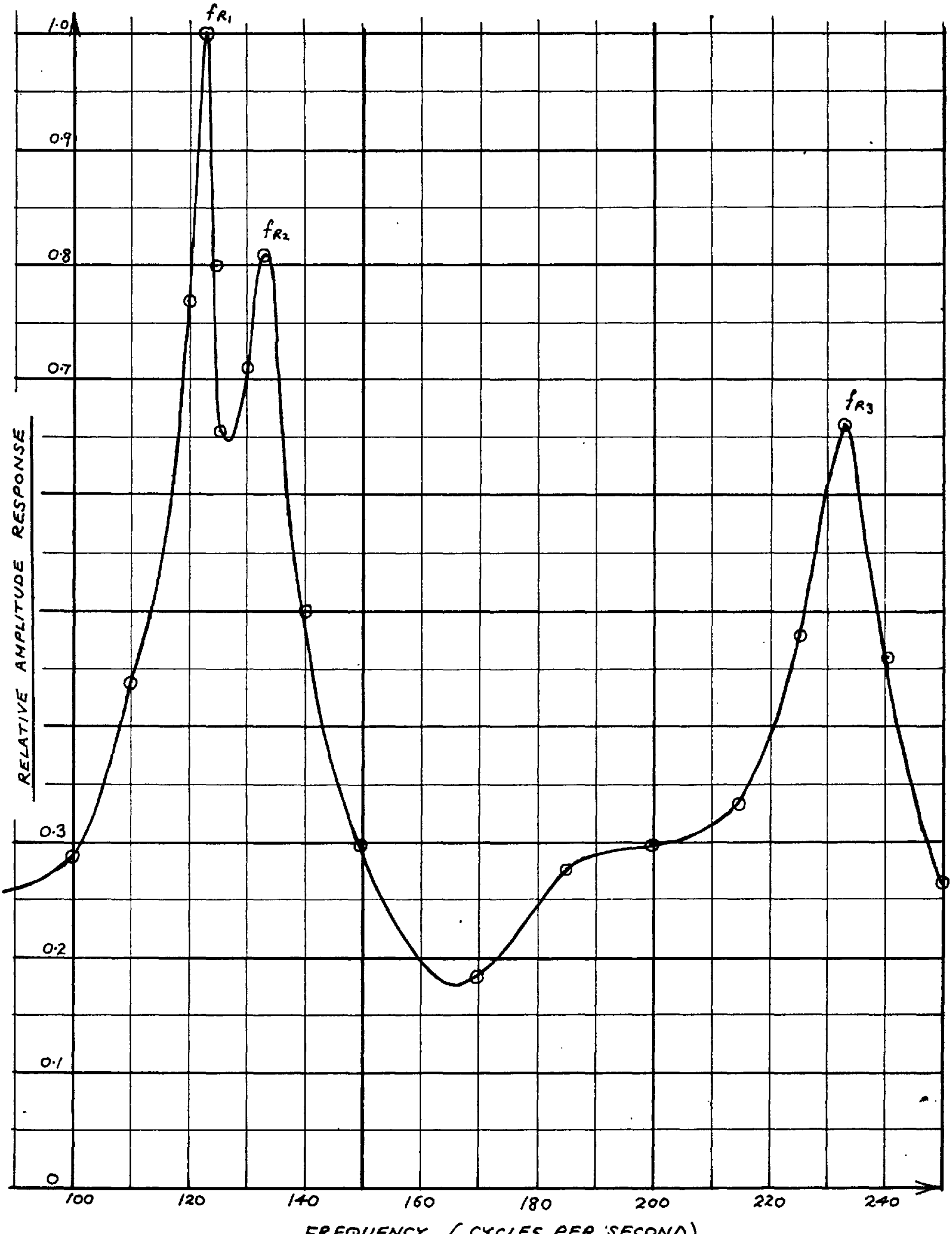

FIG. 3·26 FREQUENCY RESPONSE OF TRIAL BALANCE ARM OF THE VELOCITY MODULATOR

TABLE 3.3

FREQUENCY (C.P.S.)	PEAK-PEAK PICK-UP COIL VOLTAGE (mV)	WEIGHTED OUTPUT ($^1/f$)	NORMALISED OUTPUT
40	80	2.0	0.298
50	95	1.90	0.284
60	120	2.0	0.298
65	165	2.54	0.379
70	295	4.21	0.630
76	510	6.70	1.00
80	420	5.25	0.784
85	290	3.41	0.510
90	210	2.33	0.348
100	160	1.60	0.239
120	125	1.04	0.155
140	120	0.86	0.128
150	160	1.07	0.160
160	200	1.25	0.187
170	320	1.88	0.280
175	390	2.23	0.330
180	350	1.95	0.290
190	200	1.05	0.157
200	140	0.70	0.104

TABLE 3.4

FREQUENCY (C.P.S.)	PEAK-PEAK PICK-UP COIL VOLTAGE (mV)	WEIGHTED OUTPUT ($^1/f$)	NORMALISED OUTPUT
50	12	0.240	0.246
60	15	0.250	0.256
80	18	0.225	0.231
100	28	0.280	0.287
110	48	0.430	0.440
120	90	0.750	0.770
123	120	0.976	1.00
125	80	0.640	0.655
130	90	0.692	0.710
133	105	0.790	0.810
135	105	0.776	0.785
140	68	0.486	0.498
150	43	0.287	0.294
170	30	0.177	0.182
185	50	0.270	0.277
200	58	0.290	0.297
215	70	0.326	0.334
225	105	0.467	0.478
233	152	0.650	0.666
240	108	0.450	0.461
250	65	0.260	0.266

measurement. The natural frequency f_N on switch-off was 185 c.p.s. and lies between f_{R_1} and f_{R_3}, the previously determined forced resonant frequencies. The damping factor α was also determined by observing the successive peak amplitudes in the switch-off oscillatory decay, using the formula:

$$\alpha T/2 = \frac{y_r - y_{r-2}}{y_{r+1} - y_{r-1}} \qquad (3.20)$$

where $T = 1/f_N$, and y_r is the amplitude of the r^{th} peak from some fixed datum. Equation 3.20 gave a mean α, $\overline{\alpha} = 52$ sec $^{-1}$ for the balance arm with $f_N = 185$ c.p.s. and represents about 5 natural oscillations.

3.34 The design and Performance of the Angular Reduction Mechanism.

(1) DESIGN

The reduction gear initially contemplated, coupled the two shafts by pinning them to a perspex tube clamped at one end to the fixed aluminium support block of the balance arm; a uniform tube exhibits a linear torsion profile, and to achieve a convenient pin distance ratio, the outer radius was tapered down towards the outer shaft from the clamped end; the advantage of this method is that the mechanism provides its own restoring force and damping. The scheme was rejected when the perspex tubing was found to be too brittle; polythene tubing was tried and found to be insufficiently resilient.

The solution of the problem is shown in Fig.3.27 and Plate 3.3; the two silver steel shafts are coupled by two horizontal 28 Gauge spring steel wires rigidly end-fixed into the mirror shaft aluminium bearing block with brass bushes. Steel pins, 1/32" dia. run diametrically through the shafts and are soldered onto the spring steel wires at a radius of ⅛". The spring steel wires deflect in a combinatory mode - the angular deflection of the shaft radial pins is communicated to the wires as a CANTILEVER deflection and also as a TORSIONAL deflection, since the pin-wire joints are rigid. Cantilever deflection alone follows a cubic profile and the torsional mode is linear. The requirements of the reduction mechanism are as follows:

(i) The mechanism must provide an angular reduction ratio of 6.2 which is to be maintained dynamically when the lever arm shaft is driven with a ramp-function of angular displacement.

(ii) The reduction is to be linear up to a maximum deflection of $\pm 12.4^{\circ}$ of the driven shaft.

(iii) The natural frequency and damping of the mechanism must be compatible with the balance arm dynamics.

(iv) The stiffness of the lever-arm shaft should be within the limit set by the balance arm driving torque and lever arm to drum/flange friction.

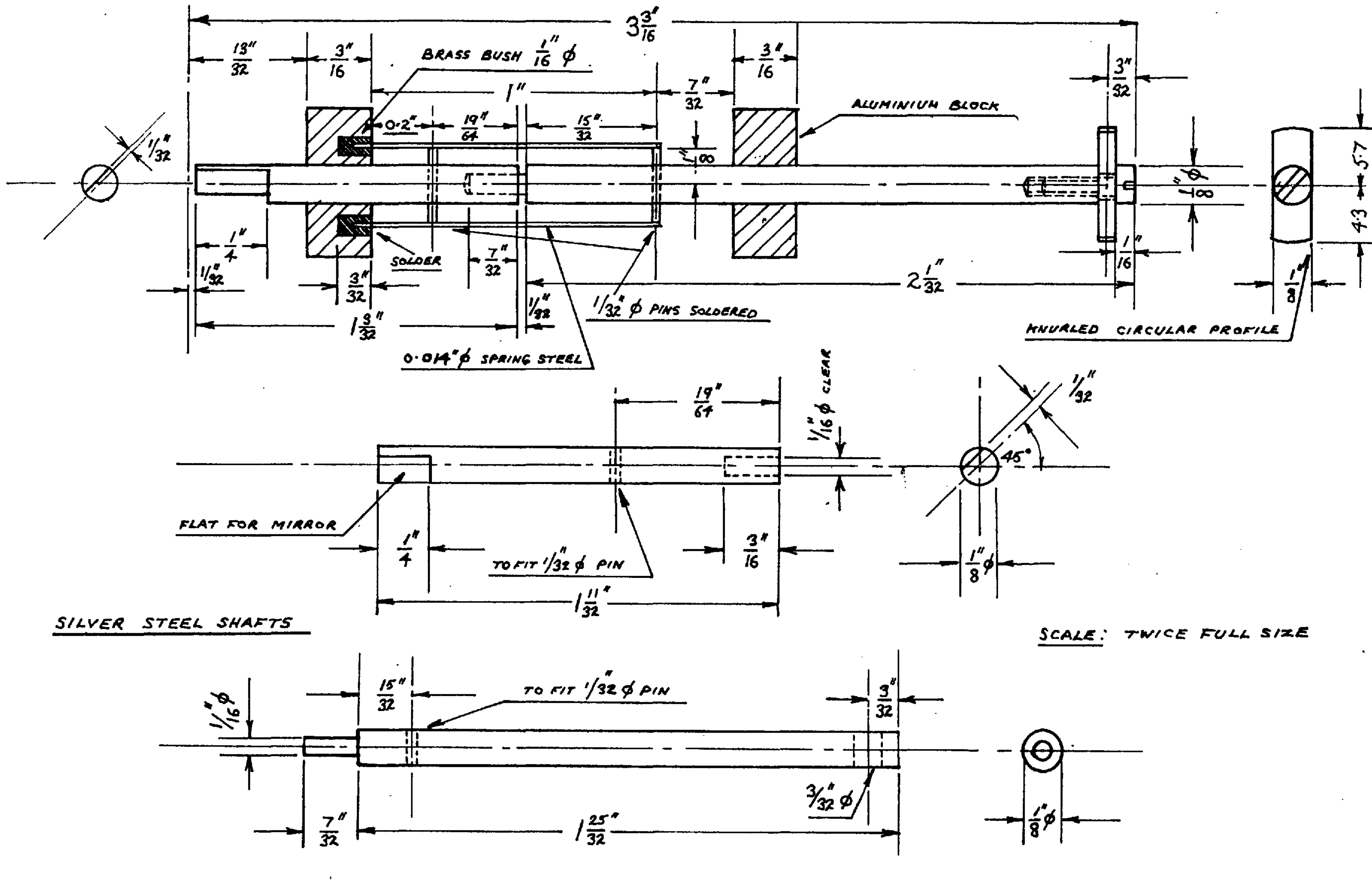

FIG. 3·27 REDUCTION MECHANISM FOR VELOCITY MODULATOR

We now show that these requirements are met by the above design. Appendix 7.1 gives an analysis of the two wire reduction mechanism and also provides design criteria. It is shown (Eq. 48) that for the above system, with shafts coupled at distances l_A and l_B ($l_A > l_B$) from the fixed ends of the spring wire, the zero-frequency design equation for an angular reduction factor of 6.2 is :

$$\frac{l_A\ (K_T - K_c/l_B^2\ -\ l_A K_T/l_B\ )}{l_B\ (K_T + K_c/l_A^2)\ -\ l_A(K_T + 3K_c/l_A^2)} = 6.2 \quad ------ \quad (3.21)$$

where $K_c = 8EIR^2g$ and $K_T = \pi Gr^5 g/R$ with $I = \pi r^4/4$; E and G are the elastic moduli of the spring wire, r its radius, R the coupling pin radius, and g the gravitational acceleration. For 28 Gauge spring steel wire, $2r = 0.0148"$, $E = 2.9 \times 10^7$ lb.in.$^{-2}$; $G = 1.12 \times 10^7$ lb.in^{-2}., inserting these into the expressions for K_c and K_T together with $R = 1.25 \times 10^{-1}$ in. and $g = 3.87 \times 10^2$ in.sec^{-2}., we have $K_c = 3.3$ and $K_T = 2.42$; l_A, the total spring wire length, has been conveniently set at $l_A = 1"$. and Eq. 3.21 then yields a cubic equation for the determination of l_B:

$$l_B^3 - 2.58\ l_B^2 + 0.068\ l_B + 0.093 = 0$$ and the

solution of this equation by Newtons Approximation Method, correct to 2 figures is $l_B = 0.21"$. The undamped natural frequencies of the system Wn_1, and Wn_2 have been given in Equations 37 and 38 of Appendix 7.1,

$$Wn_{1,2}^2 = \frac{(AE + BD) \pm \left((AE + BD)^2\ -\ 4AD(BE - CF)\ \right)^{\frac{1}{2}}}{2AD} \quad --- \quad (3.22)$$

where $A = I_1$ (inertia of driven shaft with lever arm),

$$B = \frac{K_T \ell_A + (K_c/\ell_A^2 - K_T)\, l_B}{(l_A - l_B)^2},$$

$$C = \frac{(K_c/l_B^2 - K_T)\ell_A + (K_T - 3K_c/l_B^2)\, l_B}{(l_A - l_B)^2},$$

$D = I_2$ (inertia of coupled mirror shaft with mirror),

$$E = \frac{K_T \ell_A l_B + K_c/l_B^2 - K_T \cdot \ell_A}{(l_A - l_B)^2},$$

and $F = -E/6.2$; assuming the steel shafts to be uniform cylinders, the glass mirrors and steel lever-arms to be thin rectangular plates, and the steel coupling pins to be long thin wires, the inertial moments I_1 and I_2 for the above design work out at 2.4×10^{-5} lb. in.^{2} and 1.7×10^{-5} lb.in.^{2}, respectively. Equation 3.22 then gives, on inserting $A = 2.4 \times 10^{5}$ lb.in.^{2}, $B = 4.16$, $C = 41.6$, $D = 1.7 \times 10^{-5}$ lb.in.^{2}, $E = 135$, $f = -21.8$, natural frequencies $Wn_1 = 691$ rd.sec.$^{-1}$, and $Wn_2 = 2740$ rd. sec.$^{-1}$ i.e. 110 and 436 c.p.s. respectively, and these frequencies are compatible with the torsional damped natural frequency for the balance arm of around 120 c.p.s.

The angular reduction factor of 6.2 is maintained under the dynamic conditions of its use (driving angular ramp functions), providing that the machine is run at a 'horizontal scanning bandwidth' f_s limited by $f_s \ll \frac{1}{2\pi}\sqrt{\frac{E}{D}}$ (Eq. 50 Appendix 7.1); with the above design, $f_s = 450$ c.p.s.

The static torsional stiffness k_o of the lever arm shaft is given by Eq. 40 of Appendix 7.1:

$$k_o = \mathrm{Lt}_{W \to o} \frac{A(W^2 - W_{n1}^2)\ (W^2 - W_{n2}^2)}{W_s^2 - W^2} \quad ---- (3.23)$$

and this gives $k_o = I_1 W_{n1}^2 \ W_{n2}^2 / W_s^2$ and works out at $k_o = 0.56$ gm.cm. degree $^{-1}$ which is the value which has been used in the previous actuator power output design for the balance arm.

The actual performance of the mechanism is obviously modified by inevitable damping, and indeed this is necessitated for adequate recovery of the modulator after swith-off.

(2) TESTING

Before incorporating the reduction gear with the balance arm, its actual performance was predicted by performing experimental tests on a model of the system; in particular this testing was to :

(a) experimentally confirm the design equation (3.21) for the desired reduction factor.

(b) perform a linearity test over the required angular amplitude range.

and (c) to measure the natural damping of the system. Measurements were performed electromagnetically using search coils placed on the coupled shafts.

In the model, the silver steel shafts were replaced by brass rods of the same diameter, but of increased length in order to bring the inertias equal to those of the final device including the mirrors and the steel lever arms. Brass was chosen because, being non-magnetic, it enabled a simple series magnetic circuit to be built around the mechanism without introducing interfering magnetic paths derived from the coupled shafts. The magnetic circuit was driven by a large permanent magnet and constructed from Swedish Iron bars of rectangular cross-section with two identical air gaps; these air gaps were arranged at convenient distances along each shaft and centred up to provide uniform magnetic fields at right angles to the shaft axes; a flat on the shafts at these points carried a flat rectangular paper former 7/16" x ⅛" containing a 10 turn coil of 40 Gauge enamelled copper wire. The D.C. resistance of these coils was 0.8 Ω.

For small angle deflections, the voltage v(t) picked up by each coil is given by :

$v(t) = B_g A N \dot{\theta}$, where B_g is the gap flux density, A the coil area, N the number of turns per coil and $\dot{\theta}$ the instantaneous angular velocity of the coil. For sinusoidal testing in which $\theta = \hat{\theta} \, \text{Sin} \, (wt + \phi)$, we have $v(t) = B_g A N \hat{\theta} W \, \text{Cos} \, (wt + \phi)$ and $\hat{V}(t) \propto \hat{\theta} w$, showing that the relative peak angular displacements of the two coils, at some frequency w, may be determined by measuring the peak output voltages from the coils when the coupled system is driven by a steady sinusoidally varying angular deflection function. In the experiment, this deflection function was supplied from a 100 watt De Havilland Moving Coil Vibrator with a peak linear amplitude of 0.010" at 200 c.p.s; the linear motion was transformed into angular drive by pin-coupling the Duralumin flexible drive arm of the vibrator to a $\frac{1}{8}$" long steel pin inserted into the end of the 'lever arm' brass shaft. The power amplifier of the vibrator was driven from a variable frequency audio oscillator. With plane faced air gaps and no magnetic armatures the coil voltage outputs were very low, and consequently both coils utilised the <u>same</u> 120:1 step-up audio-frequency transformer for voltage measurements on a Cossor Oscilloscope. The output signals were perturbed by noise derived from bearing vibrations, and it was found that a 0.01 μF capacitor shunted across the transformer output winding removed most of this.

With this arrangement, frequency and linearity tests were performed on reduction mechanisms constructed from 0.028" dia. and 0.022" dia. spring steel wires, with l_A = 1" and l_B , determined by solving Eq.3.21, equal to 0.19" and 0.20" respectively. The results of these tests are tabulated below in Tables 3.5,3.6 and Tables 3.7,3.8 respectively; V_A is the measured peak-peak output voltage from the coil on the driven shaft (inertia I_1) and V_B is the similarly measured peak-peak output voltage from the second coil on the coupled shaft (Inertia I_2). The amplitude characteristic for the 0.028" dia. wire mechanism (Table 3.6) has been plotted in Fig. 3.28.

Table 3.5 Frequency Characteristic for 0.028" Ø wire Reduction Mechanism.

FREQUENCY C.P.S.	V_A p-p mV	V_B p-p mV	TRANSFER RATIO V_A/V_B
50	12	2.0	6.0
70	21	3.0	7.0
100	20	3.5	5.7
150	18	3.0	6.0
200	18	3.0	6.0
500	6	1.0	6.0

Table 3.6. Amplitude Characteristic for 0.028" Ø wire Reduction Mechanism taken at 70 c.p.s.

V_A p-p mV	V_B p-p mV	TRANSFER RATIO V_A/V_B
500	75	6.65
300	44	6.85
150	22.5	6.66
97.5	15	6.50
50	7.5	6.66
32.5	5	6.50

Table 3.7 Frequency Response for 0.022" Ø wire Reduction Mechanism

FREQUENCY C.P.S.	V_A p-p mV	V_B p-p mV	TRANSFER RATIO V_A/V_B
50	150	23	6.6
70	150	24	6.15
100	150	23	6.6
150	150	24	6.15
200	150	23	6.6
300	150	23	6.6
400	140	22.5	6.2
500	82	12.5	6.6

Table 3.8 Amplitude Characteristic for 0.022" Ø wire Reduction Mechanism taken at 50 c.p.s.

V_A p-p mA	V_B p-p mA	TRANSFER RATIO V_A /V_B
375	62.5	6.0
150	22.5	6.5
105	17.0	6.2
50	7.5	6.6
32	5	6.4

FIG. 3·28

AMPLITUDE CHARACTERISTIC FOR TRIAL ANGULAR REDUCTION MECHANISM OF THE VELOCITY MODULATOR.

TAKEN AT 70 C.P.S., 0·028"ϕ SPRING WIRE, 500mV (I_1) ≡ 10° ANGLE

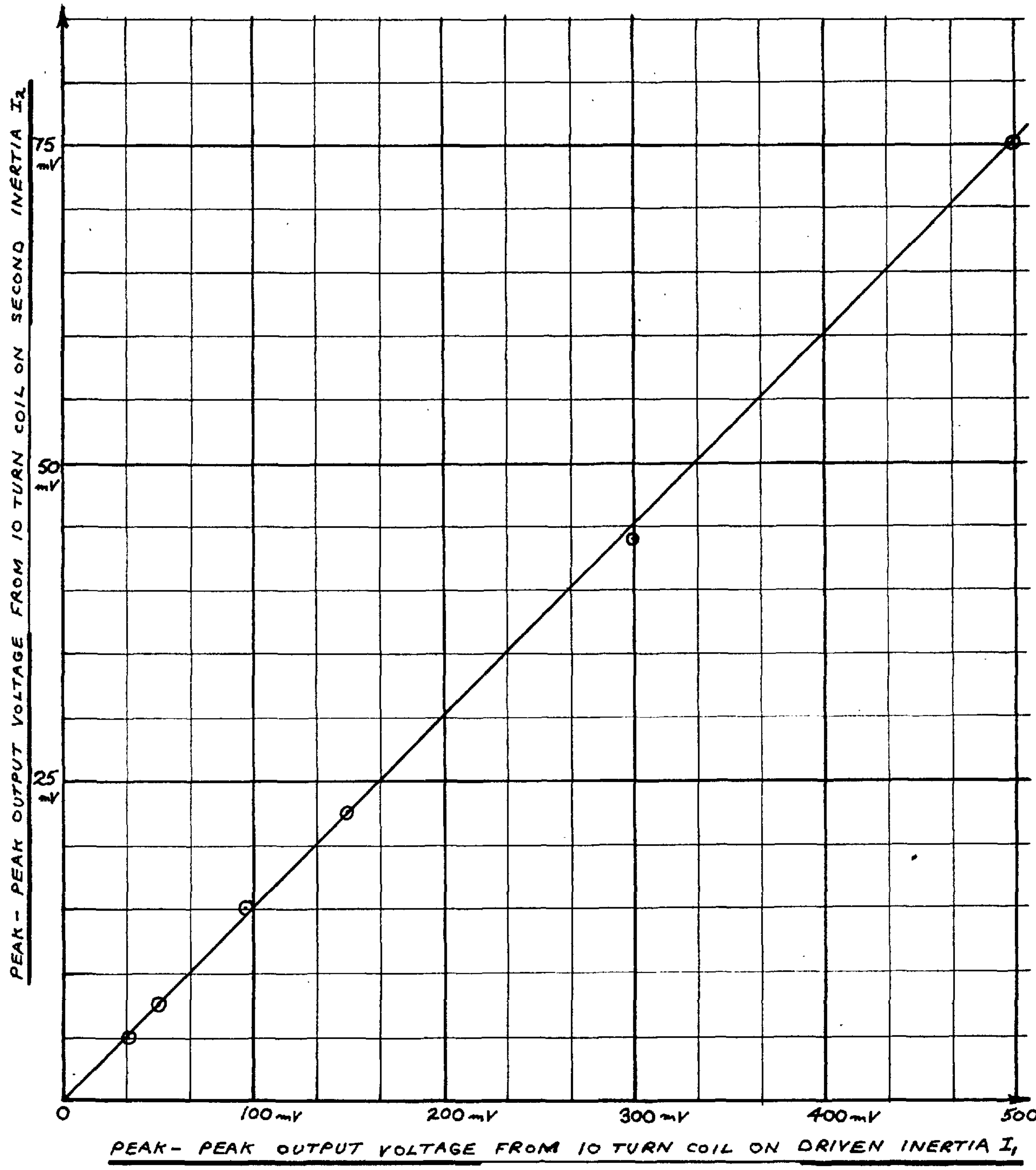

Transient tests were performed on the reduction mechanisms using the same model and pick-up arrangement as above, only with the sinusoidal drive replaced by an angle impulse generator. This generator was a 'Parvalux' D.C. motor running at 420 R.P.M. (7c.p.s.), with a short arm attached to the shaft such that it flicked the short steel pin on the 'lever-arm' shaft through about 12^{o} every revolution. The voltage waveform output from coil A was displayed on an oscilloscope and provided natural frequency and damping data. For the 0.028"Ø wire reduction gear, the observed damped natural frequency of the waveform envelope $f_{n1} = 750$ c.p.s. with a damping factor $\alpha = 160\ sec^{-1}$ which represents about $4\frac{1}{2}$ natural periods; this damping has been derived mainly from the frictional bearings; it was found to increase markedly on augmenting this friction by making the bearing diameters a near tight fit.

The above described experiments confirmed that the two-wire angular reduction mechanism was practicable, and the final device, which could not be tested in that way, was constructed and assumed to satisfy the requirements as set out in the above design criteria.

3.4 THE SIGNAL DISTRIBUTOR.

The function of this organ is to weight the intensities of the two 'alternate line' light beams according to the rule of Eq. 2.3 i.e. $S_{12} = (V_1S_1 + V_2S_2)/(V_1 + V_2)$; each time the pilot spot encounters a large brightness gradient the velocities V_1 and V_2 are step function modulated by the velocity modulator, and this requires the signal distributor to switch from the condition of transmitting each beam with half intensity to the condition in which one beam is sent with full intensity and the other completely blacked-out; this must be performed with the minimum of response time which should ideally coincide with the switch-time of the velocity modulator, so that the pilot spot advance may be set to compensate for both delays simultaneously.

The most elementary solution is to oscillate a mask between the two light beams. With a 2.25 mm radius semi-circular spot, the mask must move a distance of just over 1.125 mm in 0.001 sec, the minimum response time aimed at, and this means an acceleration of 225 g and a maximum speed of 2.25 $m.sec^{-1}$. and this is not an easy matter with massive moving parts. However, if with some kind of lever arm magnification the oscillation amplitude is reduced by a factor of 10 <u>at the actuator</u>, the latter may then be electromagnetic, since a rough calculation shows that a magnetic pull of 10 Newtons, obtainable from a conveniently small core, can accelerate a mass of 4 - 5 gms to

2.25 $m.sec^{-1}$ in 1 millisecond. This is the principle upon which the finally developed signal distributor depends.

Before describing the design and construction of this device we shall list the various possibilities in signal distribution and also describe attempts at developing a mechanically actuated distributor.

3.41 Possibilities in Optical Signal Distribution

Optical signal distribution is a special case of light modulation; light intensity modulation is a feature of sound-on-film recording and the following list contains the major fundamental methods used in this process together with comments on their suitability, or not, for application to the present problem.

(1) Galvanometer mirror (variable area recording); disadvantage is the difficulty of fitting a further deflection system into the already complicated optical circuit.

(2) Magnetic ribbon (variable area); this could probably be developed.

(3) Modulated Glow Lamp[(5)] (variable intensity); not suitable with the present optical set-up but it would be the obvious choice for writing the interpolated signal in a facsimile receiver scheme in which the line signals were available in electrical form only.

For the sake of completeness we may add to this list:

(4) Supersonic diffraction[6] [7]; this is not compatible with the present requirement.

(5) Kerr-cell (liquid) [8]; this has been used in cinematography as a light intensity modulator; it is too cumbersome for the present application.

(6) Electro-Optic Crystal Cell[9]; this is the crystal analogue of the Kerr-cell and could possibly be developed.

(7) Piezoelectric deflection of a mirror [10]; this has the same disadvantage as (1) above, and would probably be ruled out on account of the small deflections achieved.

(8) Storage Tube Light Valve [11]; applicable at TV frequencies and need not be considered for the present application.

It was felt that the problem should be tackled from scratch, using a novel distributor designed specifically for the processing requirement, rather than attempt to develop any one of the above possible known schemes.

3.42 THE MECHANICAL SIGNAL DISTRIBUTOR

In order to achieve the high accelerations required, this distributor works on the principle of restricting the full excursion of $\pm$ 1.5 mm to the mask only, and controlling this motion with massive parts which move only a small fraction of this distance.

The realisation is shown in Plate 4; in this photograph the actuators have been removed. The mask is a very light 0.010" Mica strip which is held in an equilibrium position by fine rubber bands attached to its ends and moves between two machined brass plates of the mask guide. It is moved by friction rollers at both sides which move permanently at about 5 $m.sec^{-1}$ peripheral speed; these roller-pairs, constructed from fibre material, rotate in opposite directions and are allowed to engage the mask one pair at a time. In the first prototype, the roller shafts were driven at the bottom ends by small rubber wheels spring loaded onto brass drums driven in turn from the main shaft of the picture transformer via a pulley system. This proved to be unsatisfactory and the drive was made more positive by incorporating small bevel gears.

The actuators were constructed from Barium Titanate piezoelectric bimorph elements 1" long, 1 cm. across, with a static unloaded, cantilever sensitivity of 10^{-4} mm.volt . Each pair of elements was set vertically in an Araldite base block, and at the uppermost ends were cemented P.T.F.E. bearing blocks to carry the fibre-roller shafts; these bearing blocks were fixed in position, with the actuator base fixed on the bottom platform of the distributor, and adjusted to ensure that the fibre wheel shafts just disengaged the mask.

The scheme was shown to be unworkable for the following reasons:

(i) With the necessarily close tolerances involved (with roller motion of 0.1 mm, tolerances should be within 0.001") eccentricity in the fibre wheel and its drive produced spurious motion of the moveable mask.

(ii) Vibrations from the bevel gear also produced spurious mask motion.

(iii) The stiffness of the piezo-elements was insufficient to maintain the fibre wheel shaft in its bearing to within 0.0005" - with the bimorphs attacking the shafts at their mid-points, the lever amplification is a factor of 2.

An alternative actuator design was contemplated: this employed a magnetic core system with a light 'ferroxcube' armature. The action is similar to the above - the fibre wheel shafts carry cylindrical ferroxcube armatures which run inside a split semi-cylindrical cut ferroxcube core; current drive through a coil moves the armature axis until the fibre wheel engages the distributor mask. The main features of this design are, large potential deflections compared with the piezoelectric actuator, and compatibility with the velocity modulator drive requirements; the chief disadvantage is the absence of an inherent restoring force. This scheme was never realised as it was decided that a fully electromagnetic distributor would be more practicable; this is now described.

3.43 The Electromagnetic Signal Distributor.

The final device is shown in Plate 5. The principle of working is as follows: three wound C- cores are aligned with their faces uppermost and in the same plane and with the C- planes perpendicular to the array. On top of the cores sits a 3-section armature which, in the quiescent condition, is symmetrically placed above the central core which is magnetically 'live'. The two outside armature pieces are angled, such that on switching the coil current from the central coil to one of the outer cores, the armature assembly is deflected across until the pertinent magnetic gap is closed, with the central armature piece pivoting on the central core edge. The mask is placed vertically above the central limb of the armature assembly and the magnetic gaps are arranged such that, with the fixed mask height to armature length ratio available, gap closure results in a horizontal mask motion of $\pm$ 1.5 mm.

(1) DESIGN

The design criteria for the signal distributor are derived from three major factors; firstly the geometrical requirement for producing the necessary lever arm magnification, secondly the response time requirement, and thirdly the space factor considerations. We shall list the important design equations and then describe how the final design may be optimised.

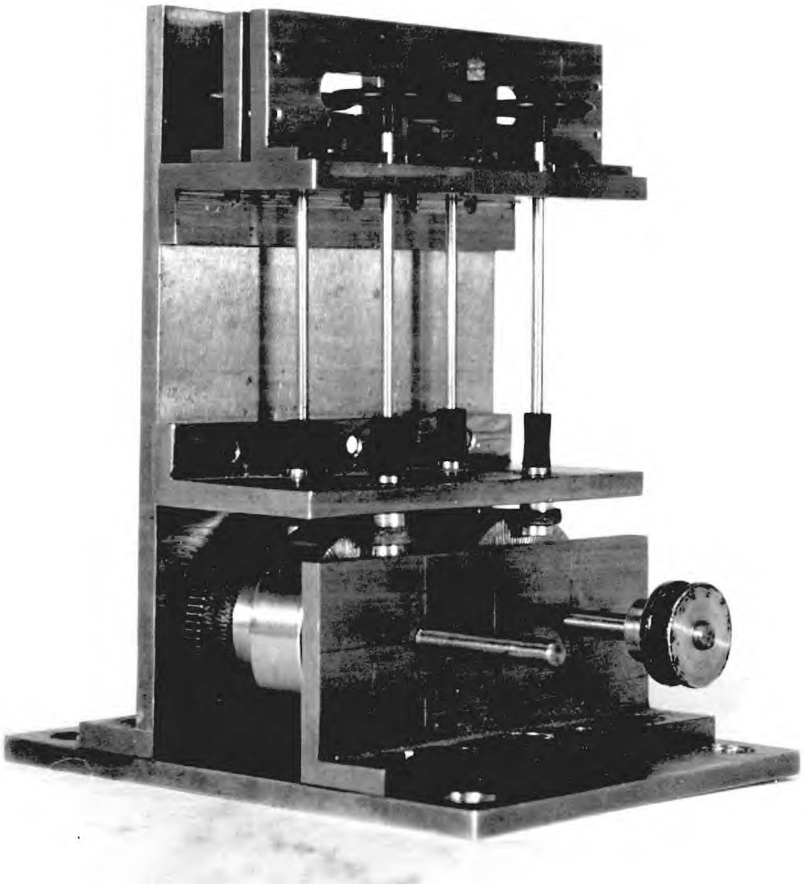

PLATE 4: THE MECHANICAL SIGNAL DISTRIBUTOR

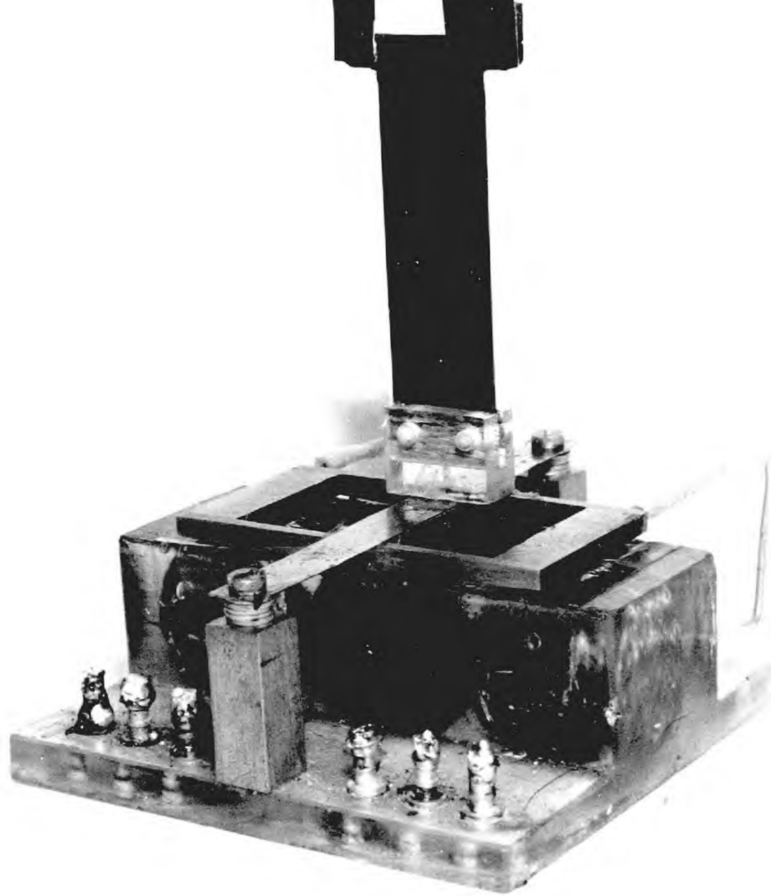

PLATE 5: THE ELECTROMAGNETIC DISTRIBUTOR

(i) With the optic axis at a fixed height H above the picture transformer base and with core faces placed at distance h from the same base line, the geometrical design equation is given by

$$\theta_0 = \frac{\Delta x}{H-h} = \frac{\Delta g}{R} \quad \text{--------- (3.24)}$$

where θ_0 is the peak angular delfection of the armature and is equal to the slope on the armature assembly base, Δx is the required mask deflection, Δg the mean magnetic gap of the outer core-armature piece, and R the radius of armature piece motion. (see sketch):

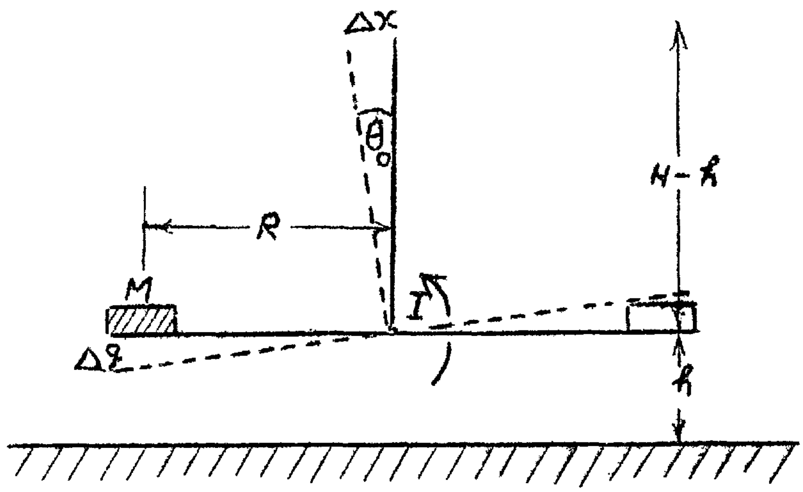

Fig. 3.29

(ii) Assuming linear motion, a constant force F_i at the outer armature section switches the assembly of inertial moment I in a period τ given by :

$$F_i = 2I\theta_0 / R\tau^2 \quad \text{----------- (3.25)}$$

(iii) The force derived from energising the outer core has an initial value F_i given by:

$$F_i = \frac{\mu_o (Ni)^2 A}{4 (\Delta g)^2} \quad \text{- - - - - - - - - - (3.26)}$$

assuming all the ampere-turns to be across the two air gaps, where the core, of face cross-sectional area A, carries a winding of N turns with a current i.

(iv) With armature pieces of mass M attached to a light superstructure, the inertial moment of the complete assembly is given by :

$$I \doteq 2MR^2 + I_M \quad \text{- - - - - - - - - -(3.27)}$$

where I_M is the inertial moment of the mask stem.

(v) With the commercial C- cores available, if A is the cross-sectional area, the winding space area (assumed square) is 2A, the core height as used is $3\sqrt{A}$ and this then gives,

$$h = R = n\sqrt{A} \quad \text{- - - - - - - - - -(3.28)}$$

where n is certainly less than 5 for the most compact winding arrangement. (see sketch):

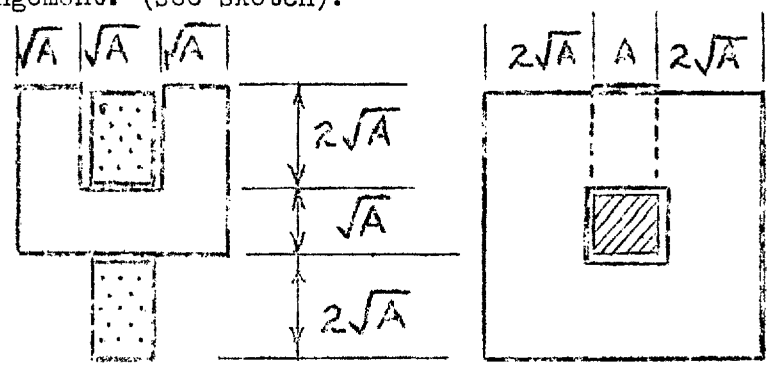

Fig. 3.30

(vi) In addition, the mass M of the armature pieces is proportional to the core cross-sectional area A, assuming that the armature height is constant; also we may take the total winding ampere turns (Ni) to be proportional to A if the available current drive is fixed.

Equation 3.25 may be solved for τ^2 and inserting 3.24, .26,.27 we have :

$$\tau^2 = \frac{8(2MR^2 + I_M)\Delta x^3 R}{\eta_c (H - h)^3 (Ni)^2 A} \quad \text{--------(3.29)}$$

Equation 3.29 shows which factors influence the response time; the height of the optic axis H, the inertia of the mask column I_M, and Δx, the mask motion, are fixed quantities. The response τ may be minimised by keeping M and R small, and choosing a core such that A and (Ni) are large with h as small as possible. These conditions are not compatible, and if we assume that the cardinal design requirement is the fastest response, the optimum choice of core size A must be derived from Eq. 3.29 by inserting Eq. 3.28 and also noting that (Ni) and M are proportional to A. We then have, assuming that we can construct an assembly with $I_M \ll 2MR^2$;

$$\tau \propto \frac{1}{\sqrt[4]{A}\,(H - n\sqrt{A})^{3/2}} \quad \text{------ (3.30)}$$

and τ is minimal from Eq. 3.30 if $\sqrt{A} = H/4n$. In the picture transformer $H = 3\frac{}{8}$" and with 'Telcon' C- cores, $n \doteq 5$ i.e. the inter-
$_{MAX}$

core distance with wound cores arranged as described is a minimum of roughly $5/\bar{A}$; the core selection is given by $\sqrt{\bar{A}} = 0.16''$. In the design we choose a $\frac{3}{4}''$ core, i.e. $A = 1/16$ in^2.

It was found that with the cores wound directly with 40 Gauge enamelled copper wire, they could carry a maximum number of 1500 turns and be spaced at a minimum distance $R = \frac{3}{4}''$ with an overall core height $h = 13/16''$ i.e. $R = h \doteq 3/\bar{A}$. With these values, Eq. 3.24 gives $\theta \doteq 2\frac{1}{2}^{\circ}$ and $\Delta g = 0.67$ mm. A signal current of 100 mA produces an initial flux density of 0.14 Wb/m^2 and initial torque $T_i = 100$ gm. cm; with an estimated inertia of 20 gm.cm^2, the response time $\tau \doteq 4$ millisecs assuming linear undamped motion. The design therefore gives a response compatible with that of the velocity modulator; a more exact calculation follows in Section 3.44.

2. CONSTRUCTION

The cores of the distributor are 3 half-section 'Telcon' grain orientated Silicon steel C- cores, 'HWR $\frac{3}{4}$'. Each core has been wrapped with thin insulating tape and wound directly with as many turns as could be accommodated; the outside cores carry 1500 turns of 40 Gauge enamelled copper wire, and the centre core 1200 turns of 38 Gauge. (the centre coil must be able to carry 40-50 mA standing current whereas the outer coils work with intermittent 80-100 mA current pulses.) The cores have been set in an 'Araldite D' base (Fig.3.31)

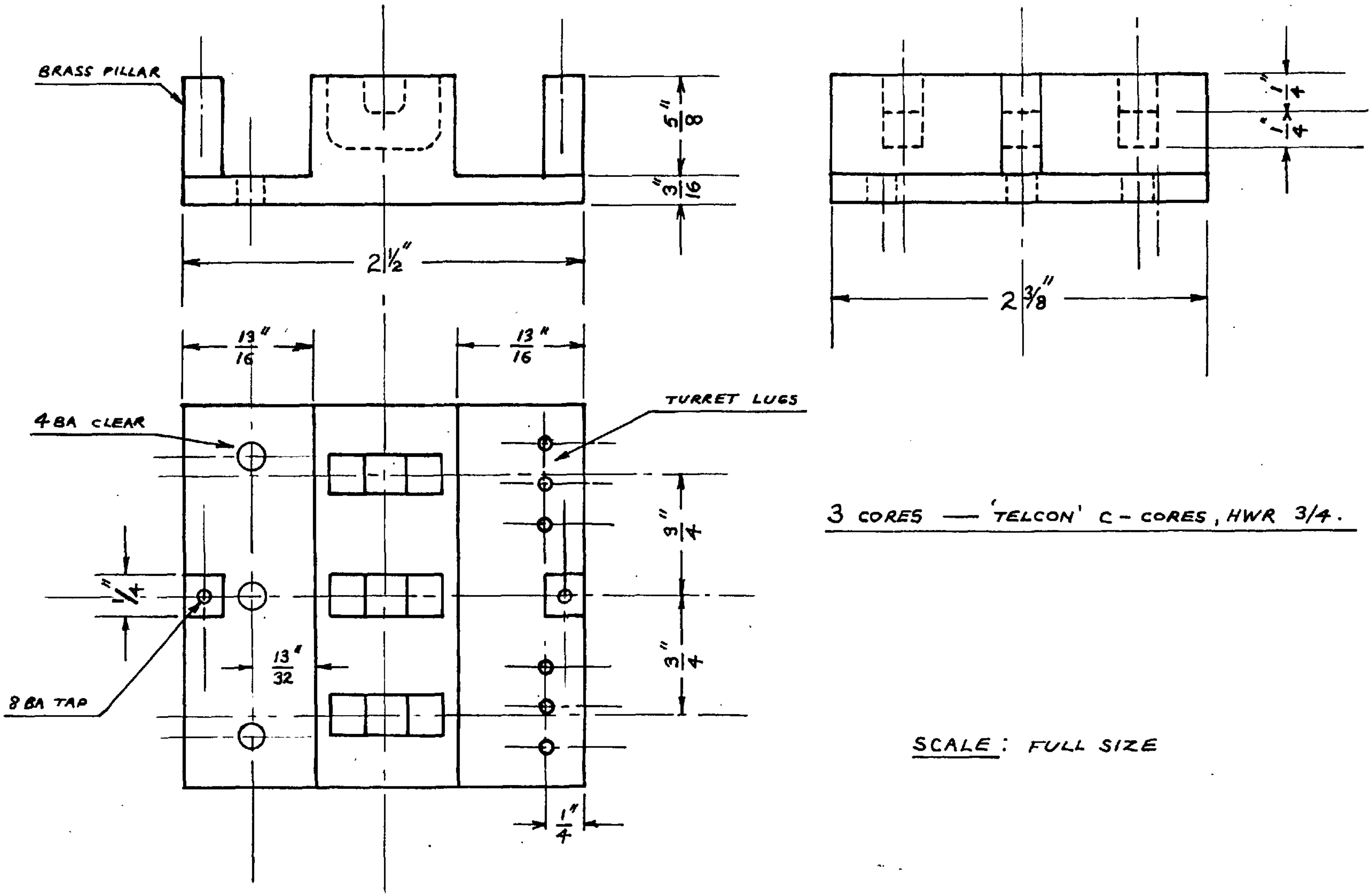

3 CORES — 'TELCON' C-CORES, HWR 3/4.

SCALE: FULL SIZE

FIG. 3·31 SIGNAL DISTRIBUTOR — 'ARALDITE' CORE HOUSING

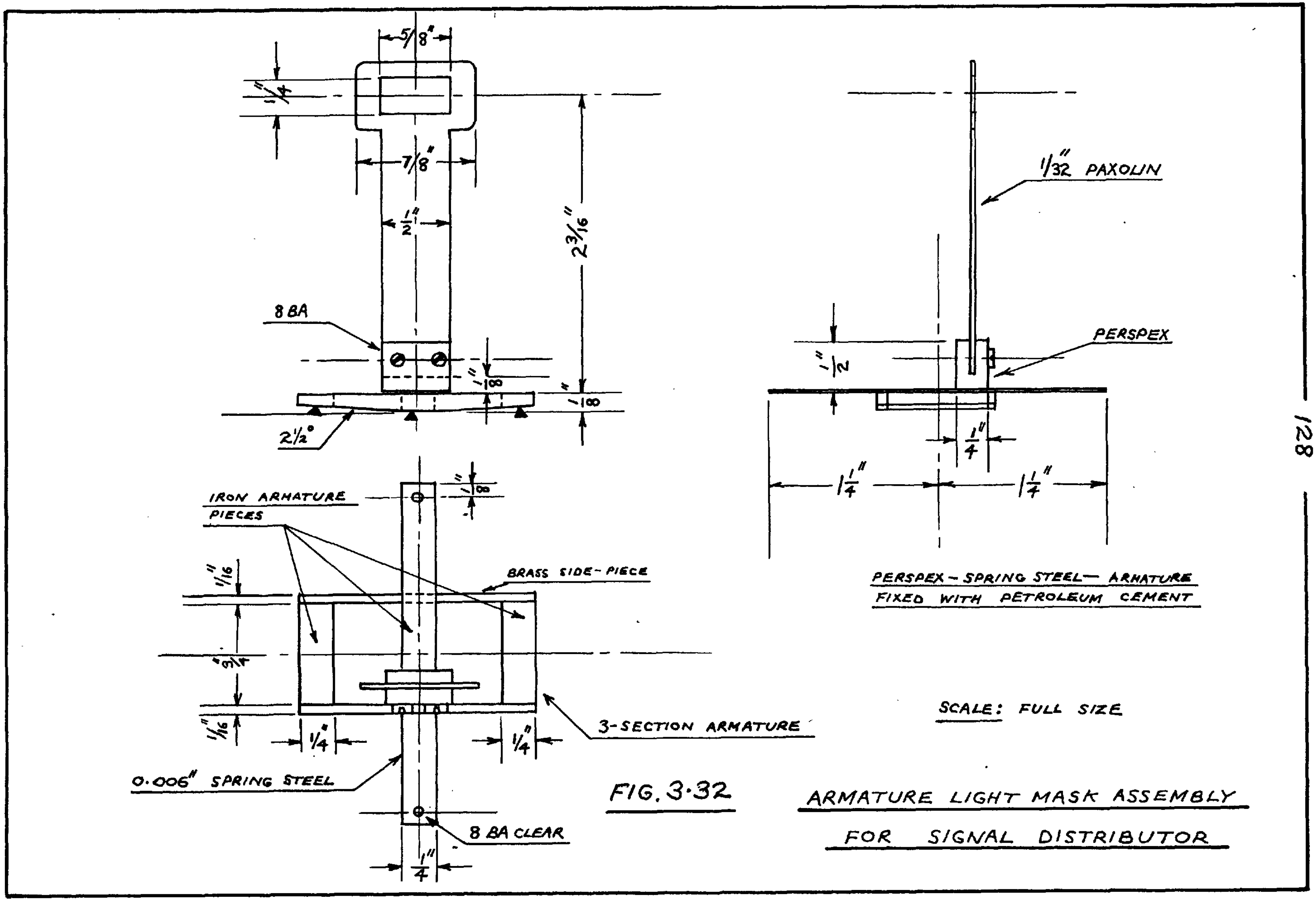

FIG. 3·32

ARMATURE LIGHT MASK ASSEMBLY FOR SIGNAL DISTRIBUTOR and were aligned by casting the base with the cores magnetically attracted to a brass template fixed above a Perspex mould-box. Two brass pillars cemented to the sides of the cast base support the armature assembly (Fig.3.32).

The armature-light mask assembly has been constructed in such a way as to minimise its pertinent inertial moment. The Swedish Iron armature pieces are pinned to light brass side supports and the $2\frac{1}{2}^{\circ}$ tilt was machined after assembly of these pieces. A Paxolin light-mask is carried in a slotted Perspex base cemented onto the central armature piece and possesses a thin cross-section (1/32") in the plane of oscillation. A 0.006" spring steel strip supports the armature assembly on the brass pillars of the distributor base, and its primary function is to ensure that the armature sections line up with the core faces; as a secondary function it also provides a small restoring torque.

The distributor is anchored to the picture transformer base with 4BA screws and the core windings are brought out to turret lugs cast into the Araldite base.

3.44 Theoretical and Experimental Response of the Signal Distributor

(a) THEORETICAL

We now calculate the theoretical response more exactly. The effects of damping, spring restoring torque and core saturation are ignored; we assume an ideal step function of signal current and account for leakage flux and the non-linear magnetic attration law for armature force versus air gap width. Eq. 3.29 above may be written

$$\tau'^{2} = \frac{8(2MR^2 + I_M)\,\theta_o^3 R}{\eta_o\, A\, Rg^2\, \phi g^2} \quad \text{--------- (3.31)}$$

where Rg is the total initial air gap reluctance and ϕg the initial gap flux, with other symbols as before. If the leakage reluctance across the core limbs is R_l, the armature reluctance R_A, and the core yoke reluctance R_Y, then from magnetic circuit considerations we have:

$$\phi g = \frac{(iN)R_l}{R_Y(R_l + R_A + R_g) + R_l(R_A + Rg)} \quad \text{-------- (3.32)}$$

With the relative permeability of silicon steel $\mu_r \doteqdot 10^3$, we have for the $\frac{3}{4}$" core system, $Rg = 2.6 \times 10^7$ AT/Wb, $R_A = R_Y = 6.25 \times 10^5$ AT/Wb and $R_l = 1.25 \times 10^8$ AT/Wb. For $\overline{iN} = 150$ Amp.turns, Eq.3.32 gives $\phi g = 5.4 \times 10^{-6}$ Wb. Inserting $M = 2.2 \times 10^{-3}$ Kgm (calculated), $R = 1.9 \times 10^{-2}$m, $I_M = 5 \times 10^{-7}$Kgm.m^2 (estimated), $\theta_o = 0.04$ rd., $\eta_o = 4 \times 10^{-7}$, $A = 4 \times 10^{-5}$m^2, $Rg = 2.6 \times 10^7$ AT/Wb and $\phi g = 5.4 \times 10^{-6}$ Wb into Eq. 3.31 we have a linear response time $\tau' = 4.5 \times 10^{-3}$ secs.

This evaluation (Eq. 3.31) assumes a linear law of motion i.e. $T = I\ddot{\theta}$; with magnetic attraction we may write the 'Torque Equation' as:

$$I\ddot{\theta}\,(\theta_o - \theta)^2 = T_i\,\theta_o \quad \text{---------- (3.33)}$$

since the attractive force varies inversely as the square of the air gap. T_i is the initial torque at $t = \theta = 0$ and the gap is proportional to $\theta_0 - \theta$ where θ_0 is the angular displacement θ of the inertia I for gap closure. The solution of Eq. 3.33 is given in Appendix 7.22(Eq.9) and is,

$$t = \frac{(I\theta_0)^{\frac{1}{2}}}{(2T_i)} \left\{ \cos^{-1}\sqrt{\theta/\theta_0} + \frac{\pi}{2} - \sqrt{\frac{\theta}{\theta_0}\left(1 - \frac{\theta}{\theta}\right)} \right\} \quad \text{-- (3.34)}$$

this is plotted in normalised form in Fig. 3.33. The total switching time τ is given by Eq. (6) of Appendix 7.22 and is shown to be

$$\tau = \frac{\pi}{4}\tau' \quad \text{------------(3.35)}$$

i,e. the non-linear response is a factor $\pi/4$ faster than the linear response τ'. Obviously in practice, the response will lie between τ and τ' because magnetic saturation occurs before $\theta = \theta_0$ and Eq. 3.33 reverts back to the linear motion case at that instant in time. In the above design, the core commences to saturate when the armature is within about $1/3^\circ$ of its full $2\frac{1}{2}^\circ$ deflection, and therefore we may take $\tau = \frac{\pi}{4}\tau'$ as the undamped response time; $\tau \doteq 3.5 \times 10^{-3}$ secs.

The motion of the distributor mask across the light beams is given by Eq. 3.34 but this response must be weighted by the 'light flux - mask position' relationship which depends upon the mask profile and the geometrical cross section of the light beams. With semi-circular beams and a rectangular mask this weighting is non-linear and asymmetrical. Appendix 7.23 produces the relationship

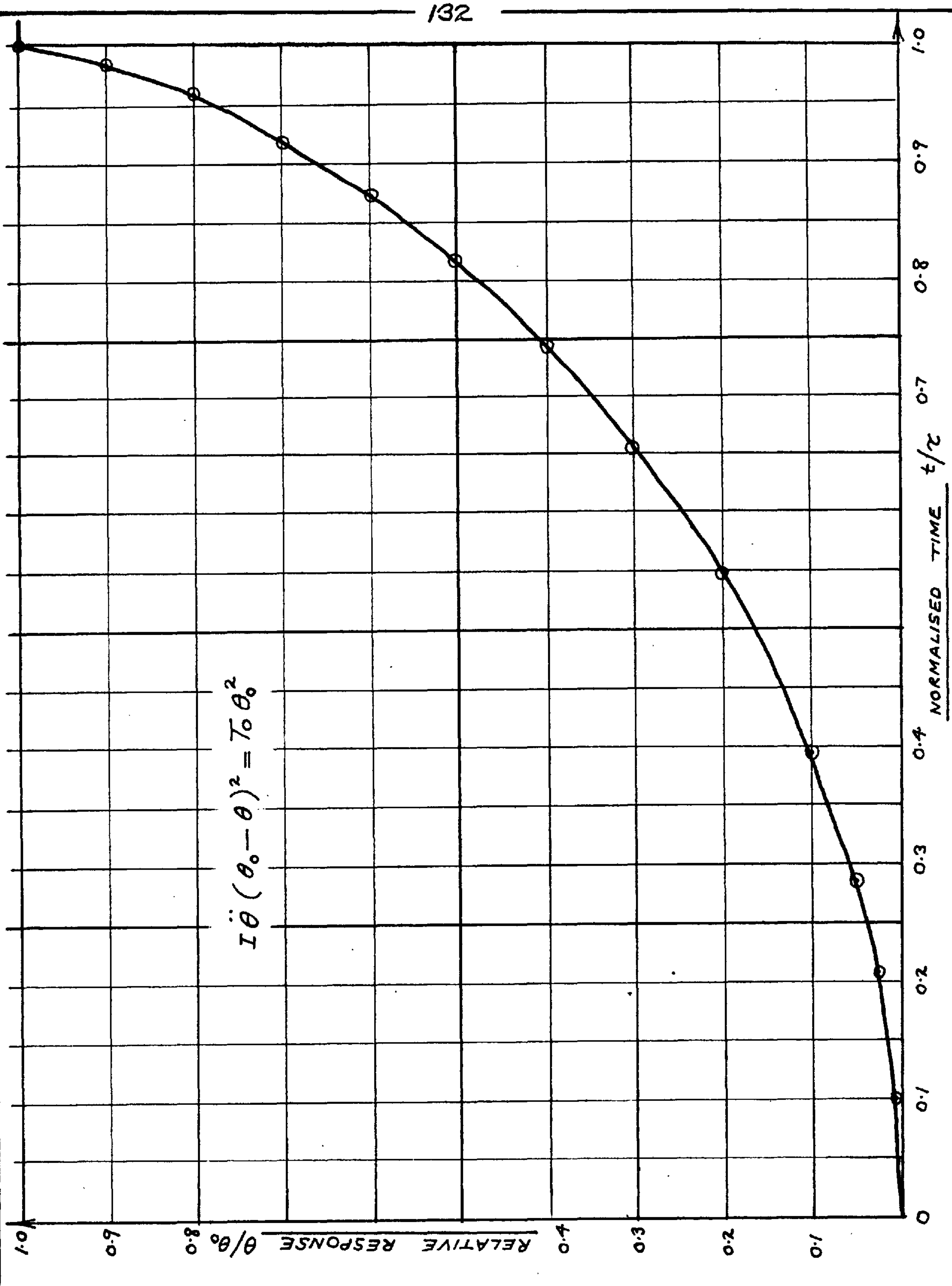

FIG. 3·33 THEORETICAL RESPONSE OF SIGNAL DISTRIBUTOR TO A STEP FUNCTION OF SIGNAL CURRENT

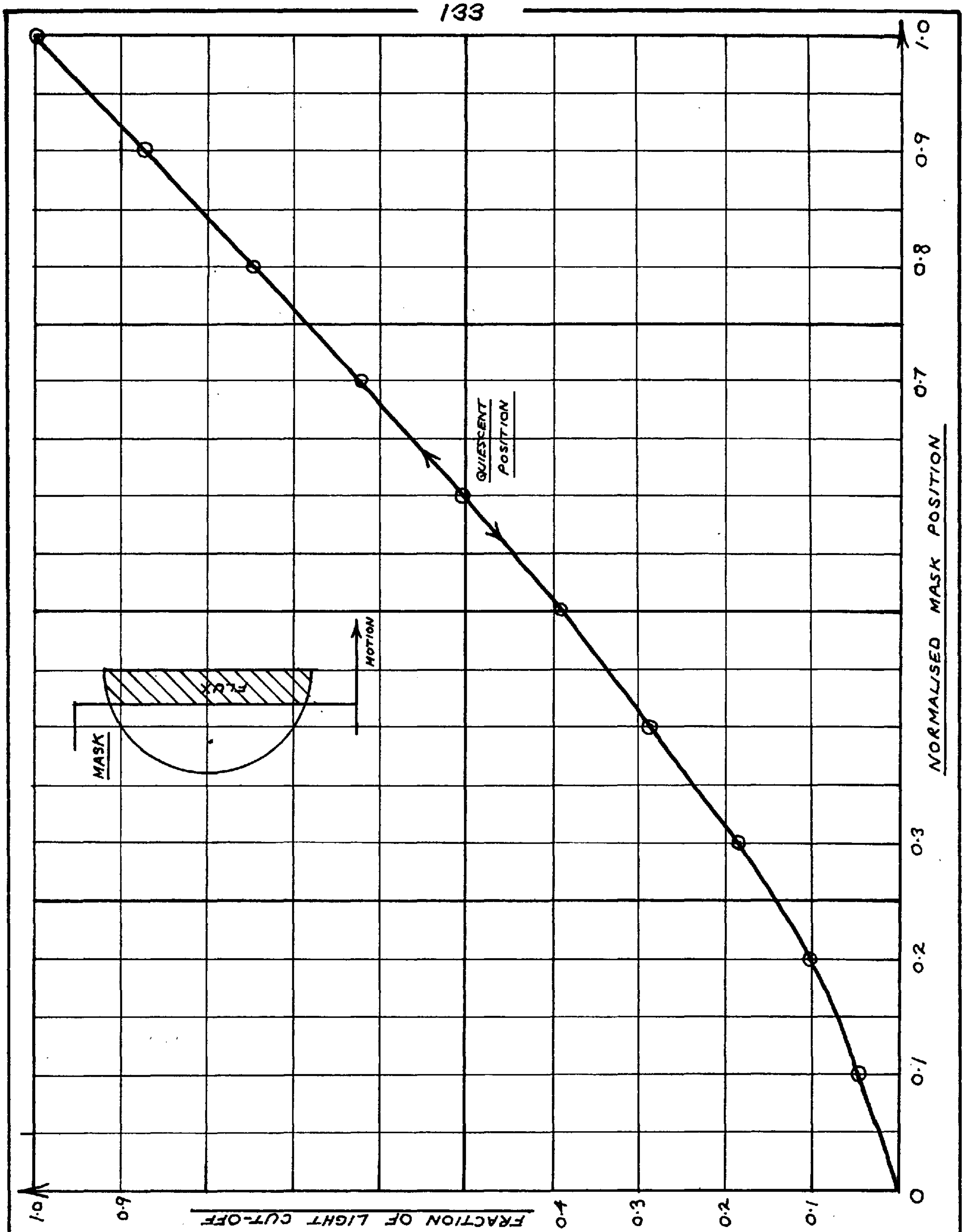

FIG. 3·34 AMPLITUDE WEIGHTING OF SEMICIRCULAR LIGHT BEAM BY A RECTANGULAR MASK between the fraction of light flux transmitted 'λ' and the normalised mask position 'n' (Eq. 11):

$$\lambda = \frac{2}{\pi}\left(\frac{\pi}{2} - \cos^{-1}(1 - n) + (1 - n)(2n - n^2)^{\frac{1}{2}}\right) \quad ----(3.36)$$

and this is plotted in Fig.3.34. The quiescent condition of $\lambda = 50\%$ is achieved when $n \doteq 0.60$. The spot which is cut off disappears before the other is fully weighted i.e. at $n_L = 1$ for the left hand spot (see sketch), the 'right hand spot' $n_R = 0.2$; on the response of Fig.3.34,

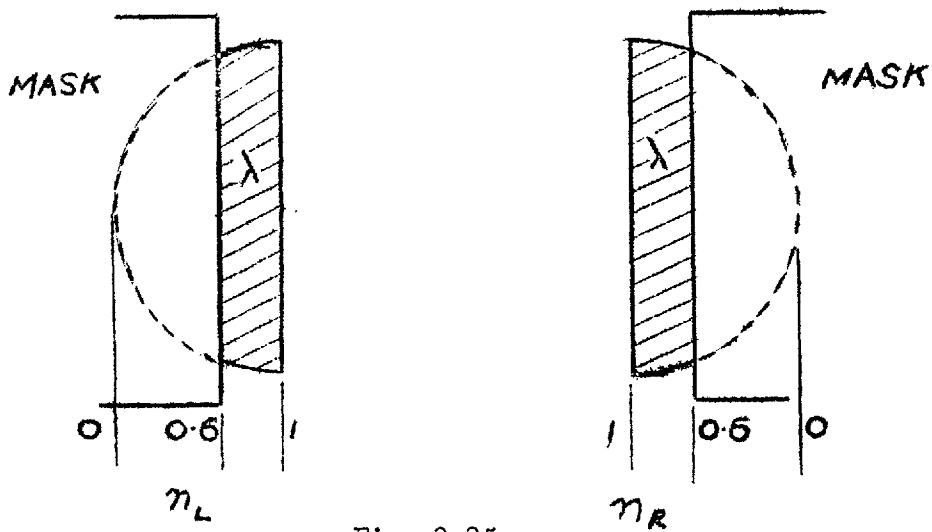

Fig. 3.35

n_R becomes $\theta/\theta_0 = 0.6$ showing that the remaining 20% of the beam flux is transmitted within the remaining 12% of the total response time. We can neglect this order of asymmetry in the distributive switching; the major effect is the non linearity in the response of <u>both</u> sides of the distributor resulting from mask acceleration (Fig. 3.33); on the film record this should sharpen the resultant contour.

(b) EXPERIMENTAL.

The response of the signal distributor has been measured experimentally in two ways:

(i) The switched flux waveform was displayed on an oscilloscope using the control tract of the optical circuit of the picture transformer. The mask height was raised to distribute the pilot beams and a stationary white picture transmitted signal flux back to the photocells. The measured switch time $\tau \doteq 4$ millisecs.

(ii) With one half of the main beam blacked out at the oscillating mirrors, a uniform raster was scanned at about 50 c.p.s. equivalent bandwidth with the signal distributor pulsed with 16 msec pulses at 20 c.p.s. P.R.F. From the known writing speed measured over many lines, the enlarged film record showed the response time as a contrast -hill distance with the interline spacing providing the scale of measurement. The photographically determined switch time $\tau \doteq 5$ millisecs. (this method is inaccurate because an enlarged contrast wedge is not well defined at the end points).

These experimental response times of 4 - 5 millisecs agree well with the theoretical value of around 3.5 millisecs for the ideal undamped distributor.

3.5 REFERENCES

1. MARCONI REVIEW, No. 50, p.27, 1934.

2. WOOD, C.B.B., SHELLEY, I.J., The transmission of News Film over the Transatlantic Cable. I.E.E. Lecture, London, Dec. 3, 1959 (to be published).

3. STRONG, J., Modern Physical Laboratory Practice, Blackie, London, 1946.

4. HOLLAND, L. The Production, Properties, and Uses of Thin Films Condensed in Vacuo, 'Vacuum' 1, No.1, January 1955.

5. TYKOCINSKI - TYCOCINER, J., Transactions of Soc. of Motion Picture Engineers, 16, p.90, (1923)

6. DEBYE, P., SEARS, F.W., Proc. Nat. Academy of Science, U.S. 18, p.410 (1932)

7. TERRY, MUMFORD, HOLLOWAY, Journal of the A.T.E. 11, No.1 January 1955.

8. ZWORYKIN, etc., Transactions of Soc. of Motion Picture Engineers 12, p.748 (1928).

9. CARPENTER, R. o' B., Journ. Acoustical Soc. of America 25 No.6, November 1953.

10. TIBBETTS, Electronics, 16, No. 4, pp 8 - 90,116,118. (1943)

11. DONAL, J.S., LANGMUIR, D.B., A type of Light Valve for Television Reproduction, Proc. I.R.E., 31, pp 208 - 213, (1943).

4. ELECTRONIC CIRCUITS FOR PICTURE TRANSFORMER

4.1 CIRCUIT REQUIREMENTS AND COMPONENTS.

The function of the circuitry is to pulse drive the picture transformer modulators according to the contour searching routine; the inputs to the circuits are derived from the optical control tract via two photocells and are next-but-one line picture signals; the output provides switching instructions to the velocity modulator and signal distributor at a sufficient power level to enable them to operate positively and fast enough to lie inside the maximum horizontal bandwidth of the machine.

The circuit function has been split into two distinct parts; the first is the twin CONTOUR SENSING CIRCUIT which detects contours of pre-selected 'importance' and provides two line trigger pulse trains, indicating contour positions in the two simultaneously scanned lines, which feed the second circuit; this is the MODULATOR CONTROL CIRCUIT which comprises a logical 'tristable' circuit, for the contour searching routine, placed in tandem with a modulator power drive circuit. The general circuit layout is given in Fig. 4.1 and the output connections to the modulator coils are shown in Fig. 4.2. In addition, a pulse generator for CONTOUR SIGNAL SIMULATION was built in order to assist in the development and testing of the tristable circuit. These

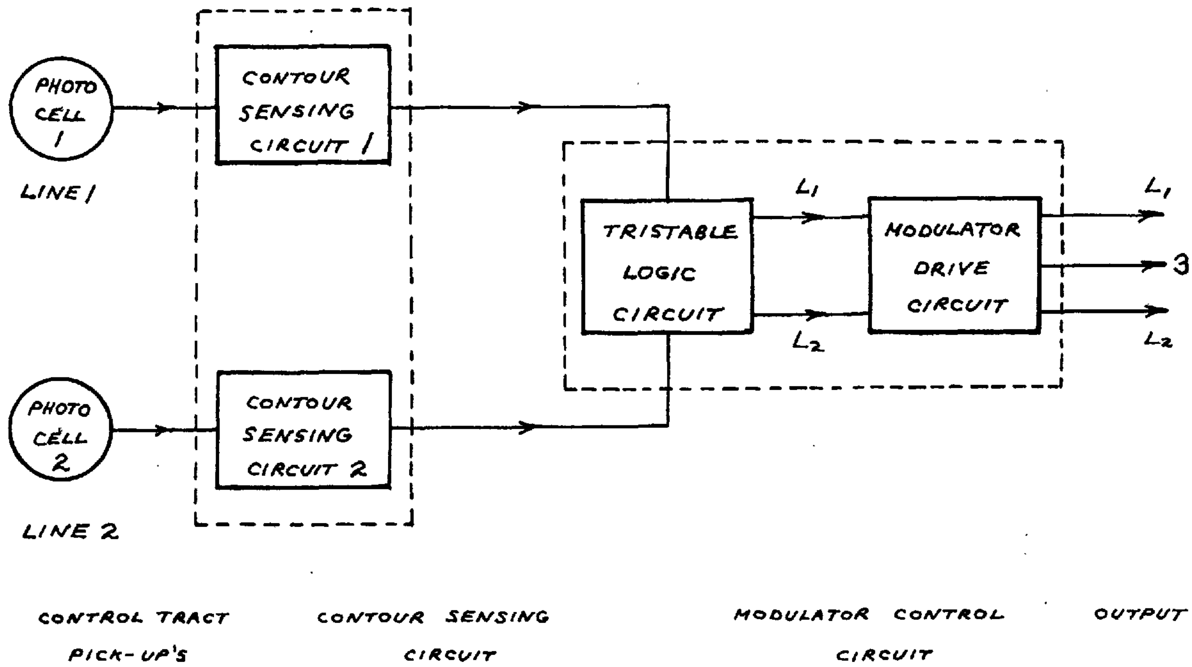

FIG. 4·1 CIRCUITS FOR PICTURE TRANSFORMER.

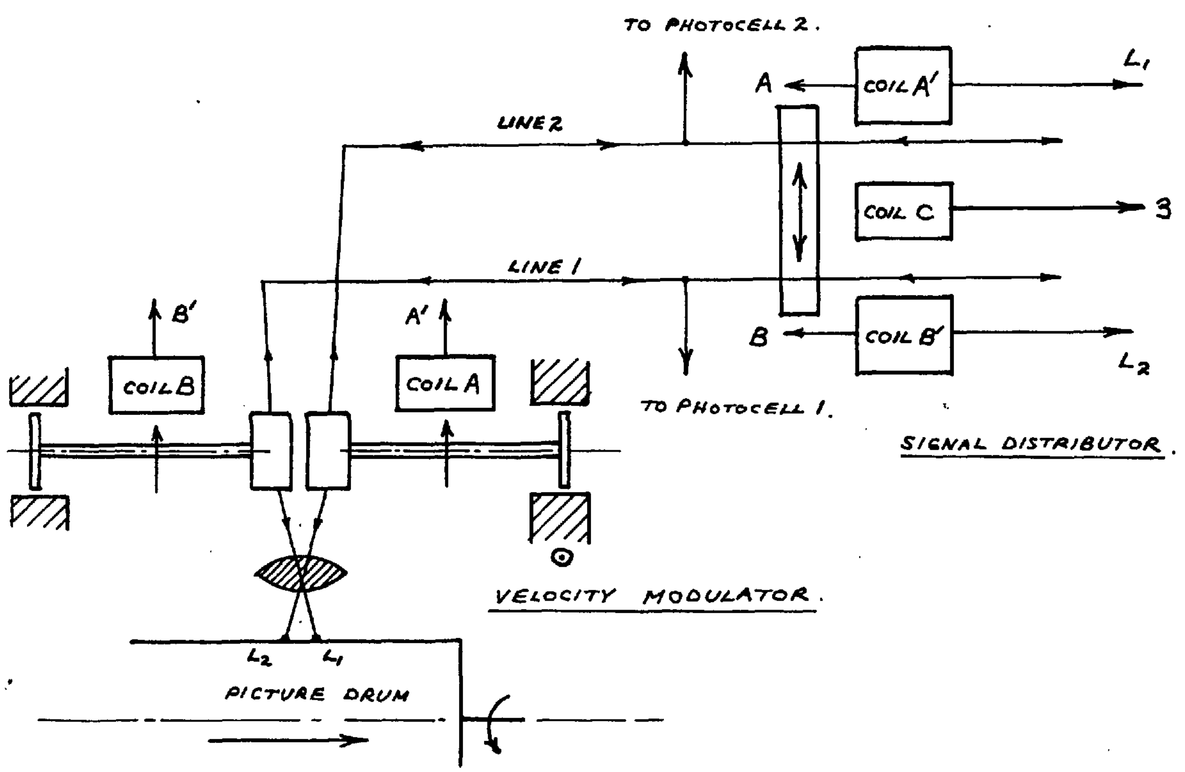

FIG. 4·2 CONNECTIONS TO PICTURE TRANSFORMER MODULATORS component circuits will be described in further detail in turn.

The Contour Sensing, Modulator Control and Contour Simulating Circuits have been built on independent chassiss suitable for 19" rack mounting and utilise separate conventional power supplies.

4.2 THE CONTOUR SENSING CIRCUIT

This comprises two identical channels and provides negative spikes indicating the existence and positions of contours (positive and negative intensity gradients) exceeding a given preset threshold in the two line signals. The contour detectors work on the principle of the picture rate-of-change amplitude criterion; independent gain controls in the two channels prior to variable contour selection allows compensation for unequal optical attenuations in the control tracts to the photocells.

4.21 Circuit Description

The basic layout is shown in Fig. 4.3. The photocell signal of each channel is amplified in two stages before differentiation and further amplification; the resultant contour signal is amplitude selected with equal positive and negative variable threshold levels in both channels, and the gated signal controls a trigger generator for the production of clean negative spikes.

The PHOTOCELL finally chosen was the Cadmium Sulphide Photoconductive cell* with a quoted sensitivity of 3A/lumen in the red region and a bandwidth of around 1Kc/sec. After experimentation, the conventional gas filled photovoltaic cell and phototransistor were rejected, the first from signal/hum considerations and the second on grounds of temperature instability. Referring to Fig. 4.4 the photocell P, which is magnetically screened by a mu-metal can, is brought into the sensing circuit via co-axial leads and is driven by a battery supply (-108 volts) through a load $R_1 = 4.7\ M\Omega$. The cell output, which is 10 mV at most is coupled to the first valve through a magnetically screened capacitor C_3 to the high stability grid resistor R_2; the input time constant is 0.5 sec.

The PRE-AMPLIFIER stage is a low noise, high gain audio pentode V_1 (EF86) providing a voltage gain of 40 dB with a low frequency cut-off of 20 c.p.s; this stage is decoupled by C_1R_6 and is resistance-capacitance coupled (C_6R_7) to a second amplifying stage $V_2/2$ $\left(\frac{1}{2}\ \text{12AX7}\right)$ with a VARIABLE GAIN control R_7; with undecoupled cathode bias (R_8) this half provides a maximum voltage gain of 30 times. M_1 is a low impedance monitoring point for the twin channel gain equalisation and is brought out via screened lead to the chassis front panel.

*These were kindly supplied by Dr. M.E. Haine, Research Manager of the Siemens Edison Swan Research Laboratory, Harlow, Essex.

The DIFFERENTIATOR is a simple RC circuit (C_7R_{12}) followed by a gain stage $V_2/2$ ($\frac{1}{2}$ 12AX7), with an undecoupled cathode bias resistor R_{13}. For 200 c.p.s. maximum working bandwidth, the RC time constant is set below 1msec. such that the picture signal sees a transfer characteristic of $/T(jw)/ = wCR$; with $C_7 = 1000$pF and $R_{12} = 330\ K\Omega$, the time constant is 1/3 msec. and the circuit attenuation at 200 c.p.s. is about 8 dB; the gain stage provides a voltage amplifying factor of 30. Picture signal with amplifier noise is transmitted with a rising frequency characteristic, and the out-of-band noise is rejected by a crude top cut filter C_9R_{14} at which point (M_2) the rate-of-change signal is brought out to a front panel monitoring socket. The complete stage V_2 is decoupled by $R_{10}C_2$.

The CONTOUR AMPLITUDE SELECTOR is a paraphase amplifier V_3 (12AX7) followed by a full-wave rectifier V_4 (6AL5) with variable clipping level (potentiometer R_{20}). The paraphase amplifier is the conventional cathode coupled difference amplifier[1] with one input grounded (R_{18}); with $R_{15} = 47K\Omega$ and R_{16}, R_{17} chosen from 1% $24K\Omega$ resistors, the gain of each half is a measured factor of around 16 with an input voltage capacity of 3 volts p-p. (the theoretical gain per half is $\pm\ \mu R_L/2\ (r_p + R_L)$ under such conditions - $R_K \gg (R_L+r_p)/\mu$, where the symbols have their usual meaning). Resistors R_{21}, R_{20}, R_{19} are chosen such that the top excursion of R_{20} picks off a voltage equal to the quiescent anode voltages of V_3, and the bottom excursion inhibits the maximum undistorted contour signal of 24 volts peak (i.e. 3/2 x 16). The selector potentiometers in the two channels are mechanically ganged. (R20)

Further AMPLIFICATION is provided by a triode stage V_5 ($\frac{1}{2}$12AX7) with a nominal stage gain of 60 times; the clipping action with the negative contour signal produces positive pulses, the leading edges of which indicate contour positions.

The PENTODE LIMITER V_6 (6 AM 6) further sharpens these pulses. This stage is normally non-conducting, bleeder bias being provided by R_{27}, R_{30}. The output pulses are differentiated by C_{15} R_{31} and the diode V_7 ($\frac{1}{2}$ 6AL5) removes the positive spikes.

A CATHODE FOLLOWER V_8 ($\frac{1}{2}$12AT7), with the cathode resistor R_{32} returned to the negative HT line, handles the negative 30 volt spike train and provides the low output impedance necessary for satisfactory operation of the following tristable circuit. This stage is decoupled by $R_{33}C_{16}$.

The normal precautions have been adopted in the circuit layout of the low level high gain stages; juxta-position of different channel leads and components were avoided wherever possible to reduce the possibility of interchannel cross talk and regeneration. The total valve line up of 4 pentodes, 6 double triodes and 3 double diodes mounts on a single 16 gauge tin chassis, and works from single

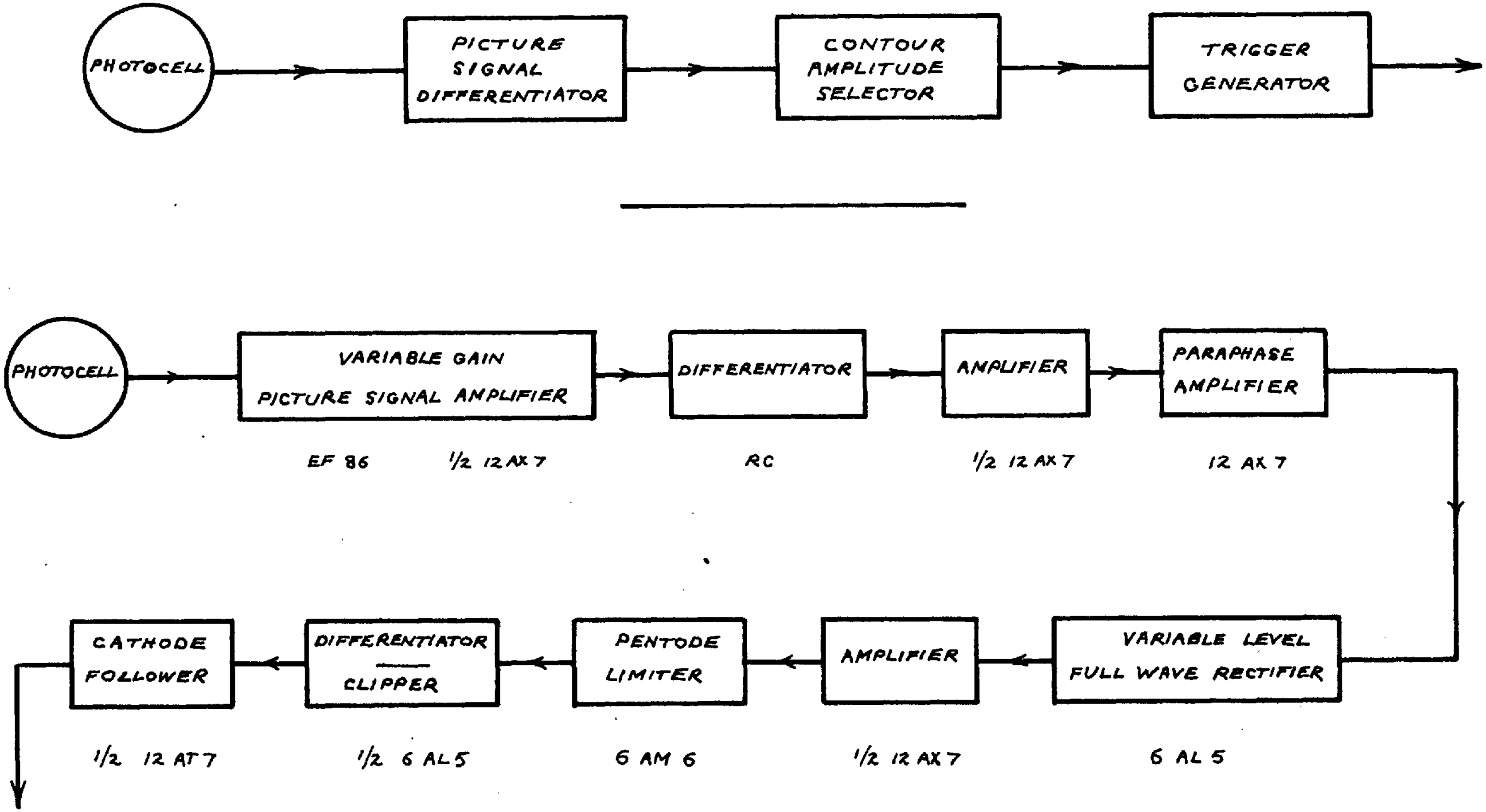

FIG. 4·3 BLOCK SCHEMATIC CONTOUR SENSING CIRCUIT (1 CHANNEL)

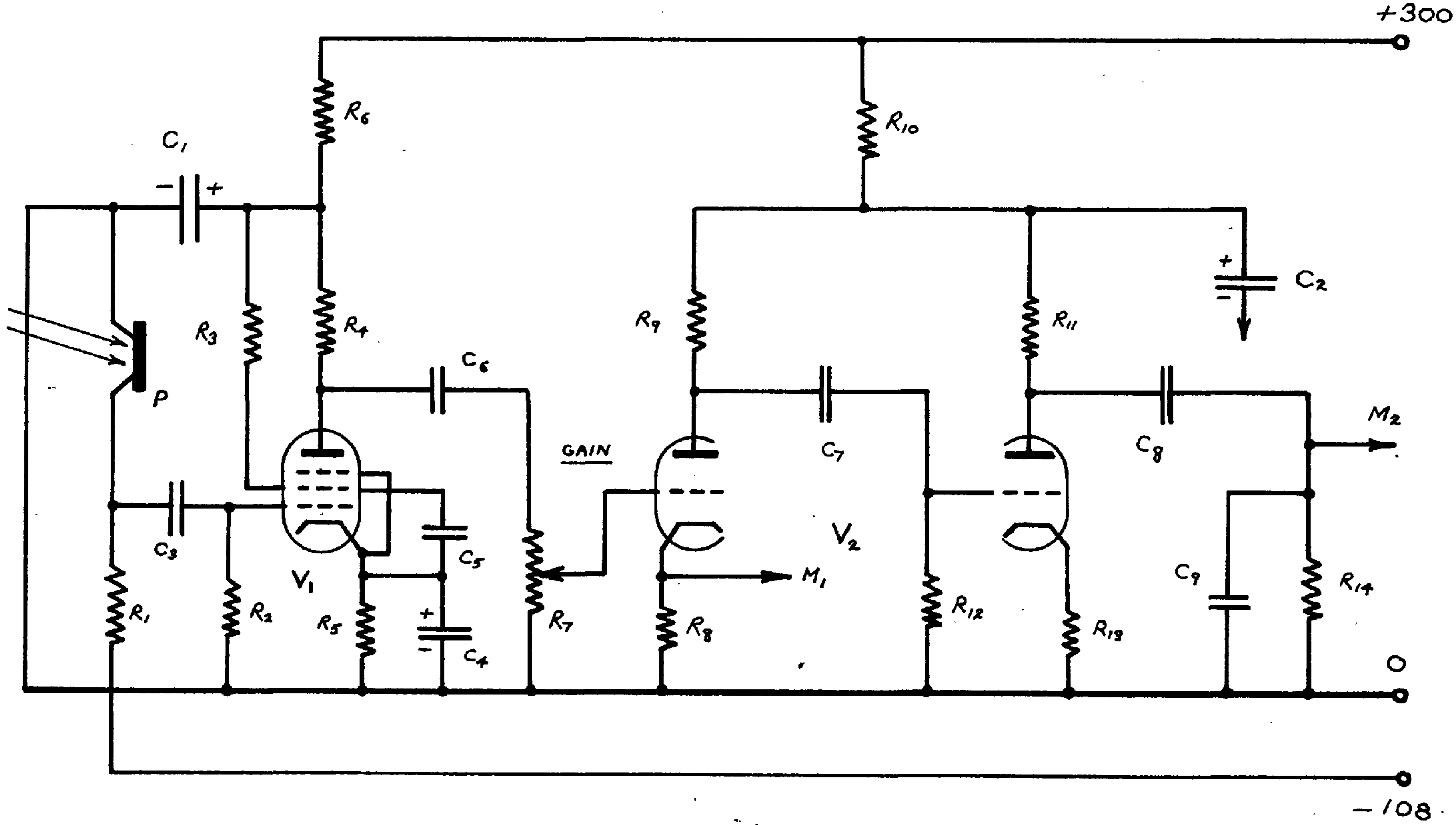

FIG. 4-4 CONTOUR SENSING CIRCUIT — PICTURE SIGNAL DIFFERENTIATOR

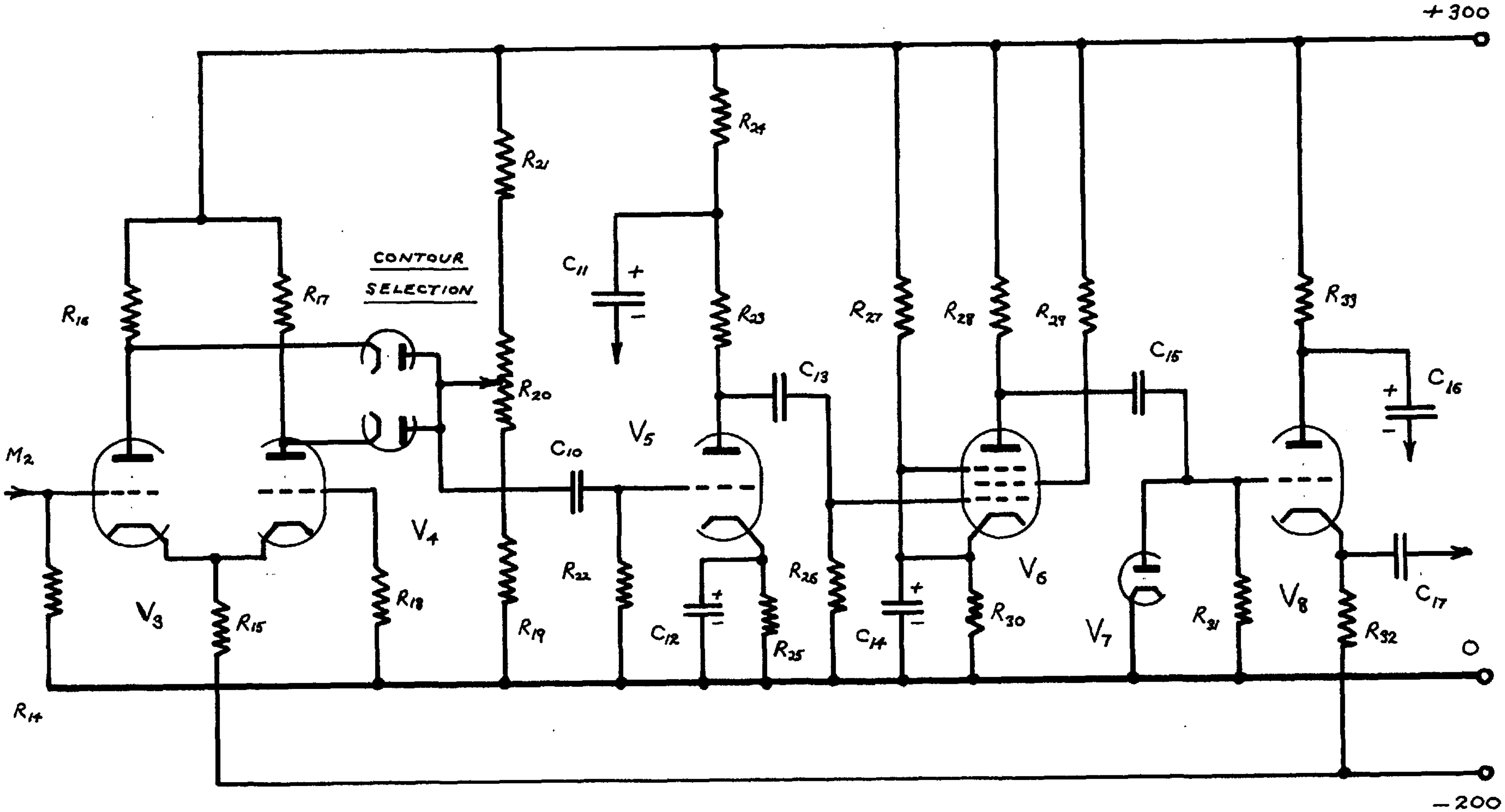

FIG. 4·5 CONTOUR SENSING CIRCUIT — CONTOUR SELECTOR, TRIGGER CIRCUIT stabilised positive and negative H.T. power supplies; to reduce hum to a minimum, the circuit runs on a DC heater supply.

The heater unit was constructed from a 230 - 24 volt transformer, a metal rectifier bridge and a smoothing π network of 2500 μF, 3.7Ω, 2500 μF, providing 3.8 amps at 6.3 volts with a ripple factor of 3½%; the series resistor of 3.7Ω was wound from 120" of 22 Gauge Eureka wire onto a ceramic former.

A graduated scale is provided for the dual contour selector potentiometer setting.

<u>4.22 Components for Contour Sensing Circuit (one Channel)</u>

RESISTORS:

R_1	4.7MΩ	1% H.S.	¼W	R_{11}	270KΩ	10%	¼W
R_2	1 M	1 H.S.	¼W	R_{12}	330K	10	¼W
R_3	390K	10	¼W	R_{13}	3.9K	10	¼W
R_4	100K	1 H.S.	½W	R_{14}	470K	10	¼W
R_5	1 K	10	¼W	R_{15}	47 K	10	1W
R_6	15 K	10	1W	R_{16}	24 K	1 H.S.	1W
R_7	500K	LOG. VARIABLE		R_{17}	24 K	1 H.S.	1W
R_8	3.9K	10	¼W	R_{18}	470K	10	¼W
R_9	270K	10	¼W	R_{19}	820K	10	¼W
R_{10}	33 K	10	3W	R_{20}	100K	LINEAR GANGED POT.	

RESISTORS (continued):

R_{21}	150K Ω	10%	$\frac{1}{4}$W	R_{28}	22 K Ω	10%	$\frac{3}{4}$W
R_{22}	1 M	10	$\frac{1}{4}$W	R_{29}	22 K	10	$\frac{3}{4}$W
R_{23}	270K	10	$\frac{1}{4}$W	R_{30}	2.7K	10	1W
R_{24}	33K	10	1W	R_{31}	100K	10	$\frac{1}{4}$W
R_{25}	3.9K	10	$\frac{3}{4}$W	R_{32}	47 K	10	$\frac{3}{4}$W
R_{26}	470K	10	$\frac{1}{4}$W	R_{33}	3.3K	10	1W
R_{27}	100K	10	$\frac{1}{4}$W				

CAPACITORS:

C_1	32 uF, 350v, Electrolytic.	C_{10}	0.05uF, Paper
C_2	16 uF, 350v, Electrolytic.	C_{11}	16 uF, 350v, Electrolytic.
C_3	0.5uF 350v, Paper.	C_{12}	25 uF, 25v,Electrolytic.
C_4	50 uF, 50v, Electrolytic.	C_{13}	0.05uF, 350v, Paper.
C_5	0.05uF, 350v, Paper	C_{14}	25 uF, 25v, Electrolytic.
C_6	1 uF, 350v, Paper.	C_{15}	120pF, Ceramic
C_7	1000pF, Ceramic	C_{16}	16 uF, 350v, Electrolytic.
C_8	0.1uf, 350v, Paper	C_{17}	0.02uF, 350v, Paper.
C9	0.05uF, 350v, Paper		

VALVES:

V_1	EF 86	V_5	$\frac{1}{2}$ 12 AX 7
V_2	12 AX 7	V_6	6 AM 6
V_3	12 AX 7	V_7	$\frac{1}{2}$ 6 AL 5
V_4	6 AL 5	V_8	$\frac{1}{2}$ 12 AT 7.

4.3 THE TRISTABLE CIRCUIT

The function of the tristable circuit is to pulse drive the Picture Transformer modulator control circuits in a way dependent upon the presence (or not) and inter-train time-displacement of trigger pulses in the two trains of contour signals derived from the contour sensing circuit.

The circuit must operate bi-symmetrically; the arrival of a pulse on either channel indicates a detected contour and the next pulse to arrive on the other channel within a period $\tau > \tau_{MAX}$, where $\tau_{MAX} = \Delta X_{MAX}/2V_S$, indicates the other end of the contour successfully found by the velocity modulator scanning at velocity $2V_S$. This operation can be conveniently condensed into a logic table (Table 4.1)

TABLE 4.1

	LINE 1	LINE 2	CONTOUR	OUTPUT 1	OUTPUT 2
1.	no pulse	no pulse	zero	zero	zero
2.	pulse, t=o	pulse, t=o	vertical	zero	zero
3.	pulse, t=o	no pulse up to t $=T_{MAX}$	Horizontal slope $> -\Delta t/\tau_{MAX}$	rectangular pulse, duration T_{MAX}	zero
4.	pulse, t=o	pulse, t=T with $T < T_{MAX}$	horizontal slope $-\Delta t/\tau$	rectangular pulse, duration T	zero
5.	no pulse up to t= T_{MAX}	pulse, t=o	horizontal slope $< +\Delta t/\tau_{MAX}$	zero	rectangular pulse, duration T_{MAX}
6.	pulse, t =T with $T < T_{MAX}$	pulse, t=o	horizontal slope $+\Delta t/\tau$	zero	rectangular pulse, duration T.

In the table, Δt is the picture element period dependent upon scanning velocity V_S and $\tau_{MAX} = \Delta X_{MAX} / 2V_S$; there is obviously an advantage in inhibiting the modulators for very near-vertical contours.

4.31 Functional Design and Operation

The realisation of the above logic table using conventional circuits with certain modifications is shown schematically in Fig.4.6; (V_1, V_2) and (V_3, V_4) are direct coupled monostable gates, A and B are amplitude selector gates, and D_1, D_2 short delay units; assuming A and B to be open, and the timing circuits to be in their monostable state (V_1 and V_3 conducting only), operation is as follows:

A trigger, say on line 1, is allowed through 'A' and flips V_2 into conduction, thus initiating the timing action of (V_1, V_2) and closing gate 'B' after a short delay (D_2) by transmitting a suitable pulse from V_2 cathode k_2; V_4 is unaffected by the arrival of the trigger at its grid g4. The timing action of the triggered gate ensues until either,

(i) (V_1, V_2) completes its quasi-stable period T_{MAX} if during that time no trigger is received by line 2; the entire circuit is then quiescent with 'B' open once more. During this period, a spurious trigger on line 1 leaves V_1 and V_4 unaffected. The output pulse is taken from V_1 anode 'a', and is positive, rectangular and of duration T_{MAX}.

or (ii) a trigger arrives on line 2 within the timing period of (V_1, V_2) and is blocked by the closed gate B; this extinguishes

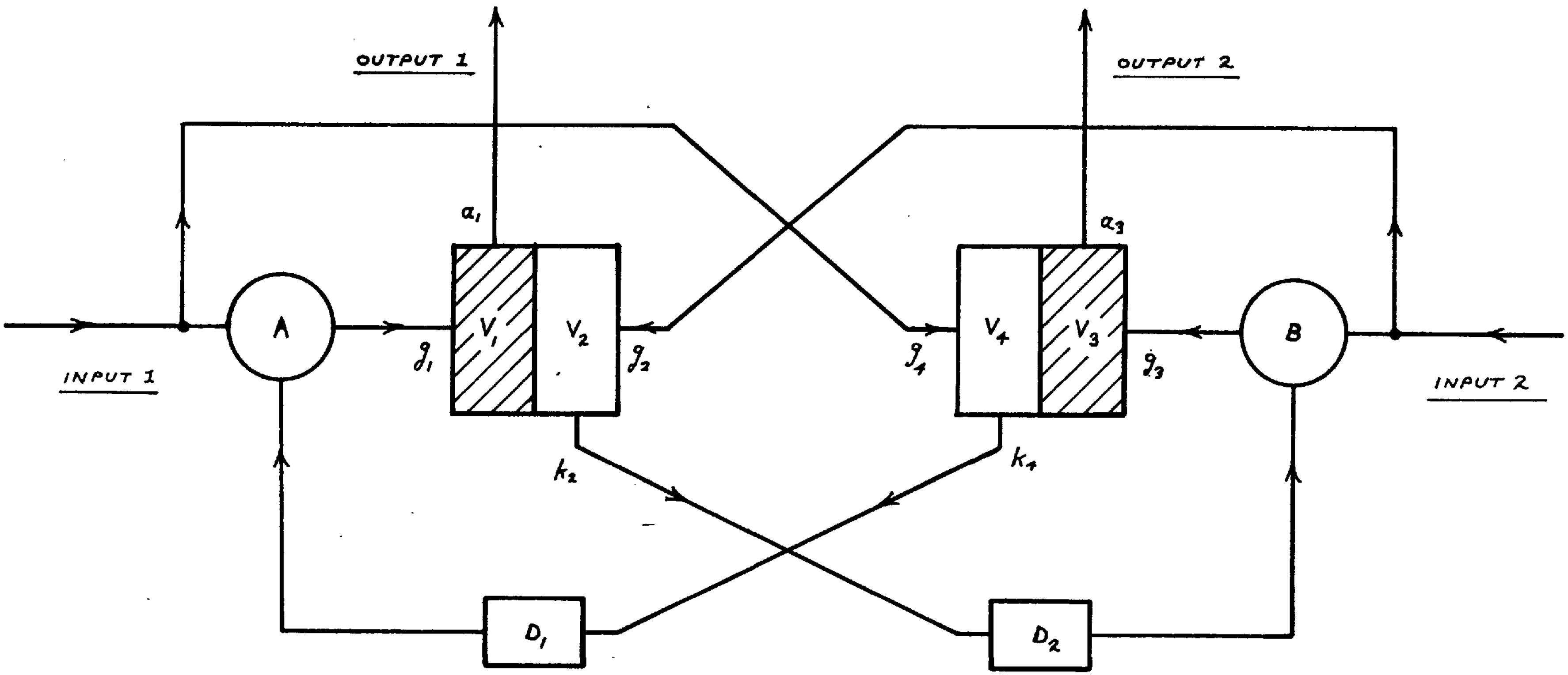

(V_1, V_2), (V_3, V_4) —— DIRECT COUPLED MONOSTABLE GATES. D_1, D_2 —— DELAY.

A, B —— 'AND' GATES DIRECT COUPLED TO CATHODES k_4, k_2 VIA D_1, D_2.

FIG. 4·6 BLOCK SCHEMATIC 'TRISTABLE' CIRCUIT FOR CONTOUR INTERPOLATION the timing action by rendering V_2 non-conducting on its grid g_2. Gate B is opened after a short delay (D_2), necessary to ensure that the trigger on line 2 has decayed sufficiently before B is finally opened. A shortened rectangular pulse is delivered by V_1 anode a_1.

This action is similar if the initial pulse is received by line 2 since the circuit topography is symmetrical about a mid-vertical line. The design of the timing circuits and gates may now be specified.

4.32 The Timing Circuits. (and Delays)

These must fulfil the following requirements:

(i) Circuit must be monostable and triggered with negative spikes.

(ii) Timing periods must be variable over range 5 - 80 msecs.

(iii) Circuit must possess a quenching facility, operational with negative spikes, but non-operational if triggered in the monostable state.

(iv) Circuit must supply a gating pulse which can be direct coupled to an 'and' gate, in addition to providing a large output pulse if triggered.

(v) The d-c gating pulse must be delayed by at least one trigger pulse period.

The circuit adopted is shown in Fig. 4.7 (a); it is a conventional D.C. Gate[2] developed to comply with the above specification; R_{k1}, R_{k2} and the diode trigger injector are normally omitted; V_2 is conducting in the monostable state. Design is as follows:

(1) R_{L1} and R_{L2} chosen to give large gain in regenerative switching; actually $R_{L1} = R_{L2}$.

(2) R_{K1} chosen to provide a gating pulse of adequate amplitude maintaining the condition $R_L \gg R_K$

(3) R_1 and R_2 are large compared with R_L and the ratio R_1/R_2 is adjusted to render V_1 normally cut-off with a convenient negative H.T. value.

(4) C and R chosen to cover the timing period range 5 to 80 msecs, C in steps and R continuously.

(5) To ensure identical operation of both D.C. Gates, R_{L1}, R_{L2}, R_1 and R_2 are 1% resistors in both circuits.

(6) The cross-gating delay is effected by delaying the cathode pulse waveform with the minimal capacitor C_K.

The quenching regeneration action is similar to the orthodox initiation, with D_2 acting as the trigger injection diode.

4.33 The Gate Circuits

These must fulfil the following requirements:

(1) The gate must be controlled by direct-coupled rectangular pulses derived from a low impedance.

(ii) It must handle negative trigger pulses.

(iii) Negative spikes must be supplied from a low impedance and

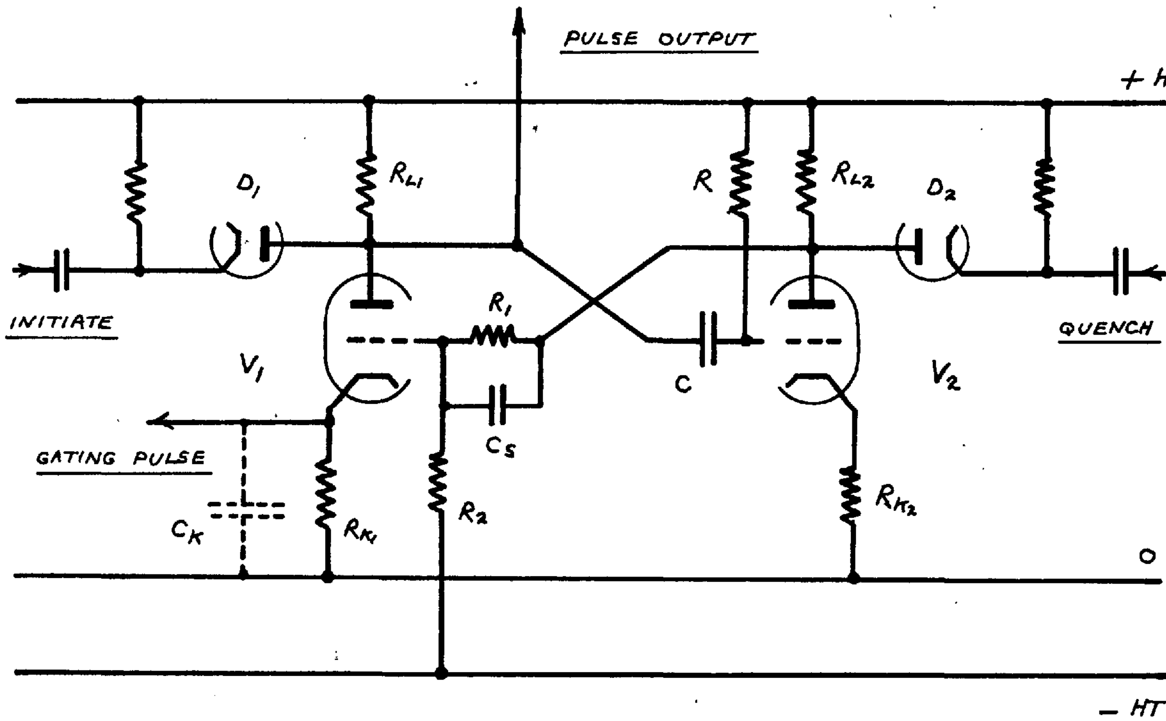

FIG. 4·7

(a) D.C. GATE WITH QUENCHING FACILITY AND GATING PULSE OUTPUT.

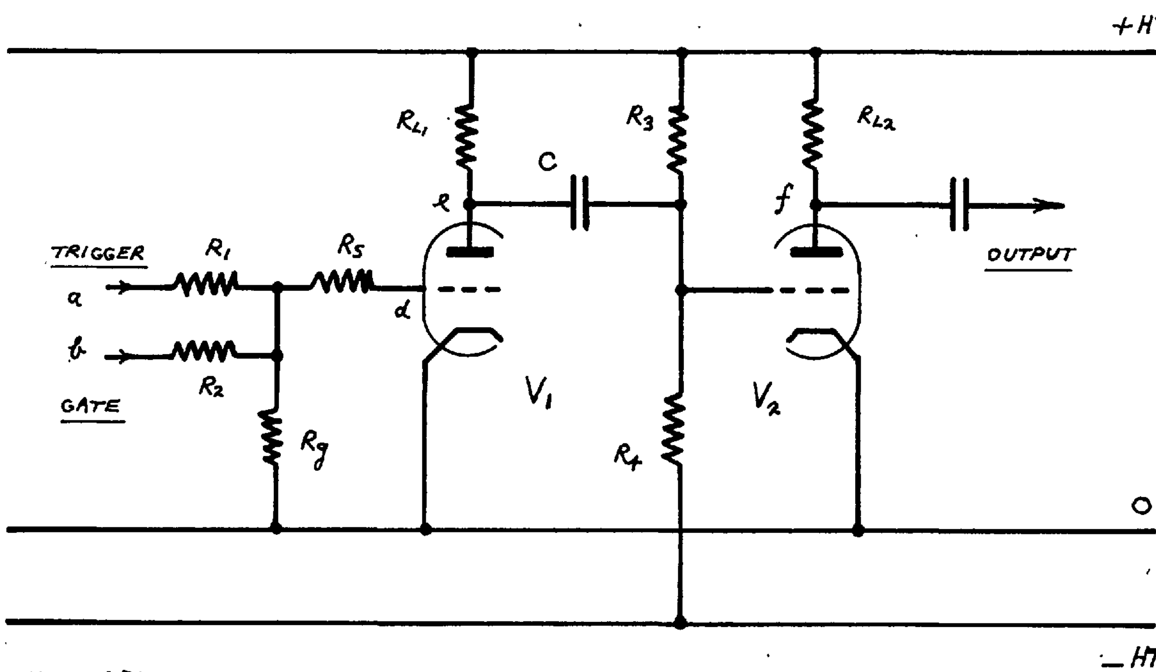

FIG. 4·7

(b) DOUBLE TRIODE AMPLITUDE SELECTOR GATE.

isolated from the gating waveform source.

The circuit adopted is a double-triode amplitude selector circuit shown in Fig. 4.7(b), (the valve (V_1, V_2) replacing the diode in the conventional selector[3] to achieve input-output isolation). The input circuit R_1, R_2, R_5, R_g sums the trigger and gating waveforms and V_1 inverts the resultant signal; V_2 is non-conducting with bleeder bias R_3, R_4 and the trigger is delivered to the output only if the gating line b (R_2) is held at zero potential such that the summed waveforms at V_2 grid exceeds the grid-base.

Design is as follows:

(1) R_1, R_2, Rg comprise an adding circuit in which $R_1 = R_2 \ll Rg$ and $R_2 \gg R_{K1}$; R_5 is a grid stopper.

(2) R_{L1} is large enough to provide sufficient gain in V_1 to allow V_2 to clip satisfactorily between wanted and unwanted signals.

(3) R_3 and R_4 are large and R_3/R_4 is chosen to allow satisfactory clipping of the gating waveform from the 'sum' signal.

(4) R_{L2} chosen to provide fast pulses of sufficient amplitude to initiate the above D.C. gates.

4.34 Components for the Tristable Circuit

The complete circuit diagram is given in Fig.4.8; (V_2 and V_3 are the D.C. Gates, V_1 and V_4 the amplitude gates) S_1 and S_2 are

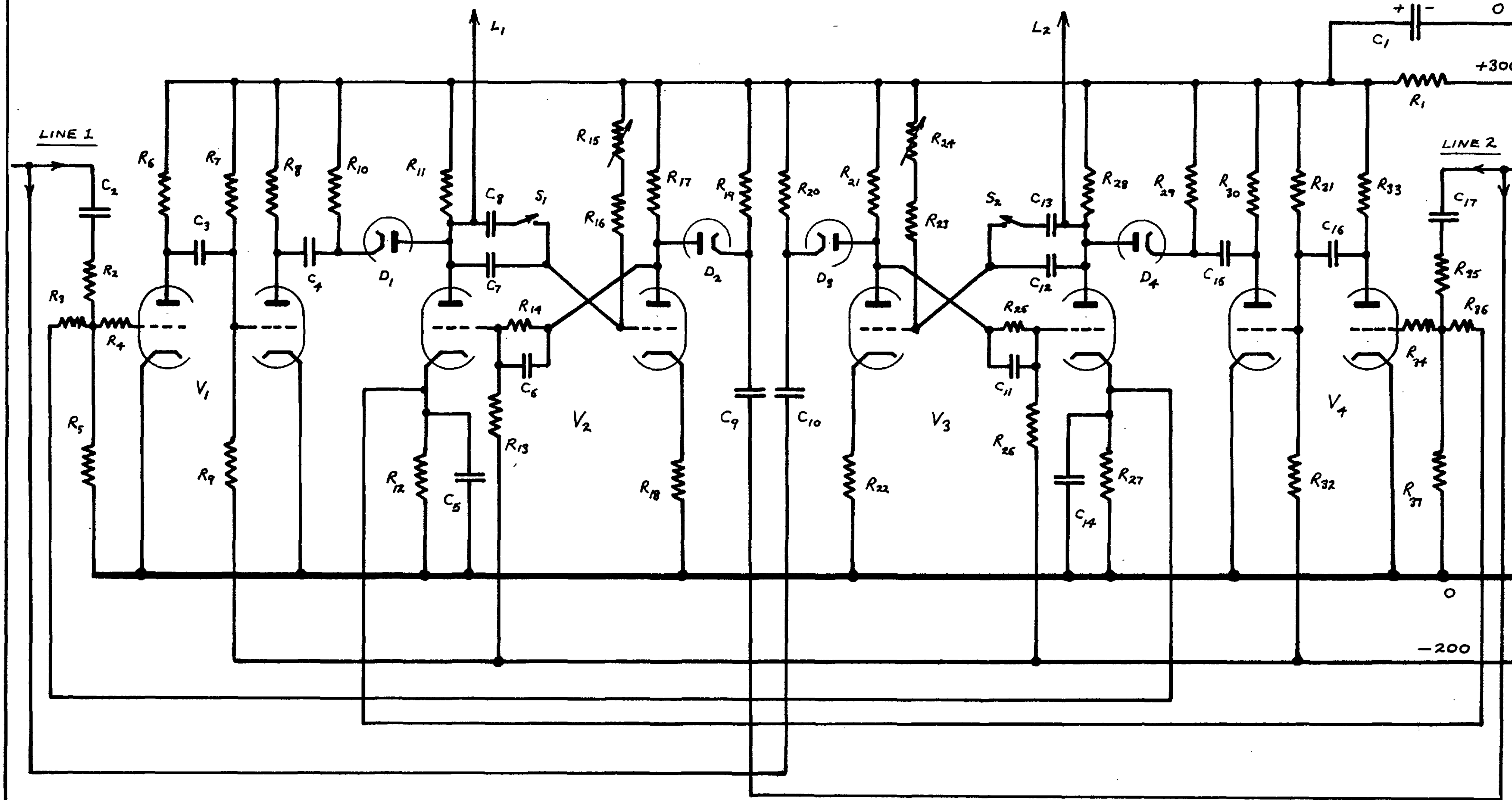

FIG. 4·8 MODULATOR CONTROL CIRCUIT FOR CONTOUR INTERPOLATION single pole switches providing 'LONG' and 'SHORT' timing period ranges and the scale calibrations for R_{15} and R_{24} potentiometers are given below in Table 4.2:

Table 4.2

DIAL POSITION	S_1, S_2 open SHORT PERIOD (mS)	S_1, S_2 closed LONG PERIOD (mS)
0	5	14
1	6.5	15
2	8	16.5
3	9	20
4	10	25
5	11	30
6	12	40
7	13	55
8	14	60
9	15	65
10	16	70

Referring to Fig. 4.8, the Components are as follows:

RESISTORS:

R_1	3.3KΩ	5%	3W	R19	100KΩ	10%	$\frac{1}{4}$W
R_2	27 K	10	$\frac{1}{4}$W	R_{20}	10 K	1	$\frac{3}{4}$W
R_3	220K	10	$\frac{1}{4}$W	R_{21}	1.5K	10	$\frac{1}{4}$W

RESISTORS (cont.)

R_4	10 KΩ	10%	$\frac{1}{4}$W
R_5	220K	10	$\frac{3}{4}$W
R_6	1M	10	$\frac{1}{4}$W
R_7	470K	10	$\frac{1}{4}$W
R_8	4.7K	10	$\frac{3}{4}$W
R_9	100K	10	$\frac{1}{4}$W
R_{10}	10 K	1	$\frac{3}{4}$W
R_{11}	1.5K	10	$\frac{1}{4}$W
R_{12}	470K	1	$\frac{1}{4}$W
R_{13}	470K	1	$\frac{1}{4}$W
R_{14}	5M	Variable	Linear
R_{15}	1M	10	$\frac{1}{4}$W
R_{16}	1.5K	10	$\frac{1}{4}$W
R_{17}	10 K	1	$\frac{3}{4}$W
R_{18}	100K	10	$\frac{1}{4}$W

R_{22}	1MΩ	10%	$\frac{1}{4}$W
R_{23}	5M	Variable	Linear
R_{24}	470K	1	$\frac{1}{4}$W
R_{25}	470K	1	$\frac{1}{4}$W
R_{26}	1.5K	10	$\frac{1}{4}$W
R_{27}	10 K	1	$\frac{3}{4}$W
R_{28}	100K	10	$\frac{1}{4}$W
R_{29}	4.7K	10	$\frac{3}{4}$W
R_{30}	1M	10	$\frac{1}{4}$W
R_{31}	470K	10	$\frac{1}{4}$W
R_{32}	10K	10	$\frac{3}{4}$W
R_{33}	220K	10	$\frac{1}{4}$W
R_{34}	27K	10	$\frac{1}{4}$W
R_{35}	27K	10	$\frac{1}{4}$W
R_{36}	220K	10	$\frac{1}{4}$W

CAPACITORS:

C_1	16uF, 350v Electrolytic
C_2	0.001uF, Paper
C_3	0.001uF, Paper
C_4	0.001uF, Paper
C_5	0.02 uF, Paper

C_{11}	0.001uF, Paper
C_{12}	56pF, Ceramic
C_{13}	0.03 uF, Paper
C_{14}	0.05 uF, Paper
C_{15}	0.1 uF, Paper

CAPACITORS (cont.)

C_6	56 pF, Ceramic	C_{16}	0.02uF, Paper
C_7	0.03uF, Paper	C_{17}	0.001uF, Paper
C_8	0.05uF, Paper	C_{18}	0.001uF, Paper
C_9	0.1uF, Paper	C_{19}	0.001uF, Paper
C_{10}	0.001uF, Paper		

VALVES:

V_1	12 AT 7	V_4	12 AT 7
V_2	12 AT 7	(D_1,D_2)	6 AL 5
V_3	12 AT 7	(D_3,D_4)	6 AL 5

4.4 THE MODULATOR DRIVE CIRCUIT.

The modulator drive circuit accepts the negative output 'searching' pulses from the tristable circuit, and produces 80 mA current pulses suitable for driving the velocity modulator and signal distributor coils in series in each channel.

4.41 Circuit Description

The circuit is given in Fig. 4.9. L_1 and L_2 are derived from similarly labelled points in the tristable circuit (Fig. 4.9) and the input pulses are coupled into PENTODE LIMITERS V_1 and V_2 via the 8 sec. time constant grid circuits R_1C_1, R_2C_2; V_1 and V_2 normally conduct heavily, R_3 and R_4 are grid stoppers. The inverted clipped positive pulses are direct-coupled to POWER PENTODES, V_3 and V_4, which are normally non-conducting with their control grids returned to the negative HT line; C_3 and C_4 are 'speed-up' capacitors, and R_{13},R_{14} grid stoppers. Clipped 200 V.pulses at the grids of V_3 and V_4 render these valves heavily conducting and drive the modulator coils Z_1,Z_2 with 80 mA current pulses of 10 μsec rise time.

The centre coil of the signal distributor Z_3 is driven by a third power valve V_5 which is normally conducting with its grid resistor R_{22} taken up to the positive HT line; this driving current of 50 mA is cut off if either V_3 or V_4 conduct by transmitting a negative pulse via the adding circuit R_{19}, R_{20} and R_{22}; Resistors R_{15} and R_{16} provide this voltage pulse and also limit the dissipation in V_3 and V_4; R_{23} limits the quiescent current in V_5.

The connections to the modulator coils Z_1, Z_2, and Z_3 are given in Fig. 4.1; Z_1 is the series combination of coils A and A^1, Z_2 the series combination of coils B and B^1, and Z_3 the signal distributor coil C.

This circuit, together with the tristable unit constitute the Modulator Control Circuit and the complete circuit has been constructed on a single 19" chassis.

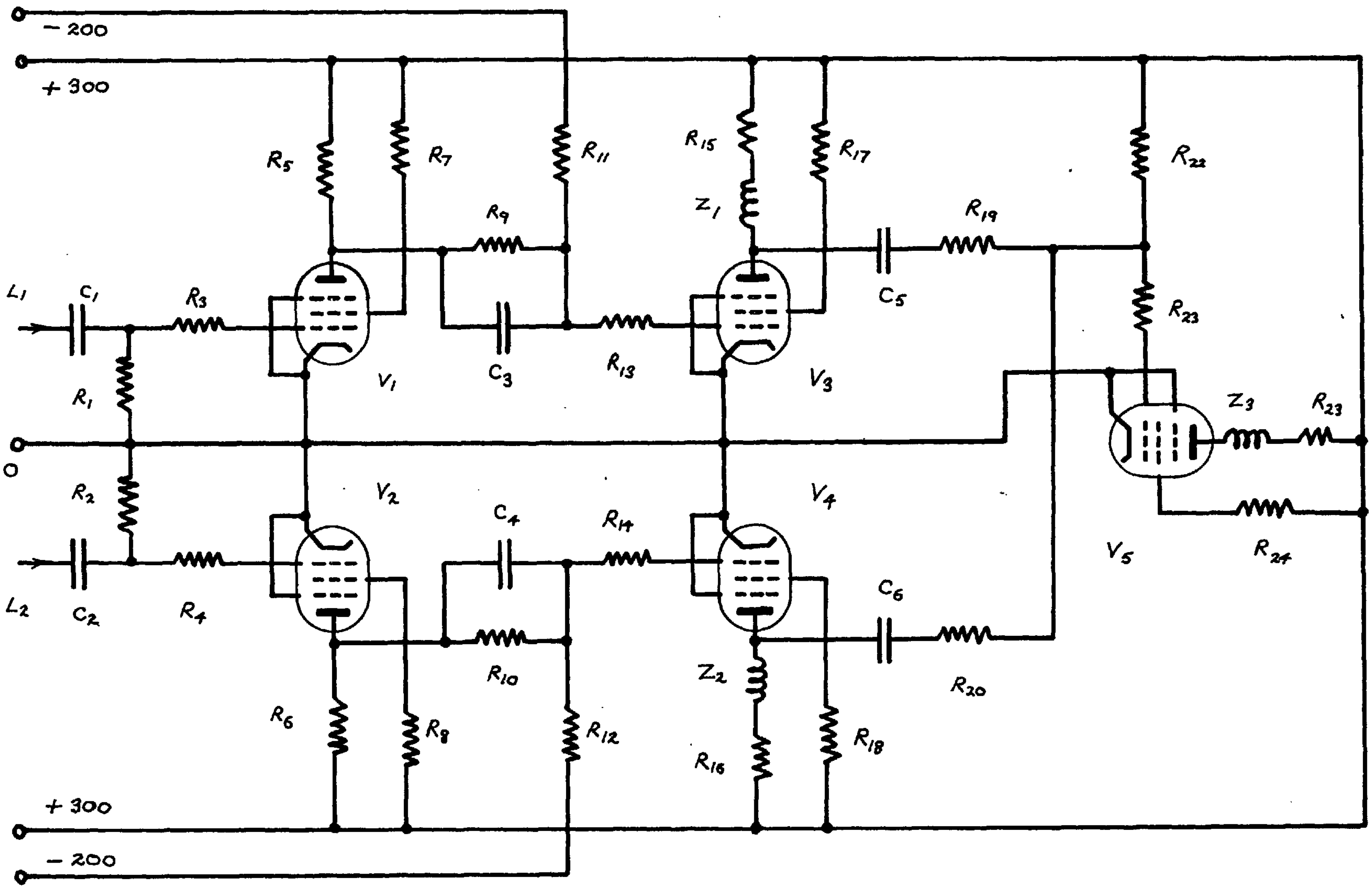

FIG. 4·9 MODULATOR DRIVE CIRCUIT.

4.42 Components for Modulator Drive Circuit.

RESISTORS:

R_1	470K Ω	10%	$\frac{1}{4}$W
R_2	470K	10	$\frac{1}{4}$W
R_3	10K	10	$\frac{1}{4}$W
R_4	10K	10	$\frac{1}{4}$W
R_5	22K	10	1W
R_6	22K	10	1W
R_7	22K	10	1W
R_8	22K	10	1W
R_9	270K	10	$\frac{3}{4}$W
R_{10}	270K	10	$\frac{3}{4}$W
R_{11}	470K	10	$\frac{3}{4}$W
R_{12}	470K	10	$\frac{3}{4}$W
R_{13}	10K Ω	10%	$\frac{1}{4}$W
R_{14}	10K	10	$\frac{1}{4}$W
R_{15}	1.5K	5	6W
R_{16}	1.5K	5	6W
R_{17}	2.7K	10	$\frac{3}{4}$W
R_{18}	2.7K	10	$\frac{3}{4}$W
R_{19}	470K	10	$\frac{3}{4}$W
R_{20}	470K	10	$\frac{3}{4}$W
R_{21}	10K	10	$\frac{1}{4}$W
R_{22}	3.3M	10	$\frac{1}{4}$W
R_{23}	4K	10	6W
R_{24}	2.7K	10	$\frac{3}{4}$W

CAPACITORS:

C_1	0.25 uF, 350v, Paper
C_2	0.25 uF, 350v, Paper
C_3	100 pF, Ceramic
C_4	100 pF, Ceramic
C_5	0.5 uF, 350v, Paper
C_6	0.5 uF, 350v, Paper

VALVES:

V_1	6 AM 6
V_2	6 AM 6
V_3	6 BW 6
V_4	6 BW 6
V_5	6 BW 6

4.5 A PULSE GENERATOR FOR SIMULATING CONTOUR SIGNALS.

This circuit was constructed in order to facilitate the development of the previously described tristable scheme. It is a free running pulse generator with a twin output, simulating the running output of the contour sensing circuit, together with other useful test pulse waveforms.

4.51 Circuit Description

The complete circuit diagram is shown in Fig. 4.10. A free running screen coupled phantastron[4] (V_1) with a cathode follower anode-control grid return (V_2) provides a variable frequency (R_5) sawtooth run-down of 70 volts D.A.P. from a low impedance, which is fed to two voltage comparators[5] (V_3, V_4). The first sections of these valves normally conduct and the second sections are cut-off. Comparator V_4 is a-c coupled (C_6) to the phantastron output and triggers at the mid-point of the sawtooth; its output, taken from R_{28}, consists of unity mark/space ratio negative pulses, 45 volts p-p amplitude. Comparator V_3 is direct-coupled to the sawtooth output and triggers at a point on the linear run-down dependent upon the setting of potentiometer R_{12} (the 'contour slope' control); the output derived from R_9 consists of variable mark/space ratio negative pulses. The positive steps of both pulse trains are coincident since the sawtooth triggers back V_3 and V_4 simultaneously.

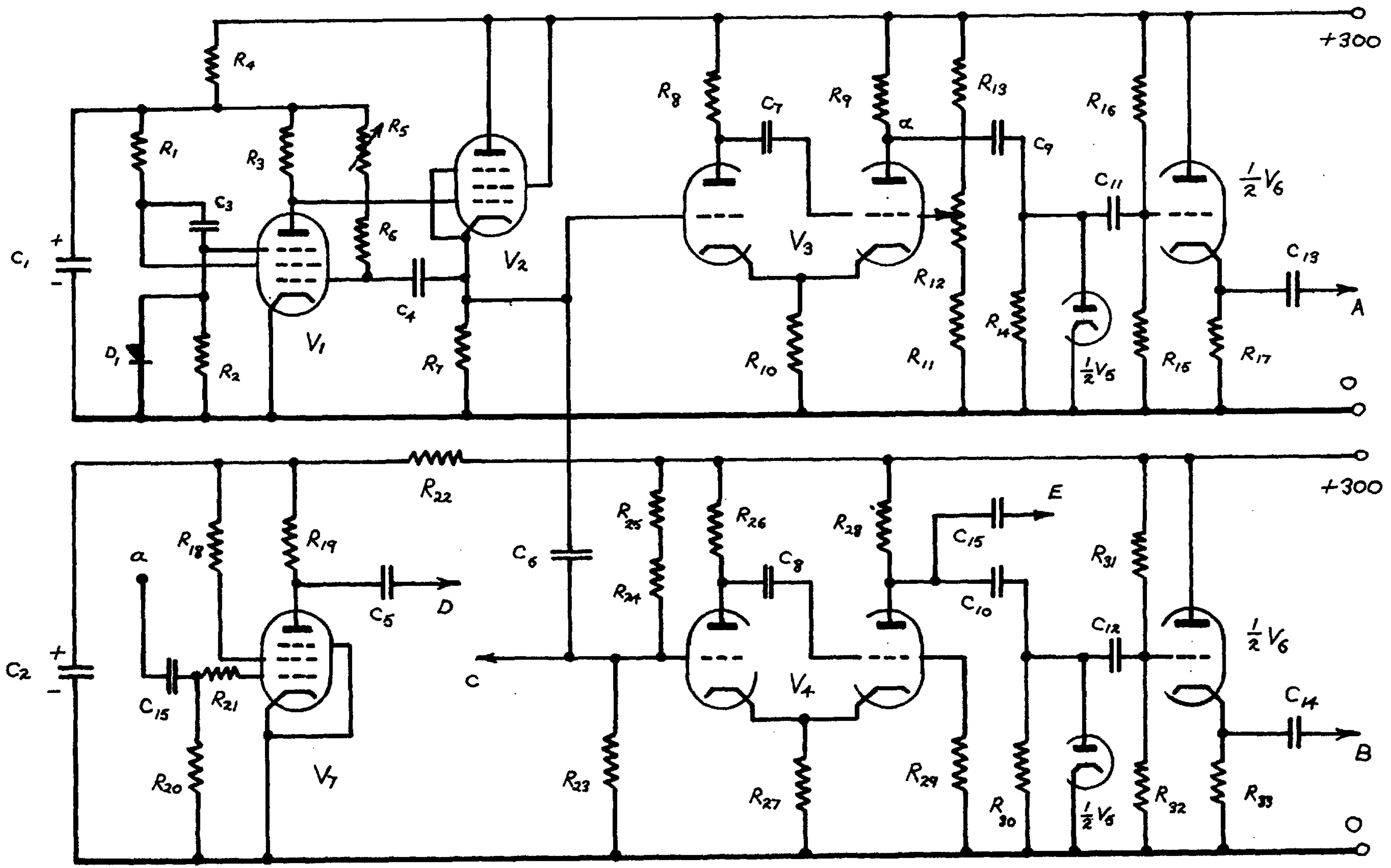

FIG. 4·10 PULSE GENERATOR FOR SIMULATING CONTOUR SIGNALS.

Both pulse trains are differentiated by C_9R_{14} and $C_{10}R_{30}$; the positive spikes are removed by diode clippers (V_5), and V_6 provides a cathode follower output (A,B) for the negative spikes, 30 volts amplitude, the necessary grid bias being provided by bleeder chains R_{15}, R_{16} and R_{31}, R_{32}.

The circuit also supplies the ac-coupled sawtooth (C), an inverted clipped version (pentode limiter V_7) of the variable P.R.F., variable mark/space ratio comparator output pulses from V_3 (D), and the square wave output of comparator V_4 (E)

OUTPUT DETAILS OF GENERATOR:

Pulse Repetition Frequency 50 - 300 c.p.s. in 1 range.

Output A	(variable shift)	negative spikes	30 volts amplitude
B	(fixed)	" " " "	" " " " "
C		Sawtooth	70 volts D.A.P.
D		Rectangular Wave	200 volts D.A.P.
E		Square Wave	50 volts D.A.P.

4.52 Components for Pulse Generator/Contour Simulator

RESISTORS:

R_1	22 KΩ	10%	$\frac{3}{4}$W	R_{18}	22 KΩ	10%	$\frac{3}{4}$W
R_2	270K	10	$\frac{1}{4}$W	R_{19}	22 K	10	$\frac{3}{4}$W
R_3	22 K	10	$\frac{3}{4}$W	R_{20}	220K	10	$\frac{1}{4}$W
R_4	3.3K	10	3W	R_{21}	10 K	10	$\frac{3}{4}$W

RESISTORS (cont.)

R_5	5MΩ	Log Variable (Carbon)	
R_6	680K	10%	$\frac{3}{4}$W
R_7	10 K	10	$\frac{3}{4}$W
R_8	47 K	10	$\frac{3}{4}$W
R_9	4.7K	10	$\frac{3}{4}$W
R_{10}	10K	10	$\frac{3}{4}$W
R_{11}	680K	10	$\frac{1}{4}$W
R_{12}	1M	Linear	Variable (Carbon)
R_{13}	470K	10	$\frac{1}{4}$W
R_{14}	100K	10	$\frac{1}{4}$W
R_{15}	470K	10	$\frac{1}{4}$W
R_{16}	3.3M	10	$\frac{1}{4}$W
R_{17}	10 K	10	$\frac{3}{4}$W
R_{22}	3.3KΩ	10%	3W
R_{23}	470K	10	$\frac{1}{4}$W
R_{24}	270K	10	$\frac{1}{4}$W
R_{25}	1M	10	$\frac{1}{4}$W
R_{26}	47K	10	$\frac{3}{4}$W
R_{27}	10 K	10	$\frac{3}{4}$W
R_{28}	4.7K	10	$\frac{3}{4}$W
R_{29}	100K	10	$\frac{1}{4}$W
R_{30}	470K	10	$\frac{1}{4}$W
R_{31}	3.3M	10	$\frac{1}{4}$W
R_{32}	10 K	10	$\frac{3}{4}$W
R_{33}	470K	10	$\frac{1}{4}$W

CAPACITORS:

C_1	8 uF, 500v, Electrolytic
C_2	16 uF, 500v, Electrolytic
C_3	33 pF, Ceramic
C_4	0.02uF, 350v, Paper
C_5	0.25uF, 350v, Paper
C_6	0.25uF, 350v, Paper
C_7	0.01uR, 350v, Paper
C_8	0.01uF, 350v, Paper
C_9	56 pF, Ceramic
C_{10}	56 pF, Ceramic
C_{11}	0.02 uF, 350v, Paper
C_{12}	0.02 uF, 350v, Paper
C_{13}	0.02 uF, 350v, Paper
C_{14}	0.02 uF, 350v, Paper
C_{15}	0.25 uF, 350v, Paper.

VALVES:

V_1	6 AM 6	V_5	6 AL 5
V_2	6 AM 6	V_6	12 AT 7
V_3	12 AT 7	V_7	6 AM 6
V_4	12 AT 7	D	GEX 66

4.6 REFERENCES.

1. SEELY, S., 'Electronic Engineering', Mc Graw-Hill Book Co., London - New York, 1956, p. 161.

2. SEELY, S., 'Electronic Engineering', Mc Graw-Hill Book Co. London - New York, 1956, p.275.

3. BRITTON CHANCE, 'Waveforms', M.I.T. Radiation Laboratory Series, Mc Graw-Hill, 1949, p.336

4. SAYRE, D., 'Waveforms', M.I.T. Radiation Laboratory Series, Mc Graw-Hill, 1949, p. 199.

5. SEELY, S., 'Electron - Tube Circuits' Mc Graw-Hill, 1950, P.430.

5. EXPERIMENTAL PICTURE TRANSFORMATION.

5.1 INTRODUCTION

The primary object of the experiments was to test and demonstrate the principles of interpolation and in particular 'contour interpolation', using the picture transformer as a device for forming pictures of 'full' vertical resolution from pictures in which only half that resolution is made available. In addition, the apparatus has been used to provide pictures of original vertical resolution so that the quality of the interpolated results may be judged subjectively by comparison with pictures containing the full number of original scanning lines. The picture transformer is thus made to simulate the receiver processing for 2 : 1 field interpolation in television and to show how feasible such a system would be, judged on the basis of subjective appraisal of the ultimate display.

The choice of pictures and patterns is an important matter in such experiments as only a limited number may be sensibly processed and it was decided to select them from two broad classes:

(i) Patterns and pictures which contain material for specifically testing linear and contour interpolation; that is, well defined large amplitude gradients of low geometrical slope.

(ii) Typical pictures which occur in television programme material, containing a wide range of detail.

The test patterns have been produced by making indian ink drawings on white card, and also by affixing black tape cut-outs to a white background; the raised pattern has the advantage of providing a high peak to peak picture signal with the black portions presenting an out-of-focus scan in addition to a low reflection coefficient. The test pictures have been produced by enlarging $1\frac{5}{8}$" x $2\frac{1}{4}$" Ilford F.P.3. negatives, taken with the author's medium-priced folding camera, up to 60 x 70 mm^2 on normal glossy bromide paper.

The processed pictures, recorded on '120' size film, have been enlarged up to $\frac{1}{4}$-plate size on papers of carefully selected contrast grades to ensure that comparison records of the same pictures are not impaired by unlike ultimate contrast 'gammas'.

The majority of the results have been taken with the picture transformer running at 100 c.p.s. horizontal bandwidth; at this speed, a medium fast (29° Scheiner) panchromatic film is adequately exposed. For the contour interpolation experiments the machine was set for 50 c.p.s. bandwidth, enabling the same film to be used despite the increased optical tract attenuation, and also allowing the modulators to function within their mechanical frequency limits with a convenient control spot advance.

5.2 EXPERIMENTAL PROCEDURE

Prior to operating the picture transformer, the previously described optical circuit must be perfectly aligned; the procedure given in the following section is for the most complex circuit, necessary for contour interpolation. Following sections deal specifically with the production of full-detail, repeated-field, linear interpolated, and contour interpolated pictures respectively, including modification and refinement details of the optical circuit necessary for the processing.

5.21 Alignment of the Optical Circuit.

The purpose of aligning the optical circuit, control and main beam tracts, is to obtain:

(a) Double line separation (0.3 mm) for the two pairs of spots focussed at the reading drum.

(b) Equal weighting from both main reading beams at the writing objective.

(c) Separation of main and control signals at the photocells and at the writing objective

(d) Freedom from stray signals in the writing tract.

The main writing tract is the most critical in alignment; any control tract inequality is compensated by gain variation in the contour sensing circuit. The alignment procedure is as follows:

(i) With the optical circuit set up according to Fig.3.11 and the control beams blacked out, the reading objective is focussed onto a peak white picture by visually maximising the writing signal at a point just beyond the auxiliary writing lens.

(ii) Prism tilts and spacings in the reading section and the signal distributor mask, are adjusted to provide roughly equal spot intensities with double line spacing at the reading drum, and to give adequate stray signal divergence at the writing masking plate.

(iii) The writing aperture plate is adjusted to give the correct spot size at the writing objective, and the latter is focussed by eye.

(iv) A low geometrical slope contour is scanned and recorded, and the resulting linear interpolation indicates the line spacing and intensity contributions (See Fig. 2.1 (a))

(v) In total darkness (necessitated by the very low level intensities involved) the writing masking plate is adjusted to further equalise the two spot contributions; this is monitored by eye, and facilitated by switching the distributor.

(vi) The control beams are now passed through the system and the main beams blacked out. The photocell-mount positions are varied to determine the position of maximum pick-up with a scanned pattern.

(vii) With both beams operating, the main beams are modulated by switching the distributor to check that the inter-tract 'cross-talk' is well below the previously observed control signal amplitudes.

(viii) Amplitude gains in the two channel contour sensing circuits are adjusted to obtain equal control signal amplitudes, prior to the contour amplitude selector.

5.22 Full-Detail Pictures

For the production of frames containing the full number of 400 original scanning lines, two methods were considered:

(i) Adjusting the bi-prism spacing such that the double beams at the reading drum are one diameter apart, and blanking out alternate beams with the signal distributor for each field scan.

(ii) Providing the main aperture with a horizontal shift between field scans.

Method (i) was found unworkable with the available biprisms and method (ii) was adopted. It was found experimentally that a $1\frac{1}{2}$ mm horizontally offset aperture provided the correct deflection at the writing objective by reversing the aperture plate for the second field scan, which then required an interlace shift of 160°. The biprisms were omitted and the control channel made inoperative for these picture runs. The film records were taken on Kodak Verichrome

Pan with a 30 c.p. light source, which was overrun for interlace intensity correction:

It was observed that exposure of the film to the first field partially exposed the interlace space as a result of spot spreading or 'irradiation', so that the second field was written with a modified film characteristic. It was found that partial compensation occurred if this second field was written with the 200v d.c. Pointolite running voltage set at 230 volts. The writing speeds were 32 mm/sec, equivalent to 100 c.p.s. horizontal bandwidth.

5.23 Field Repetition

In these experiments, the control channel was blacked out and the biprisms removed. With a fixed aperture, the same field scans were interlaced on the film record (Verichrome Pan) with an interlace shift of 135° and a Pointolite intensity of 230 volts for the second run. The writing speed was maintained at 32 mm/sec.

In addition, single field records were taken with this set-up at a Pointolite voltage setting of 250 volts and at a writing speed of 32 mm/sec.

5. 24 Linear Interpolation

The full optical circuit was used with the control channel made inoperative and the components aligned as previously described in Sec. 5.21, (i) - (v). The first field recorded was linear interpolated and this was then interlaced with the original field, scanned one line at a time, on the second run. To allow single line scanning at the full intensity, the signal distributor was switched onto Line 1 with 50 mA d.c. current derived from four 1½V dry cells such that line 1 was weighted by unity and line 2 by zero; the velocity modulator coils were made short circuit for this operation. The interlace shift was 130° and the 30 C.P. pointolite Lamp was run at 200 volt d.c. for the first field scan and 250 volt d.c. for the second interlacing field scan, in order to compensate for the distributor weighting inaccuracy and irradiation effects from the first interpolated field.

All these picture runs have been performed at a writing speed of 32 mm/sec and recorded on Verichrome Pan roll film.

5.25 Contour Interpolation

The full optical circuit was used for these experiments and aligned according to the procedure given in Sec. 5.21, (i) - (viii); necessary modifications are described later in the text.

The recording sequence was as above: the first field recorded was the contour interpolated field which was then interlaced with the original 200 line field scanned one line at a time on channel 1, with the signal distributor switched with d.c. signal current; the interlace shift was 135°.

At this stage in the experiments, the supply of 30 C.P. Pointolite was exhausted and all the contour interpolation results have been obtained with 150 C.P. bulbs modified for short focus working as previously described in Chapter 3, Sec. 3.22 (a). No overrunning facility was provided for two reasons: (i) the bulb element life was to be maximised, and (ii) irradiation or spot spreading effects were found to be negligible with the reduced film exposure present with the increased optical attenuation in the writing channel.

The following refinements to the apparatus were found to be necessary for successful contour interpolation:

(i) To allow the modulators to switch within a picture element period, the drive speed of the picture transformer was decreased to 16 mm/sec, i.e. a horizontal bandwidth of 50 c.p.s. This writing speed allowed 29° and 32° Scheiner film to be used despite the increased attenuation derived from (ii) and (iii) below.

(ii) Main-to-control beam crosstalk was present in the uncollimated optical circuit which produced spurious oscillation after distributor switching; this was reduced by placing an attenuating filter (Wratten, Red No. 25) over the main beam aperture immediately after the light source objective lens.

(iii) Electromagnetic feedback from the active modulator coils to the control channel input circuits produced spurious switching and oscillation in the modulator drive. This was eliminated by screening the photocells with earthed Mu-metal, completely screening the distributor, and placing thick sheets of Mu-metal between the velocity modulator actuators and the photocells.

(iv) Triggering was spurious with the necessarily high gain contour sensing circuits handling the very low level picture signals. Better results were obtained (a) by driving the contour sensing circuits with a D.C. Heater supply (Sec.4.21) and (b) using raised facsimile patterns for test cards.

(v) Initial results showed that a control spot advance of one diameter at the main aperture was sufficient, providing a roof prism was used to re-cross the twin beams to correct for the collimation divergence. The actual inverting prism used was a 45° - 90° reflecting prism with its longest face horizontally placed on the 'reading bar' between the microscope objective mount and the reflecting prism. (Assembly drawing, Fig. 3.1). The correct triggering advance was shown experimentally by the absence of line 'pips' in the interpolated edge just after the first writing spot encounters the contour

(vi) With the signal distributor undamped, the return to the quiescent condition was oscillatory. Some results were taken under these conditions but better roults were obtained with the distributor heavily damped; this was performed by pinning two lengths of plastic sleeving onto the extremities of the armature side bar, fixing the other ends to pins inserted into the Araldite base (Plate 5).

(vii) Printable results were obtained on Kodak Verichrome Pan for the facsimile tests; half-tone pictures required a film of double speed, 32° Scheiner; Adox 'R21' was selected.

5.26 Film Development

All the film records were tank-developed individually with D76 developer made up to the Kodak specification. Kodak Acid Fixing solution was used for film fixing and hardening; all operations were carried out at normal room temperature.

5.3 ANALYSIS OF RESULTS

The results of the experimental picture transformation obtained with the photo-mechanical device are shown in photographic form (Figs. 5.1 - 5.26). A list is provided giving details of the conditions under which each result was produced; the pictorial results are assessed and compared in order to demonstrate the subjective effects of the different picture forming processes.

5.31 Details of Photographic Results.

All the results displayed in the following twenty-six Figures have been printed on $\frac{1}{4}$-Plate Kodak Bromide Paper (WSG) and, unless stated otherwise, the magnification is $1\frac{1}{2}$X with the scanning directions conventional, that is, left to right and down the field; Table 5.1 provides a picture list together with details which supplement the information given in the figure captions.

It is observed that the enlarged contour interpolated results of Figs. 5.10 - 5.14 display edges of one geometrical slope sign only - the machine failed to successfully interpolate contours in which the 'first' line edge was sensed prior to the second. The reasons for this appear to be (i) the inability of the velocity modulator to operate successfully in that sense, and (ii) imperfect signal weighting by the signal distributor on switching to the second line writing beam; the first fault was the major cause of failure. Photographic records of these interpolations indicated that the modulator lever-arm engagements and tracking were spurious; attempts to correct this simply destroyed the working in the opposite polarity, and with time at a premium it was decided to experiment with positive-slope contours only. Contour interpolated pictures have been produced with this asymmetrical working. The 'contour amplitude' selector was adjusted to provide sufficient sensitivity for the full amplitude transitions without admitting very fine detail and thus eliminating triggering on the noise of the very low S/N ratio control signal;

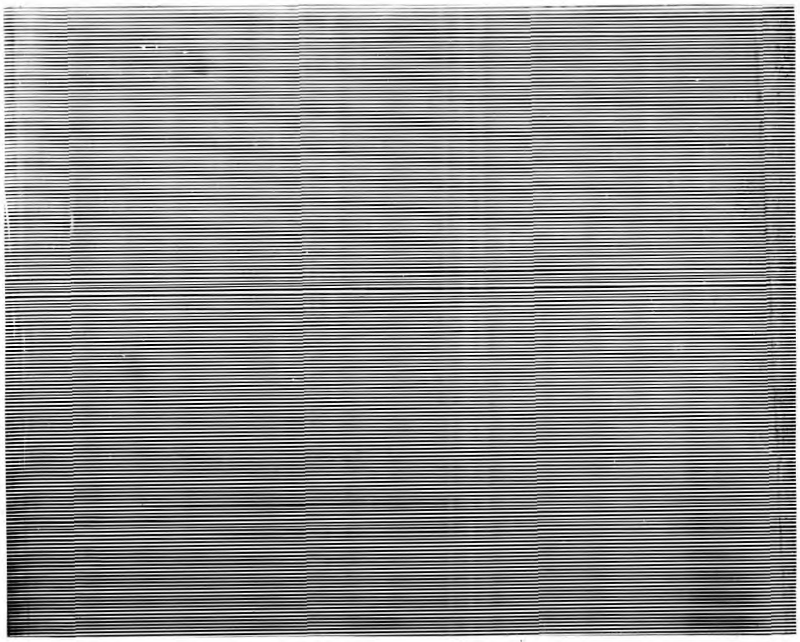

FIG. 5.1 Shading Signal. Plain Raster, Single Field, Horizontal Bandwidth 100 C.P.S; Bromide WSG 4S.

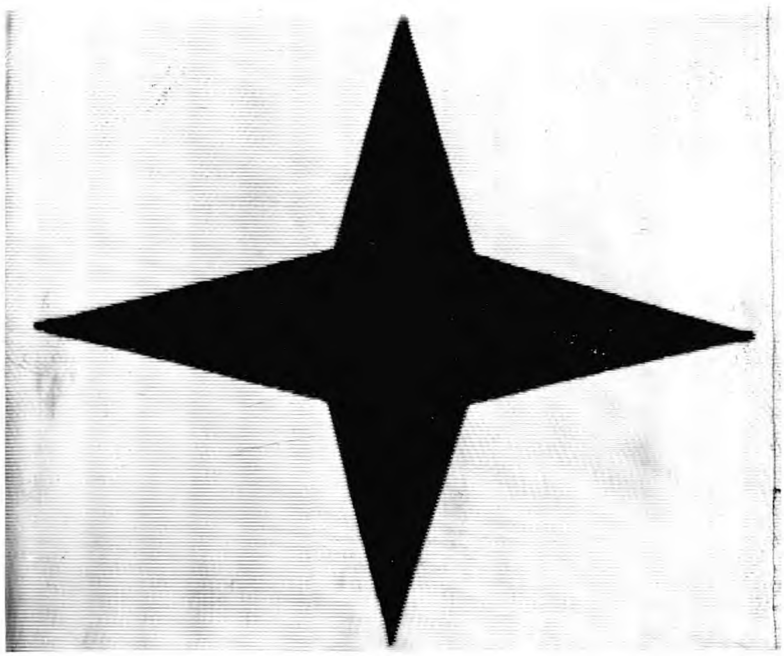

FIG. 5.2 'Full Bandwidth' Frame. Interlaced Fields, 400 Lines Horizontal Bandwidth 100 C.P.S; Bromide WSG 1S.

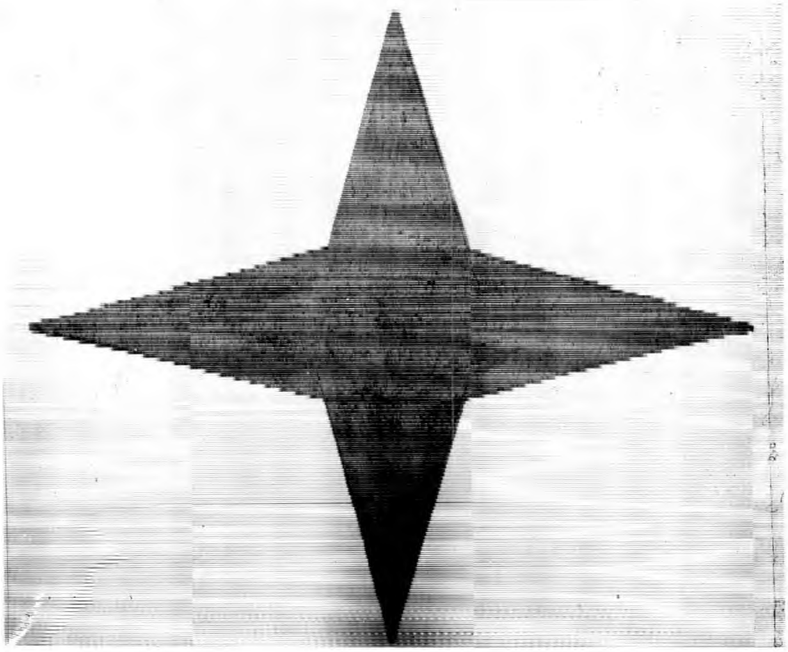

FIG. 5.3 Field Repetition. 400 lines at 100 C.P.S. Horizontal Bandwidth; Bromide WSG 1S

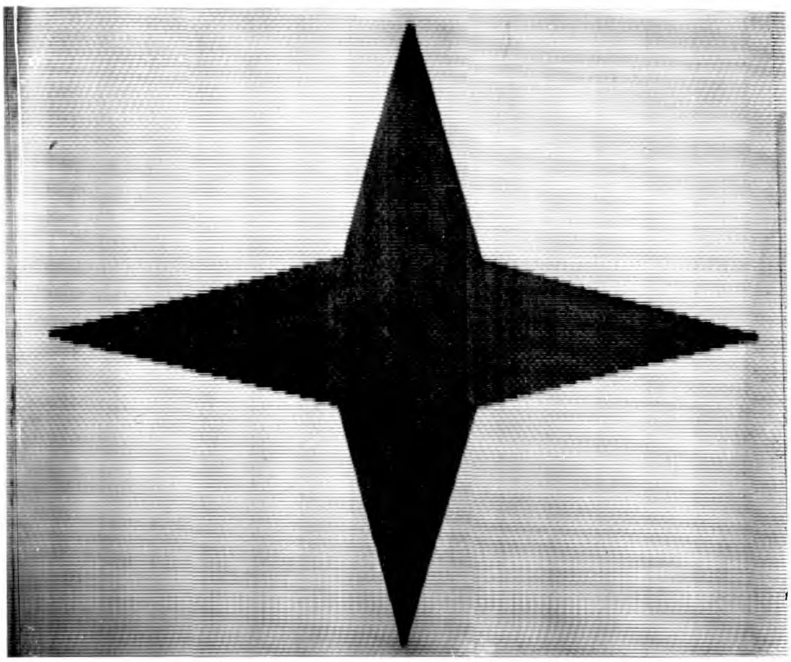

FIG. 5.4 Linear Interpolation. 400 lines at 100 C.P.S. Horizontal Bandwidth; Bromide WSG 3S

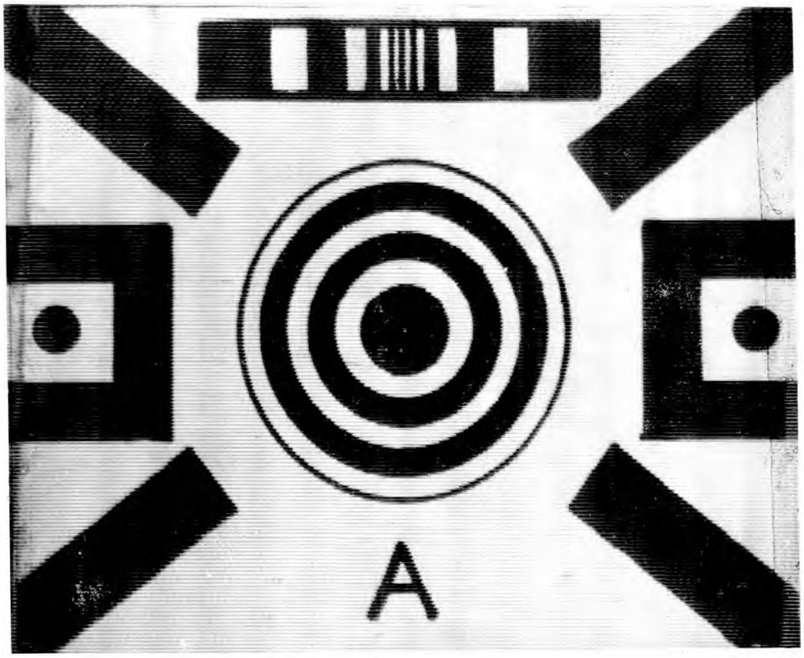

FIG. 5.5 'Full Bandwidth' Frame. 400 Lines Interlaced, Horizontal Bandwidth 100 C.P.S; Bromide WSG 1S.

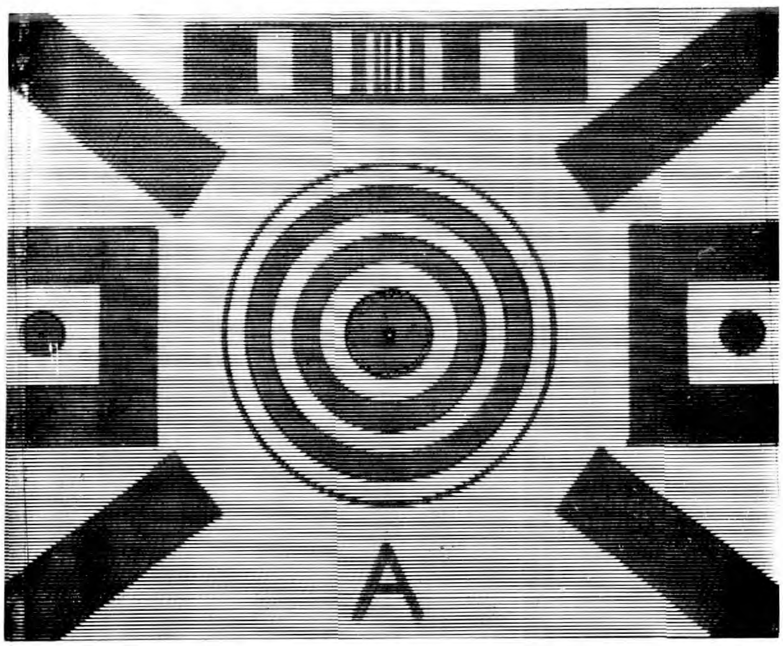

FIG. 5.6 Single Field. 200 Lines, Horizontal Bandwidth 100 C.P.S; Bromide WSG 3S.

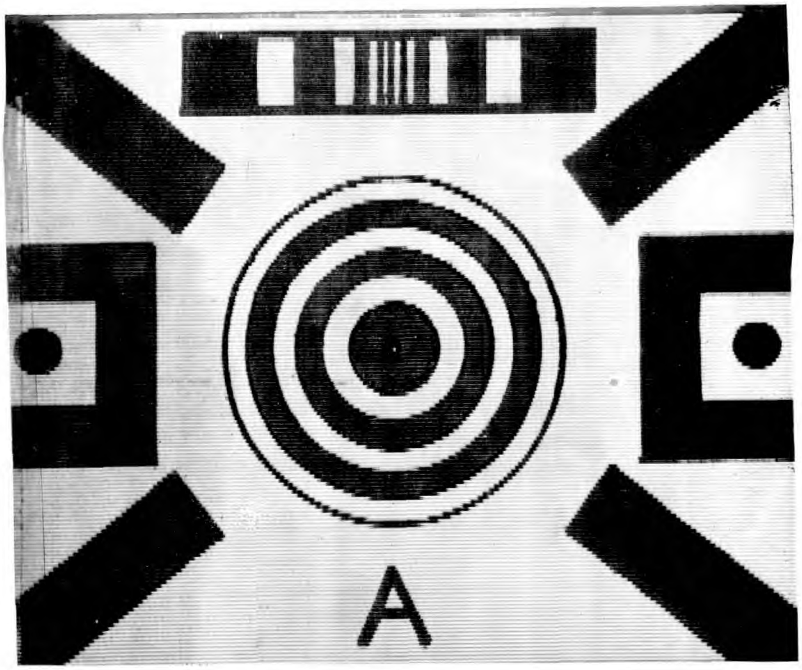

FIG. 5.7 Field Repetition. 400 Lines at 100 C.P.S. Horizontal Bandwidth; Bromide WSG 1S.

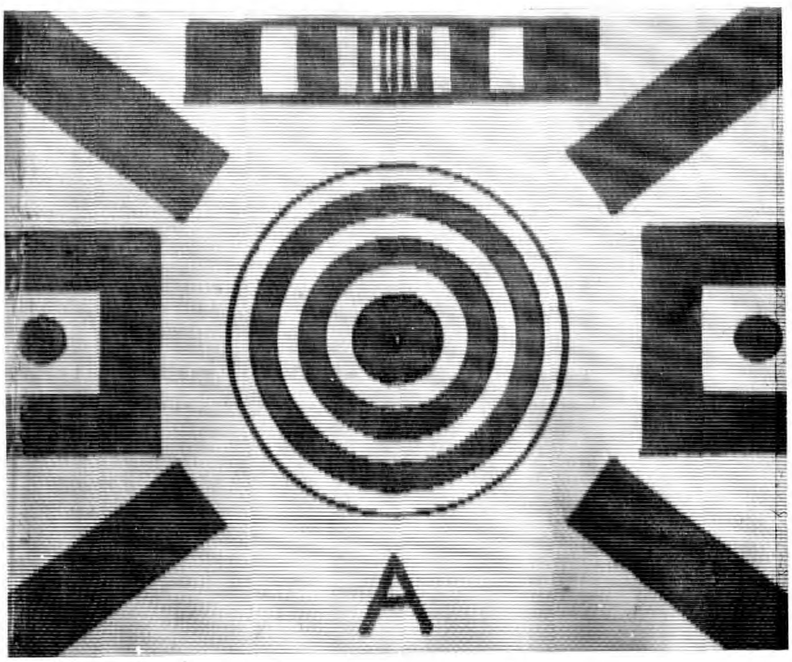

FIG. 5.8 Linear Interpolation. 400 Lines at 100 C.P.S. Horizontal Bandwidth; Bromide WSG 2S.

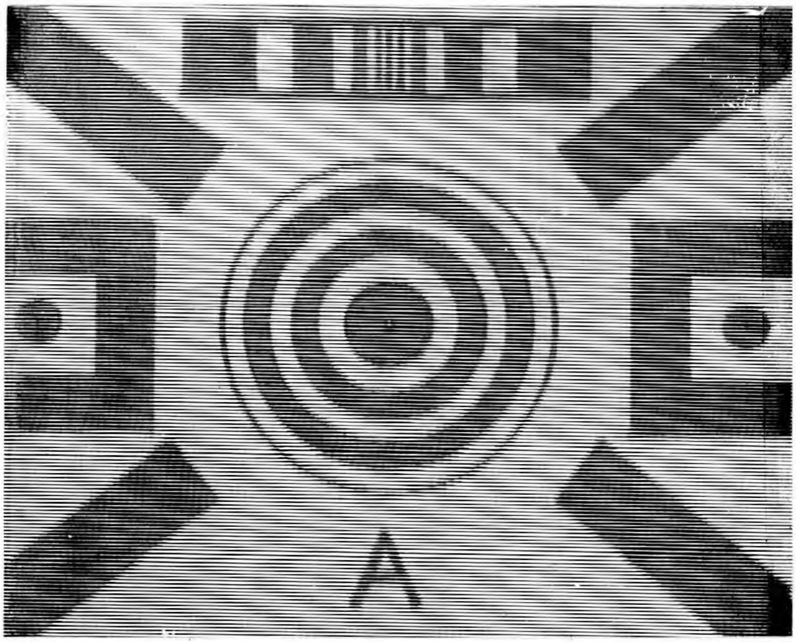

FIG. 5.9 Linear Interpolation. Single 200 Line Field only at 100 C.P.S. Horizontal Bandwidth; Bromide WSG 3S.

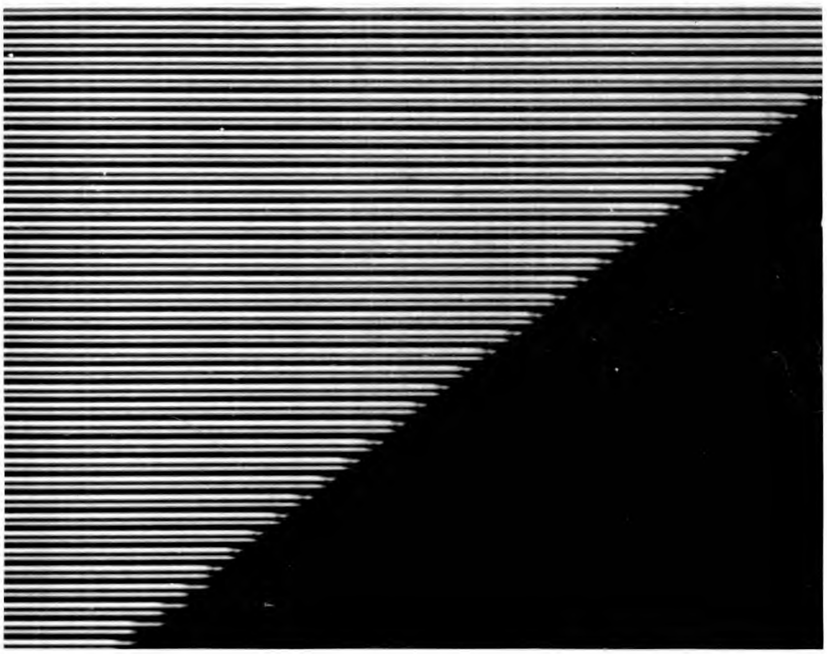

FIG. 5.10 Contour Interpolation. Interlaced Fields at 50 C.P.S. Horizontal Bandwidth; 40^{o}Contour, Magnification X7; Bromide WSG 4S.

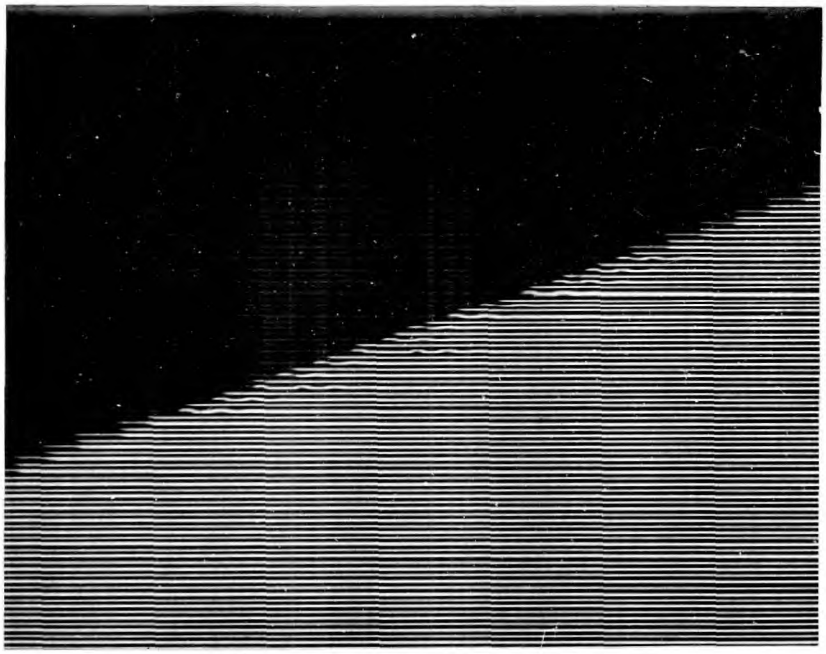

FIG. 5.11 Contour and Linear Interpolation. Overshoot on Signal Distributor; interlaced Fields at 50 C.P.S. Horizontal Bandwidth, 20° Contour, Magnification X4; Bromide WSG 4S.

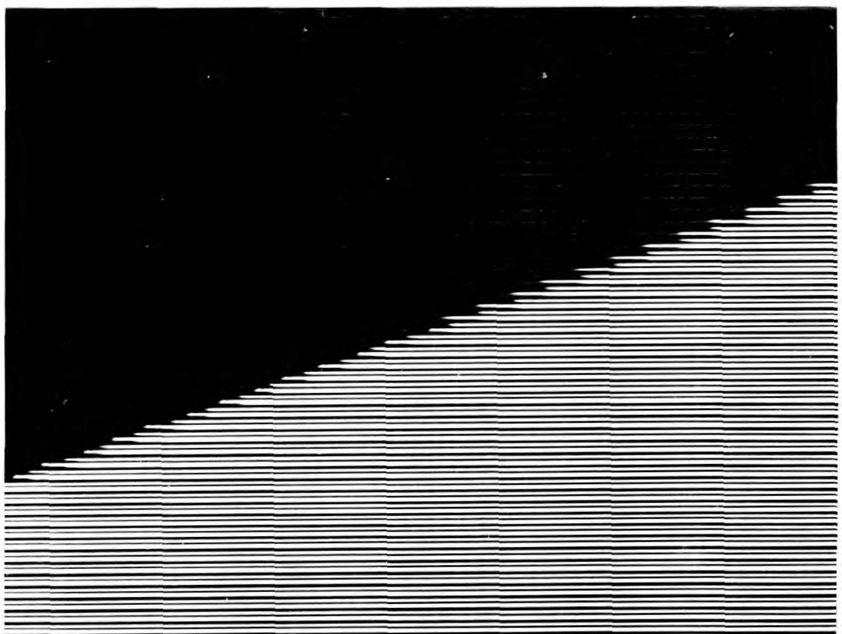

FIG. 5.12 Contour and Linear Interpolation. Signal Distributor Aperiodic; Interlaced Fields at 50 C.P.S. Horizontal Bandwidth, 20° Contour, Magnification X4; Bromide WSG 3S.

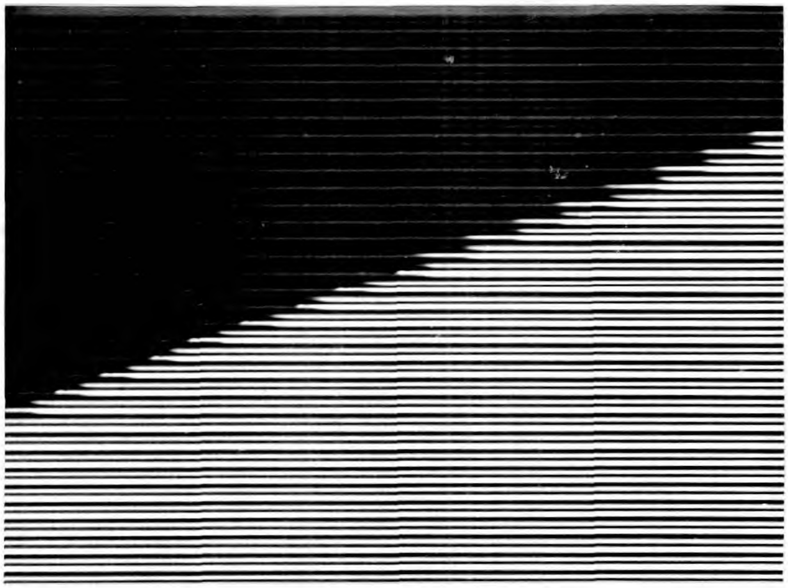

FIG. 5.13 Contour and Linear Interpolation. Signal Distributor Aperiodic; Interlaced Fields at 50 C.P.S. Horizontal Bandwidth, 20° Contour, Magnification X7; Bromide WSG 3S.

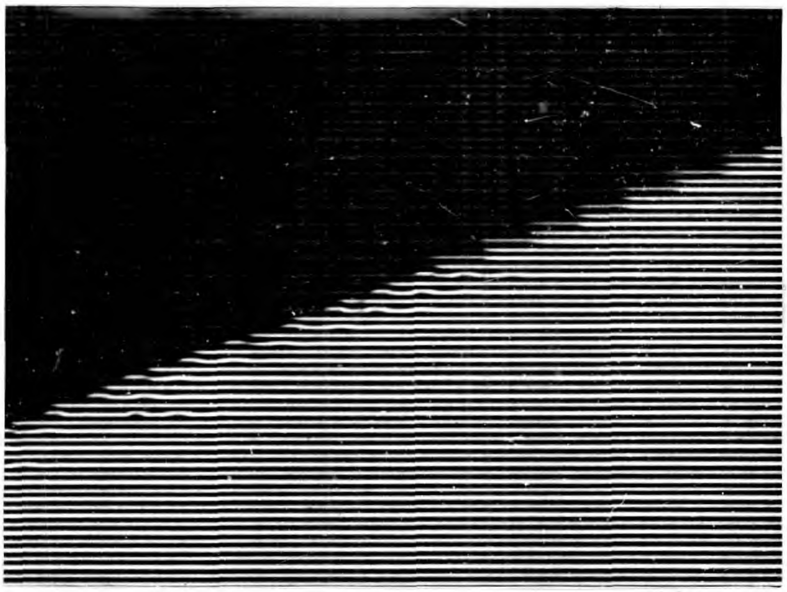

FIG. 5.14 Contour and Linear Interpolation. Overshoot on Signal Distributor; Interlaced Fields at 50 C.P.S. Horizontal Bandwidth, 20° Contour, Magnification X7; Bromide WSG 4S.

FIG. 5.15 Original. Bromide WSG 1S.

FIG. 5.16 Single Field. 200 Lines, Horizontal Bandwidth 100 C.P.S; Bromide WSG 4S.

FIG. 5.17 'Full Bandwidth' Frame. 400 Lines Interlaced, Horizontal Bandwidth 100 C.P.S; Bromide WSG 2S

FIG. 5.18 Field Repetition. 400 Lines at 100 C.P.S. Horizontal Bandwidth; Bromide WSG 2S.

FIG. 5.19. Linear Interpolation. 400 Lines at 100 C.P.S. Horizontal Bandwidth; Bromide WSG 2S.

FIG. 5.20 Contour Interpolation. 400 Lines at 50 C.P.S. Horizontal Bandwidth; Bromide WSG 4S.

FIG. 5.21. Original. Bromide WSG 2S.

FIG. 5.22 Single Field. 200 Lines, Horizontal Bandwidth 100 C.P.S. Bromide WSG 4S.

FIG. 5.23 'Full Bandwidth' Frame. 400 Lines Interlaced, Horizontal Bandwidth 100 C.P.S; Bromide WSG 2S.

FIG. 5.24 Field Repetition. 400 Lines at 100 C.P.S. Horizontal Bandwidth; Bromide WSG 2S.

FIG. 5.25 Linear Interpolation. 400 Lines at 100 C.P.S. Horizontal Bandwidth; Bromide WSG 2S.

FIG. 5.26 Contour Interpolation. 400 Lines at 50 C.P.S. Horizontal Bandwidth; Bromide WSG 4S.

TABLE 5.1

PICTURE	FIGURE	PROCESS	SCANNING SPEED	FILM	PAPER GRADE	COMMENTS
Plain Raster	1	Single Field	32mm/sec	Verichrome	4S	Shows mechanical vibrations.
Star Pattern	2	'Full Bandwidth'	32mm/sec	Verichrome	1S	400 original lines
	3	Field Repetition	" "	" "	1S	200 line vertical resolution.
	4	Linear Interpolation	"	" "	3S	400 lines interlaced.
Test Card 'A'	5	'Full Bandwidth'	32mm/sec	Verichrome	1S	400 Original lines.
	6	Single Field	" "	" "	3S	200 lines only.
	7	Field Repetition	" "	" "	1S	200 line vertical resolution.
	8	Linear Interpolation	"	" "	2S	400 lines interlaced.
	9	Linear Interpolation	"	" "	3S	200 lines only.
Test Edges (Masking Tape on White Card)	10	Contour Interpolation	16mm/sec	Verichrome	4S	Magnification X7
	11	Linear and	" "	" "	4S	Overshoot, Magnific.X4
	12	Contour Interpolation	"	Adox R.21	3S	Damped, Magnification X4
	13	Linear and	" "	" "	3S	Damped, Magnification X7
	14	Contour Interpolation	"	" "	4S	Overshoot, Magnific.X7
Portrait of Girl-Head and Shoulders	15	Original	-	FP 3	1S	Magnification X1½
	16	Single Field	32 mm/sec	Verichrome	4S	200 Lines only
	17	'Full Bandwidth'	" "	" "	2S	Full detail Transmission
	18	Field Repetition	" "	" "	2S	200 line vertical resolution
	19	Linear Interpolation	"	" "	2S	400 line interlaced
	20	Contour Interpolation	16mm/sec	Adox R.21	4S	Successful on RH shoulder.
Austrian Scene	21	Original	-	FP 3	2S	Magnification X2
	22	Single Field	32mm/sec	Verichrome	4S	200 lines only
	23	'Full Bandwidth'	" "	" "	2S	Full detail Transmission
	24	Field Repetition	" "	" "	2S	200 Lines vertical resolution
	25	Linear Interpolation	"	" "	2S	400 Lines interlaced
	26	Contour Interpolation	16mm/sec	Adox R.21	4S	No improvement

apart from electronic sources, this noise is derived from the a.c. Pointolite and the coarseness of the picture surfaces.

5.32 Assessment of Pictorial Results.

The first picture, Fig.5.1, shows a single 200 line plain white field and demonstrates the periodic shading which is superposed onto all the subsequent film records; this shading results from mechanical vibrations transmitted from the worm gear drive to the picture drums via the main transformer shaft; the single field resolution is shown directly. Another mechanical defect, wear of the threaded driving shaft, is shown up by line spreading near the bottom of Figs.5.3,8,9, 16,18,19. The remainder of the results are best described in picture groups.

The 'full bandwidth' star pattern of Fig. 5.2 shows the 400 line resolution of the system and, in particular, demonstrates that even with the full number of original lines, the low slope transitions exhibit line fuzziness. With field repetition (Fig.5.3), this effect is more noticeable but near vertical contours remain acceptable to the eye; this is better demonstrated by the field-repeated Test Card frame of Fig. 5.7 which clearly shows that contours do not become objectionable with this process unless their slope to the horizontal falls under about 50°. This picture must be compared with the full detail version (Fig. 5.5) for absolute judgement. The linear-interpolated frames (Figs. 5.4,5.8) show how the linear process breaks up the stepped edges of field repetition without giving any real improvement in the contour acuity. A single linear interpolated field is shown by Fig. 5.9 and clearly indicates how the process produces a defocussing effect at the transitions. The original single field is shown in Fig. 5.6 and, as with the latter picture, containing only 200 lines with the remaining space black, is macroscopically reduced in contrast.

The following set of Figures 5.10 - 14 contain the test results of contour interpolation suitably enlarged for demonstrating the accuracy of the interpolated edges, and the transition from linear to contour interpolation; the extra-enlargement of Figs 5.13 and 5.14 is to show the two level step produced by the linear processing and its removal with intelligent interpolation. The maximum searching distance for these pictures was set at 8 picture points on both channels; that is 40 msecs. with double velocity scanning at 50 c.p.s. mean bandwidth, thus admitting contours with slopes greater than one in four to the horizontal. Also demonstrated is the effect of overshoot at the signal distributor on switch-off; the damped oscillations so produced spoil the apparent sharpness of the interpolated edges. The quality of these results indicates the accuracy achieved in the instrumentation of the picture transformer modulation routine (unilateral working only).

The above remarks apply also to the last two groups of pictures Figs. 5.15 - 20 and Figs. 5:21-26, but with these it is far more pertinent to compare the different processes by overall picture appraisal. The original pictures, Figs.5.15,21 have been included to show the resolution of the picture sources; the true standards of comparison are the full resolution results of Figs.5.17,23. It is appreciated that only the reader himself can make a real comparative assessment of these processes but the following features are brought to his notice.

The single-field frames of Fig.5.16 and 5.22 show how well the human eye can interpolate the missing information, even in regions of fine detail, such as the hair in the portrait of Fig.5.16, and in contour regions which are also preserved correctly. Field repetition (Figs.5.18,24) is quite tolerable in most parts of the picture except for the large amplitude transitions (the shoulders in Fig.5.18 and the roof-tops of Fig.5.24) which become stepped and objectionable to the eye; certain types of subject matter take on a mosaic or 'squared' appearance as is shown by the hair in the portrait, although in this case the patterning has been augmented by spurious mechanical vibrations; although not shown here, a tree subject was found to give a similarly unnatural appearance with this process.

The linear interpolated frames of Figs. 5.19 and 5.25 certainly provide no real improvement; contours are simply blurred, an effect which to some observers, may be more objectionable than the sharp, yet incorrectly processed, stepped edges of field repetition. The improvement in the contour sharpness obtained with contour interpolation is self evident in Fig. 5.20, although as a whole, the picture is inferior to the previous results due to recording on faster film through the heavily attenuating complete optical circuit. The contour interpolation of Fig. 5.26 appears to be unsuccessful but has been included for the sake of completeness.

5.4 CONCLUSIONS

The results obtained above demonstrate some possibilities in the receiver processing of stationary pictures in a 2:1 bandwidth compression system in which only alternate frame lines are made available; they purport to show the gain of contour interpolation over two other compatible processes, namely field repetition and linear interpolation. How far this has been achieved and with what limitations is now discussed.

Despite the limited number of pictures processed, it is evident that the contour interpolation process preserves those parts of a picture for which the eye possesses a very critical acuity, and it is these large amplitude transitions which become noticeably degraded with the field repetition and linear interpolation processes. Obviously a greater range of processed pictures together with subjective testing would be more conclusive; although statistical subjective appraisal of the results has not been carried out, the above undoubtedly demonstrates the principle of contour interpolation and one possible means for its mechanisation.

The fact that it has not been possible to show contour interpolated edges with negative geometrical slopes is not a severe limitation as this was due to a purely instrumentation failure in the velocity modulator of the picture transformer. It was found impossible to balance the modulator arm in the quiescent position and both ways dynamically with the large resultant tolerances on the rotating drum/flange system and lever arms together with flexing of the arm and torsion bar; the result being that the modulator scanned accurately and without spurious mechanical triggering in one sense only. This device could possibly be further developed if the tolerances were decreased to under ± 0.001" and if the problem of balancing the arm accurately in the three positions were overcome, but from past experience, the latter would remain the major difficulty. Even if this were achieved, the above demonstrations of the interpolation principles would not be greatly enhanced. It must be emphasised that the resultant limitation in the results obtained is derived from this asymmetrical working of the velocity modulator and must not be attributed to a failure of the principles involved in the contour interpolation routine.

One interesting feature is revealed by the displayed processed pictures. The eye is easily able to tolerate linear interpolated, and even field repeated, contours if the contour slope to the vertical does not exceed about 40°. With a maximum 'searching distance' of eight picture points, this means that contour interpolation could, in principle, be restricted to contours with slopes lying between around 12° and 50° to the horizontal, providing the control channel is advanced by over the search period to supply the contour slope information in advance. The advantage of such a scheme, if practicable, is to eliminate any contour position and intensity inaccuracies which may be introduced by the system in the near vertical transitions, where such small errors become most noticeable.

The problem of mechanising field contour interpolation electronically at full speed television rates is discussed in the following chapter which also treats frame interpolation and a combined 4:1 and 8:1 compression system. The results obtained with stationary pictures cannot be used to predict the success or otherwise of a similarly instrumented frame interpolation system; it would require full-rate equipment to demonstrate the possibilities of motion interpolation.

To summarise, it is claimed that the picture transformer, despite its practical limitations, has successfully demonstrated a working system for 2:1 bandwidth compression of stationary pictures. Other known possibilities such as 'rate equalisation' and 'synthetic highs' have still to produce practicable systems; the present system, that of contour interpolation, possesses certain advantages over those alternative schemes as previously described (Sec.2.41). An electronic system incorporating the above principles should certainly provide acceptable results for 2:1 compression and it is not too sanguine to expect good results with a 4:1 bandwidth reduction scheme involving field and frame interpolation. As this form of compression can be combined with other systems to give an integrated bandwidth reduction, it yields a very attractive scheme which should be seriously considered for application to instantaneous TV transmissions over long distance narrow band cable links.

6. FUTURE DEVELOPMENTS.

This Chapter is the subject of a Provisional Patent applied for by the Author and Prof. D. Gabor, F.R.S. (Pat.App.No. 507/60)

6.1 INTRODUCTION

The experiments described above have served solely as a slow-speed demonstration of the soundness of the principles involved in television compression by interpolation. Full scale realisation of this form of band compression is shown to be theoretically possible utilising conventional devices as functional elements of the system, although this is not necessarily the optimum way unless time is at a premium. Development of special devices such as multigun charge controlled storage tubes would facilitate the problem and also provide schemes which are more economical in system components together with greater reliability. The major problems appear to be the limitations of storage tubes available at present.

This chapter discusses some of the problems involved in using conventional devices in full speed interpolation schemes; such schemes for 2:1 compression in field and frame interpolation are described in some detail. A television transmission system with 8:1 compression by contour interpolation is presented in schemmatic form. Finally there is a brief discussion of the possibilities of combining the above compression schemes with other forms of band-saving, concluding with remarks on simultaneous compression and standards conversion for instantaneous inter-continental television.

6.2 FUNCTIONAL ELEMENTS FOR CONTOUR INTERPOLATION

The functional elements required by a contour interpolation transmission system have been defined in Chapter 2; they include the information stores together with associated sensing organs, the velocity modulator and the signal distributor, and we will treat them in that order, adding a section on practical limitations.

6.21 The Stores

The major problem is at the receiver where 'stretched' fields must be stored before processing can proceed; for full speed processing the minimum storage time is (n-1) conventional field periods for n:1 compression, this being the time taken to store the fraction (n-1)/n of the incoming field. The choice of input, output, and intermediate storage devices must depend on the following considerations.

(a) The input vision signal (fields, frames or both) arrives stretched in time. The store must provide adequate retention.

(b) In field interpolation, each line of the received field is required 3 times, once for its own full speed reproduction, and twice for interpolation of lines above and below it in the interlaced field.

(c) In frame interpolation, each received line is required once for interpolation of the corresponding line in the previous frame, once for its reproduction, and once for interpolating the following frame.

(d) It is considered essential to store and process fields for a single interpolation on one store; this avoids accurate store matching.

(e) It must be possible to read out a stored signal at full speed, two lines at a time, with independent velocity modulation.

(f) A store providing many signal copies with linear half-tones and a controllable erasing action would minimise the number required for any given receiver scheme.

(g) Simultaneous reading and writing action would reduce the total delay in the receiver and also reduce the number of stores required.

The ideal store would therefore be a linear device of frame capacity with two writing organs, two independent reading organs and controllable erasing action for multiple read-outs with an erase period less than the conventional frame blanking period. Charge controlled storage tubes appear to be the only possibility at present, although there is some hope that future developments in magnetic storage will produce a variable speed magnetic scanning head. A bibliography on storage tubes is given by KNOLL and KAZAN [1].

The Graphechon, a signal-converter tube with independent reading and writing guns has been described by PENSAK; [2] it should be possible to incorporate a double writing gun in such a tube as writing is performed by primary current modulation. The disadvantage of this store is that the reading beam must be intensity-modulated at a frequency much greater than the maximum frequency of the written signal to prevent cross-talk between input and output signals; this increases the complexity of the associated circuitry with single beam interpolation; the tube also has a limited half-tone performance.

KNOLL and RANDMER [3] describe a signal-converter tube of the cathode-voltage-modulation type which employs separate reading and writing guns. Unlike the above tube, it has no read-erase action and erasing is performed by an unmodulated scan of the writing beam, thus rendering the store inoperative during that period.

In the present state of the storage tube art, the most flexible arrangement is provided by a cathode ray tube and a camera tube placed face to face optically, as shown by the success of intercontinental TV transmissions involving standards conversion [4][5] with this form of storage. [1][6] Of the many television camera tubes now available the Image Orthicon [7] and Image Isocon [8] do not suffer from the defect of superposition of the written signal on the read signal since the latter is derived separately from a collector or electron multiplier. As in the Graphechon, the output signal of the Orthicon and Vidicon tubes is derived from the signal plate of the target and separation of output and input signals may be effected by high frequency modulation of the reading beam. The Iconoscope and Image Iconoscope suffer the disadvantage of redistribution and spurious signal production. In the following discussion, it will be assumed that the most ambitious store available is an Image Orthicon optically coupled to a double beam cathode-ray tube; this arrangement possesses two semi-independent (in one field axis) writing organs and a single and separate reading organ.

6.22 Contour Interpolation in a Single Beam Camera Tube.

This is essential for interpolation of fields written on the same store, and it is proposed that it be performed as follows.

Assume that a full frame of lines for interpolation has been written onto the camera mosaic; in field or line interpolation this frame is an odd field interlaced with itself but written simultaneously, and in frame interpolation it is the sequential interlace of an odd field with the next-but-one. This frame may be read out two lines at a time by high frequency sampling at the Nyquist rate with a vertically oscillating reading beam. Let this oscillation, superposed on the Y-scan, be given by :

$$y(t) = d \sin 2\pi f_s t$$

where f_s is the sampling frequency and d half the line-spacing. Velocity modulation is effected by augmenting the X - scan with a sinusoidal oscillation x (t) in phase with y(t) and amplitude-modulated with a ramp function of sign dependent upon the geometrical slope-polarity of the contour, and of amplitude proportional to the normal scanning velocity V_s

$$x(t) = \pm V_s t \sin 2\pi f_s t$$

where V_s is the normal scan speed in the X-axis, and the onset of the contour is given by $t = 0$ so that $x(t) = 0$ for $t < 0$. These oscillatory scans combine to give,

$$x(t) = \pm V_s t. \; y(t) / d$$

and along the uppermost line we have therefore $x_1 (t) = \pm V_s t$ and along the lower line $x_2 (t) = \mp V_s t$; superposed on the main scan of $X(t) = V_s t$, this gives the required velocity modulation which may be termed 'Lissajous Scanning or Spot Wobble' (Fig. 6.1)

For modulation reversal once the contour is successfully found on the second line, the modulating ramp function is simply made to run down at the same rate until x (t) = 0 at which time, only the linear main x- scan X(t) is operative.

A possible circuit arrangement is shown in Fig. 6.2 and includes the velocity modulator, signal distributor and contour sensing circuits, following the more general scheme of Fig. 2.4. The time

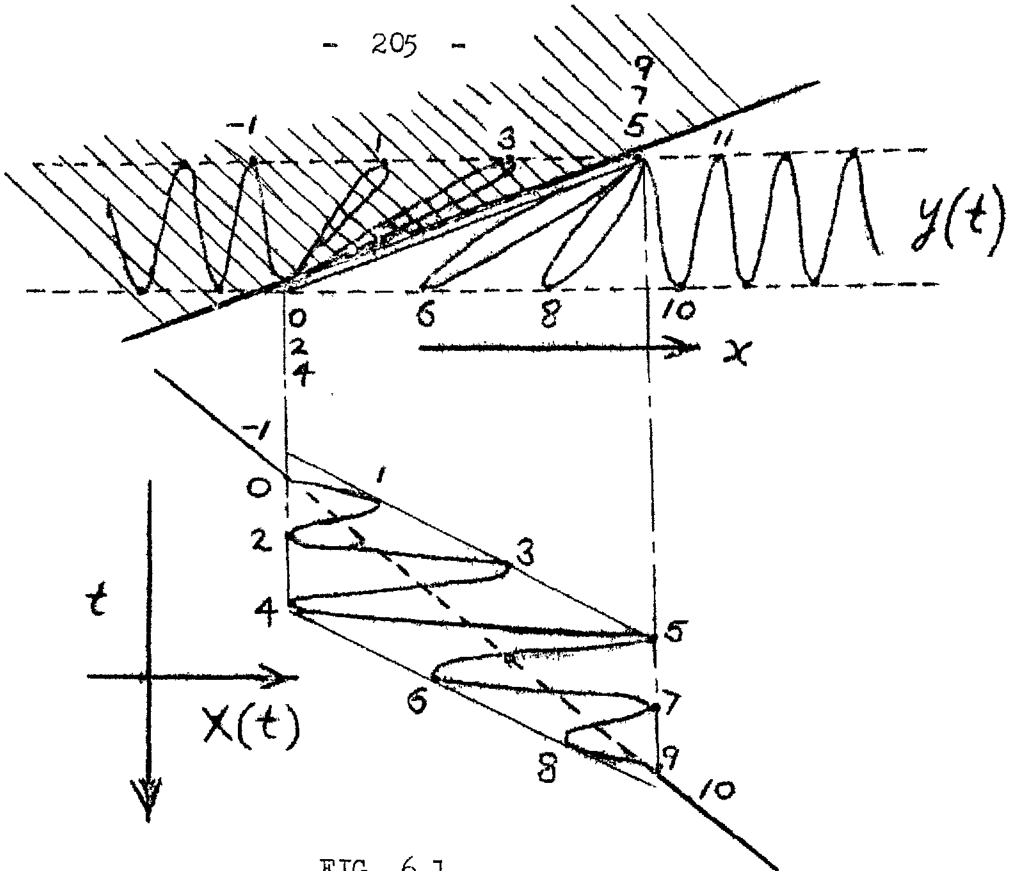

FIG. 6.1

base function for the vertical scanner is the sum of the conventional sawtooth, controlled by frame synchronisation derived from the input signal, and the double line oscillations derived from a H.F. master oscillator; this would normally be magnetic scanning. Horizontal scanning, conventionally electrostatic in orthicons, is derived from the summation of a line frequency sawtooth and the velocity modulator output of a triggered pulse ramp function-modulated sinusoid; this addition may be performed by circuitry or by using a separate deflection system for the modulator bursts (see for example the description of 'arrestor coils' by SCHLESINGER[9]). The camera output is sampled with pulses locked to twice the H.F. oscillator frequency and the resultant amplitude modulated pulses are alternately

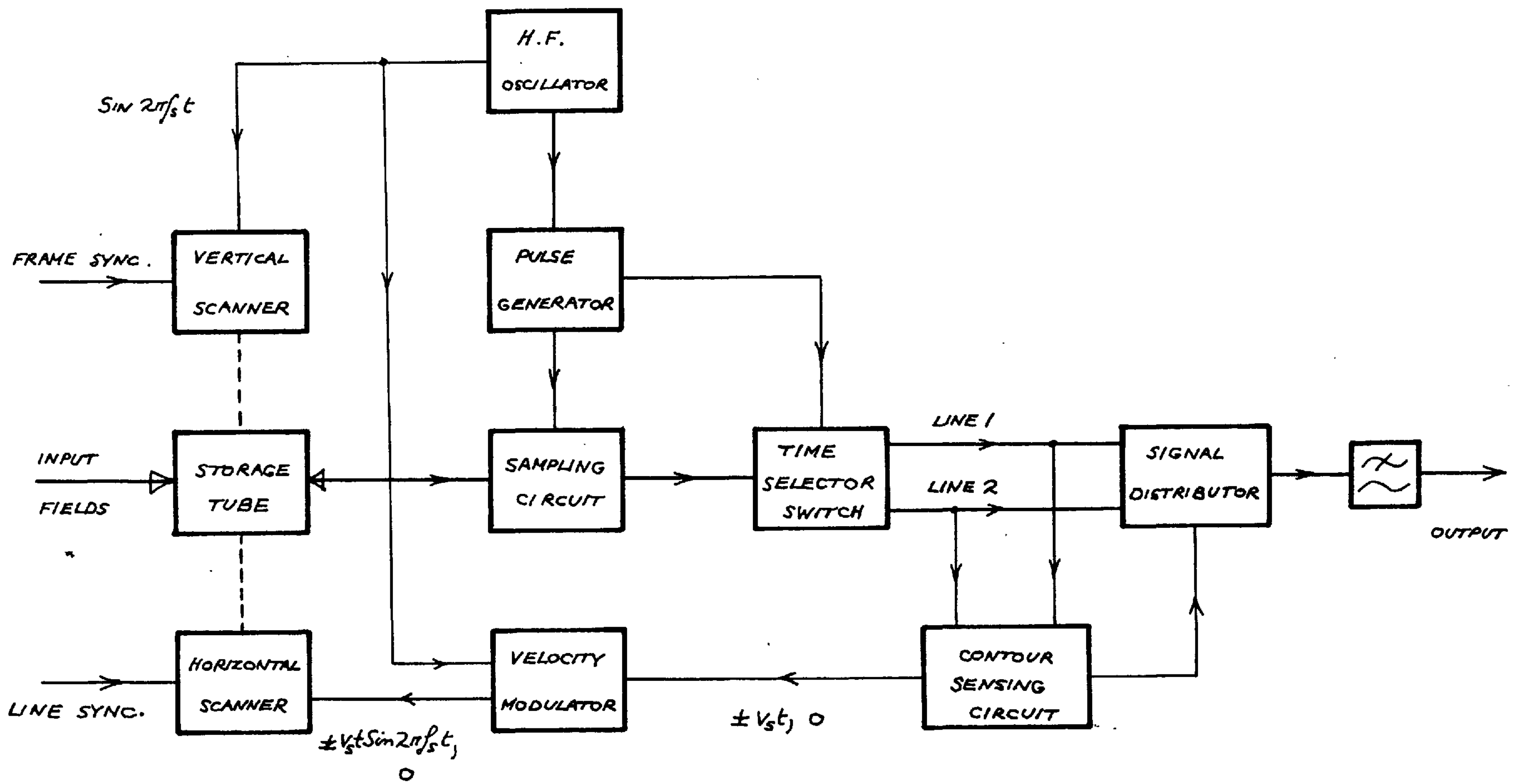

FIG. 6-2 . CONTOUR INTERPOLATION WITH 'SINGLE READ-GUN' STORE.

selected to provide separate channel line signal pulse train inputs to the contour sensing circuit; this warrants further discussion.

With line signals in pulse form, simple pulse period delay and feedback subtraction in each channel gives 'element difference' signals from which significant brightness changes may be detected. The detected points provide inputs to the logic circuit for the contour searching routine and the output of this circuit provides modulating functions for the velocity modulator and signal distributor.

The signal distributor must operate on the sampled line signals according to the velocity rule of Equation (2.3)-$S_{12} = (V_1S_1+V_2S_2)/(V_1+V_2)$, this represents a trivial circuit operation; it may be realised with a twin input adding pulse amplifier in which input gains are gated from the normal value unity to the relative values zero or two, representing the transition from linear to contour interpolation. A low-pass filter at the output restores the band-limited analogue character of the interpolated field.

Total linear interpolation is achieved in this scheme by rendering the sensing circuit inoperative; in this condition, the velocity modulator provides no additional signals to the horizontal scanner and the signal distributor equally weights the two amplitude modulated pulse trains. Alternatively, this signal may be directly derived from the sampling circuit.

6.23 Limitations in 'Single Beam' Interpolation.

Obviously it requires experimentation to demonstrate how practicable is the above system. It is useful to list certain difficulties and limitations however :-

(1) Sampling inaccuracy. With oscillatory scanning and synchronised alternate line sampling, the two derived line signals are effectively displaced by half the sampling period. In linear interpolation it might be preferable to delay one line by this period prior to signal distribution and low pass filtering. In contour interpolation, the velocity modulation routine gives an effective half sampling rate in the searching zone and the second end of the contour is therefore specified with half the accuracy of the first.

(2) Storage Tube Resolution. To ensure adequate line sample separation with sinusoidal y - scanning requires an expanded line spacing. This might necessitate a store with resolvable elements of up to two full frames.

(3) Storage Tube Erasing. The sinusoidal read-out procedure produces incomplete erasing in a tube with read/erase action; this might result in 'picture sticking' if the read-out to write-in period does not provide sufficient leakage or is not sufficient for an erase scan.

(4) Feedback Stability. The velocity modulator must respond with an accuracy of less than one sampling period and, once triggered, it becomes with the X -scanner the feedback element in a closed loop control system; the loop must satisfy the usual stability criteria.

Experiment may show that a control read-out, advanced on the main beam is essential for satisfactory working; this necessitates the development of a storage tube with two independent collectors (or multipliers) and X - scanners; the advanced scan must not erase the stored signals but might be realised with a low intensity oscillatory beam which sample-element interlaces on the main read-out.

It may be advantageous to perform the variable velocity scanning outside the storage tube by delay line circuit techniques. This might be mechanised as follows : each sampled line signal is propagated down a parallel bank of delay lines of delay $n\tau$ where τ is the element period ($\frac{1}{4}$ μsec. approx.) and n ranges from 0 to 2N, where N is the maximum number of 'search elements'. Linear interpolation is given by the arithmetic mean of the outputs from the two delay lines of delay $N\tau$ and the velocity modulation is performed by switching across the two banks at 3Mc/sec. in opposite directions.

6.3 2:1 COMPRESSION SCHEMES.

Assuming single beam interpolation to be practicable, 2:1 compression schemes with receiver contour interpolation are described; these schemes utilise conventional cathode-ray and camera tubes only.

6.31 Field Interpolation.

The transmitter requires a single store in which only the odd fields are stored and scanned at half speed for read-out (this is performed by blanking out alternate fields on a C.R.T. faced with a slow speed camera.) The transmission channel handles stretched fields of half the conventional bandwidth, and this stretched signal constitutes the receiver input.

A receiver which reconstructs the conventional sequential interlaced video signal is shown schematically in Fig. 6.3. 'A' is a storage tube of field capacity with a single writing gun and one reading gun with read/erase action (image orthicon facing cathode ray tube), 'B' is a tube of frame capacity with a double writing gun and a single reading gun with read/erase action (image orthicon facing double gun C.R.T.). Fig. 6.2 also shows the receiver scanning sequence of stores A and B; the shaded heights at any time t represent the proportion of any field stored at that moment.

The mechanism is as follows: commencing with A and B empty, let field 1 be half stored on A and also on B as a repeated-field

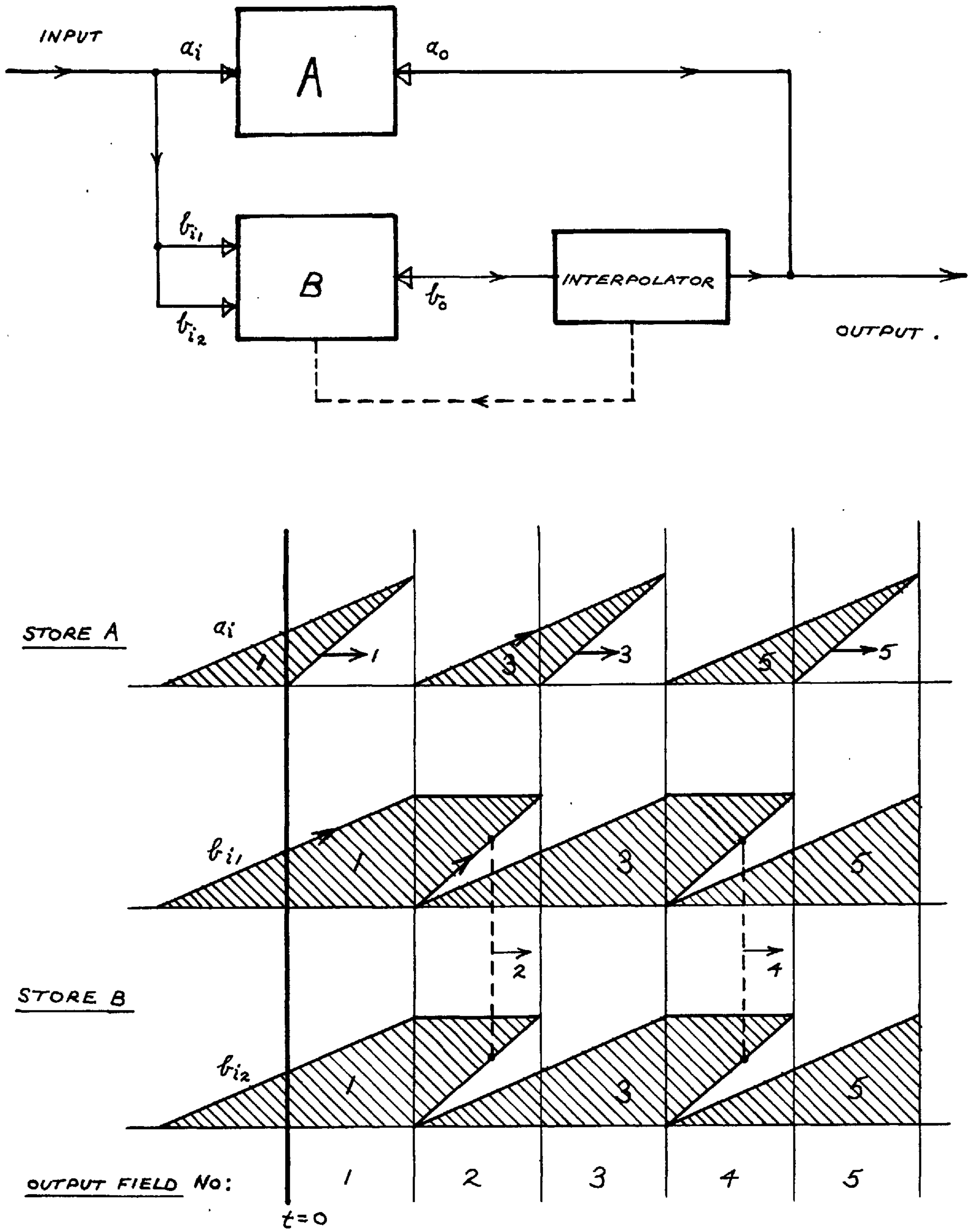

FIG. 6·3 RECEIVER WITH FIELD CONTOUR INTERPOLATION.

frame via the twin simultaneous inputs bi_1, bi_2 at $t = 0$. This field is now read out from A directly at full speed behind the second half which continues to be stored on A and B at half speed. The interlaced field 2 is now formed by reading B with contour interpolation and during this period, field 3 is half stored by A and B at half speed thus completing the cycle of 2 fields. This transmission system delays the ultimately received signal by one field period and therefore represents a technical recording.

6.32 Frame Interpolation.

Pure frame interpolation is applicable to a non-interlaced sequential system. The transmitter sends only alternate 'frames' stretched to occupy two frame periods. A receiver for reconstructing the original signal is shown schematically in Fig. 6.4 together with the store scanning sequences. A and B are stores of double frame capacity with double writing guns and single reading guns with read/erase action (image orthicon facing double-gun C.R.T.)

Receiver action is as follows: commencing with both stores completely empty, let frame 1 be completely stored as a repeated frame on store A at $t = 0$. This frame is now read out from A at full speed leaving one copy, and simultaneously, frame 3 is half stored behind it on A and also half stored as a repeated-frame on B, ai_1, being blanked out during this period. Frame 2 is now interpolated

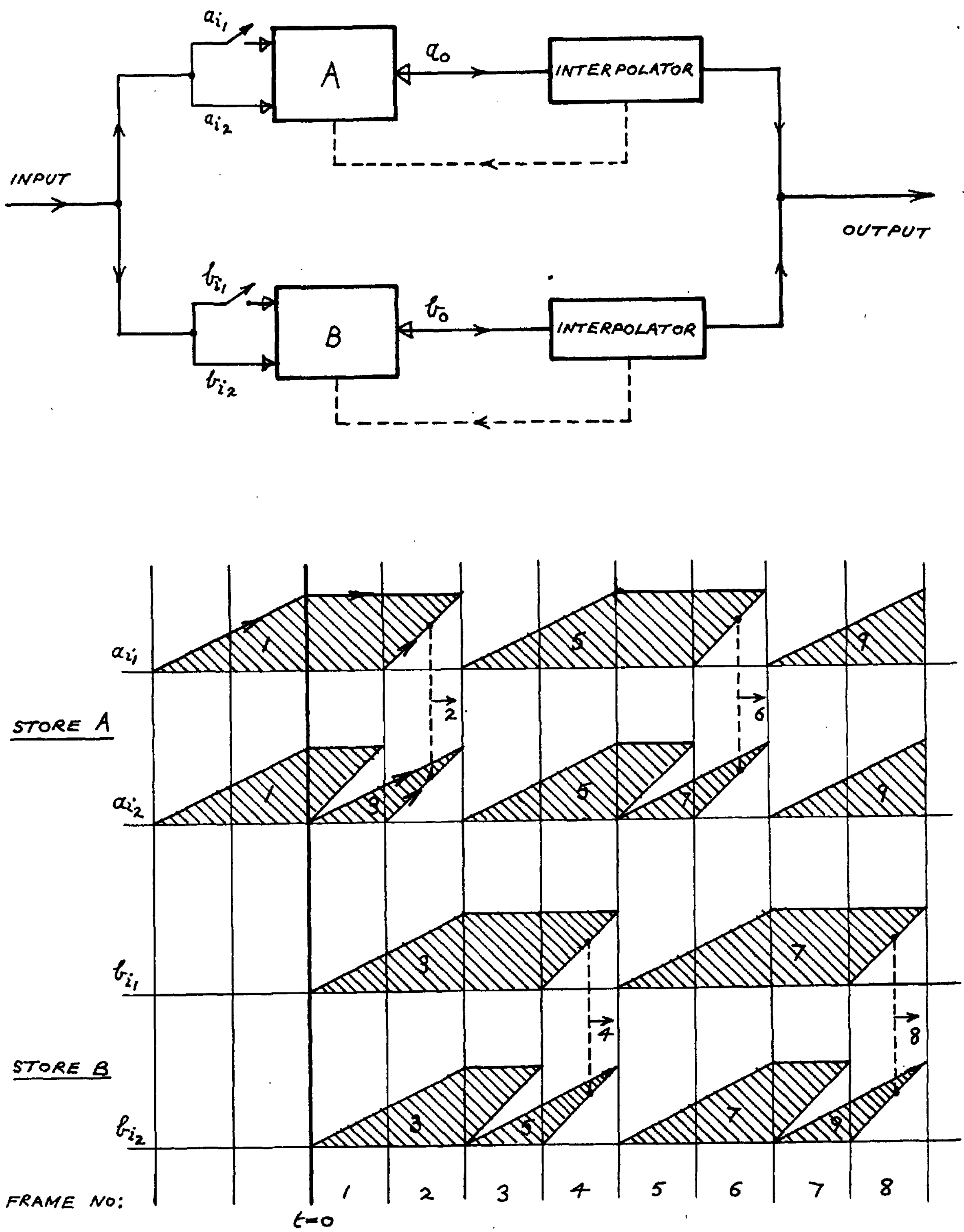

FIG. 6·4 RECEIVER WITH FRAME CONTOUR INTERPOLATION.

from frames 1 and 3 which interlace on A; on the completion of this frame, A is empty and B stores two interlaced copies of frame 3. Over the next two frames the sequence runs back from B to A, and at the end of frame 4 the stores return to the condition at t = 0; the four frame cycle then recommences. The overall delay in transmission is two frame periods; also the receiver output is asymmetrical in that the copied and the interpolated frames undergo different storage times prior to final presentation or re-transmission (this also applies to field interpolation), and also in that the interpolated frames themselves are derived from frames stored for different periods (ratio of three to one).

6.33 Synchronisation.

As in conventional transmissions, synchronising signals must be sent in the reduced waveband together with the stretched lines, fields, and frames. As the transmitter itself would normally work from full speed signals, these could be derived from half speed synchronising and blanking generators synchronised to the latter.

At the receiver, these stretched line and field synchronising pulses control the slow speed writing scanners and also provide sync. for a master synchronising and blanking generator; this generator controls the camera scanners and re-inserts full speed sync. into the receiver output.

6.4 MULTIPLE INTERPOLATION SCHEMES.

Receiver schemes for 4:1 and 8:1 compression by interpolation are described and there is a short discussion on multiple compression systems and standards conversion.

The storage tube arrangements in the following receiver schemes are dictated by the need to generate signals at conventional rates, and although attempts have been made to reduce the number of stores required to a minimum, it is not claimed that this has been achieved.

6.41 4:1 Compression with Contour Interpolation.

The transmitter stretches one field in four to four times the conventional field period, and the receiver must produce full speed copies of these fields and insert three missing fields between each pair of them; this is performed by combining 2:1 field and frame interpolation systems. In designing the receiver store logic, it is noted that each received field is required five times, and that it cannot be read out until stored for a minimum of three field periods, for producing the 'frame-interpolated' field two fields ahead. Receiver delay is thus five field periods.

It may be shown that by optically interlacing fields from two C.R.T.s onto a camera tube only three stores of frame capacity are required by the receiver (involves 3 cameras, 3 single gun C.R.T.s and 1 double gun C.R.T.). The receiver scheme to be described requires

4 stores of frame capacity (4 cameras and 4 C.R.T.s with one of these double-gun) and is shown schematically in Fig. 6.5.

The scanning sequence is given in Fig. 6.6 and the action is as follows: commencing with empty stores, assume that at $t = 0$ field 1 is stored by A_1, and C_1, and that field 5 is $\frac{1}{4}$ stored on A_2, B_2 and C_2 and D is empty.

FIELD 1 is read out from C_1 and fed back to D_1 and D_2 simultaneously. A_2,B_2,C_2 continue to receive field 5 and field 1 is completely stored on A_1.

FIELD 2 is field interpolated from repeated field 1 on D_1 and D_2 A_2, B_2,C_2 now $\frac{3}{4}$ receive field 5 and field 1 is stored on A_1.

FIELD 3 is frame interpolated from field 1 on A_1 and field 5 on A_2, and is simultaneously re-written on D_1 and D_2. Field 5 is completely stored on C_2 and B_2.

FIELD 4 is field interpolated from repeated field 3 on $D_1$and D_2. Field 9 is $\frac{1}{4}$ stored by A_1, B_1 and C_1 and B_2,C_2 store field 5.

FIELD 5 is read out from C_2 and fed back to D_1 and D_2 simultaneously. A_1,B_1,C_1 continue to receive field 9, and field 5 is completely stored on B_2.

FIELD 6 is field interpolated from repeated field 5 on D_1 and D_2. A_1,B_1,C_1 have now $\frac{3}{4}$ stored field 9 and field 5 is stored on B_2.

FIELD 7 is frame interpolated from field 5 on B_2 and field 9 on B_1, and is simultaneously re-written on D_1 and D_2. Field 9 is completely stored on A_1 and C_1.

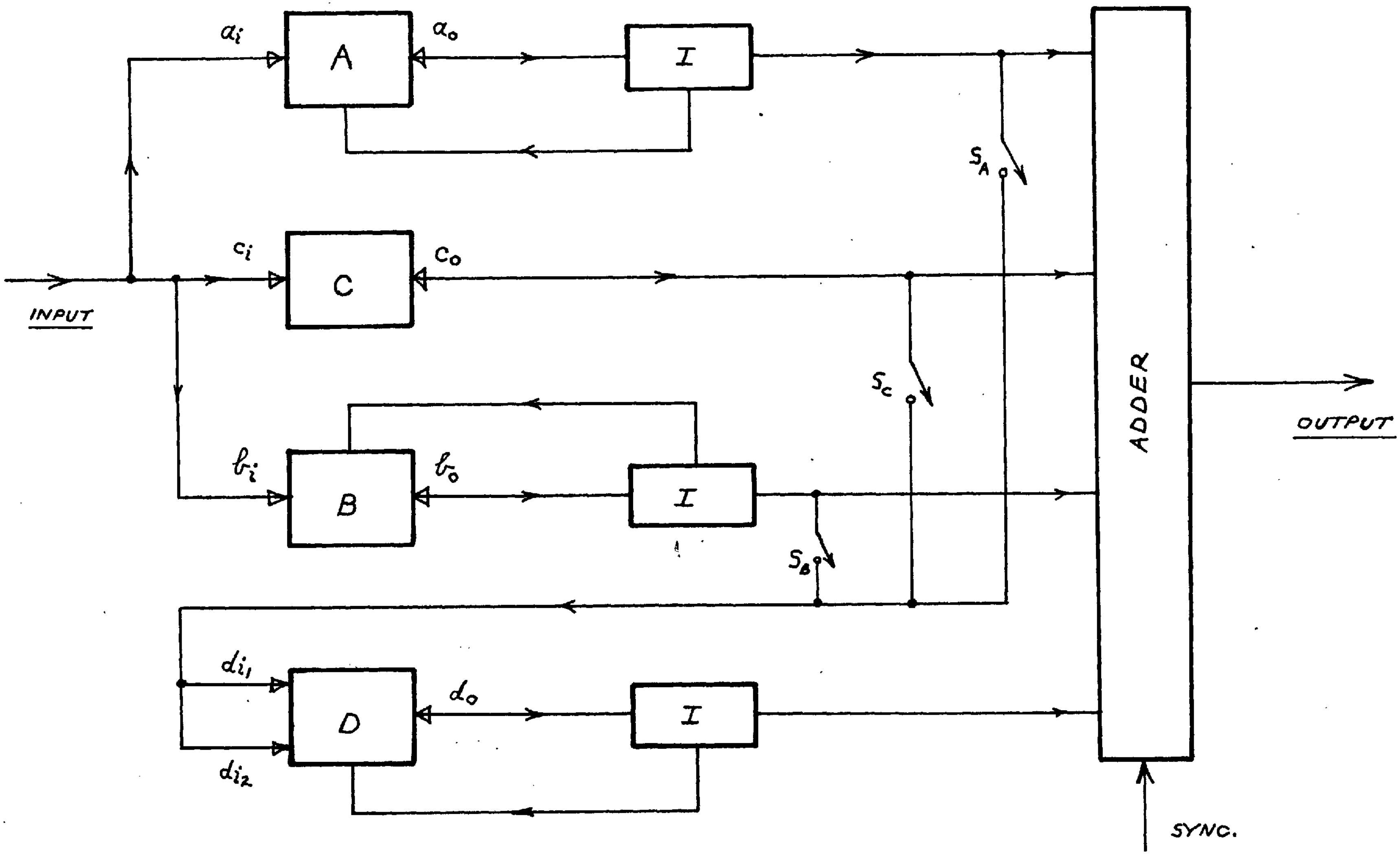

FIG. 6·5 RECEIVER WITH 4:1 FIELD/FRAME INTERPOLATION.

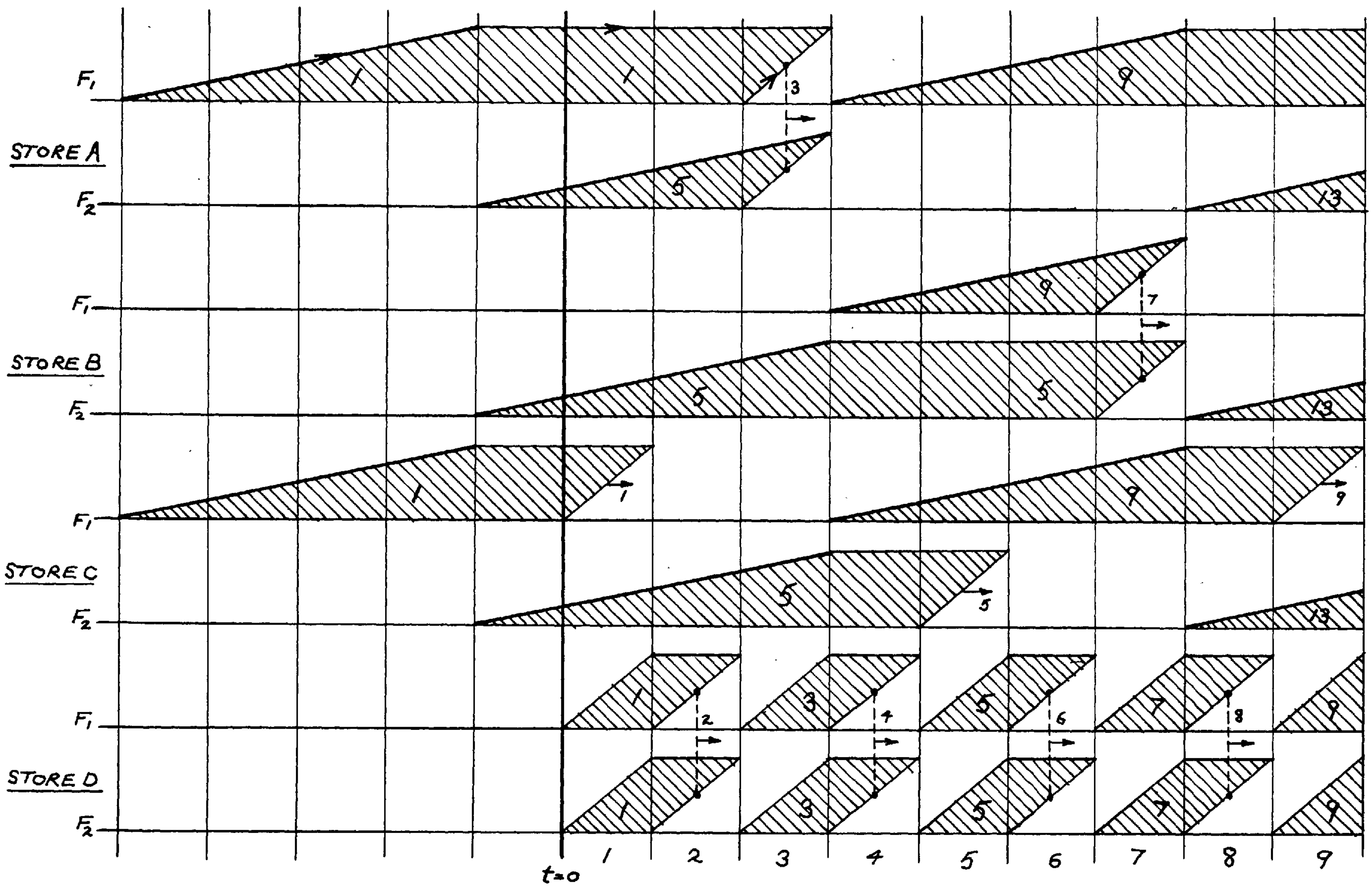

FIG. 6·6 4:1 INTERPOLATION WITH 4 STORES OF FRAME CAPACITY.

FIELD 8 is field interpolated from repeated field 7 on D_1 and D_2. Field 13 is $\frac{1}{4}$ stored by A_2, B_2 and C_2, and A_1,C_1 store field 9.

At the finish of field 8, the store condition is as at t = 0 and the four frame cycle recommences. In this system, the second interlaced field in each group (4,8,12,...) being derived from a previously interpolated field (3,7,11,...) is the one of poorest quality. (the increased processing represents a double approximation and lowers the output signal/noise ratio); also, all field interpolations are performed in the same store (D).

6.42 8:1 Compression with Contour Interpolation

The step from four-to-one to eight-to-one compression leaves two additional fields to be filled in and probably represents the limit in this form of compression. Variations in processing exist for the two missing fields, depending upon the motion detail of the programme. The transmitter simply sends one field in eight stretched to eight field periods.

For programme motion limited to 12.5 cycles/sec. we have the most economical receiver, which performs field and frame interpolation together with frame repetition. (The problem of frame repetition in storage tubes is discussed by BALDWIN[10]) and consists of the previous 4:1 receiver plus an additional store for frame repetition; this requires 5 cameras and 5 C.R.T.'s, one of these double-gun. The receiver scanning sequence is given by Fig. 6.7 and operates thus: A and B are frame-interpolating stores, C is for copying, D for field interpolation and E for frame repetition; commencing with completely erased stores, assume that at t = 0 field 1 is fully stored on A_1 and C_1 and field 9 is 3/8 received and stored by A_2,B_1, and C_2, with D and E empty; reading commences with an eleven field delay.

FIELD 1 is read out from C_1 and simultaneously rewritten on D_1,D_2 (as repeated fields) and E_1. Field 9 is half stored on A_2,B_1,C_2 and field 1 remains on A_1.

FIELD 2 is field interpolated from D_1 and D_2 and is rewritten on E_2. Field 9 is 5/8 stored on A_2,B_1,C_2 and field 1 remains on A_1.

FIELD 3 is field 1 repeated and read from E_1. Field 9 is $\frac{3}{4}$ stored on A_2,B_1,C_2 and A_1 stored field 1.

FIELD 4 is field 2 repeated and is read from E_2; Field 9 is 7/8 stored on A_2,B_1,C_2 and field 1 is on A_1.

FIELD 5 is frame-interpolated from field 1 on A_1 and field 9 on A_2, and is simultaneously rewritten on D_1,D_2 (as repeated fields) and E_1. Field 9 is fully stored on B_1 and C_2.

FIELD 6 is field-interpolated from D_1 and D_2 and is re-written on E_2 Field 17 is $\frac{1}{8}$ received and stored on C_1,B_2,A_1 and Field 9 is stored on B_1 and C_2.

FIELD 7 is field 5 repeated and read from E_1. Field 17 is $\frac{1}{4}$ stored on C_1,B_2,A_1; B_1 and C_2 store field 9 and E_2 field 6.

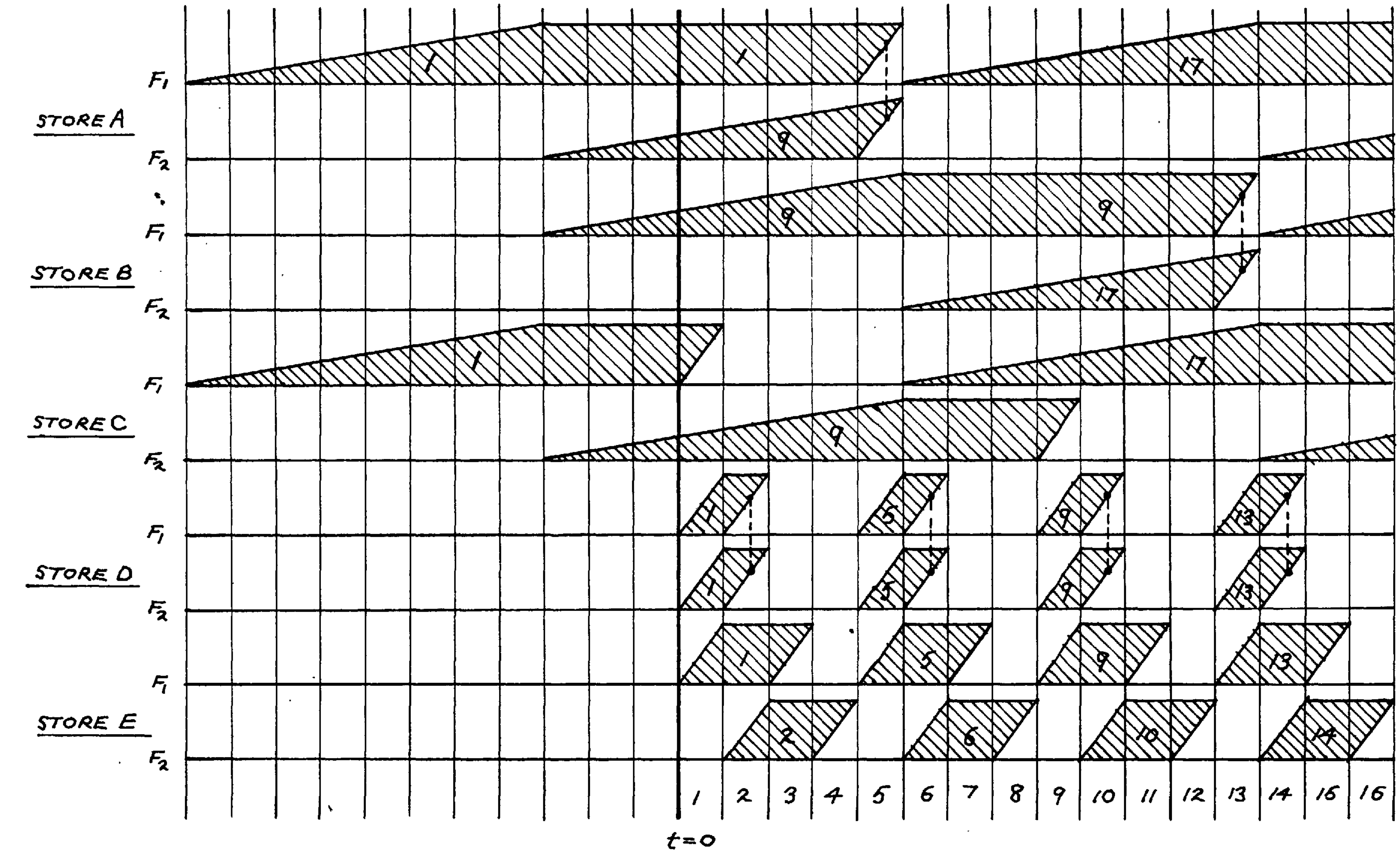

FIG. 6·7 8:1 COMPRESSION WITH 5 STORES, FIELD-FRAME INTERPOLATION, FRAME REPETITION.

FIELD 8 is field 6 repeated from E_2. Field 17 is $\frac{3}{8}$ stored on C_1,B_2,A_1 and field 9 is fully stored on C_2,B_1. Stores D and E are erased and the half-cycle is complete.

The 16-field cycle of operation should now be evident. Compared with the 4:1 compression system, this scheme suffers further degradation asymmetry since the repeated fields undergo additional storage. A poor tube E for the repetition operation would produce a 25 cycle/sec flicker.

The alternative is to field-and frame-interpolate all 7 of the missing fields; the most economical receiver is achieved if all frame-interpolations are performed at one reading, introducing intermediate storage for those fields which are required later. (this saves 2 stores). Simultaneous frame-contour interpolation of 3 fields in 8 is shown diagrammatically in Fig. 6.8 Field 3 is required directly and the mechanism is organised so that this field can be formed without the further velocity modulation which is required for the intermediate storage of fields 5 and 7. To allow for changing object brightness with movement, weighted linear interpolation is used:

Field 3, $S_3(t) = \frac{3}{4} S_1(t) + \frac{1}{4} S_9(t)$

Field 5, $S_5(t) = \frac{1}{2}S_1(t) + \frac{1}{2} S_9(t)$

Field 7, $S_7(t) = \frac{1}{4} S_1(t) + \frac{3}{4} S_9(t)$.

Referring to Fig. 6.8 for an initial contour in field 1, contour

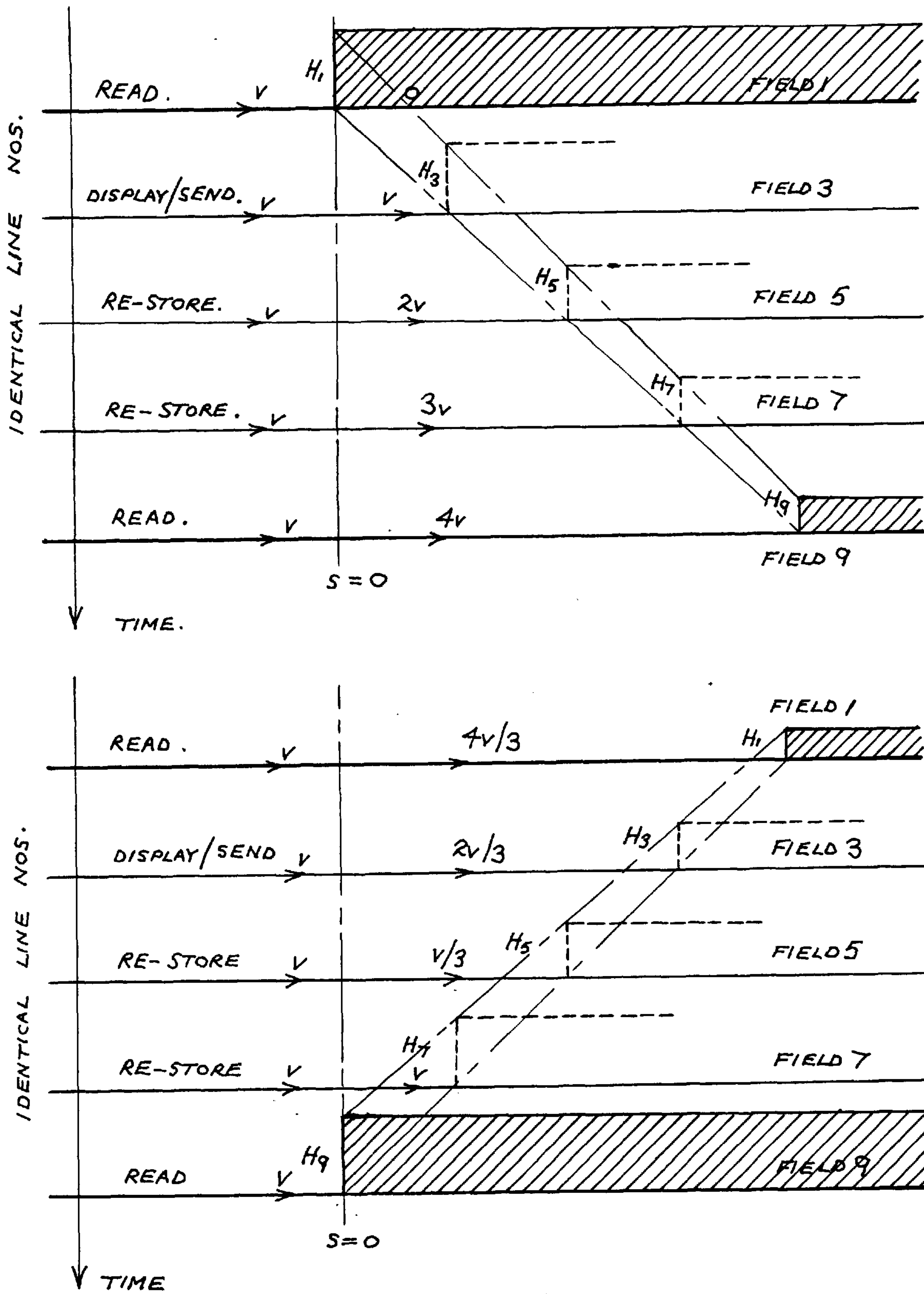

FIG. 6·8 4:1 SIMULTANEOUS FRAME CONTOUR INTERPOLATION searching in field 9 is performed at velocity $V_9 = 4V_s$ (with V_s = normal scanning velocity) and in the search period, the writing velocities and signal intensities are respectively $V_s, 2V_s, 3V_s$ and $S_9(t)$, $2S_9(t)$, $3S_9(t)$ for fields 3,5,7. For inverse geometrical contours, contour searching proceeds at speed $V_1 = 4V_s/3$ and the writing velocities and signal intensities become V_s, $2V_s/3$ $V_s/3$ and $S_1(t)$, $2S_1(t)/3$, $S_1(t)/3$. The modulated twin line reading velocities of $(0, 4V_s)$ and $(4V_s/3, 0)$ may be performed by 'Lissajous Spot Wobble' with modified modulating envelopes (the twin ramp must contain positive and negative slopes in ratio 1:3). Velocity modulation for writing fields 5 and 7 may utilise a variable velocity scanner of the BEDDOES type.(11) (12).

A receiver for complete contour interpolation requires 6 stores (6 camera tubes and 6 C.R.T.s with one of these double-gun and two with variable velocity scanners); the scanning sequence is given in Fig.6.9; A is a store for field copying, B and C are frame-interpolating stores, D is for all field-interpolations, E and F are for intermediate frame-interpolated fields. Commencing operation at t= 0, let field 1 be received and completely stored by A_1 and B_1 and field 9 $\frac{5}{8}$th. stored on A_2, B_2, and C_1 with E and F erased. Reading commences with a 13 field delay.

FIELD 1 is read out from A_1 and is simultaneously re-written on D_1, D_2

as a repeated-field frame. Field 9 is $\frac{3}{4}$ stored on A_2, B_2, C_1. Field 1 is stored by B_1.

FIELD 2 is field interpolated from field 1 on D by Lissajous or delay line technique. Field 9 is 7/8 stored on A_2, B_2, C_1. Field 1 is stored by B_1.

FIELD 3 is frame interpolated from fields 1 and 9 on B_1, B_2 by modified Lissajous technique and fields 5 and 7 are simultaneously interpolated onto E and F respectively. Field 3 is fed back to D as a repeated-field frame. C_1, A_2 fully store field 9 and A_1, B_1, B_2, and C_2 are empty.

FIELD 4 is field interpolated from field 3 on D. Field 17 is $\frac{1}{8}$ received by A_1, B_1, C_2, and A_2, C_1 completely store field 9. Fields 5 and 7 are stored by E and F.

FIELD 5 is read directly from E and re-written back on D as a repeated-field frame; field 17 is $\frac{1}{4}$ stored by A_1, B_1, C_2 and F stores field 7 with field 9 stored on A_2, C_1.

FIELD 6 is field interpolated from field 5 on D; field 17 is $\frac{3}{8}$ stored on A_1, B_1, C_2 and field 9 is stored on A_2, C_1; F stores field 7.

FIELD 7 is read directly from F and restored on D as a repeated-field frame; field 17 is $\frac{1}{2}$ stored on $A_1 . B_1, C_2$ and A_2, C_1 stores field 9.

FIELD 8 is field interpolated from field 7 on D; field 17 is $\frac{5}{8}$ stored on A_1, B_1, and C_2, and A_2, C_1 store field 9; E, F, and B_2 are empty. B and C are now at the half-cycle condition.

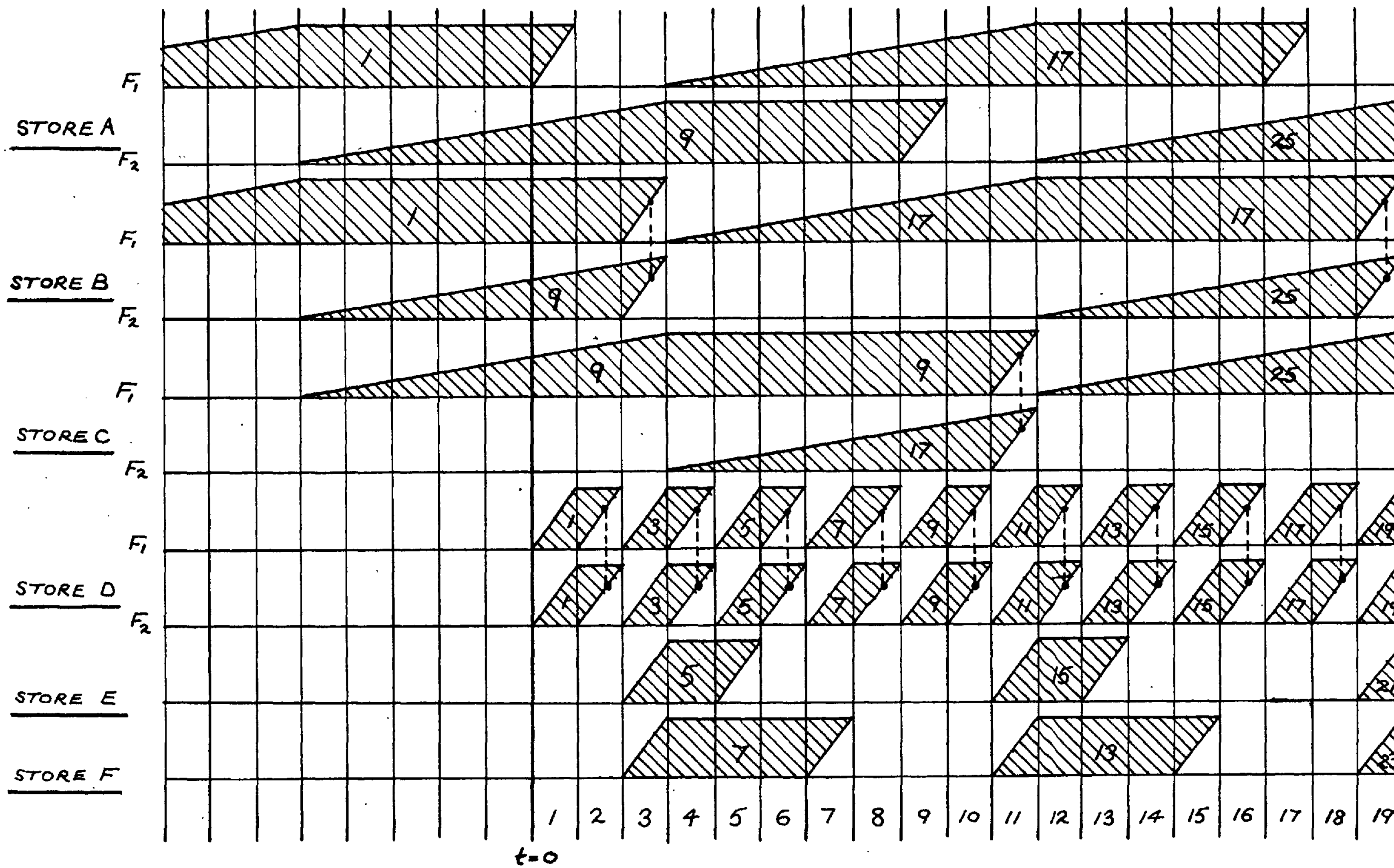

FIG. 6·9 8:1 COMPRESSION WITH 6 STORES AND COMPLETE CONTOUR INTERPOLATION.

All stores return to the t = 0 condition after 16 field periods.

6.43 Standards Conversion and Interpolation.

Two types of Standards conversion of TV signals have been reviewed by ZWORYKIN and RAMBERG (13). They are,

(1) Intermediate Film Storage Method.

(2) Instantaneous Storage Tube Method.

The instantaneous scheme is described by LORD (4), also by HAANTJES and SCHUT (5).

For Standards step-down transmission, such as U.S. (525 line, 60 cycle/sec.) to G.B. (405 line, 50 cycle/sec.), bandwidth compression and standards conversion can be combined in a single transmitter store, in which every 12th. field is selected and stretched to 10 converted field periods (1/5 second) with 202½ lines. The receiver must then operate on a 10:1 compressed signal, frame-interpolating 4 fields and field-interpolating 5 fields between every 2 stretched fields received. Five to one compression could be achieved by transmitting one frame in every six with 405 lines at 5 cycles/sec., and if complete interpolation proved too complex, limited motion programmes could be processed by combining frame interpolation with frame repetition.

The reverse transmission involves step-up standards conversion; if the 405 line, 50 C.P.S. signal is 10:1 compressed, the receiver must

12:1 interpolate and increase the number of lines per field by a factor of 5/4, which might be performed by further interpolation. (this is obviated by duplicating the initial pick-up tube with a camera working to the higher standard and then compressing 12:1 in the transmitter.)

Field contour interpolation provides a useful means for standdards conversion of systems with identical field rates and unequal field-line numbers.

6.44 Multiple Compression.

To achieve higher orders of compression, the above systems may be placed in tandem with rate equalizing schemes. If the rate equalising transmission is subsequent to the field stretching, the coder operates on conventional fields at reduced bandwidth. The receiver is simply the inverse - a decoder followed by contour interpolation.

In particular if we consider the CHERRY - GOURIET system, (14) it must be possible, at lease in principle, to combine both receiver operations, as they both depend upon indentifying brightness rates of change. If such a multiple scheme (of probable compression ratio 24:1) were to be considered practicable, this possibility shoudl be seriously investigated, as a reduction in the number of receiver operations would result in increased fidelity in the ultimate receiver output.

6.5 REFERENCES

1. KNOLL, M., KAZAN, B., Storage Tubes and Their Basic Principles. John Wiley, New York, pp 131-40, 1952.

2. PENSAK, L., The Graphecon - A Picture Storage Tube, R.C.A. Review, 10, pp.59 - 73, March 1949.
   Picture Storage Tube, Electronics, 22, pp.84 - 88, July, 1949.

3. KNOLL, M., RANDMER, Ladungs - Bildspreicherohren mit Speichergitter. Archiv El. Ubertragung, 4, 238, 1950.

4. LORD, A.V., Standards Conversion for International TV. Electronics, 26, pp.144 - 7, August, 1953.
   Conversion of TV Standards, BBC Quarterly, 8, No.2., pp.108 - 24, 1953 (Bibliography of 20 items).

5. HAANTJES J., SCHUT, T.G., A Line Converter for the International Exchange of TV Programmes. Philips Tech. Review, 15, pp.297 - 306, May 1954.

6. McGEE, J.D., Distant Electric Vision (Review of Camera Tubes). Proc. I.R.E., 38, pp. 596 - 608, June, 1950.

7. ROSE, A., WEIMER, P.K., LAW, H.B., The Image Orthicon, a Sensitive Television Pickup Tube. P.I.R.E., 34, pp 424 - 32, 1946.

8. WEIMER, P.K., The Image Isocon. RCA Review 10, pp.366 - 386, September, 1949.

9. SCHLESINGER, K., Dot Arresting Improves TV Picture Quality, Electronics, 24, No. 9, p.96, September 1951.

10. BALDWIN, M.W., Documentation of Some Visual Effects of Using Frame Storage in TV Transmission, I.R.E. Convention Record, Part 4, p.107, March, 1958.

11. BEDDOES, M.P., A Variable Velocity Scanner for Magnetic Deflection of a Scanning Spot. P.I.R.E., 104, pp.481 - 88. September 1957.

12. RAO, V.N., SANKARASUBRAMANYAN, V., An Expanded Time Base Using a Miller Integrator. Electronic Eng. 27, 273, June, 1955.

13. ZWORYKIN, RAMBERG, E.G., Standards Conversion of Television Signals. Electronics, 25, pp. 86 - 91, January, 1952.

14. CHERRY, E.C., GOURIET, G.G., Some Possibilities for the Compression of TV Signals by Re-coding, Symp. on Communication Theory, London, 1952.

7. APPENDICES.

7.1 DESIGN EQUATIONS AND THEORETICAL RESPONSE OF THE ANGULAR REDUCTION MECHANISM OF THE VELOCITY MODULATOR.

7.11 List of Symbols

I_1 = Inertia of driven shaft (lever arm shaft)

I_2 = Inertia of coupled mirror shaft.

l_1 = Length of driven shaft.

l_2 = Length of mirror shaft .

r_1 = Radius of driven shaft.

r_2 = Radius of mirror shaft.

θ_1 = Angular displacement of driven shaft.

θ_2 = Angular displacement of mirror shaft.

l_A = Coupling wire length for driven shaft. (see Fig. 7.1 (a)).

l_B = Coupling wire length for mirror shaft. (see Fig.7.1 (a)).

R = Radial displacement of coupling wires from shaft axes. (Fig.7.1(b)).

r = Radius of coupling spring wire.

T_c = Torque derived from cantilever deflection of wire coupling.

T_T = Torque derived from torsional deflection of wire coupling.

I = Coupling wire second moment of area.

J = Coupling wire polar second moment of area.

k_c = Stiffness of driven/mirror shaft resulting from cantilever deflection of coupling wire.

k_t = Stiffness of driven/mirror shaft resulting from torsional deflection of coupling wire.

E = Modulus of elasticity of coupling wire.

G = Modulus of rigidity of coupling wire.

Wn_1 = Natural frequency of driven shaft with $I_2 = 0$

Wn_2 = Natural frequency of mirror shaft with $I_1 = 0$

F_1 = Force acting on each coupling wire at distance l_A along it.

F_2 = Force acting on each coupling wire at distance l_B along it.

T_A = Torque on coupling wire at point l_A.

T_B = Torque on coupling wire at point l_B.

T_1 = Resultant torque on driven shaft.

T_2 = Resultant torque on mirror shaft.

A,B,C,D,E,F, = Parameters to be defined in text.

g = Gravitational acceleration constant.

K_T, K_C = Parameters to be defined in text.

7.12 Mode of Behaviour

The driving torque T_D derived from lever-arm location on the picture transformer drum/flange is communicated to shaft 2 via two coupling cantilevers of spring steel as illustrated in Fig. 7.1 (a). Neglecting the torsional deflection of the cantilevers, the STATIC equilibrium for small angles is given by :

$$\theta_1 = (l_A/l_B)^3 \, \theta_2 \qquad \text{------------(1)}$$

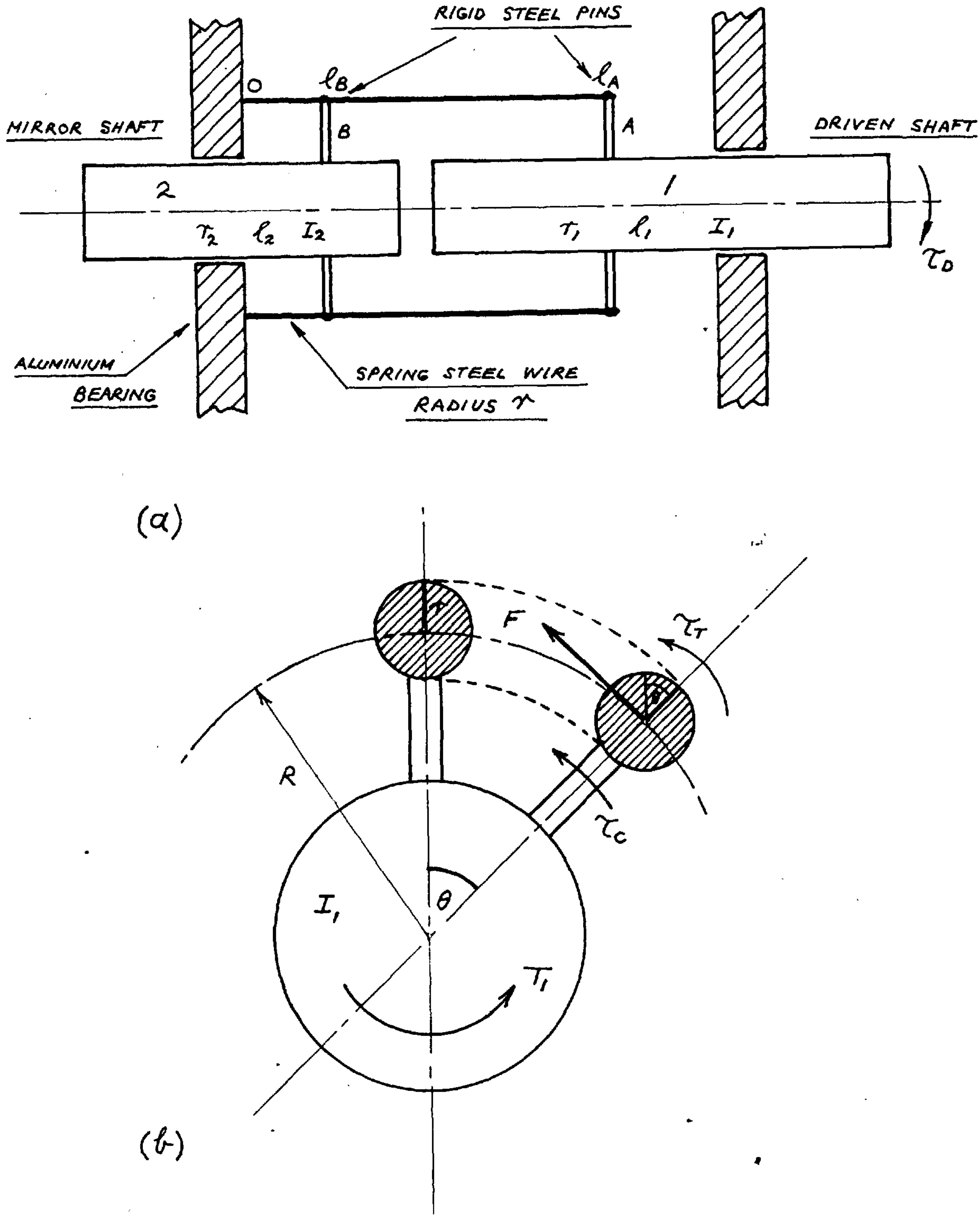

FIG.7.1 REDUCTION MECHANISM OF VELOCITY MODULATOR.

Equation (1) holds under DYNAMIC conditions providing that the working frequency of the mechanism is very small compared with the natural frequencies of the pertinent modes of oscillation of the coupled inertias. We ultimately require the response of the system to something approaching a STEP FUNCTION of DRIVING TORQUE, and ideally this response should be aperiodic and with an amplitude given by $/\theta_1/ = 6.2 /\theta_2/$.

With the coupling wires rigidly affixed to the shaft radial pins, we shall assume that the motion of the reduction mechanism is combined LATERAL CANTILEVER DEFLECTION and simple TORSIONAL DEFLECTION. Assuming the reduction coupling to have negligible mass and inertia in the pertinent vibration modes, we combine the two deflection modes in a theory for the complete behaviour, with the restriction that deflections are small enough for small-angle approximations to hold.

The Lateral Mode is given by the cantilever deflection formula:

$$y_{l} = \frac{Fl^3}{3EI} \qquad \text{------------ (2)}$$

for a point load F at x = l. Restoring torque T_c resulting is given by $T_c = FR$ for small angles, and with $y_l \to R\theta$, (2) becomes

$$T_c = \left(\frac{EIR^2}{l^3}\right) . \theta = k_c\theta \qquad \text{------------- (3)}$$

The Torsional Mode is given by the torsional deflection formula:

$$T = \frac{G\phi J}{l} \qquad \text{---------------- (4)}$$

and for a cylinrical wire $J = \pi r^4/2$, also the Torsional restoring torque on the shaft is given by $T_T = rT/R$, hence (4) becomes

$$T_T = \left(\frac{\pi G r^5}{2lR}\right) . \theta = k_T \theta \quad \text{-----------(5)}$$

Superposing (3) and (5) gives the total STATIC restoring force required to hold I_1 at $\theta = \hat{\theta}1$ peak deflection:

$$T_{Rest} = 2\ (k_c^{(A)} + k_T^{(A)}).\ \hat{\theta}1 \quad \text{-------- (6).}$$

Assuming $I_2 = 0$, the equation of motion for I_1 is:

$$I_1\ddot{\theta}_1 + 2\ (k_c^{(A)} + k_T^{(A)})g\theta_1 = 0 \text{ which gives .,}$$

$$f n_1 = Wn_1/2\pi = \frac{1}{2\pi}\left(\frac{2g.k_c^{(A)} + k_T^{(A)}}{I_1}\right)^{\frac{1}{2}} \text{------ (7)}$$

for the <u>undamped</u> natural frequency of oscillation of I_1. Similarly, the undamped natural frequency of I_2 with $I_1 = 0$ is,

$$f n_2 = Wn_2/2\pi = \frac{1}{2\pi}\left(2g.\ \frac{k_c^{(B)} + k_T^{(B)}}{I_1}\right)^{\frac{1}{2}} \text{----(8)}$$

Also, we note from (3) and (5) that

$$k_c^{(B)} = \left(\frac{lA}{l_B}\right)^3 k_c^{(A)} \quad \text{-------- (9)}$$

$$k_T^{(B)} = \left(\frac{lA}{l_B}\right) k_T^{(A)} \quad \text{---------(10)}$$

<u>7.13 Analysis of Undamped Coupled System.</u>

CANTILEVER DEFLECTION of end-fixed wire of length l_A with point loads F_1 and F_2 at $x = l_A$, l_B respectively is given by the bending moment formula:

$$M(x) = F_1(l_A - x) - F_2(x - l_B) \text{ with } y = y^{(1)} = 0 \text{ at } x = 0$$

i.e. $$EI \frac{d^2y}{dx^2} = F_1 l_A + F_2 l_B - x\,(F_1 + F_2)$$

gives on integration, $$EIy = (F_1 l_A + F_2 l_B)\frac{x^2}{2} - (F_1 + F_2)\frac{x^3}{6}$$

Putting $x = l_B$ gives the deflection y_B at $x = l_B$:

$$y_B = \frac{1}{EI}\left\{\left(\frac{l_A l_B^2}{2} - \frac{l_B^3}{6}\right) F_1 + \left(\frac{l_B^3}{3}\right) F_2\right\} \text{ - - (11)}$$

Similarly, $x = l_A$ gives the far end deflection y_A:

$$Y_A = \frac{1}{EI}\left\{\left(\frac{l_A^3}{3}\right) F_1 + \left(\frac{l_B l_A^2}{2} - \frac{l_A}{6}\right) F_2\right\} \text{ - - - - - - -(12)}$$

Also $y_A = R\theta_1$, and $y_B = R\theta_2$, hence from (12) we have

$$\theta_1 = \frac{1}{EIR}\left\{\left(\frac{l_A^3}{3}\right) F_1 + \left(\frac{l_B l_A^2}{2} - \frac{l_A^3}{6}\right) F_2\right\} \text{ - - - - - - -(13)}$$

and from (11) we have :

$$\theta_2 = \frac{1}{EIR}\left\{\left(\frac{l_A l_B^2}{2} - \frac{l_B^3}{6}\right) F_1 + \left(\frac{l_B^3}{3}\right) F_2\right\} \text{ - - - - - -(14)}$$

i.e. $$\begin{bmatrix} \left(\frac{l_A}{3}\right) & \left(\frac{l_B}{2} - \frac{l_A}{6}\right) \\ \left(\frac{l_A}{2} - \frac{l_B}{6}\right) & \left(\frac{l_B}{3}\right) \end{bmatrix} \begin{bmatrix} F_1 \\ F_2 \end{bmatrix} = \begin{bmatrix} \frac{\theta_1}{l_A^2} \\ \frac{\theta_2}{l_B^2} \end{bmatrix} EIR$$

and solving for F_1 and F_2 in terms of θ_1 and θ_2 we have:

$$F_1 = 4EIR. \frac{\left(\frac{l_B}{l_A}\right)\theta_1 - \left(\frac{3l_B - l_A}{2l_B^2}\right)\theta_2}{(l_A - l_B)^2} \text{ - - - - - (15)}$$

$$F_2 = 4EIR. \frac{\left(\frac{l_B - 3l_A}{l_A^2}\right)\theta_1 + \left(\frac{l_A}{l_B^2}\right)\theta_2}{(l_A - l_B)^2} \quad ------(16)$$

Hence the restoring torques given by the cantilever deflection of two wires are, $T_{C1} = 2RF_1$, and $T_{C2} = 2RF_2$:-

i.e. $$T_{C1} = \frac{8EIR^2}{(l_A - l_B)^2}\left\{\left(\frac{l_B}{l_A^2}\right)\theta_1 + \left(\frac{l_A - 3l_B}{2l_B^{\ 2}}\right)\theta_2\right\} \quad ---(17)$$

and $$T_{C2} = \frac{8EIR^2}{(l_A - l_B)^2}\left\{\left(\frac{l_B - 3l_A}{l_A^2}\right)\theta_1 + \left(\frac{l_A}{l_B^2}\right)\theta_2\right\} \quad ----(18)$$

TORSIONAL DEFLECTION of cantilever with point l_B constrained to deflect θ_2 and point l_A constrained to deflect θ_1 with torques T_B and T_A respectively is given by equation (4) and superposition:-

$$\theta_1 = \frac{2}{\pi G r^4} \cdot (T_B l_B + T_A l_A) \quad -----------(19)$$

and $$\theta_2 = \frac{2}{\pi G r^4} \cdot (T_B l_B + T_A l_B) \quad -----------(20).$$

Restoring torques on inertias I_1, I_2 are given by solving (19), (20) for T_A and T_B in terms of θ_1 and θ_2 and putting $T_{T1} = 2rT_A/R$ and $T_{T2} = 2rT_B/R$

i.e. $$T_{T1} = \frac{\pi G r^5}{R(l_A - l_B)} \cdot (\theta_1 - \theta_2) \quad ---------- (21)$$

and $$T_{T2} = \frac{\pi G r^5}{R(l_A - l_B)}\left(\frac{l_A}{l_B} \cdot \theta_2 - \theta_1\right) \quad ---------(22)$$

EQUATIONS OF MOTION for zero damping become :-

$$I_1\ddot{\theta}_1 + gT_{C1} + g^T{}_{T1} = T_1 \qquad \text{-------------(23)}$$

and $$I_2\ddot{\theta}_2 + g^T{}_{C2} + g^T{}_{T2} = 0 \qquad \text{-------------(24)}$$

Putting (17) and (21) in (23) we have :-

$$I_1\ddot{\theta} + \frac{\pi G r^5 g}{R(l_A - l_B)}(\theta_1 - \theta_2) + \frac{8EIR^2 g}{(l_A - l_B)^2}\left\{\left(\frac{l_B}{l_A^2}\right)\theta_1 + \frac{(l_A - 3l_B)\theta_2}{l_B^2}\right\} = T_1$$

or, putting $K_T = \pi G r^5\, g/R$ ------------ (25)

and $K_C = 8\pi EIR^2 g$ -------------(26)

we have :-

$$I_1\,(l_A - l_B)^2\ddot{\theta}_1 + K_T(l_A - l_B)(\theta_1 - \theta_2) + K_C\left\{\frac{l_B}{l_A^2}\,.\,\theta_1 + \frac{(l_A - 3l_B)}{l_B^2}\,\theta_2\right\} = T_1(l_A - l_B)^2$$

$$I_1(l_A - l_B)^2\ddot{\theta}_1 + \left\{K_T(l_A - l_B) + \frac{K_C l_B}{l_A^2}\right\}\theta_1 + \left\{\frac{K_C}{l_B^2}\,(l_A - 3l_B) - K_T(l_A - l_B)\right\}\theta_2 = T_1(l_A - l_B)^2$$

$$I_1\ddot{\theta}_1 + \left\{\frac{K_T l_A + \left(\frac{K_C}{l_A^2} - K_T\right)l_B}{(l_A - l_B)^2}\right\}\theta_1 + \left\{\frac{\left(\frac{K_C}{l_B^2} - K_T\right)l_A + \left(K_T - \frac{3K_C}{l_B^2}\right)l_B}{(l_A - l_B)^2}\right\}\theta_2 = T_1$$

which may be written:

$$A\ddot{\theta}_1 + B\theta_1 + C\theta_2 = T_1 \qquad \text{--------------- (27)}$$

where $A = I_1$ --------------- (28)

$$B = \frac{K_T l_A + (K_C/l^2{}_A - K_T)l_B}{(l_A - l_B)^2} \qquad \text{------------- (29)}$$

$$C = \frac{(K_C/l^2{}_B - K_T)\; l_A + (K_T - 3K_C/l^2{}_B)l_B}{(l_A - l_B)^2} \qquad \text{----- (30)}$$

Also, putting (18) and (22) in (24) we have :-

$$I_2\ddot{\theta}_2 + \frac{\pi G r^5 g}{R(l_A - l_B)}\left\{\frac{l_A}{l_B}\theta_2 - \theta_1\right\} + \frac{8EIR^2 g}{(l_A - l_B)^2}\left\{\frac{l_B - 3l_A}{l_A^2}.\theta_1 + \frac{l_A}{l_B^2}.\theta_2\right\} = 0$$

and inserting (25) and (26) gives:

$$I_2(l_A - l_B)^2\ddot{\theta}_2 + K_T(l_A - l_B)\left\{\frac{l_A}{l_B}\theta_2 - \theta_1\right\} + K_C\left\{\frac{l_B - 3l_A}{(l_A 2)}.\theta_1 + \frac{l_A}{l_B^2}.\theta_2\right\} = 0$$

$$I_2(l_A - l_B)^2\ddot{\theta}_2 + \left\{K_T(l_A - l_B)\frac{lA}{l_B} + \frac{K_C l_A}{l_B^2}\right\}\theta_2 + \left\{K_T + \frac{K_C}{l_A^2}.l_B - \left(K_T + \frac{3K_C}{lA^2}\right)l_A\right\}\theta_1 = 0$$

$$I_2\ddot{\theta}_2 + \left\{\frac{\left(\frac{l_A K_T}{l_B} + \frac{K_C}{l_B^2} - K_T\right)l_A}{(l_A - l_B)^2}\right\}\theta_2 + \left\{\frac{\left(K_T + \frac{K_C}{l_A^2}\right)l_B - \left(K_T + \frac{3K_C}{l_A^2}\right)l_A}{(l_A - l_B)^2}\right\}\theta_1 = 0$$

which may be written:

$$D\ddot{\theta}_2 + E\theta_2 + F\theta_1 = 0 \quad \text{--------------- (31)}$$

where $D = I_2$ --------------- (32)

$$E = \frac{\left(\frac{l_A K_T}{l_B} + K_C/l_B^2 - K_T\right)l_A}{(l_A - l_B)^2} \quad \text{----------(33)}$$

$$F = \frac{(K_T + K_C/l_A^2)l_B - (K_T + 3K_C/l_A^2)l_A}{(l_A - l_B)^2} \quad \text{--------- (34)}$$

The motion is thus defined by the simultaneous differential equations (27) and (31). To solve, we note that from (31) we have :-

$$F\theta_1 = -(D\theta_2^{(2)} + E\theta_2)$$

$$F\ddot{\theta}_1 = -(D\theta_2^{(4)} + E\theta_2^{(2)})$$ and inserting in (27):

$$AD\theta_2^{(4)} + (AE + BD)\,\theta_2^{(2)} + (BE - CF)\,\theta_2 = -FT_1 \quad \text{------(35)}$$

and similarly putting $C\theta_2 = T_1 - A\theta_1^{(2)} - B\theta_1$ from (27) in (31)

gives : $$AD\theta_1^{(4)} + (AE+BD)\theta_1^{(2)} + (BE-CF))\theta_1 = ET_1+DT_1^{(2)} \quad \text{---(36)}$$

The natural frequencies of the system are given by putting $T_1=T_1^{(2)} = 0$ in (35) or (36):-

$$ADp^4\theta_1 + (AE+BD)p^2\theta_1 + (BE-CF)\,\theta_1 = 0$$

$$p^2 = \frac{-(AE+BD) \pm \left\{(AE+BD)^2 - 4AD(BE-CF)\right\}^{\frac{1}{2}}}{2\,AD}$$

and for $p^2 = -w^2$, $p = \pm\, jw$, the natural frequencies are gived by:

$$Wn_1^2 = \frac{(AE+BD) - \left\{(AE+BD)^2 - 4AD(BE-CF)\right\}^{\frac{1}{2}}}{2\,AD} \quad \text{------(37)}$$

$$Wn_2^2 = \frac{(AE+BD) + \left\{(AE+BD)^2 - 4AD(BE - CF)\right\}^{\frac{1}{2}}}{2AD} \quad \text{------(38)}$$

The frequency response of the system is given by the solutions of (35) and (36) :-

$$\tilde{\theta}_2 = \frac{-F\tilde{T}_1}{(p^2+Wn_1^2)(p^2+Wn_2^2)} \quad \text{---------(39)}$$

and $$\tilde{\theta}_1 = \frac{(E + p^2D)\,\tilde{T}_1}{(p^2+Wn_1^2)(p^2+Wn_2^2)} \quad \text{---------(40)}$$

and for p = jw, the responses become

$$\theta_2 (jw) = \frac{- F T_1 (jW)}{(W-Wn_1)(W+Wn_1)(W-Wn_2)(W+Wn_2)} \quad ------ (41)$$

$$\theta_1 (jw) = \frac{(E - W^2D) T (jW)}{(W-Wn_1)(W+Wn_1)(W-Wn_2)(W+Wn_2)} \quad ------ (42)$$

showing resonances at $W = Wn_1$ and Wn_2 and also an infinite DYNAMIC STIFFNESS for Shaft 1 at a frequency given by

$$Ws^2 = E/D \quad ----------(43)$$

The <u>transfer function</u>, $\tilde{\theta}_2/\tilde{\theta}_1$ of the system is given by dividing (39) by (40):-

$$\frac{\theta_2(p)}{\theta_1(p)} = \frac{- F}{E + p^2D} \quad -------- (44)$$

or $$\frac{\theta_2(jW)}{\theta_1(jW)} = \frac{-F}{E - W^2D}$$

and E and F must differ in sign since it is physically abvious that

$$\left(\frac{\theta_2(jW)}{\theta_1(jW)}\right)_{W \to 0} = -\frac{F}{E} \quad ------------ (45)$$

must be positive and real. If the mechanism works at frequencies much lower than W_s given by (43) then θ_2/θ_1 is positive, real, and constant and Eq. (45), which is the STATIC condition, gives the response in this usable frequency range.

7.14 Response of Mirror Shaft I_2 to a Forced Ramp Function $\theta_1(t)$

The reduction mechanism operates in such a way that $\theta_1(t)$ is constrained to follow switched linear rises with time, the driving torque T_1 being supplied from a large inertial drive. Let $\theta_1 = mt$ for $t > 0$ and zero for negative time. The driving torque on I_1 is given by (36):-

$$T_1\ (p) = \frac{m(AE+BD) + m(BE-CF).\ 1/p^2}{E + p^2 D} \quad \text{--------(46)}$$

The inverse transform of (46) gives the time function $T_1(t)$ which is a ramp function with a superposed sinusoid of frequency $W_s = \sqrt{E/D}$.
The transfer function (44) gives the response of I_2,

$$\theta_2(p) = \frac{-F}{E + p^2 D}\ \theta_1\ (p)$$

and putting $\theta_1\ (t) = mt$ for $t > 0$ gives $\theta_1(p) = m/p^2$ and :-

$$\theta_2(p) = \frac{-F/D}{p^2 + E/D} \cdot \frac{m}{p^2}$$

$$\theta_2(p) = -\frac{mF}{E}\left\{\frac{1}{p}2 - \frac{E/D}{p^2 + E/D}\right\}$$

and inverting the transform:-

$$\theta_2(t)_{t>0} = -\frac{mF}{E}\left\{ t - \sqrt{\frac{D}{E}}\ \text{Sin}\sqrt{\frac{E}{D}}.t \right\}$$

$$\text{or} \quad \theta_2(t)_{t>0} = \theta_1(t).\left(\frac{\theta_2}{\theta_1}\right)_{W\to 0}\left(1 - \sqrt{\frac{D}{E}}\ \text{Sin}\sqrt{\frac{E}{D}}.\ t\right) \quad \text{---(47)}$$

Eq. (47) shows that for good linearity in θ_2 (t), we must have $(D/E)^{\frac{1}{2}} \ll 1$ and $Ws = (E/D)^{\frac{1}{2}}$ large; these are compatible conditions.

7.15 Design Criteria

(1) Choose l_B/l_A such that $(\theta_1/\theta_2)_{W \to 0}$ = required reduction ratio (6.2:1), and from (33), (34), and (45) this gives:

$$\frac{l_A(K_T - K_C/l_B^2 - l_A K_T/l_B)}{l_B(K_T + K_C/l_A^2) - l_A(K_T + 3K_C/l_A^2)} = 6.2 \quad \text{-------(48)}$$

(2) To maintain equation (48) under dynamic conditions requires $(D/E)^{\frac{1}{2}} \ll 1$, or from (32) and (33) :-

$$\left\{ \frac{I_2}{l_A(l_A K_T/l_B + K_C/l_B^2 - K_T)} \right\}^{\frac{1}{2}} (l_A - l_B) \ll 1 \quad \text{----(49)}$$

showing the necessity of minimising I_2.

(3) With $(D/E)^{\frac{1}{2}}$ minimised from (49), it must be checked that in addition:-

$$\frac{1}{2\pi}\sqrt{\frac{E}{D}} \gg f_{MAX} \quad \text{-----------(50)}$$

where f_{MAX}, is the maximum 'horizontal' bandwidth of the machine.

(4) In addition, to ensure satisfactory performance on switch-off, the values of Wn_1 and Wn_2 determined from (37) and (38) should be large compared with $2\pi f_{MAX}$.

7.2 THEORETICAL RESPONSE OF SIGNAL DISTRIBUTOR.

7.21 List of Symbols.

I = Inertia of armature assembly

θ = Angular deflection of armature from quiescent position.

θ_0 = Maximum angular deflection of armature from quiescent position.

τ = Total switching time.

T_i = Initial torque acting on armature.

x = Normalised angular response.

y = Axis of aperture movement across semicircular beam.

r = Radius of semicircular light beam.

L = Light flux passed by distributor aperture.

λ = Normalised light flux passed by aperture.

n = Normalised aperture position on semicircular axis.

7.22 Attraction of Armature by Magnetic Core.

We assume a freely pivoting armature located in equilibrium at a small gap distance from a matching wound core; the core is instantaneously magnetised at position $\theta = \theta_0$ providing an initial driving torque Ti. If all the energy is located in the air gap and the magnetomotive force is time invariant, then the equation of motion, assuming zero damping and restoring force, is:

$$I\ddot{\theta}\ (\theta_0-\theta)^2 = T_0\theta_0{}^2 \qquad \text{------------(1)}$$

since the magnetic pull varies inversely as the square of the air gap. Leakage flux and saturation are ignored and small angle motion is implied. Solution of this Ideal Equation is as follows:

Putting

$$\frac{T_o \theta_o^2}{I} = k \quad \text{------(2)}$$

in (1) we have

$$\dot{\theta} \frac{d\dot{\theta}}{d\theta} (\theta_o - \theta)^2 = k \quad \text{-------(3)}$$

Integrating both sides of (3) w.r.t. θ we have

$$\frac{1}{2}\dot{\theta}^2 = k\,(\theta_o - \theta)^{-1} + \text{const.} \quad \text{---- (4)}$$

and observing that $\dot{\theta} = 0$ for $\theta = 0$ this gives, const $= -k\theta_o^{-1}$,

and (4) becomes:- $\frac{1}{2}\dot{\theta}^2 = -k\theta_o^{-1} + k\theta_o^{-1}\,(1 - \theta/\theta_o)^{-1}$

or, inserting (2) and integrating both sides by separating the variables, we have :-

$$\int_0^t dt = \left(\frac{I}{2T_i\theta_o}\right)^{\frac{1}{2}} \int_0^{\theta} \frac{d\theta}{\left((1 - \theta/\theta_o)^{-1} - 1\right)^{\frac{1}{2}}}$$

and hence,

$$t = \left(\frac{I}{2T_i\theta_o}\right)^{\frac{1}{2}} \int_0^{\theta} \left(\theta_o/\theta - 1\right)^{\frac{1}{2}} d\theta \quad \text{----(5)}$$

The total response time τ is given by integrating (5) from $\theta = 0$ to $\theta = \theta_o$:-

$$\tau = \left(\frac{I}{2T_i\theta_o}\right)^{\frac{1}{2}} \int_0^{\theta_o} (\theta_o/\theta - 1)^{\frac{1}{2}} d\theta$$ and substituting

$\theta = \theta \, \text{Cos}^2 \phi$ gives,

$$\tau = \left(\frac{I}{2T_i\theta_o}\right)^{\frac{1}{2}} . \; 2\theta_o \int_0^{\pi/2} \text{Tan}\phi \; \text{Cos}\,\phi \; \text{Sin}\,\phi \; d\,\phi$$

$$\tau = \left(\frac{I}{2T_i\theta_o}\right)^{\frac{1}{2}} . \; 2\theta_o \int_0^{\pi/2} \text{Sin}^2 \phi \; d\phi \, .$$

$$\tau = \frac{\pi}{2} \left(\frac{I\theta_o}{2\,T_i}\right)^{\frac{1}{2}} \quad ------------(6)$$

The solution for constant driving torque is

$$\tau' = \left(\frac{2I\theta_o}{T_i}\right)^{\frac{1}{2}} \quad ----------(7)$$

and (6) and (7) give $\tau = \dfrac{\pi}{4}\tau'$ --------(8)

The time varying solution of (5) is :

$$t = \left(\frac{I}{2T_i\theta_o}\right)^{\frac{1}{2}} . \; 2\theta_o \int_{\text{Cos}\,\phi = o}^{\text{Cos}\,\phi = \pm\sqrt{\theta/\theta_o}} \text{Sin}^2 \phi \; d\,\phi$$

and on integration,

$$t = \left(\frac{I\theta_o}{2\,T_i}\right)^{\frac{1}{2}} \left[\phi - \frac{1}{2} \cdot \text{Sin}\, 2\phi\right]_{\text{Cos}^{-1} 0}^{\text{Cos}^{-1} \pm\sqrt{\theta/\theta_o}}$$

Taking the principal values, and writing $\text{Sin}\,2\phi = 2\text{Sin}\phi\text{Cos}\phi$,

this gives

$$t = \left(\frac{I\theta_o}{2T_i}\right)^{\frac{1}{2}} \left\{\text{Cos}^{-1}\sqrt{\theta/\theta_o} + \pi/2 - \sqrt{\frac{\theta}{\theta_o}\left(1 - \frac{\theta}{\theta_o}\right)}\right\}$$

Normalise by substituting in (6) and writing $x = \theta/\theta_o$

$$\frac{t}{\tau} = \frac{2}{\pi}\left\{\text{Cos}^{-1}\sqrt{x} + \frac{\pi}{2} - (x - x^2)^{\frac{1}{2}}\right\} \quad ------(9)$$

gives the normalised response of the ideal distributor. The following table (7.1) computes twelve points in this response :-

Table 7.1

x	0.025	0.05	0.10	0.20	0.30	0.40	0.50	0.60	0.70	0.80	0.90
1-x	0.975	0.95	0.9	0.8	0.7	0.6	0.5	0.4	0.3	0.2	0.1
$\sqrt{x}$	0.158	0.224	0.316	0.447	0.548	0.632	0.707	0.775	0.837	0.894	0.949
$\cos^{-1} x$	1.400	1.340	1.250	1.110	0.990	0.890	0.785	0.685	0.580	0.462	0.322
$\pi/2$	1.570	1.570	1.570	1.570	1.570	1.570	1.570	1.570	1.570	1.570	1.570
$\pi/2 + \cos^{-1} x$	0.170	0.230	0.320	0.460	0.580	0.680	0.785	0.885	0.990	1.108	1.248
$(x-x^2)^{\frac{1}{2}}$	0.156	0.218	0.300	0.400	0.448	0.490	0.500	0.490	0.448	0.400	0.300
$\pi/2x$ t/T	0.326	0.448	0.620	0.860	1.028	1.170	1.285	1.375	1.438	1.508	1.548
t/τ	0.208	0.285	0.395	0.548	0.655	0.745	0.818	0.876	0.916	0.960	0.985

7.23 Weighting of Semicircular Cross-section Light Beam by a Linear Mask.

We wish to determine the variation of transmitted light flux past a rectangular mask with mask position, assuming that the light flux is uniformly spread across a semicircular cross-section, and that the reading mask edge moves towards, and parallel to, the flat side of the semicircular beam.

If the mask commences to move from the beam tangent along the y-axis, then the total flux L not cut off by the mask is given by

$$L = \int_{o}^{r-y} 2(r^2 - t^2)\, dt \qquad \text{-----------} \; (10)$$

with r the beam radius and t the height of the transmitted section. Substituting $t = r \cos\psi$ in (10) we have:

$$L = \int_{\mathrm{Cos}^{-1}(r-y)/r}^{\pi/2} 2r\,\mathrm{Sin}^2\psi\, d\psi \quad = r^2 \int_{\mathrm{Cos}^{-1}(1-y/r)}^{\pi/2} (1 - \mathrm{Cos}\ 2\psi)\ d\psi$$

$$L = \quad r^2 \left[\psi - \frac{\mathrm{Sin}\ 2\psi}{2} \right]_{\mathrm{Cos}^{-1}\ (1 - y/r)}^{\pi/2}$$

$$L = \quad r^2 \left\{ \frac{\pi}{2} - \mathrm{Cos}^{-1}\left(\frac{r-y}{r}\right) + \left(\frac{r-y}{r}\right) \frac{\left(2ry - y^2\right)^{\frac{1}{2}}}{r} \right\}$$

Normalise by putting $y/r = n$,

$$L = r^2 \left\{ \frac{\pi}{2} - \mathrm{Cos}^{-1}\ (1-n) + (1-n)(2n-n^2)^{\frac{1}{2}} \right\}$$

and normalise the transmitted flux L by writing $L = \pi r^2/2\lambda$,

$$\lambda = \frac{2}{\pi} \left\{ \frac{\pi}{2} - \mathrm{Cos}^{-1}\ (1-n) + (1-n)(2n-n^2)^{\frac{1}{2}} \right\} \text{- - - - - (11)}$$

and this result is tabulated below in Table 7.2,

Table 7.2

n	0	.1	.2	.3	.4	.5	.6	.7	.8	.9	1
$1 - n$	1	.9	.8	.7	.6	.5	.4	.3	.2	.1	0
$2n$	0	0.2	0.4	0.6	0.8	1.0	1.2	1.4	1.6	1.8	2
n^2	0	0.01	0.04	0.09	0.16	0.25	0.36	0.49	0.64	0.81	1
$(2n-n^2)$	0	0.19	0.36	0.51	0.64	0.75	0.84	0.91	0.96	0.99	1
$(2n-n^2)^{\frac{1}{2}}$	0	0.436	0.60	0.714	0.80	0.866	0.916	0.954	0.980	0.995	1
$(1-n)$ above	0	0.392	0.48	0.50	0.48	0.433	0.366	0.286	0.196	0.099	0
$\pi/2$	1.570	1.570	1.57	1.57	1.57	1.57	1.57	1.57	1.57	1.57	1.57
$\pi/2$ + above	1.570	1.962	2.05	2.07	2.05	2.003	1.936	1.856	1.766	1.669	1.57
$\mathrm{Cos}^{-1}(1-n)$	0	0.454	0.645	0.795	0.928	1.050	1.158	1.268	1.370	1.470	1.57
$\pi/2 \cdot \lambda$	1.570	1.508	1.405	1.275	1.122	0.953	0.778	0.588	0.396	0.194	0
λ	1	0.96	0.895	0.812	0.714	0.607	0.495	0.374	0.252	0.127	0

7.3 LIGHT FLUX FROM SPHERICAL SOURCE INTO OBJECTIVE LENS.

7.31 List of Symbols

R = Radius of spherical source.

I = Total Candle Power of source.

L = Distance of source centre to entrance pupil of system.

B = Brightness of source, assumed uniform.

r = Radius of elemental annular ring about lens axis.

ϕ = Angle subtended by elemental ring at source centre.

θ = Angle subtended by elemental ring at entrance pupil.

l = Distance of elemental ring circumference from entrance pupil.

$dE_{\Delta\sigma}$ = Illumination at entrance pupil derived from flux emitted by elemental ring of candle power dI.

α = Ratio of R/L.

R_s = Radius of objective lens.

x = Distance of objective lens from effective entrance pupil.

D = Total source to lens distance.

7.32 Total Illumination at Entrance Pupil of Lens System

Referring to Fig. 7.2, we have:

Inverse Square Law, $dE_{\Delta\sigma} = dI \cos\theta / l^2$ - - - - - - -(1)

Lamberts Law of Emission, $dI = 2\pi r . R d\phi . B \cos(\theta + \phi)$ - - - -(2)

Sine Rule, $r = R\sin\phi = l \sin\theta$ - - - - - - - - - - (3)

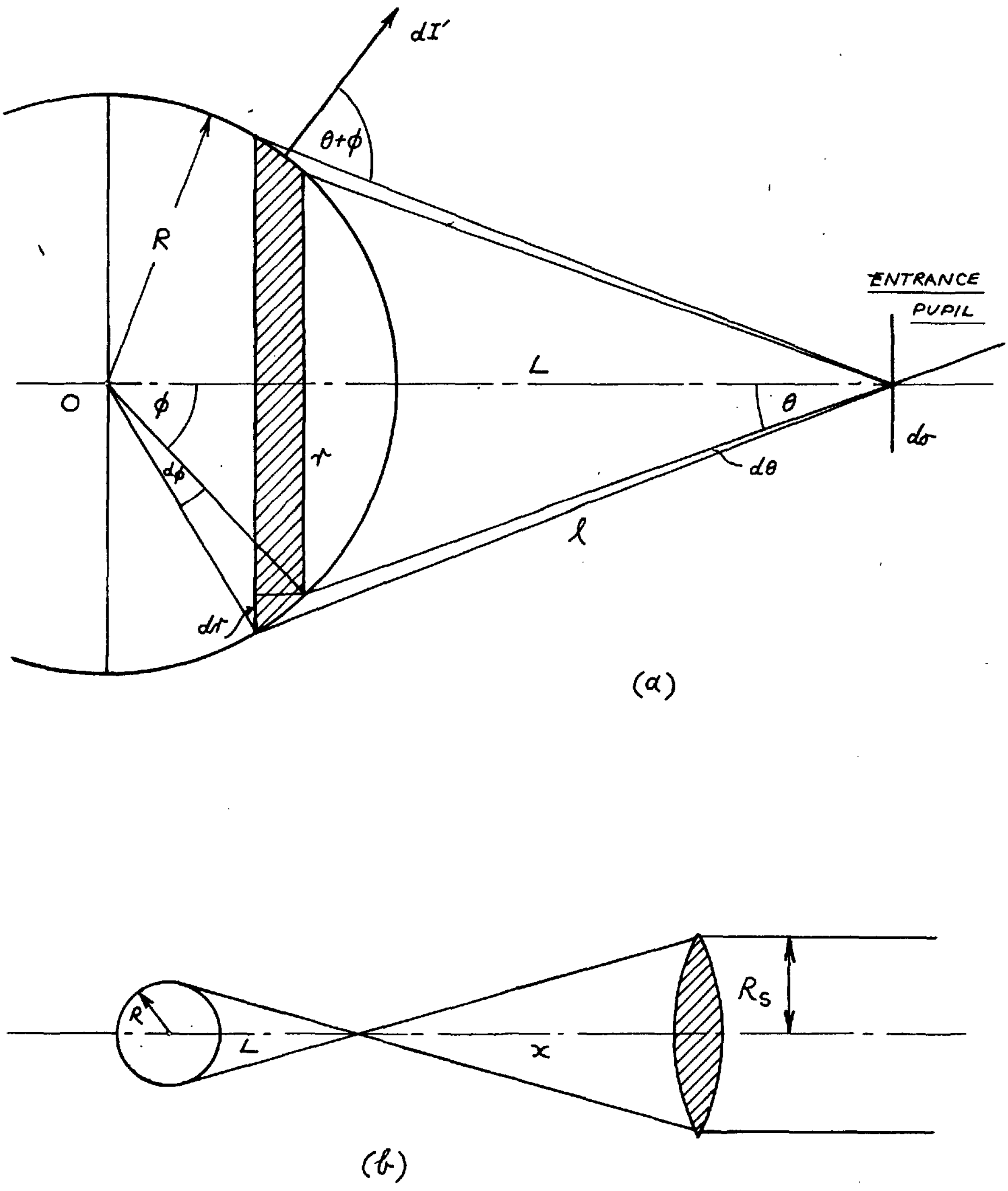

FIG. 7·2

LIGHT FLUX FROM SPHERICAL SOURCE INTO OBJECTIVE.

Projection, $L = R\cos\phi + l\cos\theta$ - - - - - - - - - - - -(4)

Cosine Rule, $l^2 = R^2 + L^2 - 2RL\cos\phi$ - - - - - - - - - -(5)

Projection, $l\cos(\phi + \theta) = L\cos\phi - R$ - - - - - - - -(6)

Inserting (4) and (5) in (1) we have,

$$dE_{\Delta\sigma} = \frac{dI(L - R\cos\phi)}{l\,(R^2 + L^2 - 2RL\cos\phi)} \quad --- (7)$$

Inserting (6) and (3) in (2) we have,

$$dI = 2\pi R.B.\ \frac{R\sin\phi}{l}\left\{L\cos\phi - R\right\} d\phi \quad ---(8)$$

Substituting (8) into (7) gives :-

$$dE_{\Delta\sigma} = \frac{2\pi R^2 B\sin\phi\,(L\cos\phi - R)(L - R\cos\phi)\,d\phi}{l^2(R^2 + L^2 - 2RL\cos\phi)}$$

and together with (5) we have :

$$dE_{\Delta\sigma} = \frac{2\pi R^2 B\sin\phi\,L^2\,(\cos\phi - R/L)(1 - R/L.\cos\phi)\,d\phi}{L^4\,(1 + R^2/L^2 - 2R/L.\cos\phi)^2}$$

and

$$E_{\Delta\sigma} = \int dE_{\Delta\sigma} = \frac{2\pi R^2 B}{L^2}\int_0^{\phi_M} \frac{(\cos\phi - R/L)(1 - R\cos\phi/L)\sin\phi\,d\phi}{(1 + R^2/L^2 - 2R\cos\phi/L)^2} \quad --(9)$$

and ϕ is given by : $\cos\phi_M = R/L$, i.e. $\phi_M + \theta = \pi/2$

Changing variable to $x = \cos\phi$ in (9) and putting $\alpha = R/L$ we have:

$$E_{\Delta\sigma} = 2\pi\alpha^2 B\int_1^{\alpha} \frac{(\cos\phi - \alpha)(\alpha\cos\phi - 1)}{(1 + \alpha^2 - 2\alpha\cos\phi)^2}\,dx$$

$$= -2\pi\alpha^2 B \int_1^{\alpha} \frac{(x-\alpha)(1-\alpha x)}{(2\alpha x - \alpha^2 - 1)^2} dx$$

which may be integrated for the case $R^2/L^2 \ll 1$, i.e. $\alpha^2 \ll 1$

$$E_{\Delta\sigma} = 2\pi\alpha^2 B \int_{\alpha}^{1} \frac{x - \alpha x^2 - \alpha}{(2\alpha x - 1)^2} dx$$

$$= 2\pi\alpha^2 B \int_{\alpha}^{1} \left\{ \frac{(1/4\alpha - \alpha)}{(2\alpha x - 1)^2} \quad \frac{-1}{4\alpha} \right\} dx$$

$$= 2\pi\alpha^2 B \left[\frac{(\alpha - 1/4\alpha)}{2\alpha(2\alpha x - 1)} - \frac{x}{4\alpha} \right]_{\alpha}^{1}$$

again noting that $\alpha^2 \ll 1$,

$$E_{\Delta\sigma} = \frac{\pi B \alpha}{2} \left\{ \alpha - \tfrac{1}{2}\alpha - 1 - 1/2\alpha(2\alpha - 1) \right\}$$

$$E_{\Delta\sigma} = \frac{\pi B \alpha^2 (2\alpha - 3)}{2\,(2\alpha - 1)}, \quad \alpha^2 \ll 1 \qquad ----- (10)$$

Note for $\alpha \ll 1$, (10) becomes $E_{\Delta\sigma} = \dfrac{3\pi B\alpha^2}{2}$ ---- (11)

<u>7.33 Light Flux into Objective Lens.</u>

Assuming uniform and unity transmission, (10) gives the illumination at the entrance pupil of the lens system, and if the objective lens - source distance is L + x (Fig. 7.2) we have

$$\alpha = R/L = R_s/x \qquad ----------(12)$$

If I is the total candle power of the source, assuming uniform diffusion,

$$4\pi R^2 B = I \qquad ------------ (12)$$

Substituting (13) in (10) for the transmitted flux density E_T

$$E_T = \frac{I}{8L^2} \cdot \frac{3 - 2\alpha}{1 - 2\alpha} \quad \text{-------(14)}$$

and α can be determined from (12), since L + x is measurable, R and R_s are known:-

$$\text{Let } D = L + x \quad \text{----------------(15)}$$

Then substituting (15) in (12) we have,

$$R(D - L) = R_s L$$

$$\text{or} \quad L/R = 1/\alpha = D/(R_s + R)$$

$$\text{and} \quad \alpha = \frac{R_s + R}{D} \quad \text{-------------- (16)}$$

Put (16) in (14) and we have,

$$E_T = \frac{I}{8L^2} \cdot \frac{3D - 2(R_s + R)}{D - 2(R_s + R)} \quad \text{-----------(17)}$$

with the condition that :

$$\alpha^2 \ll 1, \text{ i.e. } (R_s + R)^2 \ll D^2 \quad \text{--------- (18)}$$

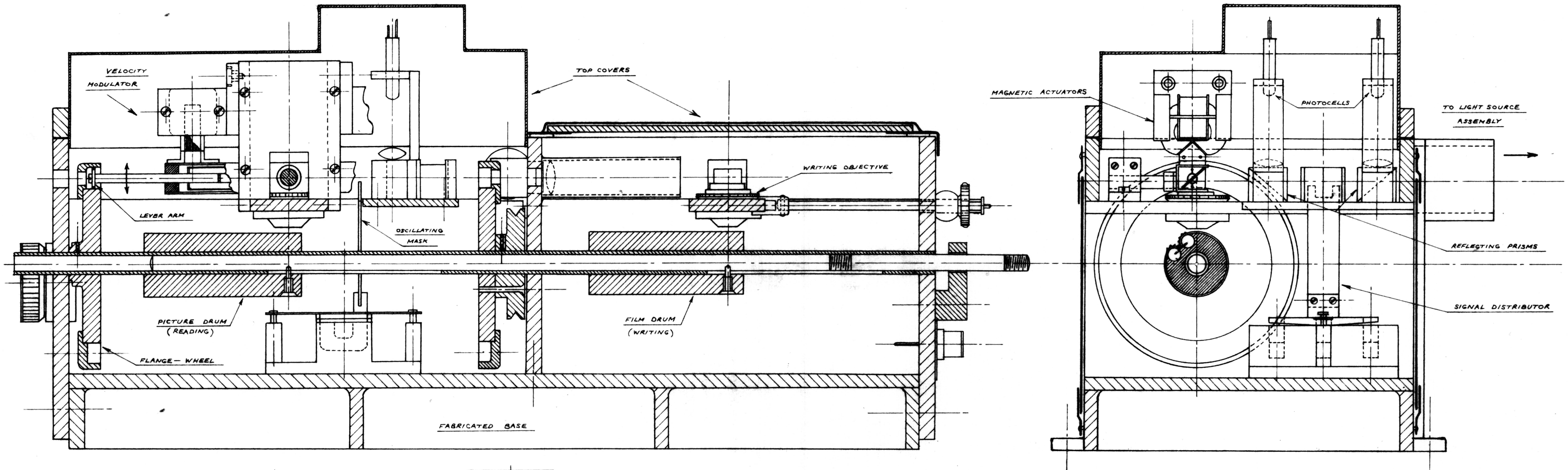

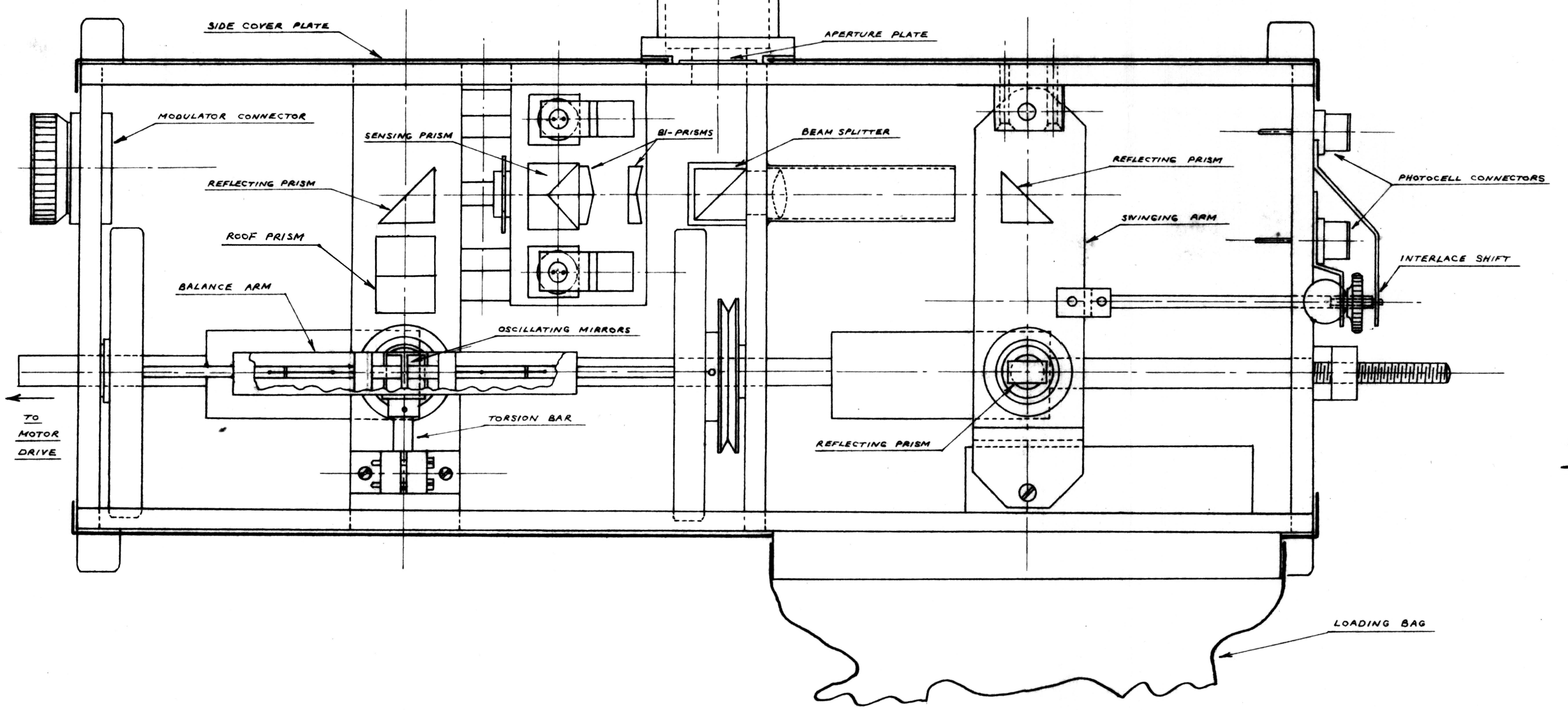

SCALE: FULL SIZE.

FIGURE 3·1

PICTURE TRANSFORMER

WITH CONTOUR INTERPOLATION